Characterization of Environmentally-Friendly Alkali Activated Slag Cements and Ancient Building Materials

A Thesis

Submitted to the Faculty

of

Drexel University

by

Aaron Richard Sakulich

in partial fulfillment of the

requirements for the degree

of

Doctor of Philosophy

September 2009

Dedication

"...we came to an archipelago where there was a little island with only one home, occupied by a weaver. He had a wife and a family, a few cocoa-palms and a small boat he used to fish and visit other islands. It also contained banana bushes, and no birds but two crows that came to greet us as we approached. And I swear I envied that man, and wished the island had been mine..."

~ Ibn Battuta, 14th century traveler

Acknowledgements

First and foremost, I would like to thank Dr. Michel Barsoum, my advisor, who took a chance on taking me on as a grad student with only my senior design project for a reference. The help of Dr. Caroline Schauer, who also sat on my Fulbright committee, was greatly appreciated. I would also like to thank Dr. Grace Hsuan, Dr. Christopher Li, Dr. Tony Addison, and Dr. Ori Yeheskel. I benefitted from the aid of a number of undergraduate students: Kyle Keen, Željko Ivošević, Edward Anderson, Chris Barr, and Frank DiCianni; as well as from my fellow researchers: Sean Miller, Alex Moseson, and Dr. Eva Jud Sierra. The help of fellow students Chris Hovanec, Tony Fast, Dr. Liz Hoffman, Dr. Shahram Amini, and Dr. Jessica Schiffman, whether training me on equipment or helping to hide equipment I had just broken, was invaluable. Of course, I would never have gotten anything done if not for the indefatigable patience of Judy Trachtman, Dorilona Rose, Daniella Ascarelli, Dee Breger, and Keiko Nakazawa.

In Morocco, I would like to thank Dr. Abderrahim Aatiq, Dr. Hassan Hannache, and Monsiuer Sidi le Moulay Rachid Tigha, at University Hassan II; Saadia Maaski and Daoud Casewit at MACECE; the staff at ALIF; Dr. George Roberson, Rajae Khaloufi, and Khalid Amine at ICPS; Dr. Lawrence Michilak in Tunis, and all the wonderful friends I made overseas and all the ma'qooda vendors I frequented.

My friends have been an indispensable, solid foundation, and my many detractors an inspiration. Finally, I'd like to thank my family, especially my father Richard and sister Alexis, who have put up with me with amazing patience.

TABLE OF CONTENTS

List of Tables

List of Figures

Abstract

Characterization of Environmentally-Friendly Alkali Activated Slag Cements and Ancient Building Materials

Aaron Richard Sakulich

Michel W. Barsoum, Ph.D.

Alternative cement technologies are an area of increasing interest due to growing environmental concerns and the relatively large carbon footprint of the cement industry. Many new cements have been developed, but one of the most promising is that made from granulated, ground blast furnace slag activated by a high-pH solution. Another is related to the discovery that some of the pyramid limestone blocks may have been cast using a combination of diatomaceous earth activated by lime which provides the high pH needed to dissolve the diatomaceous earth and bind the limestone aggregate together. The emphasis of this thesis is not on the latter – which was explored elsewhere – but on the results supplying further evidence that some of the pyramid blocks were indeed reconstituted limestone.

The goal of this work is to chemically and mechanically characterize both alkali-activated slag cements as well as a number of historic materials, which may be ancient analogues to cement.

Alkali activated slag cements were produced with a number of additives; concretes were made with the addition of a fine limestone aggregate. These materials were characterized mechanically and by XRD, FTIR, SEM, and TGA. Samples from several Egyptian pyramids, an 'ancient floor' in Colorado, and the 'Bosnian Pyramids' were investigated.

In the cements, it has been unequivocally shown that C-S-H, the same binding phase that is produced in ordinary portland cement, has been produced, as well as a variety of mineral side products. Significant recarbonation occurs during the first 20 months, but only for the Na_2CO_3-activated formulae.

Radiocarbon dating proves that the 'Bosnian Pyramids' and 'ancient floors' are not made from any type of recarbonated lime; however, Egyptian pyramid limestones were finite, thus suggesting that they are of a synthetic nature. XRD and FTIR results were inconclusive, while TGA results indicate the limestones are identical to naturally occurring limestones, and SEM/EDS analysis shows the presence of a Si-rich species.

CHAPTER 1: INTRODUCTION AND LITERATURE REVIEW

1.1 – History and Properties of Cements

1.1.1 – Lime-based Cements

The story of using materials derived from the burning of limestone to make a 'synthetic stone' for construction purposes begins at least 9,000 years ago in Asia Minor. At the site of Asikli Hüyük, buildings have been uncovered with lime-plastered floors [1], marking the oldest known use of such materials. Research has shown that inhabitants of the area must have developed some sort of crude kiln [2] with which to produce the lime by burning limestone ($CaCO_3$, or calcite.) It is generally accepted that the earliest use of this technology occurred in Asia Minor and spread south to the Levant and Egypt. [2, 3] In fact, mortars based on lime and/or gypsum have been found in a number of Egyptian pyramids [2, 4].

The kilns must have been capable of reaching temperatures between 750 ^{o}C and 850 ^{o}C, and maintaining that temperature for several hours. This would cause the CO_2 in calcite to be driven off, leaving behind CaO (equation 1.) With the rehydration of CaO, portlandite ($Ca(OH)_2$) is formed (equation 2), and the material takes on the consistency of a wet slurry that can be molded. With drying and absorption of CO_2 from the atmosphere (equation 3), the portlandite releases water and returns to $CaCO_3$ – a synthetic, recarbonated form of a natural stone [5].

$$CaCO_3 \rightarrow CaO + CO_2 \qquad \text{(eq. 1)}$$

$$CaO + H_2O \rightarrow Ca(OH)_2 \qquad \text{(eq. 2)}$$

$$Ca(OH)_2 + H_2O \rightarrow CaCO_3 \qquad \text{(eq. 3)}$$

This process is, essentially, a manner of taking naturally occurring limestone, treating it so as to make it easily worked with, and then allowing recarbonation to return it to its natural, durable, strong stone chemistry. As a building material, lime has decent compressive strength, a superior ability to bond to other materials, excellent resistance to water, high plasticity (allowing it to accommodate the expansion and contraction of other building elements), and larger pores, which allow greater air flow [6]. Because of these unique properties, using modern cement to replace lime-based mortars in historic buildings can be dangerous; often the dense, inflexible modern materials can cause extensive damage to the rest of the structure [7].

1.1.2 –True Cements

Although the first improvements over cementitious materials based solely on lime has often been credited to the Romans, recent discoveries prove that the Greeks were first, using Santorine Earth in their buildings before the Romans began to use volcanic ash. [6] The use of these 'pozzolanic' materials, which are amorphous aluminosilicates, provides Si which can react with leftover portlandite ($Ca(OH)_2$) to produce calcium silicate hydrate (C-S-H in cement chemist notation; see below.) Mixtures of lime and pozzolanic materials are superior to pure lime systems in that they are stronger, gain strength more rapidly, and are hydraulic in nature (that is, they can cure even while submerged in water; therefore they are used anywhere a waterproof coating would be needed, such as cisterns and wells.) Marcus Vitruvius Pollio (better known simply as Vitruvius, namesake of da Vinci's 'Vitruvian Man'), a Roman architect, engineer, and *praefactus fabrum* of the 1st century B.C., wrote the first book on architecture, *De Architectura*, in which he provides in-depth discussions of both cement and concrete, in

addition to describing aqueducts, siege weapons, centralized heating systems, dewatering machines, and tools for surveying. [8] The second book on architecture in the world's history was not released until Leon Battista Alberti released a new version of *De Architectura* in 1452. A list of concrete-related materials and techniques known to the Romans (Table 1.1) shows that they understood the importance of the chemistry and mechanics behind fine and coarse aggregate, proper selection of limestone, and pozzolanic additives. It was their mastery of cement and concrete chemistry that enabled the construction of the roads, aqueducts, bridges, and *insulae* (tenement houses) that made Rome the power that it was.

1.1.3 –Ordinary Portland Cement

With the disintegration of the Roman empire, much of their cement technology was lost. The next material to be seen as an improvement over Roman technology was ordinary portland cement (OPC), invented in 1824 by Joseph Aspdin, a British bricklayer, and named after the color of the cliffs in Dorchester, from which he took the limestones used as reactants in his material. Despite the presence of a number of

Table 1.1 - Cement and concrete terminology available to the Romans as early as the 1st century B.C.

Name	Type	Description
Opus incertum	Technique	Technique using fine aggregate
Opus reticulatum	Technique	Small squared tiles laid in diamond pattern
Opus quadratum	Technique	Continuous courses of blocks without mortar
Opus latericium	Technique	Coarse-laid brickwork
Opus spicatum	Technique	Herringbone-patterned brickwork
Opus vittatum	Technique	Technique used for high walls;
Opus africanum	Technique	Brickwork with alternative vertical and horizontal blocks
Opus testaceum	Technique	Thick brickwork
Opus Mixtum	Technique	Use of 2 or more techniques in 1 structure
Coementa	Material	Aggregate
Opus Caementicium	Material	Concrete

competitors, including one James Parker (who in 1796 patented 'Roman Cement,' an attempt to recreate the *opus caementicum* of the Romans), it is generally accepted that Aspdin's son William was the first to manufacture portland cement similar to that which is used today [9].

There are a number of steps in the production of portland cement, though Aspdin's original method demanded nothing more than burning limestone and clay on his kitchen stove. First, materials are mined from the earth and crushed into pieces no larger than 3 inches in size and thoroughly mixed. Then, this rubble is fed (either dry or combined with water to make a slurry) into a rotary kiln, which is often tens of feet in diameter and hundreds of feet long. Upon exiting the kiln, the material has been transformed into (red-hot) clinker. This clinker is then ground together with any additives (gypsum, fly ash, slag, etc.) and is ready for sale [10].

Table 1.2 - Basic cement chemistry notation

C.C.N.	Formula
C	CaO
S	SiO_2
A	Al_2O_3
F	Fe_2O_3
K	K_2O
N	Na_2O
M	MgO
T	TiO_2
H	H_2O
Ṡ	SO_3
Ċ	CO_2
t	tri-
m	mono-

The strength of OPC is due mainly to two chemicals present in the final product: Alite (tricalcium silicate, C_3S in cement chemist notation; see Table 1.2) and belite (dicalcium silicate, C_2S.) These hydration reactions are shown in Eqs 4 and 5, respectively. When hydrated, both of these materials form calcium silicate hydrate (C-S-H), however, as alite has more free calcium, it hydrates more quickly and gives rise to early strength. Belite hydration is slower, and gives rise to long term strength. This C-S-H can have a range of compositions, but is generally a stable, strong, 3D structure that gives strength to the cementing phase.

$$6CaO{\cdot}2SiO_2 + 6H_2O \rightarrow 3CaO{\cdot}2SiO_2{\cdot}3H_2O + 3Ca(OH)_2 \qquad \text{(eq. 4)}$$

$$4CaO{\cdot}2SiO_4 + 4H_2O \rightarrow 3CaO{\cdot}2SiO_2{\cdot}3H_2O + Ca(OH)_2 \qquad \text{(eq. 5)}$$

This is a greatly simplified view of cement chemistry; examples of more phases commonly observed in OPC, and their cement chemistry notation, can be found in Table 1.3.

Compared to other building materials, such as steel or wood, OPC clearly stands out due to its ease of manufacturing, low cost, and ease of implementation. [11] OPC, from which concrete is made through the addition of aggregate, is today's most important building material; approximately 1.7×10^9 t/year are produced, about 1 m^3 for each person on earth. [12] Unfortunately, it also stands out due to its negative impact on the environment: for every ton of OPC produced, roughly one ton of CO_2 is released into the atmosphere.[9, 13-15] Half of this CO_2 is produced during the burning of $CaCO_3$ to produce CaO and CO_2 and half is produced through the consumption of fuel to carry out this process.[16] This amounts to the cement industry being responsible for not only 5 % of total CO_2 production, but also 5 % of worldwide industrial energy consumption.[17-

19] As China and India begin to build up their respective infrastructures, this amount is only going to increase dramatically.

To decrease the environmental impact of the cement industry, a number of changes have been implemented. The first has been a drive to increase the efficiency of the kilns that are producing the raw cement. [19] Second has been the use of additives to cut the total amount of cement needed, such as natural pozzolans like metakaolin, fly ash (the byproduct of burning coal in power stations), and granulated ground blast furnace slag. [11, 16, 20] The former two of these are aluminosilicate materials which can be added to OPC without negatively affecting properties; the latter two are waste products produced in other sectors of industry which generally end up in landfills. Of the three, slag stands out, as it contains a large percentage of calcium, making it chemically similar to OPC. In fact, it can be used as a cement on its own, if activated by a high-pH solution, and is the main topic of the work discussed in this thesis.

Table 1.3– Examples of cement chemistry notation: common phases found in portland cement. Dashes, such as in C-S-H, indicate a variable chemistry

C.C.N	Formula	Name
C_3S	$3CaO•SiO_2$	Tricalcium Silicate
C_2S	$2CaO•SiO_2$	Dicalcium Silicate
C_3A	$3CaO•Al2O_3$	Tricalcium Aluminate
C_4AF	$4CaO•Al_2O_3•Fe_2O_3$	Tetracalcium aluminoferrite
C-S-H	Varies	Calcium Silicate Hydrate
C-A-H	Varies	Calcium Aluminate Hydrate
Aft	$C_3A\dot{S}_3H_{30\text{-}32}$	Aluminate Ferrite Trisulfate
AFm	$C_2A\dot{S}H_{12}$	Aluminate Ferrite Monosulfate
C_3AH_6	$3CaO•Al_2O_3•6H_2O$	Hydrogarnet

1.1.4 – Alkali Activated Slag Cements

The development of alternative cements based on the alkali-activation of slag has a relatively long history. Feret first described the use of slag in cement in 1939, while Purdon described "the action of alkalis on slag" in 1940, but it was not until the writings of Glukhovsky in the late 1950s that the notion became widespread [9, 20]. In fact, several apartment buildings and other structures were constructed using alkali-activated slag cements in Ukraine in the 1960s; despite the severe weather of that region, they still stand today in good shape [21].

The use of slag in cement is especially attractive for a number of environmental reasons. First, it consumes a waste material for which there is no other use: producing crude iron from ore containing 60 – 65 % Fe produces between 22 – 37 % its weight in slag, amounting to at least 200 Mt annually in the US alone [22]. The majority of American slag is still disposed of in landfills [20]. AAS cements are also said to excel in specific applications involving resistance to hostile environments [23-27].

The exact nature of the activation of slag by alkalis, however, is not yet fully understood. The current status of alkali-activated materials has been spelled out in a number of recent review articles [9, 15, 20, 28, 29]. These articles generally focus on the use of SEM/EDS, XRD, FTIR, thermal analysis and NMR as techniques for investigating slag cements: they conclude that C-S-H, the same phase that gives strength to OPC, is the main phase produced. A variety of minor mineral side-products have also been identified, and the general chemical reactions identified.

The name "alkali-activated slag" has received some criticism lately, mainly from Davidovits, who claims that this terminology is 'dangerous' [9]. The argument is that the

name could confuse engineers and lead them to think that the cements are prone to alkali-aggregate reaction, a degradation mechanism found in OPC. He proposes instead the name ‘geopolymers.’ In this work, *alkali-activated slag* is used to describe cementitious materials made from the activation of blast furnace slag by alkali solutions; *ordinary portland cement* is used to describe the traditional cementitious material made from limestone and clay; and ‘*geopolymer*’ is used to describe specifically the zeolite-like alkali-aluminosilicate materials originally described by Davidovits in the 1970s. The main reasons for this are that ‘geopolymer’ has too narrow a definition to describe cements produced from slag; that the term ‘alkali activated slag’ predates ‘geopolymer’; and that ‘geopolymer’ is, essentially, a marketing name for a specific product. Although the same *could* be said of ‘portland cement,’ that name has passed into common usage in the past 150 years; ‘geopolymer’ has not.

1.1.5 – ‘Geopolymers’

After a number of devastating fires in residential structures between 1970 and 1973 in France, organic chemist Joseph Davidovits turned his attention to developing fire-resistant ‘mineral plastics’ [30]. Originally struck that the same hydrothermal conditions prevail during the production of both organic polymers and zeolite minerals, these mineral plastics were an attempt to create non-flammable materials similar to organic polymers in structure, but to minerals in elemental composition. In 1979, the name ‘geopolymer’ was used to describe these materials [31], though today they are referred to variously as geopolymers, alkaline inorganic polymers, hydroceramics, hydrocements, zeoceramics, zeocretes, soil cements, alkali-activated binders, and more [32]. The term ‘alkali activated binder’ is generally accepted to be the broadest possible

category, including both ‘geopolymers’ as described by Davidovits, as well as alkali-activated slag cements and OPC.

Structurally, ‘geopolymers’ are composed of long silicate chains; Al atoms substituting for Si in these chains act as network modifiers that encourage linking, and demand an alkali ion nearby to balance the electrical charge [31]. A new terminology for these chemical species, more practical and less controversial than the name ‘geopolymers’ (which was also the name given to using plastics, as in plastic tarps, in civil engineering, for instance to prevent liquid penetration of certain areas, etc.) was developed by Davidovits. In this terminology, ‘sialate’ is used to replace silico-oxy-aluminate, and ‘siloxo’ is used to denote an O-Si bond. Thus, a geopolymer with a (Si-O-Al-O-Si-O) backbone and Na used to balance the charge on the Al would be referred to as a Na-(poly)sialate-siloxo[33].

Unlike OPC, where water is added to powder, mixed, and allowed to set, or even alkali-activated slag cements, where the water is replaced by a high-pH solution, ‘geopolymers’ require a rather elaborate production method. The starting materials must be calcined, generally at 750 ^{o}C, to remove non-linking bonds and make surfaces more reactive. After mixing with a high-pH solution, most aluminosilicate ‘geopolymers’ usually undergo a heating process, generally reported to be curing in the range of 60-80^{o}C for up to 24 hours.

‘Geopolymers’ are reported to have a number of excellent properties, such as excellent strength, acid resistance, thermal properties, freeze thaw behavior, and so on [28, 34]. Though claims have been made, due to which ‘geopolymers’ have received much attention, that they are superior to OPC in environmental footprint, these are likely

over-emphasized, as a full accounting of the environmental impact from heat treating the reactants, curing the product at elevated temperatures, and the use of concentrated industrial chemicals such as NaOH and KOH, would be less than likely to paint a rosy environmental picture for ‘geopolymers’.

In the 1980s, Davidovits developed the theory that the pyramids in Egypt were made not of carved stone, as is traditionally held, but of an ancient form of sodium-aluminosilicate ‘geopolymer’ [35]. This theory, elaborated upon in his 1988 book with Morris, will be discussed further below.

1.2 – Other Ancient Building Materials

1.2.1 – Colorado ‘Floor’ Samples

In 1934 a rancher by the name of Tom Kenney was digging an outhouse near Collbran, Colorado. A few meters into the hole, he came across a hard floor that looked like large tile slabs with mortared joints running between them. Instead of an outhouse, he decided to build a cellar with a tile floor, and a group of visiting experts declared in 1937 that there was "not the slightest doubt but that the work is of some prehistoric civilization." Archaeologists from Denver estimated that the floor had been laid by a prehistoric people between 25,000 and 80,000 years earlier. On the other hand, an Egyptologist visiting from the Archaeological Society of London declared it a geological phenomenon [36].

The matter received no more professional attention until 2007, when the floor was unearthed and inspected by geologists who declared it to be part of a natural, albeit abnormal, outcropping. Exposure to weathering had given the ‘tiles’ a polished look and

flat shape, while the ‘mortar joints’ were created by stress and weathering. However, samples from the floor have not been investigated in a materials science context [36].

1.2.2 – Bosnian ‘Pyramids’

The ‘Bosnian Pyramids’ are a number of formations near Visočica hill, northwest of Sarajevo. In October 2005, Semir Osmanagić, a Bosnian expatriate and contract metalworker, claimed that the hills were in fact the remnants of an ancient civilization. Osmanagić has claimed the discovery of numerous structures, including the Pyramid of the Sun, the Pyramid of the Moon, the Pyramid of the Bosnian Dragon, and the Pyramid of the Earth, as well as a network of tunnels, temples, and associated structures [37].

Initial reaction was fierce. Numerous archaeologists and geologists declared that the formations were of a natural, geologic origin, and that the manner in which Osmanagić carries out his excavations risks damaging genuine archaeological sites nearby (the town of Visoko was a medieval capital until its obliteration by Turkish forces.) The discovery of artifacts nearby only renewed calls for Osmanagić’s excavations to be stopped, with archaeologists going as far as to draft an open letter to the Bosnian government, claiming “This scheme… has no place in the world of genuine science.” [38]

Whatever the origins of the ‘Bosnian Pyramids,’ Osmanagić has certainly not avoided providing his detractors with ammunition. These include:

1) Grandiose statements such as “my discovery will change human history” [37]; that the Bosnian pyramid is “The Mother of All Pyramids”; and that the pyramids in Egypt, South America, and Bosnia were built by the same civilization (presumably the Maya, who he refers to as the “watchmakers of the cosmos” who are on a mission to

"adjust the Earthly frequency and bring it into accordance with the vibrations of our Sun") [39];

2) Von Däniken-like pseudoscientific claims, such as that excavations must be completed by 2012 so as to "break a cloud of negative energy, allowing the Earth to receive cosmic energy from the centre of the galaxy" [39] and that ancient builders had left messages for future generations encoded in texts that would require "numerological" study;

3) What are apparently active attempts to deceive the public, including claims that mainstream archaeologists supported or are involved with his work (including Zahi Hawass, Secretary General of the Supreme Council of Antiquities of Egypt, Canadian Chris Mundigler, leading Irish archaeologist Grace Fegan, Austrian Royce Richards, and American Allyson McDavid, none of whom are involved; attempts to track down archaeologists associated with the project by Mark Rose resulted in at least one name that was untraceable); and archaeologist Robert Schoch (invited to the site by Osmanagić) claims that a "reliable source" informed him that the "ancient inscriptions" found inside the tunnels were not there two years ago when the pyramid team first entered them.[40]

A number of geologists have investigated the site, including a team from the Faculty of Mining and Geology at the University of Tuzla, led by Sejfudin Vrabac, who claimed them to be a natural geological formation, other examples of which can be easily found elsewhere in the Sarajevo-Zenica mining basin [41]. On the other hand, Ali Abdullah Barakat, who Osmanagić claimed to be a pyramid expert recommended by Zahi Hawass (and who Hawass claimed is not a pyramid expert and for whom he did not offer a recommendation) came to the conclusion that traces of 'glue' similar to what was used

in the Egyptian pyramids were present, and that the site was, in fact, a “primitive pyramid.” (For the record, the word ‘glue’ is probably a confabulation due to translating between Egyptian Arabic, English, and the Bosnian languages, and probably refers to mortar.) [42]

However, limited investigations from a materials science perspective have taken place. Joseph Davidovits concluded after investigating several samples that Osmanagić’s theory was reasonable, and could possibly be another example of early ‘geopolymer’ technology. The Gliwice Radiocarbon Laboratory, under the direction of Professor Anna Pazdur, performed radiocarbon dating on a sample from a ‘stalagmite’ found inside the tunnels; the date came back to 5139 ± 75 years old. [43]

1.2.3 – Egyptian Pyramids

The pyramids of Egypt, in contrast to those in Bosnia, are among the most recognizable structures created in human history. It is unknown how many were originally built; over 80 remain today, the majority of which are but traces of ruins. The largest, the Great Pyramid on the Giza plateau, is the only of wonder of the ancient world that remains, and was the tallest building on earth from its construction around 2560 BC until the completion of the spire of Lincoln Cathedral in England. The spire, it should be noted, collapsed a mere 238 years later. In fact, the first building to exceed the Great Pyramid in height without collapsing soon thereafter was not built until 1874 (the spire of the Church of St. Nikolai, in Hamburg, Germany, beat it by 1.8 feet.)

The manner by which the pyramids were constructed is still a matter of debate, a debate characterized by seemingly incomprehensible mysteries: how was a structure like the Great Pyramid built in, as we know from archaeological records, only 23 years? How

were enormous 70-ton beams positioned above the king's chamber, hundreds of feet in the air? How is it that the casing stones were produced with such perfection that they fit so tightly together? And so on.

The traditional theory states that limestone and granite blocks were quarried, hauled to the work site, and then hoisted in position either by ramp or some other device. In 1988, Joseph Davidovits posited an entirely unorthodox theory: that the blocks of the pyramids were not, in fact, carved but are actually an ancient form of 'geopolymer' concrete. In his version, naturally occurring clays were mixed with limestone rubble and various alkalis (ashes, naturally occurring salts, and so on.) This material was then allowed to react over the course of a few days, carried to the work site in buckets, and then tamped into wooden molds. After a few days, the material was strong enough to build on and had the appearance of natural limestone.

Davidovits' main objections to the carve-and-hoist theory were that the Egyptians did not have tools sufficiently durable to carve limestone and granite; that they had no method to carry the dressed blocks to the work site; and that they did not have a mechanism by which to hoist the blocks into place, especially to the tops of the pyramids (ramps being problematic for a number of reasons.)

The objections to Davidovits' theory, as proposed in his book *The Pyramids: an Enigma Solved* with Margaret Morris, were numerous and vociferous. Geologists and archaeologists alike argued against many of his claims, from a variety of angles. However, despite Davidovits obtaining samples from the inner casing of the ascending passageway of the Great Pyramid, most of the evidence came from an archaeological or

geological background. Little investigation had been done from a materials science perspective.

1.3 – Objective

This work hopes to produce and characterize several environmentally-friendly slag cements, based on NaOH/waterglass, which should provide the highest possible strength, and Na_2CO_3, which would be the most practical activator in real life situations. The latter has received some attention in the literature, but not as much as the former. These basic formulae will then be investigated with a number of additives, meant to enhance properties, encourage the formation of 'geopolymers,' or improve cost/practicality/environmental friendliness. The reaction products (i.e. AAS materials or 'geopolymers') will be identified and characterized by materials science methods, along with mechanical properties, and their similarities with, or differences from, 'geopolymers' discussed. Long-term characterization, of which there is little in the literature, will also be provided. Finally, ancient building materials will also be characterized using the same materials science techniques in an effort to identify their 'geopolymeric' origin. Should these ancient materials prove to have a synthetic origin, their characterization could provide important clues as to how to optimize formulae using modern materials such as slag.

CHAPTER 2: EXPERIMENTAL METHODS AND MATERIALS

2.1 – Sample Preparation

Reactants used in the basic formulae were: ground granulated blast furnace slag (St. Lawrence Cement Co., Camden, NJ), NaOH pellets (Alfa Aesar, Ward Hill, MA), Na_2CO_3 powder (Dharma Trading Co., San Rafael, CA), and type N soluble silicate (PQ Corp., Valley Forge, PA). Tap water was used throughout. NaCl (Alfa Aesar) was investigated as a retardant; fine limestone (Old Castle Stone Products, Charlotte, NC) was used as a fine aggregate; diatomaceous earth (PermaGuard, Inc., Albuquerque, NM), Al_2O_3 (Alfa Aesar), Type F (Low CaO) Fly ash (Hossein Rostami, Philadelphia University), metakaolin (Concrete Countertop Institute, Raleigh, NC), and acid rock treatment sludge (Halifax International Airport, Halifax, Canada) were each investigated as additives. The compositions of the formulae investigated can be found in Table 2.1.

To prepare a specimen, dry ingredients (slag, aggregate, and whatever additives) were weighed and added to a Nalgene mixing bottle. The bottle was then rotated at 28 rpm on a rotary mixer for approximately 5 minutes. Meanwhile, the activating solution was prepared, either by combining NaOH or Na_2CO_3 with water and mixing on a stir plate. Once dissolved, the soluble silicate was added to the NaOH solution. The mixed powders were placed in a container, combined with the activating solution, and mixed with a tabletop paint mixer for roughly 2 minutes. The resulting slurry was then poured into 5x10 cm cylindrical polypropylene sample molds (Jatco Industries, Union City, CA), sealed with plastic wrap, and allowed to cure under ambient conditions until testing.

After mechanical testing, broken specimens were placed in zipper-top bags, labeled, and put in storage in case they were needed for chemical testing.

Table 2.1 – Composition (g) of alkali-activated concretes investigated. Abbreviations: agg = limestone aggregate, DE = diatomaceous earth, sludge = acid rock treatment sludge. Samples with NaCl as a retardant contained 79g. Formulae with fly ash, metakaolin, and acid rock treatment sludge were scaled up to minimize waste per batch.

Formula	Slag	Agg.	Water	Water-glass	NaOH	Na_2CO_3	DE	Al_2O_3	Fly Ash	Meta-kaolin	Sludge
A	397	480	125	144	42	-	-	-	-	-	-
A+DE	397	480	175	144	42	-	50	-	-	-	-
A (Si:Al=1)	397	480	125	144	42	-	-	163	-	-	-
A (Si:Al=2)	397	480	125	144	42	-	-	61	-	-	-
A (Si:Al=4)	397	480	125	144	42	-	-	7	-	-	-
A+Fly Ash	450	600	196	180	52	-	-	-	50	-	-
A+ Metakaolin	450	600	196	180	52	-	-	-	-	50	-
A+Sludge	450	600	196	180	52	-	-	-	-	-	50
B	397	480	225	-	-	31	-	-	-	-	-
B+DE	397	480	225	-	-	31	32	-	-	-	-
B (Si:Al=1)	397	480	225	-	-	32	-	69.3	-	-	-
B (Si:Al=2)	397	480	225	-	-	32	-	12.2	-	-	-
B(Si:Al=4)	397	480	225	-	-	32	82	-	-	-	-
B+Fly Ash	450	600	281	-	-	39	-	-	50	-	-
B+ Metakaolin	450	600	281	-	-	39	-	-	-	50	-
B+Sludge	450	600	281	-	-	39	-	-	-	-	50

During the year spent in Morocco at the Université Hassan II in Casablanca, research was performed beginning with a number of reactants, including the ashes of oil shale from the Tarfaya and Temhedit fields (Office National de Recherche et d'Exploitation Pétrolière, ONAREP), runoff from a surface treatment plant, slag from a mining operation (Sefrioui SARL, Fes, Morocco), marble powder from a marble quarry south of Casablanca, clay from the Bizou region, and clay-heavy soil from the Tata region. Reactants (NaOH, sodium silicate solution, and Na_2CO_3) were obtained from

Société Cadilhac, Casablanca, Morocco. Saltwater was collected from the Atlantic Ocean on the southwestern city limits of Casablanca (1 km north-east of the marabout of Sidi Abderrahman.) Almost all of these materials were provided through the agency of Dr. Abderrahim Aatiq and Dr. Hassan Hannache.

To make samples, the reactant (oil shale, clay, etc.) were broken into smaller pieces with a hammer and then burned in a laboratory furnace at 750 ^{o}C for three hours in 3 kg batches. The ashes were removed and allowed to cool overnight, then ground by hand in a steel mortar and pestle. The resulting fine powder was then used to produce small exploratory specimens and, later, larger mortar specimens for mechanical testing. To make the exploratory specimens, 40 g of powder was combined with activator (either NaOH, Na_2CO_3, or waterglass solution) and hand-mixed with a steel spatula for ≈ 3 minutes. The resulting slurry was then poured into molds, sealed with plastic wrap, and cured at either 60 ^{o}C or room temperature for 24 h followed by 6 d of room temperature curing.

After one week, the specimens were inspected and those formulae that had hardened were marked for production of larger cement paste and mortar specimens. These specimens were produced in the same manner as the exploratory specimens, except that they were larger (70 g of ashes and 30 g fine sand as an aggregate.)

2.2 – Compressive and Tensile Splitting Strengths

After curing, samples were removed from their molds and mechanically tested on a load frame (Instron 5700, Norwood, MA) in accordance with the compression testing standard ASTM C39. Three samples were tested for each data point. For some formulae 3 other samples were tested according to the tensile splitting strength standard ASTM-

C496. Here, cylindrical samples are laid on their side, and the tensile splitting strength is determined through:

$$T = 2P/\pi lD \qquad \text{(eq. 6)}$$

where T is the tensile splitting strength (MPa), P is the maximum load in (N), and l and D are the length and diameter (mm) of the sample, respectively. For specimens produced in Morocco, compressive strength was tested on an MTS tester (Model 810, Minneapolis, MN) on 10 mm x 20 mm cylinders.

2.3 – X-Ray Diffraction (XRD)

XRD experiments were performed using a Siemens model D500 diffractometer (Karlsruhe, Germany.) All scans were performed on powdered samples that had been obtained by either a) drilling into bulk samples or b) removing and grinding portions of samples fractured during mechanical testing. The powders were placed on glass microscope slides onto which acetone was dripped. After the acetone dried, the sample was loosely affixed to the slide and placed in the diffractometer. Scan conditions were identical for all samples: a step size of 0.02^o and a dwell time of 0.5 s over the range of $10 – 90^o$ 2θ. Each scan took 50 minutes to complete. Data were smoothed in plotting software using a 5-point adjacent-averaging filter; as few peaks were detected in the $70 – 90^o$ 2θ range, the data was cropped and only the $10 – 70^o$ 2θ range was displayed. Peaks were identified according to the literature [44-57], a summary of which can be found in Table 2.2. In Morocco, samples were run on a Bruker AXS model D5 Advance (Madison, WI) using a step size 0.05^o and a dwell time of 0.5 s over the range of $5 – 60^o$ 2θ.

XRD experiments were carried out on cement pastes which contained no aggregate and the same amount of water as the concretes. Crystalline limestone aggregate in the concrete would have masked the peaks associated with poorly crystalline C-S-H and the minor mineral side products commonly reported for alkali activated slag cements (see below). Additionally, they would have masked the presence of $CaCO_3$ due to the recarbonation of the cement paste.

At no point in these studies, regardless of activating solution or additive, were any

Table 2.2– Mineral products in alkali activated slag cements determined by XRD as reported in the literature.

Name	Formula	Source
Calcite	$CaCO_3$	[44, 48, 49, 51, 52]
Vaterite	$CaCO_3$	[52]
Gaylussite	$Na_2Ca(CO_3)_2 \cdot 5H_2O$	[58]
Hydrotalcite	$Mg_6Al_2CO_3(OH)_{16} \cdot 4H_2O$	[47, 48, 51, 53, 54, 57]
C-S-H	var.	[44, 46-48, 52, 53, 55, 57, 59]
C_4AH_{13} or $(C,M)_4AH_{13}$	var.	[44, 48, 52, 57]
AFt	var.	[54]
Portlandite	$Ca(OH)_2$	[44, 51, 52]
Scawtite	$Ca_7(Si_6O_{l8})CO_3 \cdot H20$	[52]
Gehlenite	$Ca_2Al_2SiO_7$	[52]
Hibschite	$Ca_3Al_2(SiO_4)_2(OH)_3$	[52]
Hematite	Fe_2O_3	[48]
Merwinite	$Ca_3Mg(SiO_4)_2$	[48]
Xonotlite	$Ca_6Si_6O_{17}(OH)_2$	[59]
Strätlingite	$Ca_2Al_2SiO_6 \cdot 8H_2O$	[44]
Magnetite	Fe_3O_4	[49]
Maghemite	$\gamma\ Fe_2O_3$	[49]
Thermonatrite	$Na_2CO_3\text{-}H_2O$	[49]
Trona	$(Na_3)(CO_3)(HCO_3) \cdot H_2O$	[49]
Fayalite	Fe_2SiO_4	[49]
Hydroxysodalite	$Na_8Al_6Si_6O_{24}(OH)_2 \cdot (H_2O)_2$	[49]
Totally Amorphous	var.	2,8

zeolitic phases, sometimes reported with the production of 'geopolymers' found. Additionally, the presence of an amorphous hump centered around 30^{o} -2θ is sometimes mentioned as a hallmark of 'geopolymers.' As the raw slag used here also produces an amorphous hump at this position, it is more likely that the amorphous content comes from unreacted slag rather than the formation of 'geopolymers.'

2.4 – Fourier Transform Infrared Spectroscopy (FTIR)

FTIR experiments were carried out using a microspectrometer (Varian model Excalibur FTS 3000MX, Paolo Alto, CA) with a pellet-holding accessory. Scans were performed on powdered samples obtained by drilling into bulk samples. Specimens were made by mixing powdered samples with KBr in a mortar and pestle; the mixture was then compressed under 10 tons of force for 10 minutes to create a solid pellet. Scan conditions were identical for all samples: 4 cm^{-1} resolution and 128 scans run in transmission mode. After addition of a purge-gas generator to the system, the generator was run for 10 minutes before scans were initiated. In Morocco, samples were run under similar conditions on a spectrometer (Bruker Vertex 70, Madison, WI) at the Laboratoire de Spectroscopie Infrarouge, Département de Chimie, Faculté des Sciences in Rabat. When smoothing of data was required, a 5-point adjacent averaging filter was used in the plotting software. Peak identification was based on the literature; a summary of this literature can be found in Table 3.2 below.

FTIR experiments were carried out on cement pastes which contained no aggregate and the same amount of water as the concretes in order to remove peaks due to limestone aggregate, simplify peak identification, and to avoid masking peaks due to $CaCO_3$ from recarbonation.

2.5 – Thermogravimetric Analysis (TGA)

TGA experiments (PerkinElmer TGA-7, Waltham, MA) were conducted on some formulae using 19±1 mg of powder in a Pt crucible heated at 10 ^{o}C/min over the range of 50 – 800 ^{o}C. Powder was obtained by crushing specimens in a mortar and pestle. Peaks were identified according to the literature [60-64], a summary of which can be found in Table 2.4. TGA experiments were carried out on cement pastes which contained no aggregate and the same amount of water as the concretes in order to avoid masking signals due to $CaCO_3$ from recarbonation.

2.6 – Scanning Electron Microscopy (SEM)

SEM experiments were conducted on a Zeiss Model Supra 50 VP (Thornwood, NY.) Samples were mounted in epoxy (occasionally bakelite, which was avoided as it must be processed at relatively high temperatures) and ground. Samples were then polished with 3 and 1 μm diamond polishing solution, and coated with Pt/Pd using a sputter coater (Cressington Scientific 208HR, Watford, England). Fracture surface specimens obtained from samples fractured during mechanical testing were affixed to Al sample stubs with carbon tape and also sputter coated. A variety of accelerating voltages, aperture sizes, and working distances were used.

Table 2.3– Location (^{o}C), and origin, of peaks in TGA, according to the literature.

Unbound H_2O	Gypsum Dehydration	C-S-H Dehydration	$Ca(OH)_2$ Dehydroxylation	$CaCO_3$ Decarbonation	Source
<120	160-186	95-120	350-550	600-900	[60]
-	-	70-400	450	600-700	[65]
130	-	225	500	825	[66]
<105	110-170	180-300	450-550	700-900	[63]
<120	-	110-400	400-490	680-800	[64]
<120	-	200-600	-	>600	[61]
<105	120-163	250-350	450-550	600-800	[62]

2.7 – Backscatter Electron (BSE) Image Analysis

Image analysis was used to determine the quantity of unreacted slag in some formulations. Ten BSE images were obtained under identical conditions (300 x magnification, 20 keV accelerating voltaged, 30 μm aperture.) Each image was then processed using the ImageJ software developed by the National Institutes of Health (Bethesda, MD.) The BSE images, in which unreacted slag appeared light gray and the cementing phase appeared dark gray, were turned into binary (black and white) images. The "Analyze Particles" technique was then used to count the number of black (unreacted slag) particles, as well as the dimensions of each particle and the overall percentage of the image displaying those particles.

2.8 – Energy Dispersive Spectroscopy (EDS)

Energy Dispersive Spectroscopy experiments (Oxford Inca X-Sight, Oxfordshire, UK), were performed on all formulae to determine elemental compositions. All elemental analyses were performed on specimens being examined by SEM as described above. A variety of accelerating voltages, aperture sizes, and working distances were used, but generally were not below 15 keV accelerating voltage, not below 60 μm aperture, and not more than ±3 mm from a working distance of 15 mm.

2.9 – Radiocarbon Dating

In the course of the investigation of samples from the pyramids in Egypt, it was speculated that they may have been made of a cement-like material containing lime (CaO.) For this reason, samples were sent for radiocarbon dating (CO_2 from the atmosphere is absorbed by the material, enabling accurate carbon dating; for a more complete discussion, see Ch. 4.) All radiocarbon dating was performed by Beta Analytic

of Miami, FL using accelerator mass spectrometry (AMS.) All samples were in bulk form and roughly 1 cm^3 in size. According to the laboratory that carried out the work, in all cases, they had more than enough material to carry out an accurate measurement. Acid washing was used to remove any layer of contamination due to exposure to the elements.

2.10 – Characterization of Raw Materials

2.10.1 – Slag

Water-quenched, ground granulated blast furnace slag was used as the main reactant in the cements produced here. The composition of the slag as determined by XRF was provided by the manufacturer and verified using EDS. The two compositions were in close agreement and (see Table 2.5). When observed in the SEM, the slag appeared as blocky particles roughly 5 μm wide. XRD diffractograms of the raw slag (Fig. 2.1) showed only a broad amorphous hump, centered at roughly 30^o-2θ, due to the short-range order in the glassy CaO-MgO-Al_2O_3-SiO_2 structures within the slag. No crystalline phases were detected.

Table 2.4 – Composition of initial reactants, as determined by EDS, with the exception of XRF data for slag (column 1) as provided by distributor.

	Slag (XRF)	Slag (EDS)	Diat. Earth	Al2O3	NaCl	Fly Ash	Metakaolin	Sludge
CaO	42.1	44.8	-	-	-	1.7	-	6.7
SiO_2	34.6	36.7	89	-	-	61.1	55	20.7
Al_2O_3	11.7	12	4	100	-	27.5	40	28.2
Fe_2O_3	-	0.4	1.7	-	-	4.5	1	21.9
MgO	6.6	6.6	0.6	-	-	<1	<1	5.5
MnO	-	-	-	-	-	-	-	4.8
TiO_2	0.8	-	-	-	-	-	<1	-
K_2O	0.2	-	0.5	-	-	<1	<1	-
SO_3^{2-}	1.1	-	-	-	-	<1	-	11.1
Other	2.9	3.3	4.2	0	100	3	1	1.1

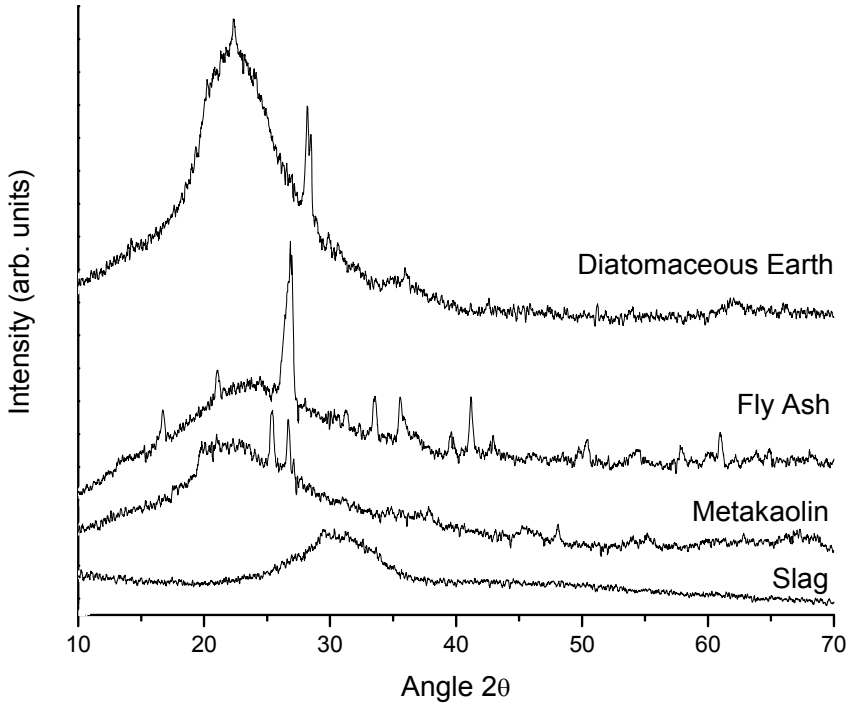

Figure 2.1 – XRD diffractograms of raw materials used in the making of AAS cement and concrete. Featureless diffractogram of acid rock treatment sludge not shown.

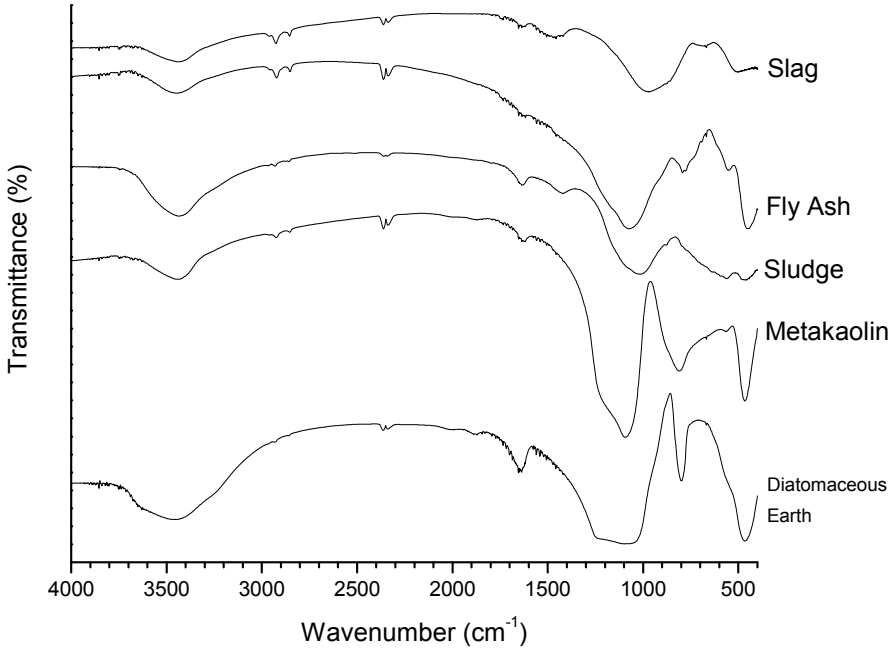

Figure 2.2 – FTIR spectra of raw materials used in the making of AAS cement and concrete.

The FTIR spectrum of unadulterated slag (Fig. 2.2) shows three main peaks. The first, a broad peak centered around 3400 cm^{-1}, together with a smaller peak around 1630 cm^{-1}, represent the –OH stretching vibrations of water; the second, a broad peak with a possible shoulder on the right centered around 968 cm^{-1}, represents Si-O and Al-O stretching; the final peak, centered around 500 cm^{-1}, represents Si-O-Si and O-Si-O bending. A number of other minor peaks are present, but are not well defined enough to be certainly identified.

2.10.2 Diatomaceous Earth

Diatomaceous earth was used as an additive to the cement in the hopes of boosting the quantity of Si present with which to form C-S-H. Diatomaceous earth is essentially the Si-rich skeletons of plankton; in the SEM these skeletons were observed as complex, varied shapes. The majority appeared in the form of barrels with evenly spaced rings of evenly spaced holes; each of these holes had a five-sided bridge structure inside. Many of these barrels showed a seam in the center, which looked as though two barrels had been stitched together. The median length was approximately 10 μm. Other diatoms appeared as flat leaves with more or less elaborate vein-like structures. EDS analysis showed the bulk of the diatomaceous earth to be made up of SiO_2; results can be found in Table 2.2.

The XRD diffractogram of diatomaceous earth (Fig. 2.1) showed an amorphous hump, smaller than that of the slag, centered at 23^{o}-2θ; a few minor peaks around 28^{o}-2θ could not be identified. During microscopy occasional grains of an aluminosilicate-rich impurity, likely a clay, were observed.

The FTIR spectrum of diatomaceous earth (Fig. 2.2) contains mainly peaks representing water (3400 cm^{-1} and 1640 cm^{-1}), a broad peak centered around 980, a sharper peak at 750, and a peak at 500 cm^{-1}. This group of peaks represents the presence of Si-O bonds, being indicative of Si-O stretching, O-Si-O stretching, and Si-O bending, respectively.

2.10.3 Fly Ash

Fly ash, a common additive to OPC, was investigated here as an additive. The waste product of coal burning, fly ash was observed in the SEM to consist of microscopic spheres, many of which were hollow and many of which were broken. These spheres were approximately 5 μm in diameter. EDS analysis (Table 2.2) on the raw fly ash showed it to be a predominantly aluminosilicate material (61.1 wt.% SiO_2 and 27.5 wt.% Al_2O_3) with a slight iron impurity.

The XRD diffractogram of raw fly ash (Fig. 2.1) after calcination at 750 ^oC for 2 h contains an amorphous hump, but not as broad as the one seen in the diffractogram of the raw slag, centered around 22^o-2θ. A sharp peak at 27^o-2θ, due to the presence of quartz, is present, as well as a number of other peaks all of which correspond with mullite, a common aluminosilicate mineral.

The FTIR spectrum of fly ash (Fig. 2.2) again shows the broad peaks around 3400 cm^{-1} and 1640 cm^{-1} indicative of water; a broad peak centered around 1100 cm^{-1} which could indicate a range of aluminosilicate bonding (Si-O, O-Si-O, Al-O, etc.); a weak, broad peak at 792 cm^{-1} likely to indicate Si-O or Al-O stretching vibrations, a weak peak at 560 cm^{-1} of unclear origins; and a broad peak at 451 cm^{-1} which indicates Si-O bending vibrations. A pair of minor peaks near 2920 cm^{-1} are a harmonic due to the carbon atom

in calcite, while the minor double peak at 2350 cm^{-1} is an artifact due to differing levels of CO_2 in the chamber during the scan compared to when the background scan was taken. This information paints an overall picture of an aluminosilicate material, in agreement with the EDS analysis.

2.10.4 Metakaolin

Metakaolin, a naturally occurring clay and another common additive to OPC, was used here as an additive. In the SEM, metakaolin was observed to take the form of roughly rectangular particles about 5 μm in length. EDS analysis (Table 2.2) showed it to be primarily aluminosilicate (55 wt.% SiO_2, 40 wt.% Al_2O_3), similar to the fly ash.

The XRD diffractogram of raw metakaolin (after 2 h of calcination at 750 ^oC; Fig. 2.1) contained an amorphous hump centered at 25^o-2θ, though slightly less broad than the amorphous hump of raw slag. Aside from that, the only two features are a sharp peak at 27^o-2θ, due to the presence of quartz, and a sharp peak at 25^o-2θ, due to the presence of anhydrite ($CaSO_4$.)

The FTIR spectrum of metakaolin (Fig. 2.2) contains four distinct regions. The peaks at 3400 cm^{-1} and 1640 cm^{-1} indicate water; the deep, broad peak with a probable left side shoulder, running from about 1000 cm^{-1} to 1250 cm^{-1}, indicates the stretching of a variety of bonds of the Si-O, O-Si-O, Al-O, etc. type; a broad peak centered around 850 cm^{-1} indicates Si-O and Al-O stretching; and, finally, the peak around 460 cm^{-1} indicates Si-O-Si, Al-O-Si, and O-Si-O bending. Again, the pair of minor peaks near 2920 cm^{-1} are due to the calcite harmonic, while the minor double peak at 2350 cm^{-1} is an artifact due to CO_2.

2.10.5 Acid Rock Treatment Sludge

Acid rock treatment sludge from the Halifax International Airport was investigated as a component of the alkali activated slag cements here reported. A sticky, foul-smelling brown solid, it was investigated not so much as an additive, but to see if cement would be a good place to dispose of it. After either drying at 200 ^{o}C or750 ^{o}C, the material became a light brown powder that could now be crushed by hand in a mortar and pestle.

In the SEM, the dried sludge took the form of a fine powder with, particle sizes no larger than 5 μm, and in backscatter imaging mode, it appeared quite bright due to its high iron content. EDS analysis (Table 2.2) showed it to contain an aluminosilicate portion (20.7 wt.% SiO_2 and 28.2 wt.% Al_2O_3) as well as some CaO content (6.7 wt.%), but the main components were Fe_2O_3 (21.9 wt.%) and SO_3^{2-} (11.1 wt.%, surely as a compound with some other element.) While S is known to prevent flash setting in OPC, iron is known to cause problems in the formation of geopolymers.

The XRD diffractogram of the sludge dried at room temperature, 200 ^{o}C, and 750 ^{o}C were completely featureless (not shown), indicating no crystalline or semi-crystalline components. In addition to the presence of water, the FTIR diffractogram (Fig. 2.2) of the sludge indicates only the presence of O-Si-O bending at 460 cm^{-1} and various forms of aluminosilicate stretching with a broad, shallow peak at about 1050 cm^{-1}.

2.10.6 Moroccan Materials

Raw materials in Morocco were analyzed by XRD, FTIR, and XRF. Characterization of these materials is discussed in Appendix A as part of a discussion on why the materials did produce viable materials.

CHAPTER 3: MECHANICAL AND MICROSTRUCTURAL CHARACTERIZATION OF AAS CEMENTS

3.1 – Basic NaOH/waterglass Formula

This formula was one of the two initial benchmarks against which all other formulae with additives were compared. However, for every set of experiments, a new batch of samples was produced and their compressive strengths measured in order to ensure fair comparisons. For this reason the strength of the basic formula varies somewhat from section to section. NaOH was selected to provide a high pH and thus faster dissolution of slag; waterglass was used as a source of reactive Si to increase C-S-H production.

3.1.1 – Mechanical Properties (Fine Aggregate Concrete)

The NaOH/waterglass formula was originally tested by grinding the ends of the samples to ensure parallelism. Tested in this manner, the samples had good early strengths of 44 ± 6 MPa at 1 day, 44 ± 9 MPa after 7 d, and increasing slightly to 46 ± 5 MPa after a full 28 d (Fig. 3.1.)

This formula was later produced and tested using steel caps with rubber inserts to ensure parallelism between the top and bottom surfaces; the results showed a significant strength increase from 73 ± 2 MPa at 1 day, 81 ± 1 MPa after 7 d, and 103 ± 2 MPa after 28 d. This represents not just a jump in strength, but a substantial lowering of the standard deviation of the data. After this was observed, it was determined that grinding was insufficient for ensuring parallelism in high-strength samples, and the steel cap method was afterwards used exclusively.

These results are higher than those reported by Puertas *et al*. [67] for a similar slag activated by 10M or 2M NaOH at room temperature (~ 50 MPa at 28 d), by Palacios *et al.* [68] for a slag activated solely by waterglass (~ 65 MPa at 28 d), and by Cheng *et al.* [69] for a 'geopolymer' produced from slag activated by either KOH or waterglass (~ 70 MPa at 28 d); these results are at the high end of the range reported by Brough *et al*. [45] for slags of varying fineness (~ 60 – 100 MPa at 28 d); and roughly the same as reported by Wang *et al*. [57] for a slag of similar composition activated by waterglass (~ 98 MPa at 28 d, though this strength increased to ~ 110 MPa with finer grinding of the slag, and to ~ 117 MPa when cured for 24 h at 80 ^{o}C.) The strengths reported here are also at the high end of the range reported by Komnitsas *et al.* in a recent review [34] of 'geopolymers' in general (70-100 MPa is reported as a range for the final strengths of 'geopolymers,' depending on activator, curing time, etc.)

The overall higher strengths of the formula reported here can most likely be attributed to the mixture of NaOH and waterglass in the activator. NaOH provides a sufficiently high pH to rapidly dissolve slag, while the large amount of waterglass provides sufficient soluble Si to ensure both rapid formation of C-S-H and an amorphous Si gel to ensure a dense microstructure (as discussed below.) As shown by Wang *et al*., other factors, especially fineness of the slag and variations in temperature, can have a pronounced effect, which are the most likely sources for the range of strengths reported in the literature. It should be noted, however that the formula reported here was developed solely for strength; other, weaker formulae in the literature may perform better in a variety of other ways (shrinkage, acid resistance, cost, etc.)

The tensile splitting strengths of NaOH/waterglass activated samples were determined in accordance with ASTM standard C496 are listed in Table 3.1. Over the first 28 d of curing, the tensile splitting strength increases slightly, from 2.6 ± 0.2 MPa to 4.2 ± 0.6 MPa (tensile strength is determined with the cylinder in a horizontal position; thus caps were not used, as with compressive strength testing.)

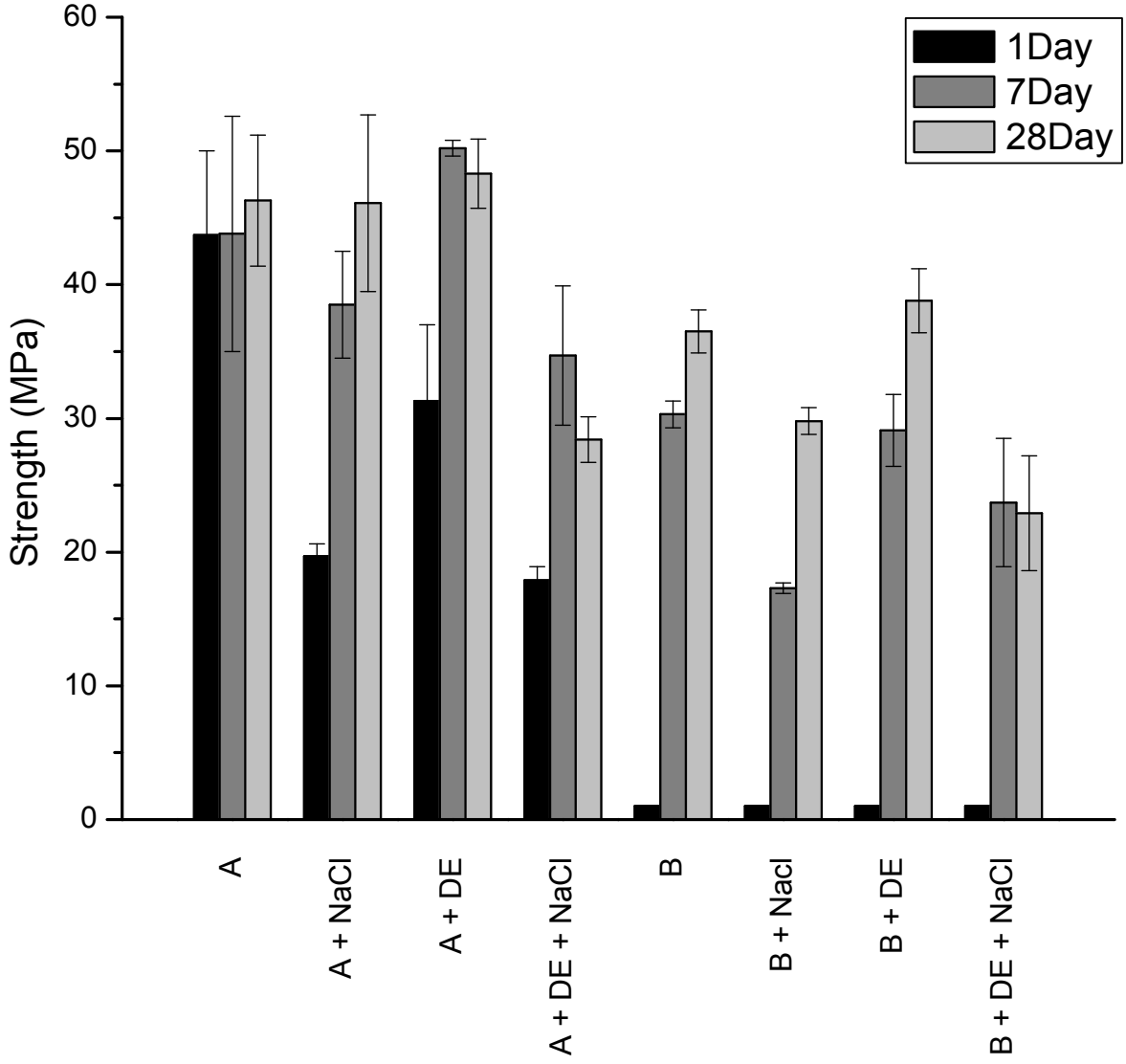

Figure 3.1 – Compressive strength of formulae activated by NaOH/waterglass (formula A) or Na_2CO_3 (formula B) with and without NaCl, diatomaceous earth (DE), or both, without steel caps.

3.1.2 – XRD (Cement Paste)

XRD diffractograms of the basic NaOH/waterglass activated formula were taken after 7, 28, or 55 d and after 20 months of curing (Fig. 3.2a) This formula changed little over these time periods: the main feature was a wide amorphous hump due to unreacted slag between roughly 25^{o} and 35^{o}-2θ and a wide, but generally well defined, peak at approximately 30^{o}-2θ. This broad peak (the (100) reflection), and much weaker peaks that may be present at approximately 50^{o} and 55^{o}-2θ (the (020) and (310) reflections) are indicative of poorly crystalline C-S-H. Identification of further peaks related to C-S-H is hampered by the presence of the amorphous hump from the slag, as well as the general low degree of crystallization in the C-S-H. The position of the main peak, at 30^{o}-2θ, is also the position of the main peak of $CaCO_3$, however, the lack of secondary peaks due to $CaCO_3$ rule out its presence, as does the width of the peak, which indicates the poorly crystalline nature of the C-S-H.

Over the period between 55 d and 20 months the intensity of the C-S-H peak appears to decrease, possibly indicating that it is becoming less crystalline over time; however, as an internal standard such as Si was not used, this is not clear. It is also possible that these differences are due to plotting issues or differences in scan settings, though these appear not to be the cause.

These diffractograms are similar to those produced by Wang *et al.* [56] for a similar slag activated by a 4M NaOH solution (Fig. 3.2b). Their interpretation of the

Table 3.1 – Tensile splitting strength of NaOH-activated formulae, with diatomaceous earth (DE), NaCl, and Al_2O_3 (Si:Al ratios of 1, 2, or 4), and combinations thereof, as additives.

Formula	1 Day (MPa)	7 Days (MPa)	28 Days (MPa)
A	2.6 ± 0.2	3.1 ± 0.2	4.2 ± 0.6
A + DE	2.7 ± 0.5	3.0 ± 0.4	2.3 ± 0.5
A + NaCl	1.7 ± 0.2	2.5 ± 0.2	3.5 ± 0.6
A + DE + NaCl	1.8 ± 0.5	2.4 ± 0.4	2.4 ± 0.5
A - Si:Al =1	3.4 ± 1.1	3.2 ± 0.5	2.7 ± 0.2
A - Si:Al = 2	2.3 ± 0.9	3.6 ± 1.3	3.9 ± 0.3
A - Si:Al = 4	2.2 ± 0.4	4.0 ± 1.0	2.8 ± 0.4
A + NaCl - Si:Al =1	2.3 ± 1.0	2.2 ± 0.8	2.2 ± 0.3
A + NaCl - Si:Al = 2	1.4 ± 0.5	3.5 ± 0.8	2.3 ± 0.8
A + NaCl - Si:Al = 4	1.2 ± 0.3	2.0 ± 0.2	2.6 ± 0.5

main peak near 30^o-2θ is complimented by DTA and EDS analyses. It should be noted that while they identify hydrotalcite as a reaction product, it is not seen in the NaOH/waterglass formula reported here; however, it is present in diffractograms of the Na_2CO_3-activated formulae reported below. More recently, Mozgawa *et al.* [70] reported similar diffractograms for a slag activated by waterglass (Fig. 3.2c.) It should be noted that Mozgawa *et al.* refers to the final products as 'geopolymers' despite the fact that only C-S-H and possibly Si-rich gel are observed. In fact, the existence of 3D, alkali-balanced zeolite-like materials as described by Davidovits [31] are specifically ruled out. The identification of the only peak, again at roughly 30^o-2θ, is supported by FTIR and NMR studies. Other researchers have identified this peak as C-S-H as done here, most notably Escalante-García *et al*. [48] (confirmed by EDS); Fernández-Jiménez [71], in a study on slags activated by NaOH, waterglass, or Na_2CO_3, (confirmed by NMR and TEM; hydrotalcite, some carbo-aluminates, the mineral gaylussite were also detected, as well as calcite at later ages); Duda [72], who observed C-S-H in slags activated by NaOH or water (confirmed by EDS and TGA); Rajaokarivony-Andriambololona *et al*. [52], who

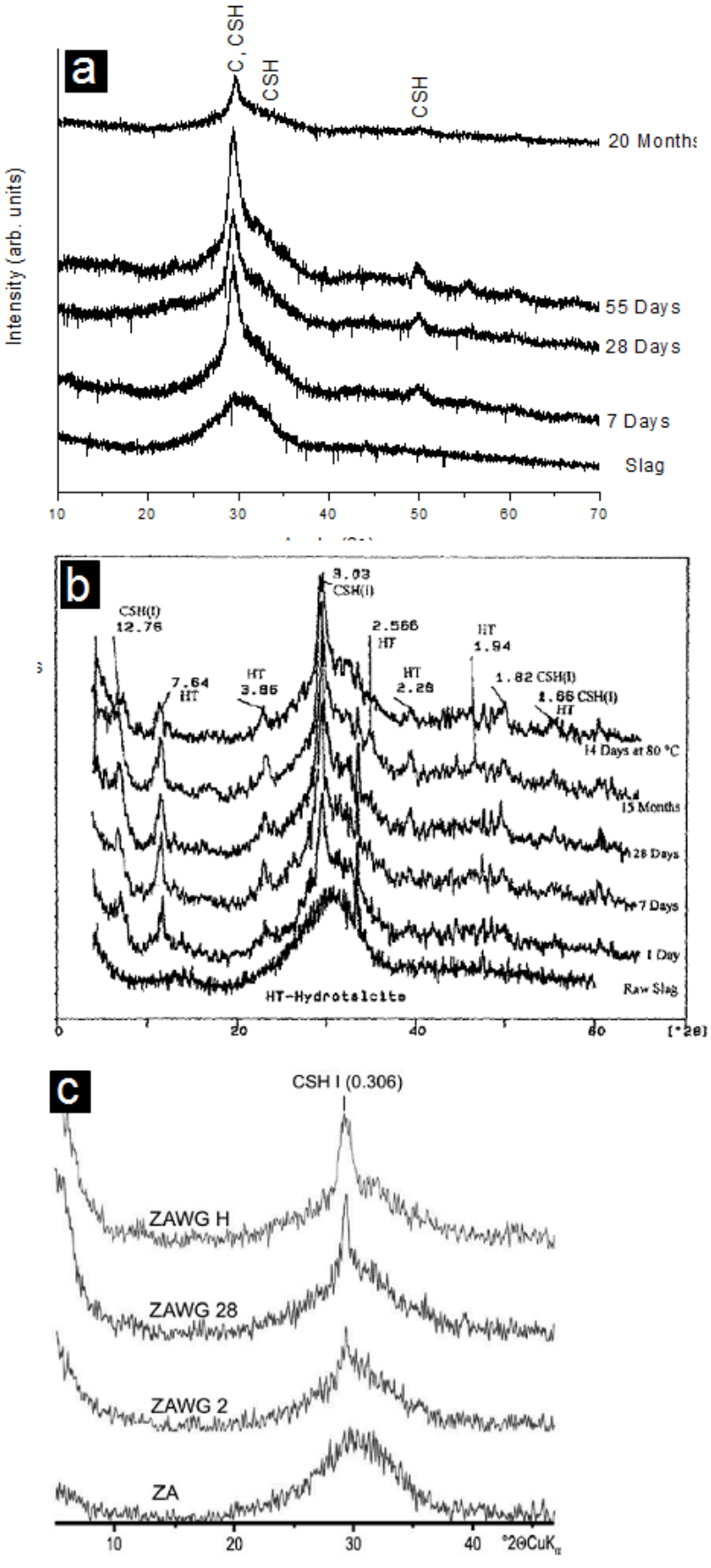
a
C, CSH
CSH
CSH
20 Months
55 Days
28 Days
7 Days
Slag
Intensity (arb. units)
10
20
30
40
50
60
70
b
3.03
CSH(I)
CSH(I)
12.76
7.64
HT
HT
3.86
2.566
HT
HT
1.94
HT
2.28
1.82 CSH(I)
1.66 CSH(I)
HT
14 Days at 80 °C
15 Months
28 Days
7 Days
1 Day
Raw Slag
HT-Hydrotalcite
0
20
40
60
[°2θ]
c
CSH I (0.306)
ZAWG H
ZAWG 28
ZAWG 2
ZA
10
20
30
40
°2ΘCuK$_\alpha$

Figure 3.2 – (Overleaf) a) XRD diffractograms of the basic NaOH/waterglass activated formula after 7, 28, 55 d and 20 months. Diffractogram of raw slag (bottom) provided for comparison. b) Similar XRD diffractograms of slag activated by NaOH between 1 d and 15 months after Wang *et al*. [56]. c) XRD diffractograms of 'geopolymers' produced by the alkali activation of slag (bottom) by waterglass at 2 d, 28 d, and after 'hydrothermal treatment' (ZAWG2, ZAWG28, and ZAWGH, respectively), from Mozgawa *et al.* [70]. Diffraction angle is from 5 to 50. C = Calcite, CSH = Calcium silicate hydrate (C-S-H), HT = Hydrotalcite.

report C-S-H as well as a number of silico-carbonates and calcite/vaterite in artificial slags activated by NaOH or KOH (confirmed by EDS, TEM, and XPS); and Schneider *et al.* [55], who report C-S-H in slags activated by waterglass, NaOH, or $Ca(OH)_2$ (confirmed by NMR.)

On the other hand, Lecomte *et al.* [50] ignore a peak at 30^o-2θ in the diffractogram of a slag activated by potassium silicate (i.e. potassium-based waterglass) and conclude their AAS cement to be totally amorphous. As the peak is so weak, and broad, its existence is essentially in the eye of the beholder. By FTIR and NMR, however, they confirm the existence of C-S-H. Puertas *et al*. [67] do not show their diffractogram, but report $CaCO_3$ to be the only crystalline phase present in a slag activated by NaOH at different concentrations and cured at various temperatures. A later paper by Puertas *et al.* [51] reports $CaCO_3$ and hydrotalcite to be the only products of a slag/fly ash blend activated by NaOH; however, in both cases it is known that C-S-H and $CaCO_3$ both produce a peak at 30^o-2θ; it is possible that the $CaCO_3$ peak simply overwhelms that of C-S-H, whose existence was confirmed by FTIR and NMR. A similar problem with the intensity of the $CaCO_3$ peak hiding a possible C-S-H peak was reported by Pan *et al*. [73] who did not observe C-S-H in slag/red mud mixtures activated by waterglass, but confirmed C-S-H through use of FTIR, TGA, and EDS. Finally, Brough

et al. [45] report that their (not shown) XRD diffractograms of KOH- or waterglass-activated slag are totally featureless; the presence of C-S-H, however, is proven by the complimentary use of calorimetry, EDS, and NMR.

Due to the evidence in the literature, in which C-S-H is repeatedly identified and confirmed with complimentary techniques, the interpretation of the poorly defined peak at 30^{o}-2θ as indicative of C-S-H is preferred, as the broadness of the peak suggests poorly crystalline material, thus ruling out $CaCO_3$, the only reasonable alternative. Additionally, none of the secondary peaks related to $CaCO_3$ are in evidence. Further, at least one secondary C-S-H peak can be observed. In general, it is noted that while XRD can be used to prove the existence of C-S-H, complimenting XRD evidence with other techniques (see below) is preferred. Finally, XRD cannot be used to rule out the presence of C-S-H (which may be either amorphous, as shown by Lecomte and Brough, or disguised by the $CaCO_3$ peak, as shown by Puertas and Pan.)

3.1.3 – FTIR (Cement Paste)

A brief summary of the most common cement/'geopolymer' related peaks identified in the literature can be found in Table 3.2. This table was compiled from the work of Yu *et al*. [74], who report spectra for C-S-H in OPC; Mozgawa *et al*. [70], who report spectra of alkali-activated slag 'geopolymers'; Barbosa *et al*. [75], who report spectra of Na-polysialate 'geopolymers'; the theses of Ichcho [76] and Oumam [77], who report spectra for materials made of shale oil and other natural minerals; García Lodiero *et al*. [78], who report the effect of alkali on fresh C-S-H; Farcas and Touzé [79], who provide exhaustive spectra of OPC, cement additives, and cement-related products; Varas *et al*. [80], using FTIR to identify 'natural cements,' the forerunner of OPC; Delgado

Table 3.2 - FTIR Peak locations as identified by the literature.

Location (cm^{-1})	Origin
3650	Hydrated Minerals (i.e. $Ca(OH)_2$)
3600-3100	S-O (Gypsum)
3400	OH Stretching (H_2O)
2930, 2850	Calcite Harmonic
	S-O (Gypsum)
1650	H-O-H Bending (H_2O)
1430	C-O Asymmetric Stretching
	S-O (Gypsum)
1100	Si-O-Si and Al-O-Si Asymmetric Stretching
1035-1030	'aluminosilicate bonding'
1010-1000	Calcium Silicates
960-800	Si-O, Al-O Stretching
872	C-O Bending
480	Si-O-Si and O-Si-O Bending

et al. [81], who report efficacy of various spectroscopic techniques for use with OPC, and Gao *et al.* [82] who report IR results for OPC with different stress histories. It should be noted that there is unanimous agreement by these authors as to the identification of the various peak locations and the general meaning of trends in FTIR (i.e. shifts in peak position, etc.) despite reporting on a disparate group of materials.

The FTIR spectrum of the NaOH/waterglass activated formula (Fig. 3.3a) contains a broad, deep peak stretching from roughly 3750 cm^{-1} to 3000 cm^{-1} that is indicative, along with the peak at roughly 1660 cm^{-1}, of the stretching and bending, respectively, of -OH bonds in water. The stretching peak could also be hiding the presence of peaks due to other OH-bearing minerals, such as portlandite ($Ca(OH)_2$), however, since no such minerals appeared in the XRD spectra, this is unlikely. A peak at 1410 cm^{-1} is due to the bonding in CO_3^{2-} ions, indicating the presence of some sort of carbonated mineral, possibly due to absorption of CO_2 from the atmosphere. Broad peaks at 960 cm^{-1} indicate the Si-O, O-Si-O, etc., stretching vibrations of silica tetrahedra of

various coordination states. The peak at 470 cm^{-1} is due to Si-O and Al-O bending vibrations.

A slight peak is present around 700 cm^{-1}, the origin of which is unclear. This peak is so weak as to be essentially negligible, however. A final peak corresponding to out of plane Si-O bending is centered around 530 cm^{-1}. The double peak appearing around 2300 cm^{-1} is an artifact of the machine, produced because more CO_2 was present during collection of the spectra than had been present during collection of the background scan.

Recent work by Lecomte *et al*. [50] provides a comparison between OPC, alkali-activated slag, a metakaolin 'geopolymer,' and a 'geopolymer'/alkali activated slag mixture. (The alkali activator, in this case, was potassium silicate.) The spectra (Fig. 3.3b) show the same peaks as observed here. Further, the four different materials are all relatively similar; peak positions have shifted slightly, and the peaks of OPC are generally less broad, indicating superior crystallinity. The peaks related to Si bonds are also much deeper, due to the Si in the potassium silicate taking on a wide variety of bonds; it also hints at the presence of the amorphous Si gel associated with the use of waterglass. When combined with NMR results, Lecomte concluded that the FTIR spectra were indicative of C-S-H with a more highly polymerized Si-rich region, more analogous to the products of OPC than to 'geopolymers' (except, of course, in the case of the Ca-free 'geopolymer' sample.)

Mozgawa *et al*. [70] reported spectra of 'geopolymers' produced by the activation of slag by either NaOH or Na_2CO_3 (Fig. 3.3c; the data are presented in absorption, rather than transmission, so are essentially 'upside down' to the data presented here.) These

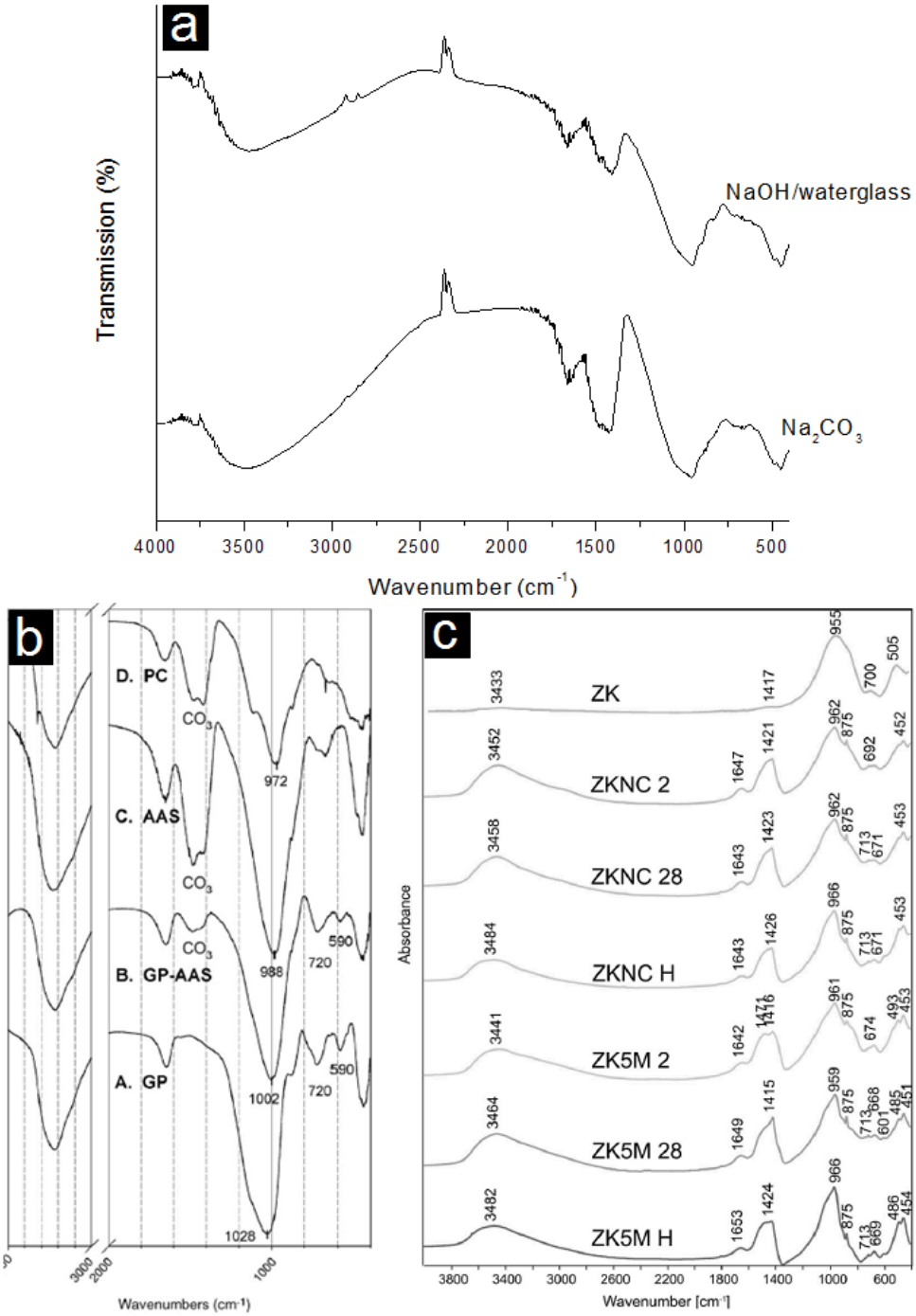

Figure 3.3 – a) FTIR spectra of basic NaOH/waterglass-activated (top) and Na_2CO_3-activated (bottom) cements at 7 d. b) FTIR spectra of OPC and alkali activated slag (AAS), slag/metakaolin mix (GP-AAS), and metakaolin (GP) activated by potassium silicate by Lecomte *et al*. [50], and c) FTIR spectra of raw slag (top), slag activated by 5M NaOH (ZK5M-2, -28 and –H for samples at 2 d, 28 d, and after hydrothermal treatment), and by Na_2CO_3 (ZKNC-2, -28, and –H as above) by Mozgawa *et al*. [70]. This data is displayed by absorbance, essentially an upside-down version of a) and b).

spectra contain the same general peaks, for the same reasons, although peak intensity and exact position have changed slightly. Combined with XRD and NMR, Mozgawa et al. conclude that the FTIR spectra are indicative of C-S-H.

In a study on the effect of salt contamination on 'geopolymers' produced from fly ash/metakaolin activated by sodium and potassium silicates, Lee *et al*. [83] reported spectra with similar peaks, though the Si-O peak at 900 – 1000 cm^{-1} was substantially broader. Criado *et al.* [84] provide a detailed analysis of the FTIR spectra of 'geopolymers' produced of fly ash activated by NaOH/waterglass, as does Panias *et al.* [85], Bakharev [86], and Álvarez-Ayuso (NaOH only) [87]. All of these spectra contain the same peaks, with slight differences in location and intensity. The same can be said of materials made from the alkali activation of slag/red mud blends [73], slag/OPC blends [27], OPC [78, 79, 81], and aged OPC pastes going back to their introduction in Europe at the beginning of the 20th century, as observed by Varas et al. [80].

Rees *et al.* [88] and Ŝkvára *et al.* [89] report data for fly ash 'geopolymers' activated by NaOH or waterglass, the spectra of which seem similar to those presented here, however, they performed detailed analysis of only the most important peaks, and the overall spectra are not shown. Finally, Phair *et al.* [90] investigated fly ash activated by waterglass, with the addition of slag, OPC, or metakaolin, and produced spectra with the same general peak positions.

These spectra are also similar to those obtained by Miller *et al.* [91] in a study combining hydraulic lime with DE. In that study, XRD identified C-S-H as the main phase produced; the FTIR spectra show some differences in width due to larger amounts of DE, and thus a larger variety of Si-O bonds, but the main peaks are in the same general

locations. The only difference was the presence of a highly crystalline -OH peak identified as $Ca(OH)_2$, in accordance with their XRD results. This highly crystalline -OH peak, at 3640 cm^{-1}, is more thoroughly described in a review of the use of FTIR in the characterization of cements by Farcas *et al*. [79] who also report spectra for clinkers, hydrated OPC, additives, and many other materials related to cements. The spectrum reported for OPC is, as above, similar to the ones reported here.

Taking all of this into account, it can be seen that FTIR alone should not be used for identifying final products: as geopolymers, OPC, and AAS cements contain Si-O and Al-O bonds, as well as hydroxides and carbonates, and therefore the general shape of the spectra are quite similar. However, FTIR still has some value, as some reactions, such as recarbonation or the continuing polymerization of the Si-rich gel in C-S-H, can be monitored over time. Recarbonation is observed simply by the existence of sharp, crystalline peaks around 875 and 710 cm^{-1}. The ability to observe continuing reactions has been described by Yu *et al*. [74] in C-S-H, and by Puertas *et al*. in slag/fly ash mixtures [51]; this ability is essentially provided by the ability of FTIR to describe not just the types of bonds, but their environments. The peak occurring around 1000 cm^{-1} due to Si-O bonds, for example, will shift to higher wavenumbers as the environment of the Si-O bonds becomes more ordered. That is to say, as the Si-rich gel portion of C-S-H becomes more highly polymerized, or the gel becomes more highly cross-linked, a shift in the position of the peak will be observed. Also, according to Mozgawa *et al*. the peak around 500 cm^{-1} due to Si-O and Al-O bonds will shift to lower wavenumbers for the same reason, or because Al is substituting for Si.

For the NaOH/waterglass formula reported here, however, the FTIR spectra after 20 months of curing showed minor differences. The peaks at 960 cm^{-1} shifted to slightly higher wavenumbers, while the peaks at 470 cm^{-1} shifted slightly lower. Though a manner by which these changes could be quantified remains elusive, it is a clear indicator that reactions are continuing, as Si (and possibly Al) enter more 'ordered' systems.

When compared to the raw materials (Fig 2.2), the spectra of both the NaOH/waterglass and Na_2CO_3-activated formulae (discussed below) show significant differences at two points: the appearance of the peak at 1420 cm^{-1}, and the shifting of the peak at 950 cm^{-1} from higher wavenumbers (1100 cm^{-1}), which is known to indicate effects due to structural changes in the Si-O environment; in this case the incorporation of isolated tetrahedra into larger, more ordered (relatively speaking) molecules of C-S-H or an Si-rich gel produced by excess Si in the waterglass.

3.1.4 – SEM (Cement Paste, Fine Aggregate Concrete)

Several distinct constituents of the cement or concretes were easily identifiable in the SEM (Fig. 3.4.) These include unreacted slag; an outer product (Op), essentially the cementing phase, which likely contains low-density C-S-H, mineral side products, and alkali ions from the activator; a transition zone called the inner product (Ip; sometimes called Inner Transition Zone, or ITZ), which, when observed, appears as a white ring of approximately 2 μm thickness around particles of unreacted slag in BSE mode with extremely high contrast. Large limestone aggregate particles were clearly evident in the concrete samples.

None of the microstructures commonly associated with C-S-H in OPC (long fibers, etc.) were observed, implying that the C-S-H formed here is somewhat different. It

has been suggested [21] that the lack of such microstructures is due to the lack of a sufficiently powerful driving force (i.e. concentration gradients due to localized variations in pH, high temperatures, etc.); that is, transport of atoms over short distances (nanometers) is relatively easy, and as slag particles dissolve they can form nanocrystals of C-S-H or other side products, however, long-range transport (several microns) is sufficiently difficult that nanocrystals do not coalesce into larger structures. In a study of blended slag/OPC cements, Richardson and Groves [54] concluded that as the content of slag increased, the morphology of C-S-H changed from 'fibrillar' in pure OPC to a finer, 'foil-like' morphology. This morphology became finer and finer, until at significant loadings of slag the microstructures were only observable by TEM, being but several tens of nanometers in size. This finer morphology is, according to Richardson and Groves, one of the reasons for superior mechanical performance and lower diffusion rates that produce superior durability for slag cements in aggressive environments; the lack of larger structures is briefly mentioned as due to 'space constraints.' C-S-H intimately mixed with hydrotalcite are shown to be the final products, with hydrotalcite occurring on a scale below that of TEM resolution; diffraction patterns confirm the very poorly crystalline nature of the C-S-H. These results are reproduced in a later study using 'synthetic slags' blended with as little as 10 wt.% OPC [92].

The lack of obvious similarities to the microstructure of OPC has been noted by Fernández-Jiménez [71], who, in a study on slag activated by NaOH, waterglass, or Na_2CO_3, found 'foil like' C-S-H morphologies of only a few tens of nanometers in size via TEM; by Song *et al*. [93], who report 'smooth and homogeneous' microstructures similar to those seen here in NaOH-activated slags; and Mozgawa *et al*. [70], who report

similar microstructures in slag activated by Na-alkalis, but note that 'plate like' structures are formed when autoclaved (that is, when a sufficient 'driving force' is applied to encourage coalescence).

Garci Juenger *et al*. [94], in a study of French slag activated by KOH or K_2SO_4, eschew the use of SEM/TEM due to the results being tainted by sample preparation (drying, polishing, etc.) and prefer the use of soft x-ray transmission microscopy for imaging the hydration of slag particles. When activated by alkali solutions, they observed 'globular,' 'sheaf of wheat,' and 'angular' morphologies on the sub-micron scale; they conclude that these hydration products are C-S-H or, for samples with added portlandite, 'silica poisoned calcium hydroxide.'

As no TEM work was performed here, the question of differences between the C-S-H produced here and the C-S-H produced in OPC cannot be conclusively answered. That fibrillar C-S-H, as occurs in OPC, is not observed is the sole data point. Based on the literature, however, it seems likely that due to 'space constraints,' or the inability to transport atoms over micron-scale distances, poorly formed nanocrystals of C-S-H simply do not coalesce into larger 'fibers.' A TEM study would likely find 'foil-like' morphologies, and could help to elaborate on the structure of the C-S-H here produced (see Ch. 6, below.)

Above the nanoscale, however, both the cement pastes and concretes appear essentially the same as their OPC counterparts in imaging mode (that is, they contain Ip, Op, unreacted slag, and/or aggregate particles.) Even at low magnification (Fig. 3.4a) grains of unreacted slag were discernable from the Op in the NaOH/waterglass formula, and some larger-scale morphologies such as pores were observed. At higher

magnification (Fig. 3.4b) both the unreacted slag and the Op were easy to identify; the morphology of the Op appeared smooth, but with substantial cracking, possibly from the production of the sample or stresses created during polishing. They may also be drying cracks. At the highest magnification (Fig. 3.4c), the bonding between grains of unreacted slag and the Op was clear; sometimes cracking was evident. The Op still appeared relatively smooth at these magnifications.

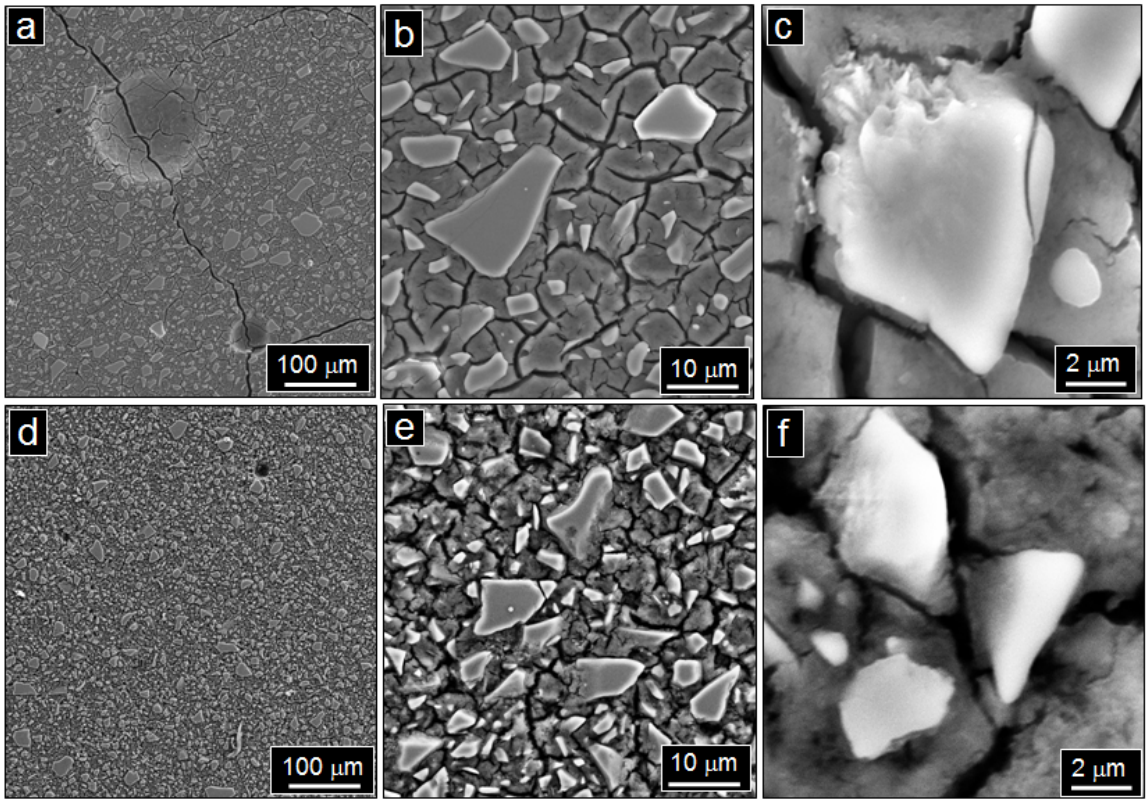

Figure 3.4 –Secondary electron micrographs of cement pastes. a) low magnification image of formula A, showing cracking in the Op and a pore; b) medium magnification image of formula A featuring grains of unreacted slag and cracking in the Op; c) high magnification image of formula A showing unreacted slag (center), Op, and Ip (white ring around the grain of slag; d) low magnification image of formula B, containing much more unreacted slag than formula A and at least one pore; e) medium magnification image of formula B, with an Op of somewhat different morphology of that found in formula A, and f) high magnification image of grains of unreacted slag in formula B, with less clear Ip. All images were taken at an age of 7 d.

BSE images were similar (Fig. 3.5.) At low magnification the particles of unreacted slag (Fig. 3.5a), with their relatively higher average atomic weight, appeared as bright white particles against a dark gray Op. At higher magnification (Fig. 3.5b) the difference was quite obvious, and even the smallest particles of unreacted slag could easily be differentiated from the Op. At the highest magnification (Fig. 3.5c) images were somewhat blurry, but in high contrast mode the Ip could be identified as a bright ring around the slag particles. Finally, in samples containing aggregate (Fig. 3.6) little change was noticed at low magnification (Fig. 3.6a) aside from the presence of large particles of aggregate, and neither the Op nor grains of unreacted slag seemed much affected (Fig. 3.6b) by the aggregate's inclusion.

Brough *et al*. [45, 95], Wang *et al*. [56], Richardson *et al.* [54], Bohác *et al*. [96], and Bakharev [24] have published results similar in appearance (Op, Ip, slag, and aggregate) for slags activated by various alkalis. Such morphology is also well known in OPC [97].

BSE images of the NaOH/waterglass formula were investigated after 7 d as well as after 20 months (Table 3.2) using automated image analysis software (Fig. 3.7), which determines the percentage of unreacted slag in pure cement pastes by turning BSE images

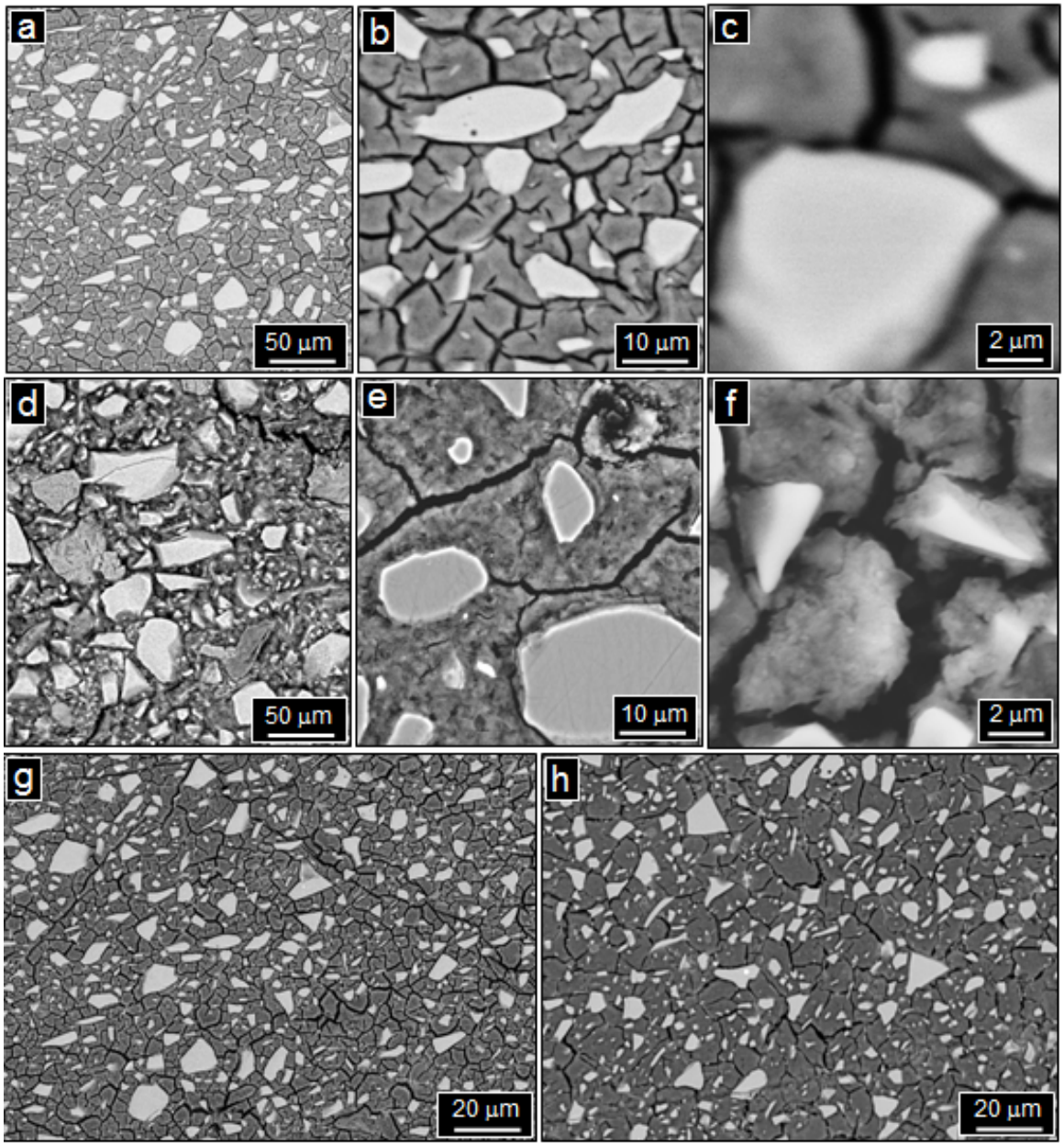

Figure 3.5 – SEM-BSE micrographs of cement pastes. a) low magnification image of formula A, showing cracking in the Op and well defined grains of unreacted slag; b) medium magnification image of formula A featuring grains of unreacted slag and detailed cracking in the Op; c) high magnification image of formula A showing unreacted slag and cracking between the slag and Op d) low magnification image of formula B, which was more difficult to polish and shows more angular grains of unreacted slag; e) medium magnification image of formula B, with an Op of somewhat different morphology of that found in formula A as well as well polished grains of slag with clear Ip rings, f) high magnification image of grains of unreacted slag in formula B, with less clear Ip and some Op cracking. All images were taken at an age of 7 d. g) low-magnification BSE image at 7 d for comparison with h) low-magnification BSE image at 20 months.

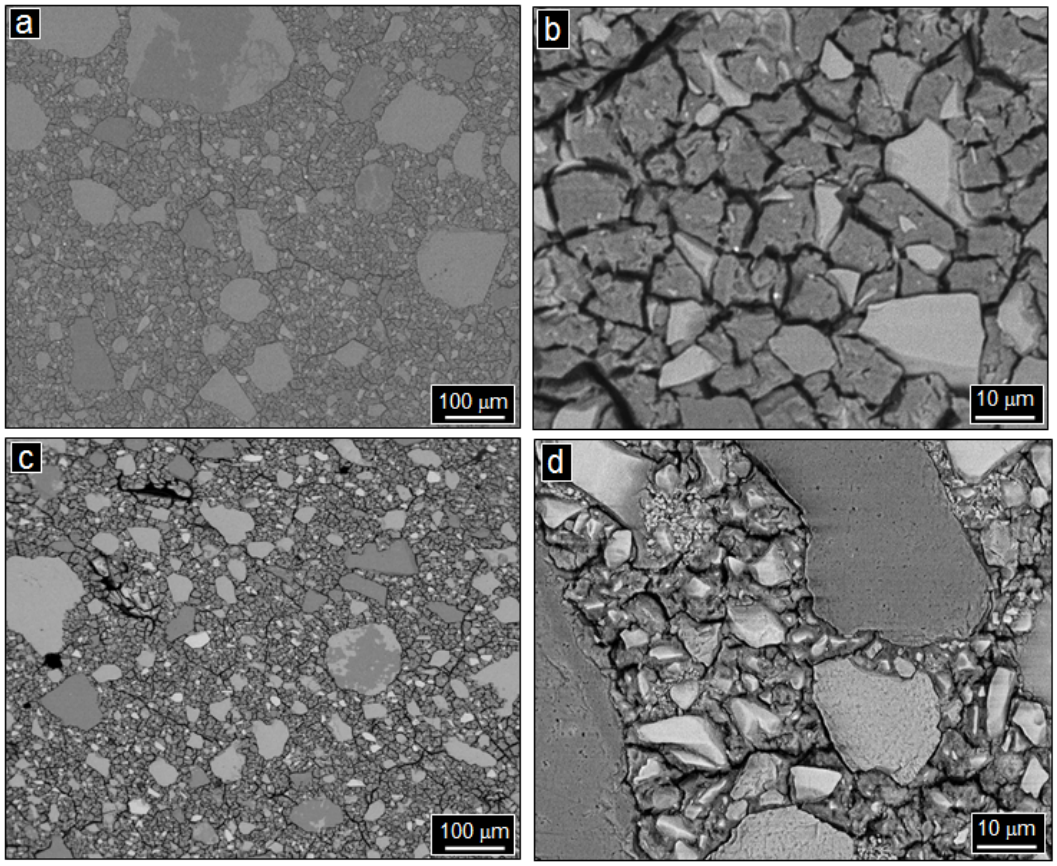

Figure 3.6 – BSE images of basic formula cements with fine limestone aggregate. a) low-magnification image of formula A showing aggregate (large particles) and unreacted slag (smaller particles) as well as cracking in the Op; b) high-magnification image showing grains of unreacted slag as well as cracking in the Op; c) low-magnification image of formula B, showing some cracking in the Op, aggregate (larger particles) and unreacted slag (smaller particles); d) high-magnification image of formula B, showing unreacted slag, aggregate (top center and left) and Op morphology. All images were taken at an age of 7 d.

into binary images and then analyzing them. This formula contained 26.5±2 vol.% unreacted slag, going down to 21±2 vol.% after 20 months. While these numbers are only estimates of the unreacted slag content, as these numbers are still quite close together, it is clear that over the course of the first 20 months the slag in the NaOH/waterglass activated formula either does not continue to react or that the reaction slows down significantly. The analysis also measures the average area of the unreacted slag particles

Table 3.3 – Image analysis of basic formulae cements with and without diatomaceous earth at 7 d and 20 months, and analysis of formulae containing Al_2O_3 after 7 d.

Formula	Objects Measured (#)	Avg. Size (μm^2)	Unreacted Slag (vol. %)	Age (m or d)
A	3,244	4.4 ± 1.2	26.5 ± 2.1	7 d
A + DE	12,466	4.5 ± 0.5	23.5 ± 1.2	7 d
B	34,010	1.8 ± 0.4	41.8 ± 3.2	7 d
B + DE	35,674	3.3 ± 3.2	30.3 ± 4.1	7 d
A	17,141	1.4 ± 0.2	21.3 ± 1.5	20 m
A + DE	26,322	0.9 ± 0.1	22 ± 1.1	20 m
B	14,244	2.1 ± 0.3	27.4 ± 0.9	20 m
B + DE	19,081	1.7 ± 0.2	29.5 ± 3.2	20 m
A1	49,493	2.3 ± .07	16 ± 2	7 d
A2	38,132	3.0 ± 0.5	13 ± 1.5	7 d
A4	70,760	3.3 ± 0.8	26 ± 7	7 d
B1	72,213	3.0 ± 0.3	23 ± 1.5	7 d
B2	73,410	2.7 ± 0.4	21 ± 1	7 d
B4	73,946	2.2 ± 0.1	18 ± 1.5	7 d
C1	11,548	4.5 ± 0.2	28 ± 2.5	7 d
C2	67,144	3.5 ± 0.4	24 ± 1	7 d
C4	60,014	3.0 ± 0.3	25 ± 2	7 d

(Table 3.2.) The average area decreases from 4.4 ± 1.2 μm^2 after 7 d to 1.4 ± 0.2 μm^2 after 20 months (μm^2 is used, as 2D micrographs are being investigated), a somewhat surprising result, as the volume of slag grains did not decrease by such a large amount. This opens the possibility that the previous analysis was wrong, and that the reaction continued to eat away at unreacted particles; it is also possible that the scale was set incorrectly (though this was rechecked and does not seem to be the case), that large particles are breaking up into smaller ones, or that more well-defined Ip zones are playing a role at 20 months. Examination of two BSE images at identical magnifications (Figs. 3.5g and h at 7 d and 20 months, respectively) appear to show fewer unreacted particles at 20 months. However, there also seems to be less cracking, so a ready answer with certainty is not forthcoming. When taken with the FTIR and EDS (see below) results, however, it is clear that the reaction is continuing.

Brough *et al*. [45] used a similar image analysis procedure to investigate slag cements activated by waterglass. By their estimation, only 5 % of the slag had reacted after 1 day, increasing to 64 % after a year. They note a number of difficulties in using this technique, however, including the fact that cracking and shrinkage in general will lower the apparent amount of reacted slag. NMR and other techniques were then used to determine the extent of reaction, and provided what the authors considered more satisfactory evidence (that is, 61 % reaction as determined by NMR, compared to 49 % reaction by image analysis after 1 month. They also provide estimates based on loss on ignition (LOI), though they note that such a technique is wildly inaccurate, as temperature increases to ignite the samples causes slag to react and changes the total amount of unreacted slag.) It should therefore be reiterated that the measurements taken here are for identification of trends, not concrete numbers.

3.1.5 – EDS (Cement Paste, Fine Aggregate Concrete)

The Ip and Op of the NaOH/waterglass activated formulae were analyzed after 7 d and 20 months of curing, with 40 points in the Op and Ip, and 30 points in unreacted slag grains analyzed. As hydrogen is not detected in EDS, analysis (Table 3.3) shows the main

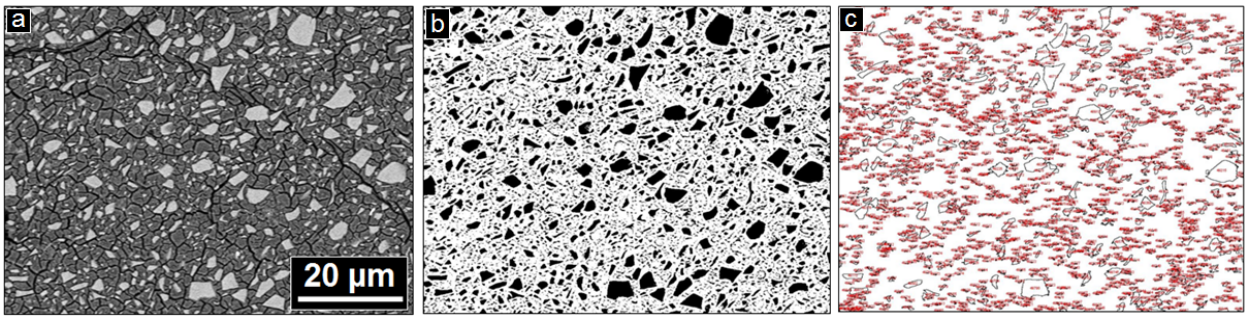

Figure 3.7 – Methodology of image analysis. a) BSE image; b) binarization of the BSE image; c) particle size analysis marking each particle and critical information about it. This method was performed on at least 10 images per data point reported.

Table 3.4 - Concentration of selected elements (at. %) and Ca/Si and Ca/Al ratios of NaOH/waterglass- and Na_2CO_3-activated formulae at 7 days and 20 months, and for concrete after 20 months.

		Cement - 7 Days		Cement - 20 Months		Concrete - 20 Months	
NaOH/ Waterglass	Slag	Inner Product	Outer Product	Inner Product	Outer Product	Inner Product	Outer Product
# of Points	30	40	40	40	40	40	40
Al (at.%)	4.6 ± 0.3	3.7 ± 0.7	4 ± 0.6	4.1 ± 0.5	3.9 ± 0.2	3.9 ± 0.5	4.1 ± 0.4
Si (at. %)	12.8 ± 0.4	10.8 ± 1.8	15.9 ± 3.3	12 ± 1.3	15.8± 0.8	11.6 ± 1.5	14.5± 3.0
Ca (at. %)	15.1 ± 0.7	10.1 ± 4	1.1 ± 0.5	11.9 ± 3.4	2.9 ± 0.4	11.0 ± 4.0	1.5 ± 0.5
Na (at. %)	0 ± 0	1.9 ± 1.1	5.4 ± 1.2	1.6 ± 0.9	5.1 ± 0.6	1.6 ± 0.8	3.3 ± 1.1
Ca/Si	1.2	0.93	0.1	1	0.2	0.9	0.1
Ca/Al	3.3	2.7	0.26	2.9	0.8	2.8	0.4
Na_2CO_3 Activated	Slag	Inner Product	Outer Product	Inner Product	Outer Product	Inner Product	Outer Product
# of Points	30	40	40	40	41	40	40
Al (at.%)	4.7 ± 0.3	3.8 ± 0.7	4.9 ± 1.1	3.8 ± 0.4	3.1 ± 0.3	4.6 ± 0.6	4.5 ± 0.8
Si (at. %)	13.2 ± 0.3	9.6 ± 2.2	9.7 ± 2.9	10 ± 1.4	9 ± 0.9	11.8 ± 1.7	10.9± 2.1
Ca (at. %)	16.4 ± 0.5	8.9 ± 4.4	5.1 ± 3.1	8.6 ± 2.7	9 ± 0.9	10.6 ± 3.1	5.3 ± 1.4
Na (at. %)	0 ± 0	2.4 ± 1.0	4.0 ± 1.1	1.6 ± 0.7	3.1 ± 0.3	0.9 ± 0.4	1.7 ± 0.4
Ca/Si	1.2	0.93	0.5	0.8	1	0.9	0.5
Ca/Al	3.5	2.36	1.06	2.2	2.9	2.3	1.2

constituent of all samples to be O, some of which is in the form of water (as evidenced by FTIR and TGA, see below) and some in the form of hydrated minerals (as observed by XRD, FTIR, and possibly TGA.)

The data from the center of the unreacted slag particles are clustered tightly together, as are the data for the Op, to a lesser extent. Data for the Ip have a wider scatter. which is probably due to the uncertain thickness of the Ip and the fact that the signal from either the slag or Op could have bled through due to the strength of the electron beam, which created an interaction volume on the order of 1 μm^3. The concentration of Na is essentially constant (6.1±1.5 at.%) throughout the Op; possible dispositions for the Na include substituting for Ca in C-S-H gel, balancing charge where Al has substituted for Si, forming minor side products in the pore solution and/or in the interlayer space of the

C-S-H. Between 7 d and 20 months, these values change only slightly (Table 3.4), although a roughly 2 % increase from 1.1 at.% to 2.9 at.% does mean that Ca concentration doubles, a trend also seen in the Na_2CO_3 formula, discussed below.

The exact concentrations of Na are complicated by a number of factors. It is known that Na materials are easily 'removed' from samples [56], either through dissolution in the fluids used during polishing, sublimation by the electron beam, or the vacuum produced in the SEM chamber. This seems to be an unavoidable cost of using SEM/EDS; but it can be accounted for by reiterating that these values should be viewed as minimum amounts and not exact concentrations. The likely final dispositions of the Na atoms have not changed.

Regardless of age, the Si/Ca ratios (Fig. 3.8a) follow the same general trend: that of a line (the Ip) connecting two points (the Op, with low Ca and high Si, and the unreacted slag, with high Si and Ca.) Some variation is expected, as it is well known that visual identification of the Ip is an imperfect art and prone to errors [95]. The center of the unreacted slag particles are tightly grouped around a value of about Si/Ca = 0.8. This value is the same as the Si/Ca ratio measured in the unreacted slag powder (Table 2.5) At both 7 d and 20 months (Fig. 3.8a), the Ip is scattered along a line that runs from Si/Ca = 0.8 to roughly Si/Ca = 2, due to a drop in Ca. The Op is a little less tightly grouped, at around Si/Ca = 15 (after 7 d) and Si/Ca = 5.3 (after 20 months.)

The Si/Ca ratios of the unreacted slag agree with the EDS/XRF analyses of the unreacted material (Ch. 2) and that of the Ip is in accord with what would be expected from the literature. Brough *et al.* [45] reported Si/Ca values of ~ 0.8 for the Ip of slags activated solely by 5M KOH; Rajaokarivony-Andriambololona *et al.* [52] reported values

of 0.4 – 1.4 for the Ip of NaOH activated slags; Wang *et al.* [56] report values of 1-2 for NaOH-activated slags at 1 d and 1 year. The Ip reported here covers a range of roughly 0.5 - 1.

The values for the Op, however, show a wild divergence, being at least 4 times greater than would be expected based on the literature. The most likely answer for this huge ratio is that the cement receives a substantial quantity of extra Si from waterglass.

The Si/Ca ratio of the Op of AAS cements depends heavily on the activator. When blended with OPC (wherein $Ca(OH)_2$ acts as the activator) the ratio is much higher, as the amount of Ca is increased. For example, Richardson and Groves [54] report Op Si/Ca ratios of 1.7 for pure OPC, 1.55 for a 50/50 blend, and 1.18 for a pure AAS material: increasing the Ca content of the activator lowers the Si/Ca ratio by providing extra Ca.

In a similar manner, the use of waterglass, which contains ~ 30 wt. % Si, would have the opposite effect, raising the Si/Ca ratio by providing more Si. In a study of slags activated by NaOH, waterglass, or a 50/25/25 mixture of Na_2CO_3/Na_2SO_4/$Ca(OH)_2$, Escalante-García *et al*. [98] measured Si/Ca ratios using EDS. The NaOH- and 50/25/25-activated formulae had Si/Ca ratios of 0.65 and 0.67, respectively; when waterglass was used, this ratio increased to 0.89, a roughly 35 % increase. This was despite the fact that the waterglass used was only 5% of the slag's weight; the value used here is closer to 40% of the weight of the slag, and should thus produce a substantially more pronounced effect.

While the use of NaOH/waterglass could possibly dissolve Si from the slag more rapidly than Ca, the high Si/Ca ratio is certainly at least partially due to the fact that the

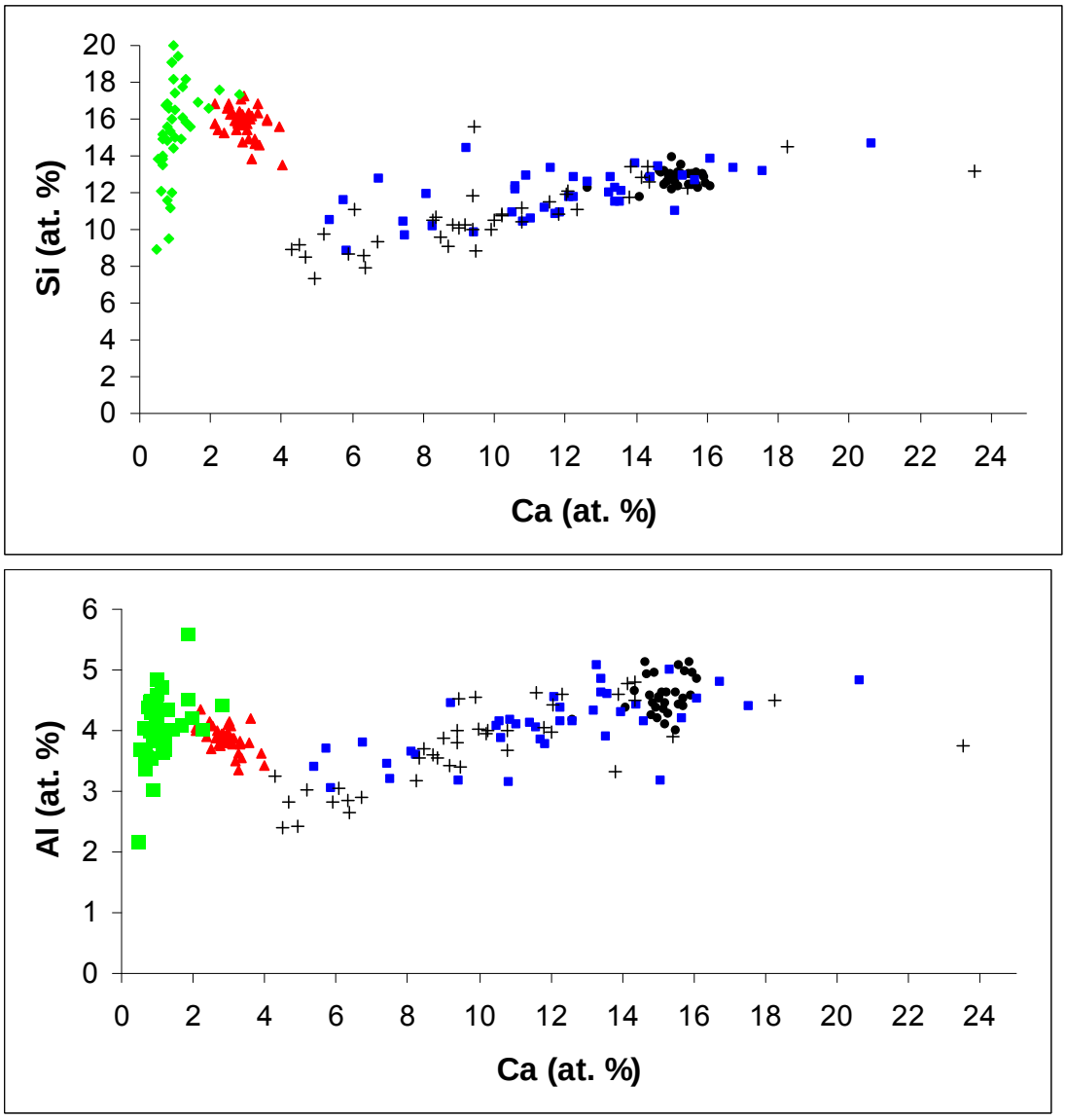

Figure 3.8 – Elemental analysis of the NaOH/waterglass activated cement formula: Si/Ca and Al/Ca concentrations of slag (●), Ip after 7 d (+) and 20 months (□), and Op after 7 d (x) and 20 months (Δ), as determined by EDS.

waterglass simply contains additional Si. This makes analysis of the exact nature of the C-S-H produced here difficult without more powerful techniques (TEM, etc.) to separate the C-S-H from the Si-rich gel that is being produced by excess Si from the waterglass. Such methods would also be needed to identify if a second source were a contributing

cause, i.e., if Si were being dissolved from the slag at a higher rate due to the high pH of the activator used.

Overall, similar trends are observed in the Al/Ca ratios (Fig. 3.8b), where the Ip is a line that runs from the unreacted slag (high Al and Ca) to the Op (lower amounts of each.) The unreacted slag (Fig. 3.8b) is tightly grouped around a value of Al/Ca = 4 (which is the same value found in unreacted slag, see Table 2.2); it falls gradually to around Al/Ca = 0.75 with the Ip, and then has a value of Al/Ca = 3-5 (after 7 d) and Al/Ca =1.3 after 20 months. The reason why the Op contains less Al than some of the Ip, which implies that Al prefers the Ip over the Op or the center of the slag particles is not clear but it has been hypothesized that the Ip preferentially contains various aluminate phases [45]. That the amount of Ca in the Op increases between 7 d and 20 months while the Al value stays roughly the same, however, is clear.

Overall, trends can be observed in this data. First, the concentration of Ca falls going from the slag, through the Ip, to the Op. In the Op, however, there is substantially more Si, the majority of which is, as noted above, due to the Si in the waterglass. Second, Al concentrations falls only slightly, despite the large drop in Ca concentrations. It is thus clear that Al is easily dissolved by the activating solutions, but due to the low concentration of Al and lack of distinct Al-rich phases, it is likely that the Al is either forming mineral side products (such as hydrotalcite) and/or occasionally substituting for Si in the C-S-H gel. Third, the Ca concentration in the Op increases between 7 d and 20 months, while the overall amount of scatter decreases. This implies that not only does the reaction continue between 7 d and 20 months (i.e., Ca continues to be dissolved out of the unreacted slag particles) but also that the Op is becoming more homogeneous, at least as

far as the SEM is concerned. This increase in homogeneity could be partially due to a greater distance between smaller particles of unreacted slag, lowering the likelihood of the electron beam impinging on a slag particle and thus adding scatter to the EDS results.

At both ages, samples containing fine limestone aggregate were also investigated (Table 3.3.) Analyzing cement paste in close proximity to aggregate particles was avoided, to ensure the chemistries were representative of the cementing phase and not of the aggregate, but aggregate contributing to the signal cannot be discounted. Overall, the numbers are fairly close; almost all changes in the elemental concentration are either less than 1 at. %, or are within the standard deviations of the two values. Ca and Na concentration falls by 1.4 and 1.8 at. %, respectively, in the Op while C rises by 2.9 at. %. Such small changes may arise for a variety of reasons, such as different evaporation rates between the cement paste and concrete, or the relatively coarse accuracy of the EDS technique. For example, comparing the composition of the unreacted slag between the cement and concrete shows a 3 at.% increase in the concrete's O concentration, certainly due to some combination of the above factors. The Ca/Si and Ca/Al ratios are in relatively good agreement with those of the pure cement paste.

It should be noted that early results [99] are different than those presented here. EDS analysis 5 points in cement pastes at an age of 7 d produced results wherein the Si/Ca ratio was roughly 1:1, or at worst, 2:1, substantially lower than what was found when the experiment was repeated 3 years later on samples aged for 7 d (the data presented above.) The reason for this is not clear; a review of the data seems to suggest that things are in order, though errors were made in estimating the expected values of each element. The overall difference is likely due to a combination of operator error

(incorrect sample preparation, misidentification of phases, sub-optimal microscope or software settings, etc.) and the fact that only 5 points were analyzed; however, the length of time between the error being made and the error being discovered makes it unlikely a detailed, certain explanation will be arrived at. Notebooks and the original data seem to be in order. Re-performing the experiment with 40 points, above, provided new data that should be viewed as more accurate, if only because a higher number of points were analyzed to produce statistically meaningful results, which are backed up by the data from the 40-point analysis for aged cements at 20 months.

3.1.6 – TGA (Cement Paste)

TGA curves were obtained after curing for 1 week and 20 months (Fig. 3.9, lower curves.) Two regions are observed: Weight loss below 150 ^{o}C (~ 15 wt.% for either formula) can be attributed to the loss of unbound water [100]. The weight loss between 150 and 550 °C, roughly an additional 5 wt. % for each sample, can be attributed to bound water, such as that found in hydrated minerals (such as hydrotalcite), C-S-H, calcium aluminate hydrates, calcium aluminates, and gypsum [65]. Weight loss below 150 ^{o}C is now only between 4–8 wt.%, due either to the loss of unbound water from evaporation or from that water becoming incorporated into C-S-H or hydrated minerals. In the second region, each sample lost approximately 10 wt. % between 200 and 550 ^{o}C, due to bound water in the form of C-S-H or hydrated minerals. Unfortunately, the TGA analysis is hampered by the lack of sharp decreases; further, in the literature [60-66] there is little agreement on the exact temperatures at which various reactions occur (see Ch. 2.) It had been hoped that that weight losses would be sufficiently abrupt so as to facilitate estimation of the weight content of the various phases (i.e., if the weight of CO_2 lost is

known, the weight of $CaCO_3$ in the sample can be calculated.) This technique was used by Lawrence *et al*. [63, 101] to measure residual amounts of $Ca(OH)_2$ in OPC cements; and by Miller [102] to estimate various phases in freeze-dried lime/DE mixtures.

Stepkowska *et al*. [64] performed TGA experiments on fresh and aged OPC cement pastes, the results of which are generally similar to those shown here, with the exception that their data contained considerable peaks due to the dehydration of portlandite, $Ca(OH)_2$. This phase does not occur in AAS materials due to a substantial surplus of Si, ensuring that each Ca atom that dissolves can be turned into C-S-H. It should be noted that Stepkowska *et al*. observed both vaterite and aragonite, the two polymorphs of calcite, by XRD, and used TGA and FTIR to confirm their presence. The results of ageing are similar to those presented here: over time, the amount of unbound water decreases dramatically due to evaporation to the atmosphere, while the amounts of bound water in C-S-H, the weight loss due portlandite (not seen here), etc., change little.

Thermal analysis by Wang *et al*. [56] on a slag similar to the one used here activated by NaOH or waterglass solutions of varying concentrations identified similar regions (unbound water and bound water,) however, the decreases were too broad to estimate total content; subtle changes in the curves were used to identify hydrotalcite (begins ~ 330 ^oC) and an "AFm-type phase" (begins ~ 130 ^oC.) These phases cannot be identified from the data collected here.

Much research has been done on 'geopolymers' in terms of their fire-resistance properties. As opposed to the AAS literature there is some agreement as to what the exact temperature at which reactions occur: Lyons *et al*. [103] reported ~ 5 wt.% loss at 200-400 ^oC ; Duxson *et al*. [104] found that all weight loss occurred below 300 ^oC (although

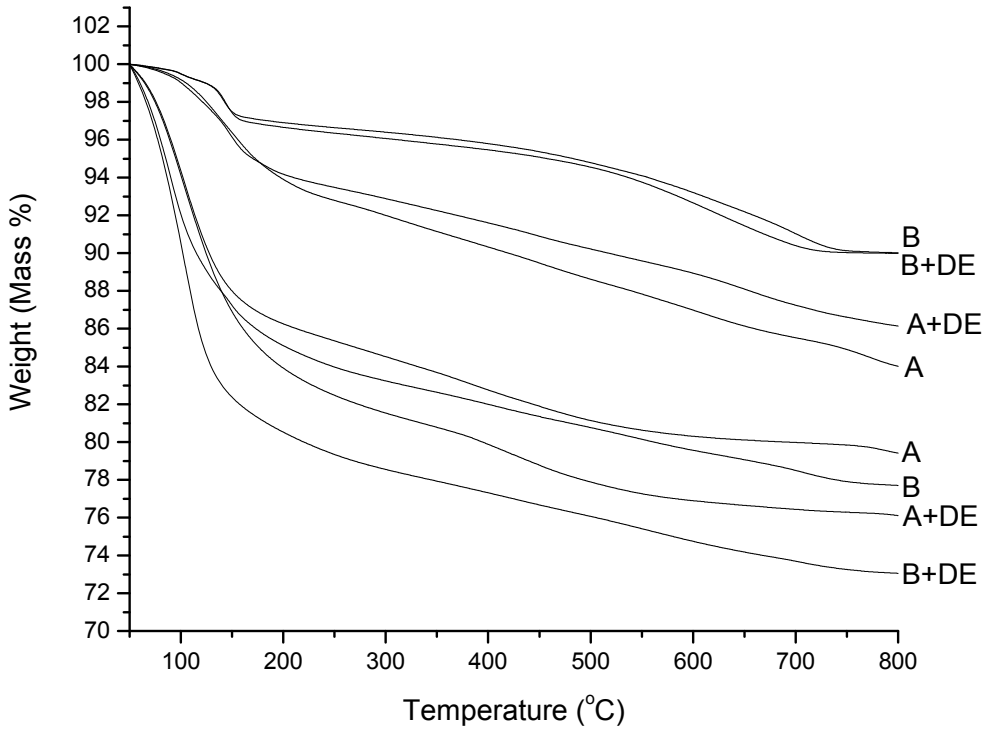

Figure 3.9 – TGA curves of formulae activated by NaOH/waterglass (A) and Na_2CO_3 (B) with and without diatomaceous earth at 20 months (upper set) and 7 d (lower set.) After 20 months (Fig. 3.9, upper curves.), these two regions are still evident.

the total amount is not mentioned); Barbosa *et al.* [105] described a loss of about 10 wt.% below 200 °C. These losses are all attributed to the evaporation of unbound water from pores; there is a general agreement that 'geopolymers' are stable at moderate to high temperatures [28, 31, 33, 89, 104-108]. If it were a purely geopolymer system, therefore, it would be expected that there would be no weight loss above ~ 200 °C.

Unfortunately, comparison to the literature does not illuminate the TGA behavior of the samples investigated here. While it is true that there is a weight loss in the region attributed to unbound water, this is a behavior also known to occur in AAS and OPC materials [60-66, 109]. The weight losses that are seen are too broad for accurate

determination of the makeup of the final product. That TGA can be a useful tool is clear; that it can be a useful tool with the materials made herein is less clear.

3.1.7 – Conclusions

This basic formula, activated by NaOH/waterglass, has a sufficiently high strength (73 MPa compressive strength and ~ 2 MPa tensile strength at 1 day) to be used for many applications. The use of steel caps proved to be a superior method for compression tests compared to grinding, providing more accurate data, and should be used exclusively. Analysis by XRD shows the presence of C-S-H, which is supported by FTIR and EDS. TGA analysis is insufficient to rule out the presence of 'geopolymers,' however, weight loss at higher temperatures implies that, at the very least, other materials are present (as geopolymers are known to be thermally stable), thus possibly confirming the presence of C-S-H. The lack of distinct peaks prevents estimation of the amount of each phase in the material.

While any single analysis method could be interpreted in favor of a pure system of one kind or another, the weaknesses of each method make this a flawed approach. A complimentary combination of methods, as used here, however, leaves little doubt that 'geopolymers' are not being produced, and that C-S-H intimately intermixed with a second phase (likely a Si gel from the excess Si contained in the waterglass, as described in the literature.)

This second phase is the most likely reason for the extremely high Si/Ca ratio in the Op of this material; that the Si-rich gel portion of the C-S-H is becoming more polymerized over time and thus consuming more Si atoms (as shown by FTIR) is also likely to be a portion of the explanation. Microstructures commonly associated with C-S-

H in OPC were not observed, implying a possible difference between the C-S-H seen here and that seen in OPC. This is not, however, a unique position and is reported by other researchers and is likely due to the preference for localized reactions over long-range transport and coalescence of nanocrystals. Finally, little if any difference is seen between the elemental analyses of the cement paste and those of the fine-aggregate concrete.

The most important conclusion of this part of the work is that to identify the final products of AAS cements, a complimentary combination of analysis techniques must be used: any one technique could argue either way, but taken as a whole, they describe a C-S-H/ Si-rich gel system more similar to OPC than to 'geopolymers.'

3.2 – Na_2CO_3 Activated Basic Formula

This formula is the second of the two basic formulae used as benchmarks. Na_2CO_3 is an effectively carbon neutral activator, safer to handle than NaOH, cheaper than waterglass, and more likely to be used in practical, real-world applications. For every set of experiments, a new batch of samples was produced and their compressive strengths measured in order to ensure fair comparisons.

3.2.1 – Mechanical Properties (Fine Aggregate Concrete)

The Na_2CO_3 activated formula was also originally tested after the ends had been ground to ensure parallelism. After 1 d, the samples had barely set, with strengths of less than 5 MPa. After 7 d, the strength had increased to 30 ± 1 MPa, and reached a strength of 36±2 MPa after 28 d (Fig. 3.1.)

As before, this formula was later tested using steel caps. At 1 d the sample was still soft, with a strength of only 14.7 ± 0.3 MPa. After 7 d, the strength had risen to 25.1

± 0.1 MPa, and ended at 47 ± 1 MPa after 28 d. While the strength gain here (33 %) is not as impressive as that of the NaOH/waterglass activated samples (60%), the differences are still substantial enough to indicate that grinding was a flawed method for attaining parallelism between the tops and bottoms of the cylinders tested.

In the literature, strengths for formulae activated by Na_2CO_3 solutions are somewhat less common than those activated by NaOH or waterglass. Xu *et al.* [21] report a strength of 25 MPa (in 1964) and 40 MPa (in 1971) for an Na_2CO_3-activated slag mortar (cement with sand) used in the production of an irrigation chute in Ukraine. Wang *et al*. [57] reported a strength of 35.5 MPa at 28 d for one Na_2CO_3–activated mortar, which was increased to 53 MPa by more fine grinding of the slag and 70 MPa through the use of elevated curing temperatures. Bakharev *et al*. [110] have reported a 28 d strength of 26 MPa for a slag activated by Na_2CO_3 with an additional 7 % NaOH. Yongde *et al.* [111] report 28 d strength of 60 MPa for a Na_2CO_3–activated mortar; Fernández-Jiménez *et al.* [112] achieved strengths of ~40 MPa at 28 d and ~ 60 MPa at 180 d for a Na_2CO_3-activated mortar, which was not as strong as an NaOH-activated mortar at early ages, but stronger at later ages. The authors attribute this to carbonate ions continuing to react with slag, forming calcium aluminate/carbonate phases over long periods of time (see below.) These strengths describe a range of roughly 20 – 60 MPa, a fairly wide range, due to differences in activator concentration, slag composition/fineness, water:binder ratio, curing methods, etc.

Overall, the activation by Na_2CO_3 produces formulae that are weaker than NaOH-activated formulae in the short term, as the Na_2CO_3 solution has a lower pH and therefore less ability to dissolve the slag. They are generally also weaker than formulae

based on a combination of NaOH and waterglass; the extra Si in the waterglass provides more Si for C-S-H as well as a densifying Si gel, which gives a large boost to initial strength that Na_2CO_3–activated seem to be unable to accommodate, even at long time scales.

The strength seen here is within the general range reported in the literature and also follows the trend of being weaker than the NaOH/waterglass formula. Over time, if the mechanisms proposed by Xu and Fernández-Jiménez (that is, carbonate ions continuing to increase strengths; see EDS section below) are at work, this formula may be stronger in the long term. However, it is unlikely to catch up to the strength of the NaOH/waterglass-activated formula.

The tensile splitting strength of the Na_2CO_3 activated formula (samples without caps; Table 3.4) follows the same general trend as the NaOH/waterglass activated formula, but at lower values, increasing from 0 to 2.2 ± 0.2 MPa. While values for the tensile splitting strength of Na_2CO_3 activated slag cements could not be found in the literature, that they are lower than those of the NaOH/waterglass formulae, as is the compressive strength, is not surprising.

Table 3.5 – Tensile splitting strength of Na_2CO_3-activated formulae, with diatomaceous earth (DE), NaCl, and Al_2O_3 (Si:Al ratios of 1, 2, or 4), and combinations thereof, as additives. The number in parenthesis below tensile splitting strength in MPa is tensile splitting strength as a percent of compressive strength at the same age.

Formula	1 Day (MPa)	7 Days (MPa)	28 Days (MPa)
B	0	1.4 ± 0.2	2.2 ± 0.2
B + DE	0	2.0 ± 0.1	2.2 ± 0.6
B + NaCl	0	1.8 ± 0.2	2.0 ± 0.2
B + DE + NaCl	0	1.7 ± 0.0	2.9 ± 0.6
B - Si:Al =1	0	1.7 ± 0.6	2.9 ± 0.3
B - Si:Al = 2	0	2.1 ± 0.8	2.4 ± 1.3
B - Si:Al = 4	0	2.3 ± 0.6	2.6 ± 0.1

3.2.2 – XRD (Cement Paste)

The diffractograms of the Na_2CO_3 activated formula (Fig. 3.10a) are more complex than those of the NaOH/waterglass activated formula at all ages. After just 7 d, the broad hump due to unreacted slag and the wide peak at 30^o -2θ are both present; the wide peak is now somewhat sharper. For reasons discussed above in the XRD section of the NaOH/waterglass activated formula, this peak is identified as C-S-H, either more crystalline than that found in the NaOH/waterglass formula, or with some crystalline calcite contributing to the signal. The peak is nearly identical to that described by Mozgawa *et al*. (Fig. 3.10b), which they identify as C-S-H and confirm through FTIR and NMR. They also observe calcite, which can be differentiated from C-S-H by the presence of secondary peaks.

Peaks at 11^o, 23^o, 35^o, 40^o, and 60^o-2θ are also present. These peaks correspond to hydrotalcite ($Mg_6Al_2CO_3(OH_{16})\cdot 4H_2O$) As seen in the discussion of the diffractogram of the NaOH/waterglass activated formula, hydrotalcite has been identified in diffractograms by Wang *et al*. [56], as well as Puertas *et al.* [51]. Although they do not provide XRD data, Bohać *et al*. [96] speculate on the presence of a hydrotalcite phase due to evidence from EDS analyses, as do Escalante-Garcia *et al*. [47, 113] and Brough *et al*. [45]. Gruskovnjak *et al.* [114] observed hydrotalcite by XRD (confirmed by TGA), however, they were using a slag cement activated by anhydrite. Based on TEM data and structural models, Richardson [115] has identified hydrotalcite as finely intermixed with C-S-H in OPC/slag blends.

Compared with the literature in which hydrotalcite is not identified, there seems to be no correlation between the presence of hydrotalcite and strength or other properties.

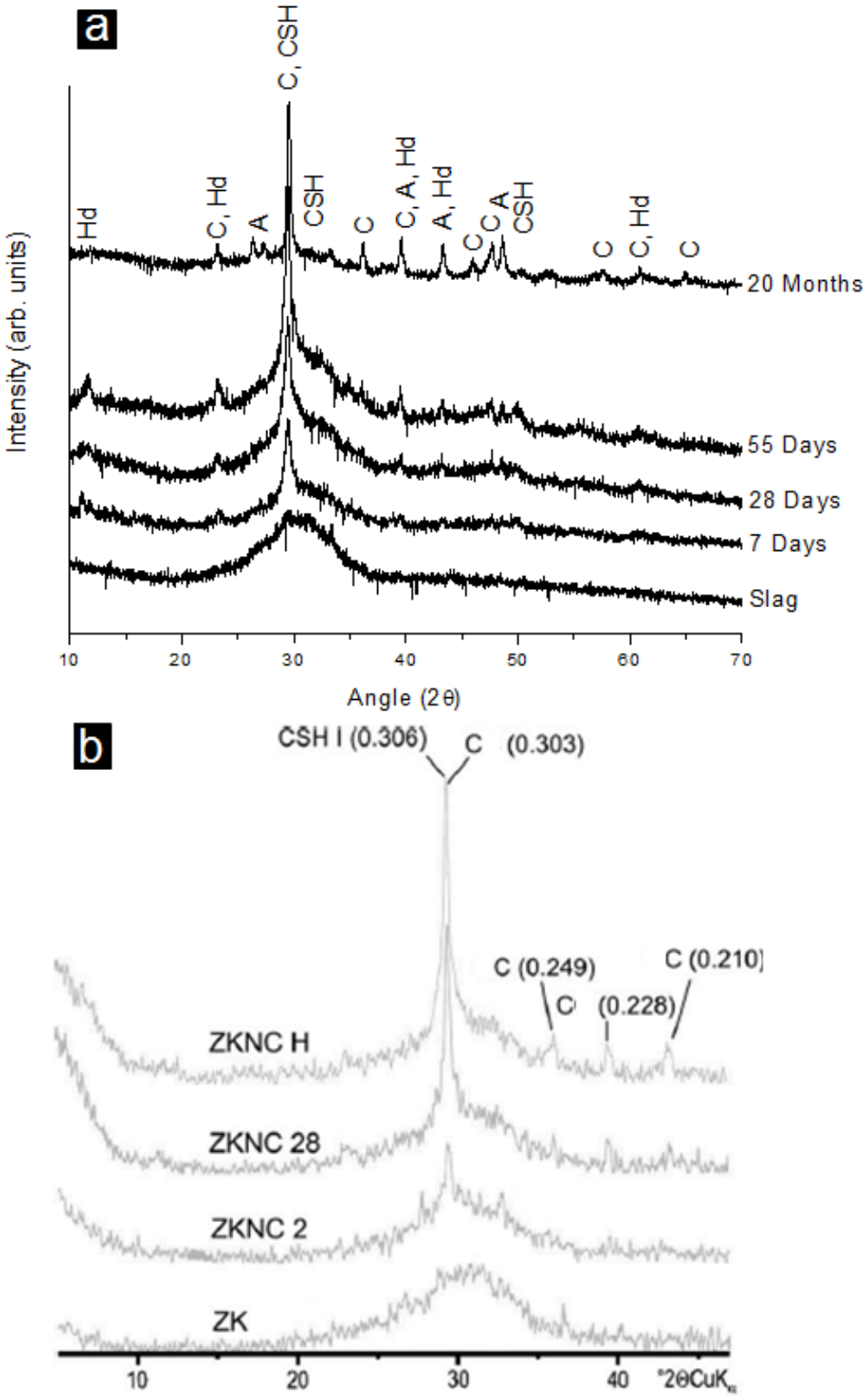

Figure 3.10 – a) XRD diffractograms of the basic Na_2CO_3-activated formula after 7, 28, 55 days and 20 months. B) Diffrctograms of Na_2CO_3-activated formulae at 2 d, 28 d, and after hydrothermal treatment, as reported by Mozgawa *et al*. [70]Diffractograms of raw slag (bottom) provided for comparison. C= Calcite, A = Aragonite, Hd = Hydrotalcite, CSH = Calcium Silicate Hydrate (C-S-H.)

It is, therefore, likely a mineral side product that plays a perhaps interesting, but not necessarily critical, role in the microstructure of the material.

After 20 months, neither hydrotalcite nor C-S-H are present. Instead, a new set of well-defined, sharp peaks have appeared, all of which can be attributed to one of two polymorphs of $CaCO_3$, calcite and aragonite. The appearance of $CaCO_3$ over time in alkali activated slag cement systems is not unusual, and occurs due to the recarbonation of Ca in the cement by either absorbing CO_2 from the atmosphere or the CO_3^{2-} ions present due to the Na_2CO_3 in the activating solution. As no $CaCO_3$ was observed in the formula that was activated by NaOH/waterglass, the latter is the more likely cause. Finally, while aragonite is unstable at ambient temperature and pressures, it is known to occur in isolated regions such as certain caves and areas of the ocean. It has been reported as occurring in samples taken from plaster mortars in Andalusian palaces [116], as well as in building materials from Ottoman constructions in modern Tunisia [117] and 5-6 year old OPC samples [64]. The presence of aragonite implies that the recarbonation of Na_2CO_3-activated cement is occurring in localized regions, such as the pore solution or the space between sheets of C-S-H, where ‘ambient temperature and pressure’ may not necessarily occur.

The recarbonation of Ca in the C-S-H of cements leads to calcite as well as a decarbonated Si-rich phase. Volume changes between C-S-H and calcite can lead to cracking, deteriorating mechanical properties, as well as, a higher susceptibility to acid attack. On the other hand, it is the mechanism by which basic lime building materials

harden [91], and is proposed as the mechanism by which certain ancient building materials gained strength [118].

Xu *et al* detected calcite [21] via XRD in samples poured in the 1960s; these samples still showed satisfactory mechanical properties. In a review of cement work in Britain, Osborne [119] concludes that adding slag to OPC increases the risk of recarbonation and the associated damaging side effects only in special situations or environments. Vaterite, another polymorph of calcite, similar to aragonite, was produced by Rajaokarivony-Andriambololona *et al.* [52] in AAS materials, and observed by Stepkowska *et al.* [64] in aged OPC pastes, however, the former required the use of elevated temperatures. The connection between recarbonation and the choice of activator, as opposed to atmospheric CO_2, appears not to have been previously mentioned. At 20 months, there were not sufficient samples for mechanical characterization. However, the works mentioned above show that, even with recarbonation, slag cements can last effectively for many decades. Lowering the amount of activator used here is one possible method that could counteract recarbonation at later ages.

Recarbonation would have one definite negative effect, however: if the process described by Fernández-Jiménez *et al*. is indeed taking place, wherein carbonate ions continue to increase strength by continuing to dissolve slag and create calcium aluminate carbonate phases, locking carbonate ions up in calcite would hamper continued strength increases. On the other hand, if Xu *et al.* are correct and calcite is simply a step in a cyclic process (Ca and Si dissolve from slag to create calcite and dissolved Si species; at a certain saturation of Si, C-S-H is formed, releasing the carbonate ion to dissolve more

Ca and Si from the slag, and so on), then recarbonation is not a worry so much as a guarantee of future strength. This process is discussed further in the EDS section below.

3.2.3 – FTIR (Cement Paste)

The FTIR spectrum of the Na_2CO_3 activated formula (Fig. 3.3) was quite similar to that of the NaOH/waterglass activated formula. There were, however, a few differences: the peak at 1426 cm^{-1} due to the bonding in CO_3^{2-} ions, indicating the presence of some sort of carbonated mineral, is more intense and shifted to a slightly higher wavenumber than that of the NaOH/waterglass formula. This is almost certainly due to the presence of carbonate ions introduced with the activator. It is possible that this is indicative of $CaCO_3$, as the peak at 30^o 2θ in the XRD is sharper than that of the NaOH/waterglass activated formula; it is, however, not conclusive. A peak corresponding to out of plane Si-O bending, centered around 530 cm^{-1} in the NaOH/waterglass activated formula, appears more as a shoulder than a distinct peak for the Na_2CO_3 activated formula, likely due to lower quantities of Si (waterglass was not used.)

The FTIR spectrum of the Na_2CO_3 activated formula after 55 d of curing was essentially the same, with only some minor shifting of peak positions. After 20 months, the Si-O bending peak at 530 cm^{-1} has shifted to a slightly lower wavenumber, while the stretching peak at 960 cm^{-1} has shifted slightly higher

For reasons described more elaborately described in the FTIR section of the NaOH/waterglass formula, these FTIR spectra are interpreted as representative of C-S-H; the shifting of peak position is interpreted as Si entering more ordered environments, specifically, the Si-rich gel portion of the C-S-H is continuing to polymerize.

3.2.4 – SEM (Cement Paste and Fine Aggregate Concrete)

As with the NaOH/waterglass activated formula, three regions (Op, unreacted slag, and an Ip around grains of unreacted slag visible only at high contrast) were observed (Fig 3.4b.) Also, large particles of aggregate were clearly evident in concrete samples (Fig 3.6.) BSE images were investigated after 7 d as well as 20 months using automated image analysis software, which determines the percentage of unreacted slag in pure cement pastes (Table 3.2.) The Na_2CO_3 activated formula went from 42 ± 3 vol.% of unreacted slag at 7 d to 27 ± 1 vol.% after 20 months. While these numbers are only estimates of the unreacted slag content, the same caveat as above applying, it is clear that over the course of the first 20 months, slag in the Na_2CO_3 activated formula continues to react. Little change was seen in the average size of unreacted slag particles in the Na_2CO_3 activated formula: it varied only from 1.8 ± 0.4 μm^2 after 7 d to 2.1 ± 0.3 μm^2 after 20 months.

3.2.5 – EDS (Cement Paste and Fine Aggregate Concrete)

For the Na_2CO_3-activated formula, the data from the center of the unreacted slag particles are clustered tightly together; data for the Ip have a wider scatter. The data for the Op are scattered at 7 d and clustered more tightly at 20 m. The concentration of Na is essentially constant (3.5 ± 0.3 at.%.) Regardless of age, the Si/Ca ratios (Fig. 3.11a) follows the same general trend as that of the NaOH/waterglass activated formula: that of a line (the Ip) connecting two points (the Op, with low Ca and high Si, and the unreacted slag, with high Si and Ca.) Again, the center of the unreacted slag particles are tightly grouped around a value of about Si/Ca = 0.8, which is in agreement with the value expected based on both EDS or XRF analysis (Table 2.2.) The Ip runs from a value of

Si/Ca = 0.8 (in the slag) to around Si/Ca = 1.3 (in the Ip), ending with a Si/Ca ratio of between Si/Ca = 1 to 8 (after 7 d) and at roughly Si/Ca = 1 (after 20 months.) The reason for the greater amount of scatter in the Na_2CO_3 activated formula is not clear, but the

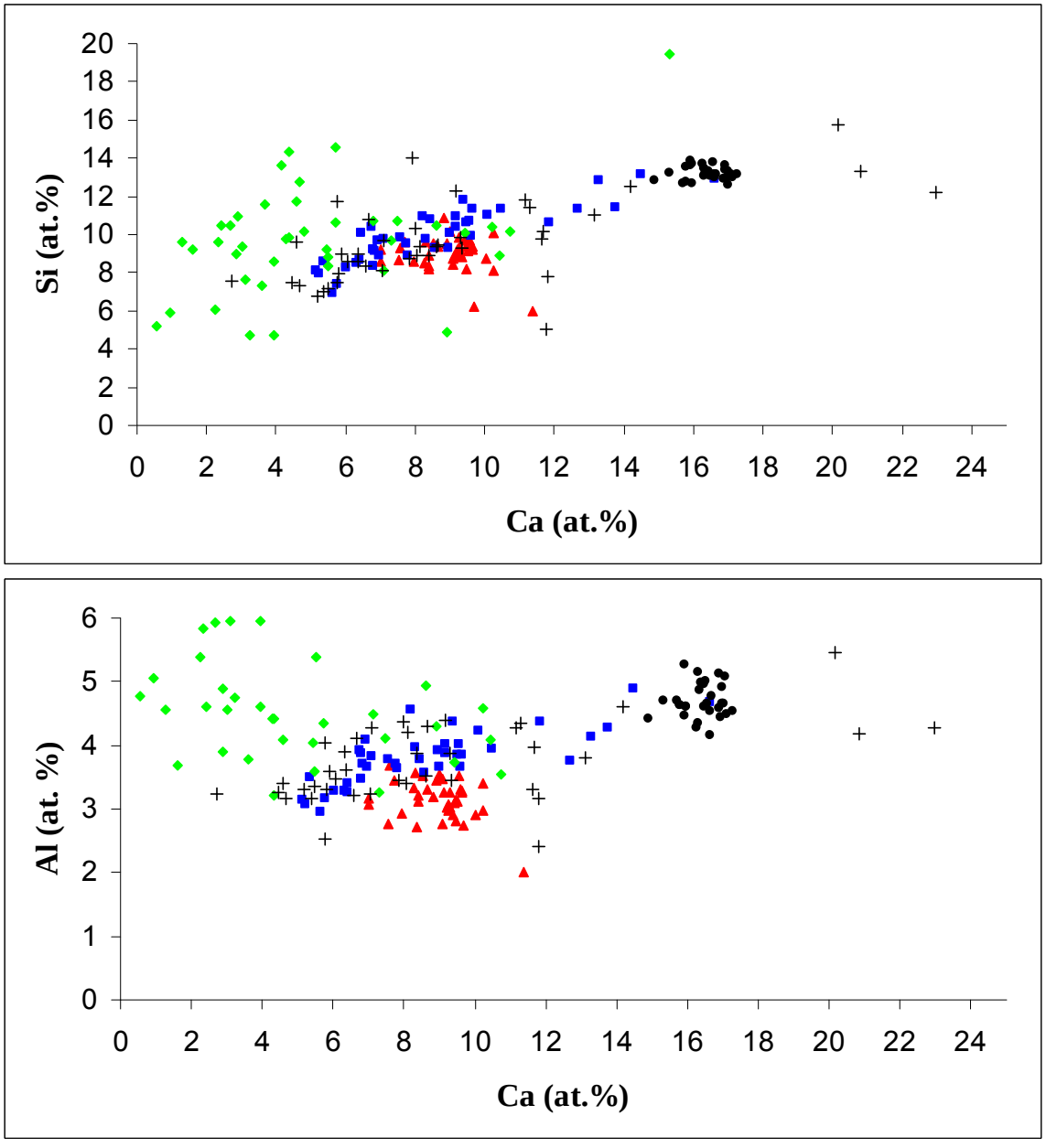

Figure 3.11 – Elemental analysis of the Na_2CO_3 activated cement formula: Si/Ca and Al/Ca concentrations of slag (●), Ip after 7 d (+) and 20 months (□), and Op after 7 d (x) and 20 months (Δ), as determined by EDS.

trend of Ca and Al decreasing from slag to Op, as well as Ca increasing over the 20 month time period, remains clear.

A similar trend is observed in the Al/Ca ratios (Fig. 3.11b), where the Ip is a line that runs from the unreacted slag (high Al and Ca) to the Op (lower amounts of each.) In the Na_2CO_3 activated formula (Fig. 3.11b), data again shows a great deal more scatter. From a ratio of Al/Ca = 4 in the unreacted slag, the Ip is a line that runs to about Al/Ca = 0.8, with the Op having Al/Ca = 0.3 after 20 months. After 7 d the values for the Op are fairly scattered, however, they seem to be vaguely centered around Al/Ca = 1. As before, why the Op contains more Ca than the Ip in some cases is not clear. The Ca concentration in the Ip and Ops are roughly the same (and lower than in the unreacted slag) and again, only a slight drop in Al content is seen.

In a recent paper, Xu *et al*. [21] performed chemical characterization on 5 AAS cements produced between 1964 and 1982, activated by at least 85% Na_2CO_3, the remainder generally being NaOH. All were taken from field service locations and were noted to have a 'good' appearance (i.e. no cracking, alkali-aggregate reaction, etc.) Four of the five samples followed the trends seen here: decreasing Ca and Si going from the unreacted slag, through the Ip to the Op.

The first sample, purely Na_2CO_3 activated (the original slag contained 5% more of both Ca and Si than that used here) from an irrigation chute, had a Ca/Si ratio of 1.3 in the Ip and 1.2 in the Op. Here, the Na_2CO_3 activated formula had a Ca/Si ratio of 0.9 in the Ip at 7 d (0.8 at 20 months) and 0.5 in the Op at 7 d (increasing to 1 at 20 months.) These numbers are lower than those reported by Xu et al.; however, the Ca/Si ratio in the unreacted slag here is also lower than what they report. Different starting slag chemistries

is a more likely cause than an increase in the ratio over time (their sample being roughly 520 months older than the one reported here.) The rest of their samples (one with 15% K_2CO_3, one with 15% NaOH and some $Ca(OH)_2$, and two with 15% NaOH in place of Na_2CO_3 in the activators) have Ca/Si ratios that vary from 1 to 2 in the slag, Op, and Ip. It should be noted that comparisons are complicated by the variety of slag compositions (going as high as 55 % Ca and 39 % Si, compared to the 42 % and 35 % used in this work), by one sample that had Ca in its activator, and by one sample containing coarse slag aggregate.

The results presented here, therefore, fall in the general range described by Xu *et al*. In their paper, they speculate (as do Brough *et al.*) that while NaOH-activated samples have superior early strength, the carbonate ion in the Na_2CO_3 activating solution may play an important role by continuing to dissolve slag, resulting in continual strength increases. As evidence that this may be true, they show a very thoroughly hydrated slag particle with a wide Ip, as well as a quartz particle with a hydrated outer layer (due to the leaching of Si.)

Their proposed mechanism is essentially that carbonate ions strip Ca from the slag to produce $CaCO_3$; hydroxide ions then strip both Ca and Si from the slag until Si reaches a saturation point, where it begins to behave as an acid, stripping Ca from the $CaCO_3$ and forming C-S-H, while also leaving the original carbonate ion free to begin attacking the slag particle once again. In this manner, $CaCO_3$ is simply a step in a cyclic process which leads to continuous production of C-S-H over time, and thus may continue increasing strength. That the $CaCO_3$ seen here is the less-stable aragonite, as opposed to calcite, may be a point in favor of this process, as it would more easily give up Ca to

form C-S-H. This, however, is hypothetical. That this process would limit the amount of recarbonation (as some $CaCO_3$ molecules are created, others are destroyed to form C-S-H) seems likely in theory, but the effect of this and of such cyclic volume changes (if any) on long-term strength is not clear, and was not the focus of this study.

The mechanism of continued reactions cannot be commented on here; however, the EDS results confirm that between 7 d and 20 months the amount of Ca in the Op increases and FTIR confirms that Si moves into a more 'ordered' structure. The conclusion can thus be drawn that, in the Na_2CO_3 activated formula, the reactions do indeed continue over time. This was also seen, but only to a lower degree, in the NaOH/waterglass activated samples above. This cyclic mechanism may also be a part of the cause of the high Si:Ca ratios seen in the Op of both cements; if the Si must reach a saturation point before it can attack the $CaCO_3$ and form C-S-H, there would be good reason for higher than normal levels of Si in the cements.

At both ages samples containing fine limestone aggregate were also investigated by this method (Table 3.4.) Analyzing cement paste in close proximity to aggregate particles was avoided, to ensure the chemistries were representative of the cementing phase and not of the aggregate, but aggregate contributing to the signal cannot be discounted. The Na_2CO_3 activated formula concrete was a little more complex (Table 3.4) than the NaOH/waterglass activated formula. The Ip of the concrete corresponds well to the Ip of the cement paste, both in terms of elemental distribution and Ca/Si and Ca/Al ratios. In the Op, however, there are a number of differences. Both Mg and Si show slight rises within the standard deviation, while Al and Na show modest changes (+1.4 and -1.6 at.%, respectively.) The main changes are in C (+5.2 at.%), O (-5.2 at.%)

and Ca (-3.7 at.%) The reasons for this change, and the effect it may have on the chemistry or overall strength of the concrete compared to that of the cement paste are unclear, but are likely to be negligible. The accuracy of EDS, combined with likely slightly different hydration conditions and the presence of aggregate possibly impinging on the EDS interaction volume make analysis difficult for such small numbers. Due to the lower amount of Ca in the Op, the Ca/Si and Ca/Al ratios are roughly half of what they were in the Op of the cement paste.

3.2.6 – TGA (Cement Paste)

The TGA curves of the Na_2CO_3 activated formula (Fig. 3.9) were quite similar to those of the NaOH/waterglass activated formula, however, a third region was now apparent: a sharp weight loss between 550 and 650 °C, presumably due to the calcination of poorly crystallized $CaCO_3$, produced by recarbonation and confirmed by both XRD and FTIR. At 7 d the differences between the curves of the two basic formulae were negligible, however, after 20 months, the Na_2CO_3-activated formula lost ~ 5 wt.% less in the range due to unbound water (or, possibly, low in the range due to bound water.) This could possibly be due to a different distribution of pore sizes, thus facilitating natural evaporation in the Na_2CO_3-activated formula, but this is speculation. The exact reason remains unclear, as the transitions between weight loss due to different causes are not sharp enough for definite identification. As before, TGA can neither rule out nor positively show the presence of 'geopolymers.'

3.2.7 – Conclusions

The second basic formula, activated by Na_2CO_3, while not as strong as the formula activated by NaOH/waterglass, still has a sufficiently high compressive strength

to suggest a wide range of possible applications. The lower strength is due to a lack of high pH provided by NaOH (ensuring rapid dissolution of slag) and a lack of the abundance of Si from waterglass (assuring rapid formation of C-S-H and possibly a Si-gel reported to densify the overall system.) However, this lowering of strength is somewhat mitigated by being more environmentally friendly, less dangerous to handle, cheaper, and all around more practical. Further, over long time scales, EDS and FTIR have shown reactions in the cement to continue, possibly leading to higher long-term strengths.

XRD unambiguously shows the presence of C-S-H and hydrotalcite, and is supported by FTIR and TGA. No evidence for 'geopolymers' was observed, though they cannot be ruled out. Some minor differences are seen between the elemental analyses of the cement paste and concrete, the reasons for which are unclear. Recarbonation occurs in this formula by the age of 20 months; this is most likely from carbonate ions introduced in the activating solution, as this behavior was not seen in the NaOH/waterglass activated formula, and may or may not have an adverse effect on long term strength.

As before, the cementing phase was observed to be homogeneous; the same microstructure as the previous formula (Op, Ip, unreacted slag, and aggregate) was again observed. Si/Ca ratios in the Op varied from 0.5 – 1. Again, the general trend of unreacted slag clustered in one position, with the Ip as a line pointing in the general direction of the Op was apparent.

3.3 – TGA-Based Speculation (Cement Paste)

High and low estimates for unbound water, C-S-H dehydration, and $CaCO_3$ decarbonation from TGA data are given in Table 3.5. High and low estimates are given

based on the temperature ranges described in the literature (Table 2.5.) Between 7 d and 20 months, the main changes are a marked drop in unbound water content (from 6-15 wt.% to 2-4 wt.%) and an increase in $CaCO_3$ due to recarbonation (from roughly 1 wt.% to 4 wt.%.) Freeze-drying the samples totally removes the unbound water; other than that, it has little, if any, effect.

If some assumptions are made (i.e., that the weight loss in the unbound water region is due to total evaporation of water; that water makes up 20% of the weight of C-S-H, and that CO_2 makes up 44% of the weight of $CaCO_3$) the total weights of those three phases can be calculated. This data is provided in Table 3.5 and show the various formulae to be 2-3 wt.% unbound water after 20 months (falling from 6-15 wt.% after 7 d); 30-90 wt.% C-S-H; and little, if any $CaCO_3$ due to recarbonation until an age of 20 months, when this value can reach 10 wt.%. That the C-S-H is at one point estimated to be 95 wt.% of a formula, despite the fact that it is known from image analysis that at least 30 vol.% of the cement is unreacted slag, illustrates the limitations of estimating composition by this method.

Table 3.6 – Low and high estimates of weight loss due to unbound water (UBW) evaporation, C-S-H dehydration, and $CaCO_3$ decarbonation for cement paste samples after 1 week of curing, freeze-dried after 1 week of curing (FRZ), and 20 months of curing. All values are weight %.

		UBW Low	UBW High	CSH Low	CSH High	$CaCO_3$ Low	$CaCO_3$ High
Sample	Age	<105 °C	<120 °C	105<400 °C	105<600 °C	>700 °C	>600 °C
A	1 wk	6	9	10	13	1	1
A+DE	1 wk	6	9	13	17	1	1
B	1 wk	9	10	9	12	1	1
B+DE	1 wk	11	14	12	15	1	1
A FRZ	1 wk	1	1	8	12	1	1
A+DE FRZ	1 wk	1	1	9	15	1	1
B FRZ	1 wk	1	2	9	12	1	1
B+DE FRZ	1 wk	1	2	11	12	1	1

A	20 mo.	3	4	8	14	1	3
A+DE	20 mo.	3	4	13	19	1	1
B	20 mo.	2	3	6	14	1	4
B+DE	20 mo.	2	3	6	14	1	3

3.4 – Conclusions

Two basic alkali-activated slag cements and fine limestone aggregate concretes were prepared. Regardless of activator, strengths were sufficiently high after 7 days (or even after a few hours for the NaOH/waterglass activated formula) for a wide range of applications. XRD identified C-S-H as the main binding phase, confirmed by FTIR and TGA, likely coupled with an amorphous Si gel. Evidence for the presence of 'geopolymers' was not found but cannot be totally ruled out. The Op of the cement appears homogeneous by SEM. Recarbonation occurs over 20 months in the formula activated by Na_2CO_3.

From EDS, the exact final disposition of the Na ion is unclear, but could replace Ca in C-S-H, form mineral side products (such as hydrotalcite), or could congregate in the pore solution, and so on. Extremely high Si/Ca ratios in the NaOH/waterglass formula are due to additional Si provided by the waterglass used here. The Si/Ca ratios for the Na_2CO_3 formula are generally similar to those reported in the literature. Finally, this formula shows ample evidence by EDS and FTIR that reactions continue over long time scales, thus increasing the amount of C-S-H and possibly increasing strength.

Due to limitations of every analysis method used here, a single method is insufficient for characterizing alkali-activated slag based materials. It is therefore suggested that a complimentary suite of techniques, as used here, always be used.

CHAPTER 4: MECHANICAL AND MICROSTRUCTURAL CHARACTERIZATION OF AAS CEMENTS WITH VARIOUS ADDITIVES (NaCl, DE, FLY ASH, METAKAOLIN, ACID ROCK SLUDGE)

4.1 – Addition of NaCl (Fine Aggregate Concrete)

NaCl was added in an effort to retard the set time of the NaOH/waterglass activated formulae, which was approximately 5 minutes. This had the desired effect, with set time increasing to 30 minutes with the addition of 20 wt.% of the weight of the slag. Lower amounts of NaCl did not significantly increase set time (Fig. 4.1.) The NaCl was added as a powder with the other powdered reactants, in an effort to produce a 'one bag' material. It is known [46] that had the NaCl been pre-dissolved instead of by being added directly to the activating solution, its effectiveness would have been increased.

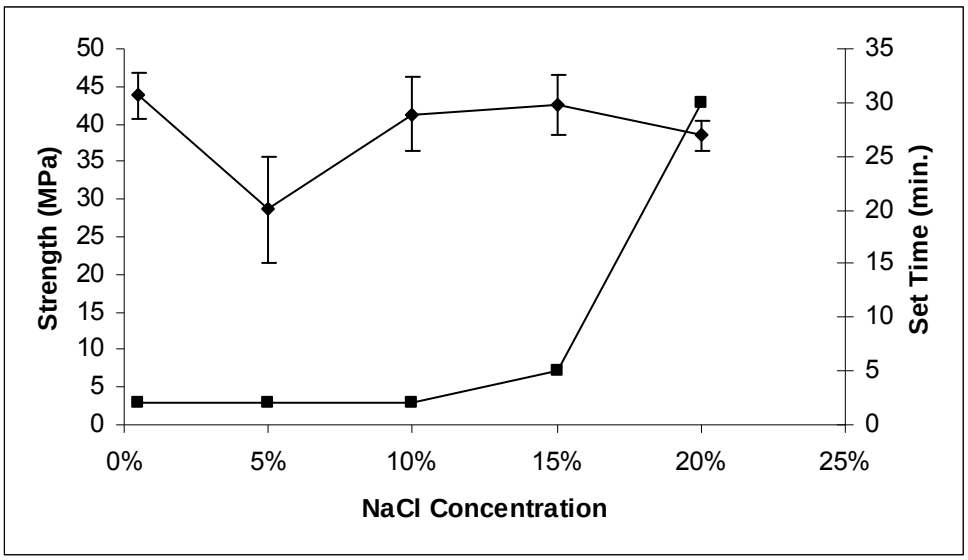

Figure 4.1 – Effect of NaCl addition on strength and set time.

4.1.1 – Mechanical Properties (Fine Aggregate Concrete)

Samples of NaCl containing concrete were tested with the ends ground to ensure parallelism (Fig. 3.1.) At 1 d, the strength of the NaOH/waterglass activated formula was

only 20 ± 2 MPa, rising to 38 ± 4 MPa after 7 d and attaining 46 ± 7 MPa after 28 d. Although the strength gain is much slower compared to the basic formula after 28 d the strength reached the level of the unadulterated formula.

NaCl was also added to the Na_2CO_3 activated formulae for comparison purposes, although this formula has a sufficiently long set time. After 1 d, the strength was still negligible, rising to 17.3 ± 0.4 MPa after 7 d and 30 ± 1 MPa after 28 d (Fig. 3.1.) Although this strength is only 81.6 % of the basic formula after the same length of time, it is likely that the samples would have continued to gain strength and eventually level off with no net loss.

The addition of NaCl had the curious effect of scrambling the data as regards the tensile strengths of the samples (Tables 3.1 and 3.3.) For formulae activated by NaOH/waterglass, the addition of NaCl resulted in an increase from 1.7 ± 0.2 MPa at 1 d to 3.5 ± 0.6 MPa at 28 d; however, when taken as percent of compressive strength, this is a decrease from 8.6% to 7.9 %, going through 6.3% after 7 d. For the Na_2CO_3 activated formula, a similar trend is observed. Although the tensile splitting strength increases from 0 at 1 day to 1.8 ± 0.2 MPa and 2.0 ± 0.2 MPa, at 7 and 28 d, respectively, this represents a drop from 9.6 % of compressive strength at 7 d to 6.9 % of compressive strength at 28 d. These trends are surely due to the difference in strength gain due to the use of NaCl as a retardant, which suppresses early (but not final) compressive strength, while not severely curtailing tensile strengths.

4.1.2 – SEM (Cement Paste and Fine Aggregate Concrete)

Formulae containing NaCl were not investigated with image analysis, as the NaCl would be considered ‘unreacted slag’ by the interpretation program. In the SEM,

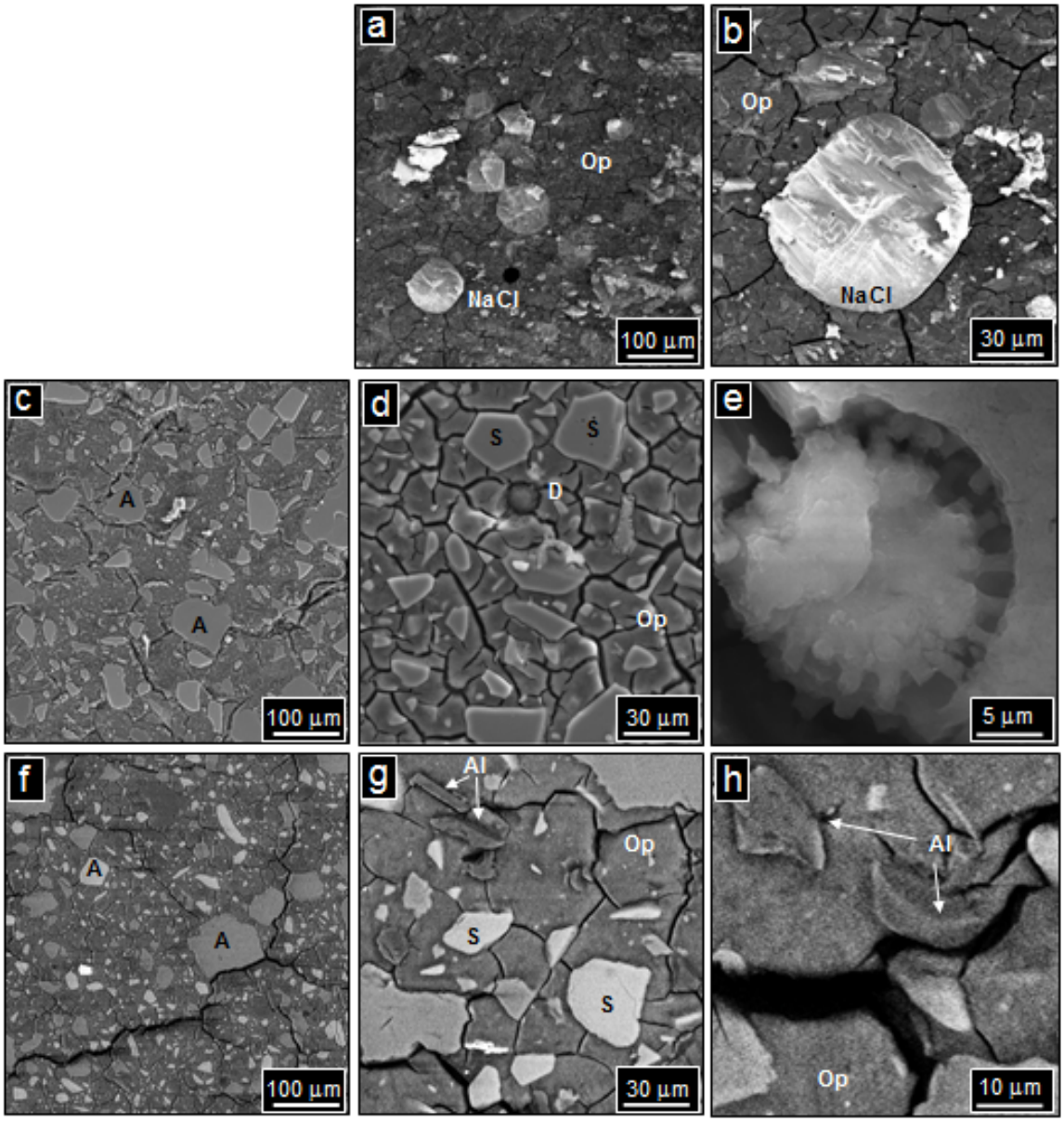

Figure 4.2 – SEM BSE micrographs of alkali activated cement with additives at 28 days. a) Low magnification image of NaOH/waterglass based formula with several large particles of undissolved NaCl; b) Higher magnification image of individual unreacted NaCl particle; c) low magnification image of basic formula containing DE and fine limestone aggregate; d) higher magnification image of basic formula containing DE, showing unreacted slag, outer product, and an undissolved diatom; e) high magnification image of a partially dissolved diatom; f) basic formula containing Al_2O_3 and fine limestone aggregate; g) higher magnification image in which unreacted slag, outer product, and unreacted Al_2O_3 are evident; h) high magnification image showing unreacted alumina. A = aggregate, S = unreacted slag, Op = outer product, D = diatomaceous earth, and Al = unreacted Al_2O_3.

however, unreacted NaCl particles appeared as large, light-colored spheres (Fig. 4.2a) and were not difficult to spot. At higher magnification (Fig. 4.2b) they appeared as solid, poorly polished areas, not dissimilar to aggregate. Had the NaCl been added to the activating solution rather than mixed in with the powders, and thus been entirely dissolved, it is unlikely that it would have appeared in this form. Little, if any, difference was noted between NaCl particles in the NaOH/waterglass and Na_2CO_3 activated formulae.

4.1.3 – Conclusions

Clearly, NaCl is not the perfect retardant and, in fact, could pose substantial problems if metal reinforcement of the cement is used. However, it can be concluded that NaCl would be a good retardant for use in developing nations or in applications where metal reinforcement is not used. Chang *et al*. [120, 121] described the use of phosphoric acid in retarding the setting of slag cement; though it had no adverse effects and created no new phases in the cement, it is more expensive than NaCl, a corrosive material, and Chang's study showed it to be highly temperamental: increasing the concentration of phosphoric acid from 0.84 M to 0.87 M increased set time from 1 h to 6 h, much more than would be needed. Gong *et al*. [122] investigated the use of sodium phosphate as a retardant in slag/red mud mixtures (red mud being similar to slag, but with less Si and more Fe), finding that 2 wt.% increased set times by 4 h. Unfortunately, it also created a new phase, which could interfere with future properties. Finally, Brough *et al.* [46] investigated the use of both NaCl and malic acid; both were shown to be effective retarders, with neither the cost nor safety worries of phosphoric acid or sodium phosphate; as NaCl is the more common of the two, it was chosen here for investigation.

Adding the NaCl to the other powdered reactants in order to have a 'one bag' approach is possible, but demands the use of more NaCl; if the salt is added to the activating solution, it would ensure total dissolution and less could be used. Finally, while the long term effects are not known and were not investigated here, over the course of the first 28 d, NaCl does not seem to have a deleterious effect on strength. XRD analyses (not shown) showed no new crystalline products, aside from halite (NaCl), while FTIR spectra (also not shown) were identical, as NaCl is infrared transparent. It is possible that, to lower the total amount of NaCl needed and reduce the stress on potable water sources, seawater could be used.

4.2 – Addition of Diatomaceous Earth

Diatomaceous earth (DE) an amorphous form of silica, was added to both of the basic formulae in order to encourage either the formation of additional C-S-H or 'geopolymers' through the presence of extra Si.

4.2.1 – Mechanical Properties (Fine Aggregate Concrete)

For the NaOH/waterglass activated formula, the addition of DE had only a slight effect on strength (Fig. 3.1.) These samples were tested using the end-grinding method that had previously produced lower strengths in the basic formula (compared to the use of steel caps.) From 31 ± 6 MPa after 1 d, to 50 ± 1 MPa after 7 d and 48 ± 3 MPa after 28 d, the final strengths of the samples with added DE end at a little under 104 % of the unadulterated samples.

The basic formula with added DE was also investigated with added NaCl as a retardant, as the addition of DE did not slow the set time. As with the addition of NaCl to the unadulterated formula, the strength after 1 d is lower, at 18 ± 1 MPa, 35 ± 5 MPa after

7 d, and 28 ± 1 MPa after 28 d. This number is only 61 % of the final strength of the basic formula, likely due to the compounding effect of NaCl and DE both lowering early strength.

When added to Na_2CO_3 activated solutions, DE had a similar effect (Fig. 3.1.) From no strength after 1 d, to 29 ± 3 MPa after 7 d and 39 ± 3 MPa after 28 d, DE provided an 8 % increase over the basic formula at the same age. With the addition of NaCl, however, lower strengths are again seen: 24 ± 5 MPa after 7 d and 23 ± 4 MPa after 28 d, a drop of 38 % with no apparent increase in the already long set time.

The effect of adding DE on tensile splitting strength (Tables 3.1 and 3.3.) is not entirely clear. For the NaOH/waterglass activated formula, the tensile splitting strength drops from 2.7 ± 0.5 MPa after 1 d to 2.3 ± 0.5 MPa after 28 d, however, it goes through a maximum of 3.0 ± 0.4 MPa after 7 d. In terms of percentage of compressive strength, this is a steady decrease from 8.7% to 4.8 %. The same is true for the Na_2CO_3 activated formula. Although it increases from 0 MPa at 1 day (the samples had not yet set) to 2.0 ± 0.1 MPa after 7 d and 2.2 ± 0.6 after 28 d, this represents a decrease from 6.8 % to 5.6 % of compressive strength between 7 and 28 d. As with the addition of NaCl, this confusion is likely due to the retarding effect of DE, which delays the bulk of strength gain until after the first day.

When DE is added to a formula that also contains NaCl as retardant, similar high-low-medium behavior is seen (Tables 3.1 and 3.3), although the tensile splitting strength in terms of MPa continuously increases: from 1.8 ± 0.5 MPa after 1 d to 2.4 ± 0.5 MPa after 28 d for the NaOH/waterglass activated formula, and from 0 MPa after 1 day to 2.9 ± 0.6 MPa after 28 d for the Na_2CO_3 activated formulae.

4.2.2 – XRD (Cement Paste)

Regardless of activator, the addition of DE (Figs. 4.3 and 4.4) had no effect on the number, size, or position of peaks in the diffractograms of the base formula at any age. The DE itself is amorphous, and the peaks corresponding to minor impurities (which are now a small fraction of a small fraction of the cement) are likely too small to be recognized. As was explained above, the preferred explanation for these diffractograms is C-S-H, coupled with hydrotalcite at early ages and $CaCO_3$ at later ages in the Na_2CO_3 activated formulae.

4.2.3 – FTIR (Cement Paste)

The FTIR spectra of formulae containing diatomaceous earth (Figs 4.5 and 4.6, top spectra) were very similar to spectra without DE, regardless of activator. The main difference was the peak at 960 cm^{-1}, indicating the stretching vibrations of silica tetrahedra of various coordination states, which became somewhat wider and deeper. This is most likely due to unreacted DE, which provides plenty of Si-O and O-Si-O bonds to affect the spectra; this widening of the bands makes it somewhat more difficult to determine whether or not the peak positions have shifted, and thus track the progress of the reaction. As with XRD, the arguments made above still stand in terms of identification of the spectra; while they cannot differentiate between C-S-H and 'geopolymers,' when taken with all other evidence, it indicates poorly crystalline C-S-H with substantial modification to the Si-O bonds, due to unreacted DE and Si-rich gel.

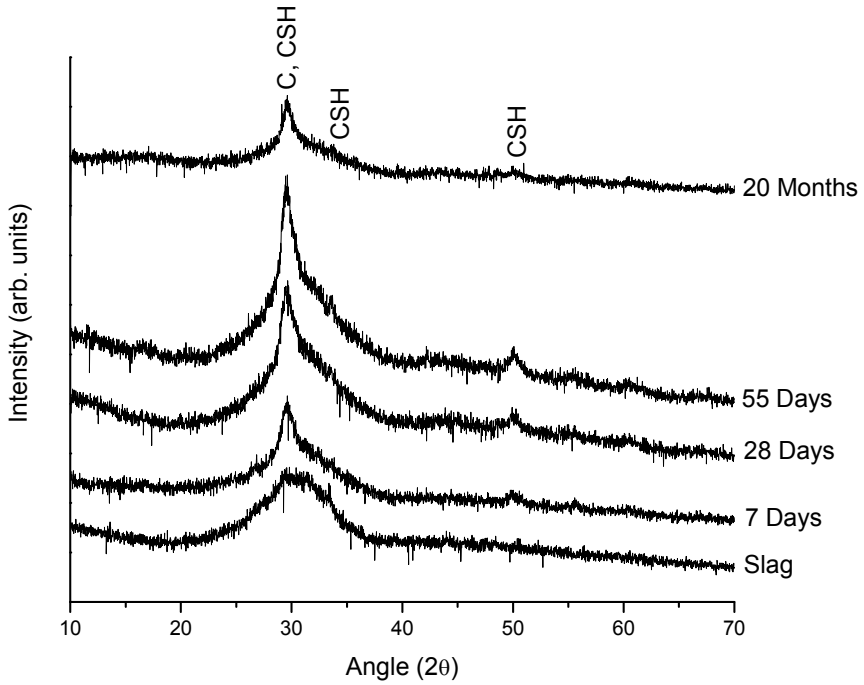

Figure 4.3 – XRD diffractograms of the NaOH/waterglass activated formula with the addition of diatomaceous earth after 7, 28, 55 days and 20 months. Diffractogram of raw slag (bottom) provided for comparison. C = Calcite, CSH = Calcium Silicate Hydrate (C-S-H.)

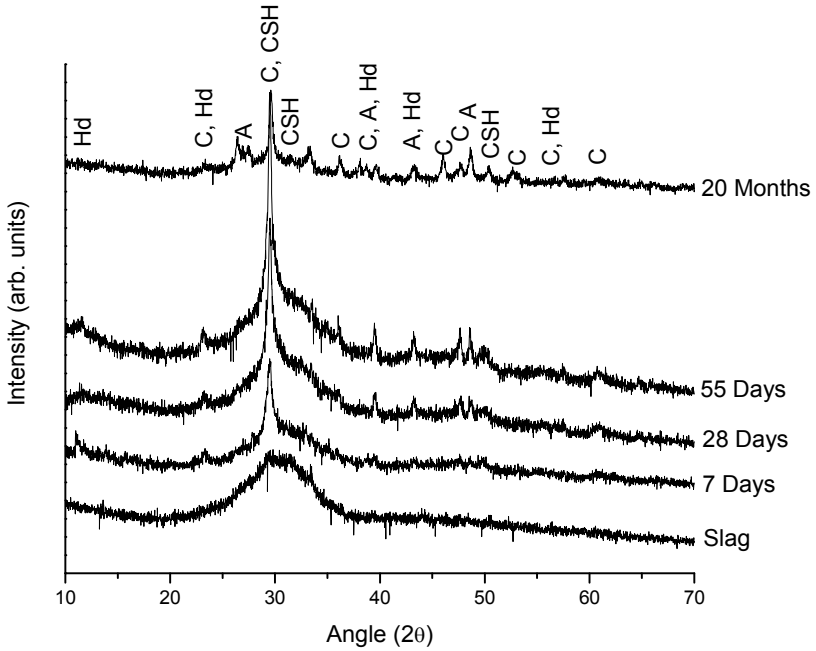

Figure 4.4 – XRD diffractograms of the Na_2CO_3 activated formula with the addition of diatomaceous earth after 7, 28, 55 days and 20 months. Diffractogram of raw slag (bottom) provided for comparison. C= Calcite, A = Aragonite, Hd = hydrotalcite, CSH = Calcium Silicate Hydrate (C-S-H.)

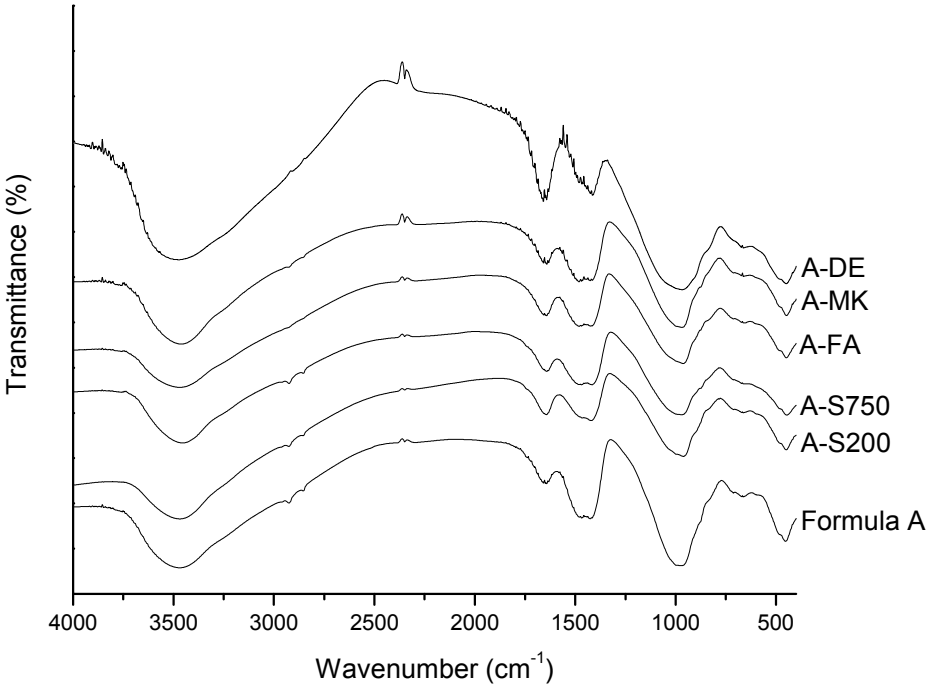

Figure 4.5 – FTIR spectra of NaOH/waterglass activated (formula A) cements at 28 d with various additives: sludge dried at 200 ^{o}C (A-S200) and calcined at 750 ^{o}C (A-S750), fly ash (A-FA), metakaolin (A-MK), and diatomaceous earth (A-DE.)

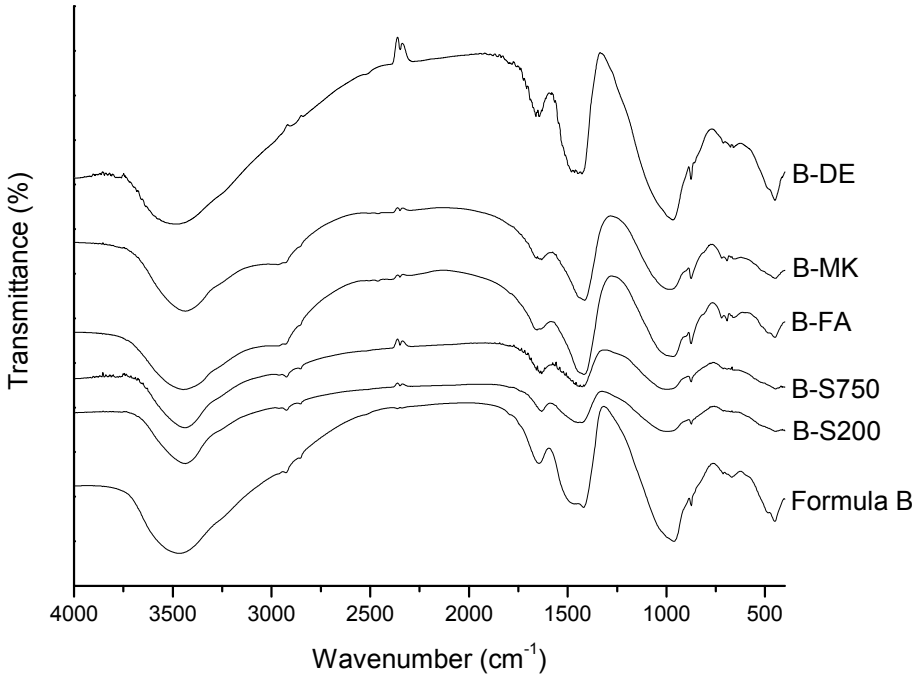

Figure 4.6 – FTIR spectra of Na_2CO_3 activated (formula B) cements at 28 d with various additives: sludge dried at 200 ^{o}C (B-S200) and calcined at 750 ^{o}C (B-S750), fly ash (B-FA), metakaolin (B-MK), and diatomaceous earth (B-DE.)

4.2.4 – SEM (Cement Paste and Fine Aggregate Concrete)

At any age, at low magnifications of either the concrete (Fig. 4.2c) or the cement paste (Fig. 4.2d), undissolved diatoms were difficult to spot due to their small size and the dominance of such microstructural features as the aggregate. At higher magnification (Fig. 4.2d) they could be found with little difficulty due to their round shape; more often than not, anything at medium magnification that looked like a small black 'o' in an image was an undissolved diatom being viewed end-on. These unreacted diatoms were in evidence even at long ages. At the highest magnifications, the identification of diatoms was certain, as the microstructures associated with the porous nature of the diatoms were obvious (Fig. 4.2e.) That some DE remains undissolved in the solution is quite clear; further, the Op around individual diatoms appears homogenous. Any additional phases in the Op due to extra Si from the diatoms are apparently very similar, morphologically. Finally, no difference was noted between diatoms appearing in the NaOH/waterglass and Na_2CO_3 activated formulae, aside from the differences in the morphology of the Op, as previously noted.

The NaOH/waterglass and Na_2CO_3 activated formula containing DE as an additive were also investigated after 7 d as well as 20 months (Table 3.2) by image analysis. The NaOH/waterglass activated formula with DE decreased only slightly from 23.5 ± 1.2 vol.% unreacted slag at 7 d to 22 ± 1 vol.% at 20 months. The Na_2CO_3 activated formula with DE behaved similarly, falling slightly from 30 ± 4 vol.% after 7 d to 29.5 ± 3 vol.% after 20 months. One caveat is that DE appears in BSE imaging as a

Table 4.1- Concentration of selected elements (at. %) and Ca/Si and Ca/Al ratios of NaOH/waterglass- and Na_2CO_3-activated formulae containing diatomaceous earth at 7 d and 20 months.

NaOH/waterglass +DE	Slag	Inner Product	Outer Product	Inner Product	Outer Product
# of Points	30	40	41	40	40
Al (at.%)	4.6 ± 0.2	3.6 ± 0.5	3.7 ± 0.6	3.8 ± 0.4	3.2 ± 0.2
Si (at. %)	13.2 ± 0.5	11.0 ± 1.6	17.1 ± 3.2	11.2 ± 1.1	16.4± 1.5
Ca (at. %)	16.6 ± 1.2	9.9 ± 2.6	1.3 ± 0.3	10.4 ± 2.4	1.7 ± 0.3
Na (at. %)	0 ± 0	1.3 ± 0.5	3.1 ± 0.7	2.8 ± 1.1	7.1 ± 1.0
Ca/Si	1.3	0.9	0.1	0.9	0.1
Ca/Al	3.6	2.74	0.35	2.8	0.5
Na_2CO_3 + DE	Slag	Inner Product	Outer Product	Inner Product	Outer Product
# of Points	31	40	40	40	40
Al (at.%)	4.6 ± 0.3	3.8 ± 0.7	3.6 ± 0.9	3.8 ± 0.4	2.9 ± 0.3
Si (at. %)	13.2 ± 0.6	10.7 ± 2.4	12 ± 3.3	11.2 ± 1.6	12.4± 1.8
Ca (at. %)	12 ± 1.3	9.7 ± 4.0	5.7 ± 3.3	11.6 ± 2.9	7.9 ± 1.3
Na (at. %)	0 ± 0	1.7 ± 0.8	3.3 ± 1.0	2.2 ± 1.5	3.8 ± 0.4
Ca/Si	1.3	0.91	0.5	1	0.7
Ca/Al	3.7	2.54	1.57	3.1	2.7

darker color, thus making it appear to be cementing phase. However, the relatively small amount of DE does not explain the drop in the amount of unreacted slag at 7 d. The exact reason for this is unclear, but it is possible that extra Si from the DE encourages the production of at least some C-S-H.

The average size of the slag particles in the cements containing DE fell over time, from 4.5 ± 0.5 μm^2 after 7 d down to 0.9 ± 0.1 μm^2 after 20 months for the NaOH/waterglass activated formula, and from 3 ± 3 μm^2 after 7 d down to 1.7 ± 0.2 μm^2 after 20 months (Table 3.2.) As with the formulae without additives, the reason for the discrepancy between change in particle size and change in the amount of unreacted slag is not clear. The caveat made above about image analysis stands.

4.2.5 – EDS (Cement Paste and Fine Aggregate Concrete)

Elemental analyses of the NaOH/waterglass activated cement paste, as well as Na_2CO_3 activated cement paste, containing DE were performed at 7 d and 20 months (Figs 4.7 and 4.8.) Regions close to undissolved diatoms were avoided, however, in the Op of either cement paste at either age the amount of Si shows a marked increase. The Na levels are again roughly the same as in the cement pastes, and the likely final dispositions for Na have not changed (Table 4.1.)

In the NaOH/waterglass activated formula (Fig. 4.7) the increase in Ca between 7 d and 20 months is somewhat less; however, the data also has less scatter. The same trends are observed as in formulae without DE. Between 7 d and 20 months, the Ca increases slightly and the Al concentration becomes more tightly grouped. This implies that the reactions in the Op of the cement continues somewhat between 7 d and 20 months.

In the Na_2CO_3 activated formula (Fig. 4.8) all data have an even greater amount of scatter, making analysis difficult at best. As observed by XRD, this is almost certainly due to a larger number of microconstituents (hydrotalcite, calcite and aragonite at 20 months) making the Op less homogeneous. The 7 d data for the Op show a huge scatter, covering the entire range described by the Ip. Over time the scatter decreases. The same general trends as those seen in the NaOH/waterglass activated formula are observed, but the scatter makes thorough analysis difficult. As before, the reason for this is unclear, but scatter in the 7 d data could be attributed to both larger amounts of

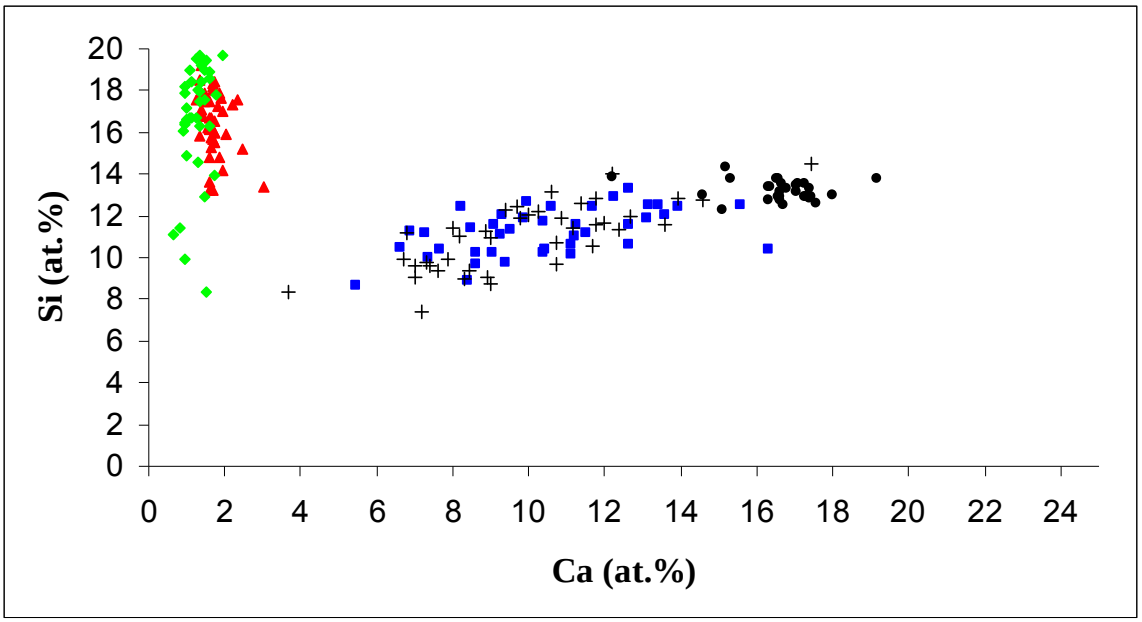

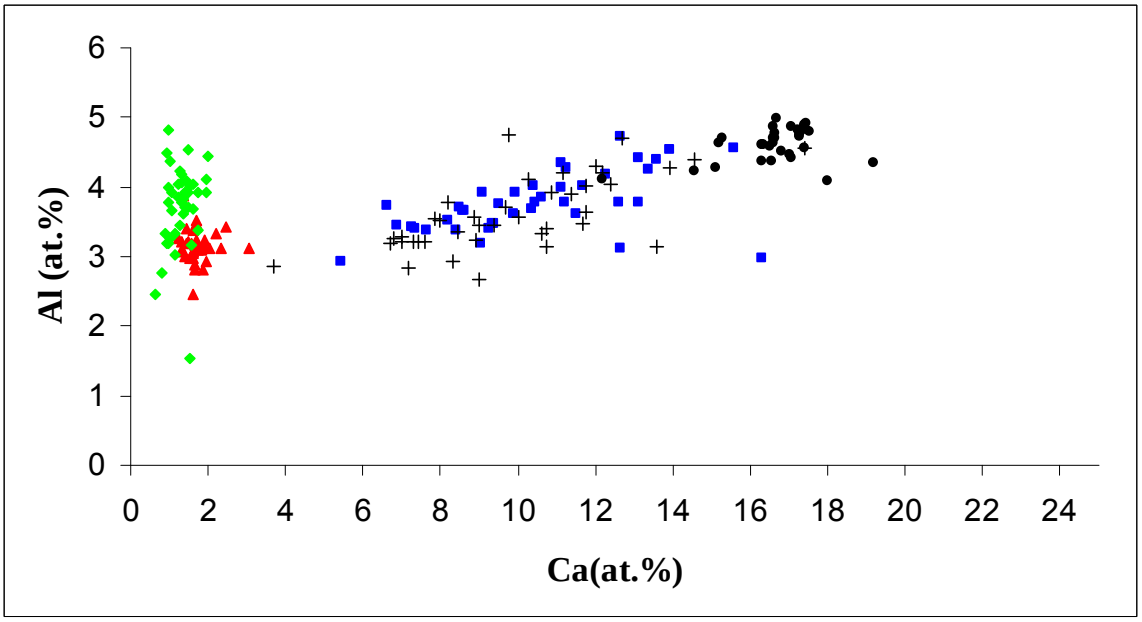

Figure 4.7 – Elemental analysis of the NaOH/waterglass activated cement formula with added DE: Si/Ca and Al/Ca concentrations of slag (●), Ip after 7 d (+) and 20 months (□), and Op after 7 d (x) and 20 months (Δ), as determined by EDS.

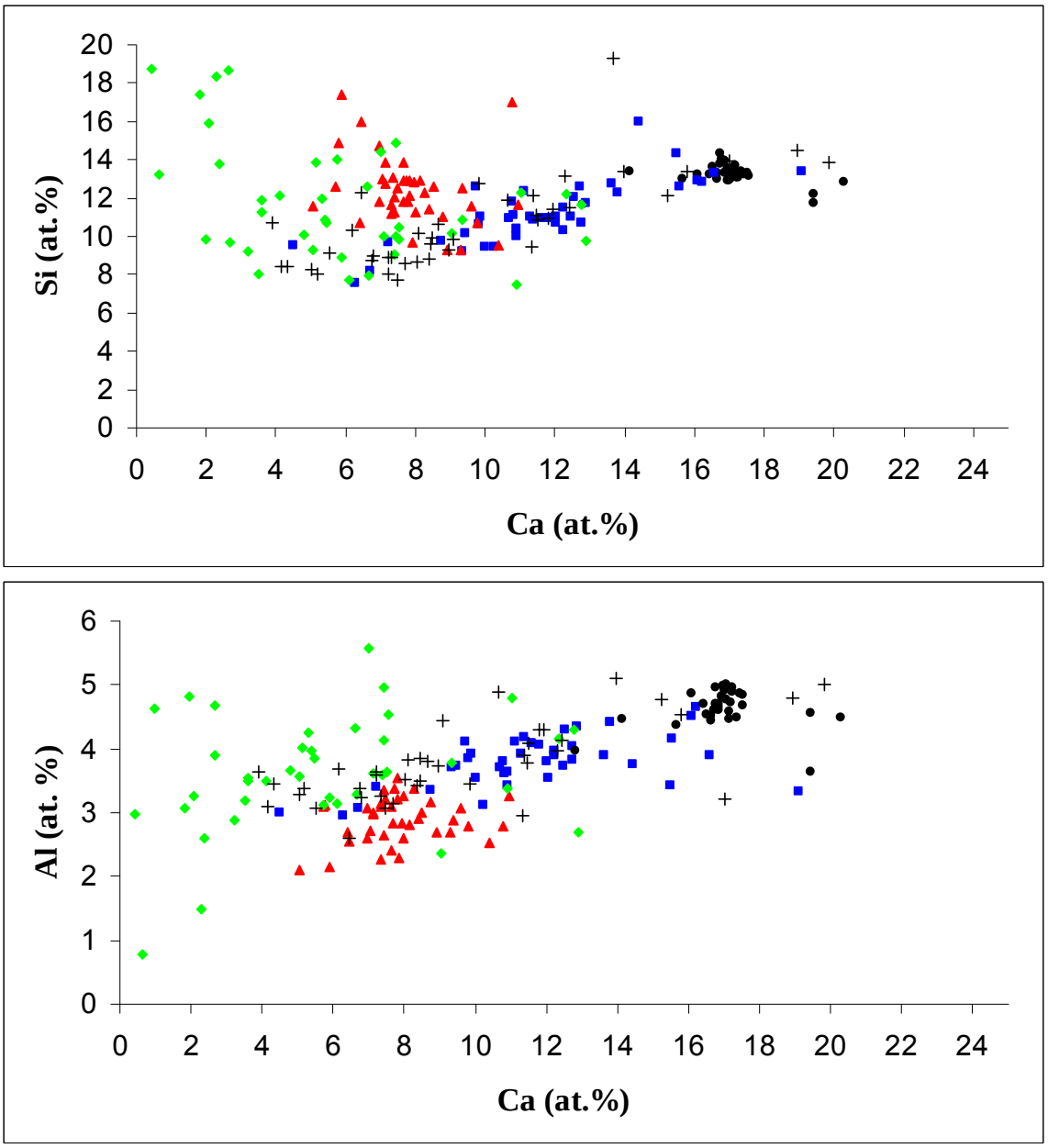

Figure 4.8 – Elemental analysis of the Na_2CO_3 activated cement formula with added DE: Si/Ca and Al/Ca concentrations of slag (●), Ip after 7 d (+) and 20 months (□), and Op after 7 d (x) and 20 months (Δ), as determined by EDS.

unreacted slag than in the NaOH/waterglass activated formula (as seen in image analysis) as well as unreacted diatoms lying under the sample surface and impinging on the interaction volume of the electron beam in addition to the more complicated, less homogenous nature of the Op (hydrotalcite, calcite, etc.)

4.2.6 – TGA (Cement Paste)

The two formulae containing DE were also investigated by TGA after 7 d and 20 months (Fig. 3.9.) At either age, the samples with and without DE looked essentially the same; differences generally amounted to no more than 3 wt.% above 200 ^{o}C. The same regions for the curves of formulae containing DE were observed as in the curves of formulae without DE. The portion of the TGA curve due to unbound water generally dominates the weight loss; the formula with the least water (NaOH/waterglass) has the highest curve/least water loss, and the curves proceed in order of water content to the Na_2CO_3 formula with DE, which has the most water and thus the bottom curve.

After 20 months (Fig. 3.9, upper curves), three regions were now evident. As with the samples that did not contain DE, only 4 – 8 wt.% was lost below 150 ^{o}C, and the samples lost approximately 10 wt. % between 200 and 550 ^{o}C. The Na_2CO_3 activated formula again underwent a weight loss between 550 and 650 °C, due to the presence of $CaCO_3$ from recarbonation. The Na_2CO_3 formulae were ‘drier’ than those activated by NaOH/waterglass at 20 months, despite containing more mixing water. The reason for this is unclear, as the transitions between different regions in the TGA curves are insufficiently well-defined.

4.2.7 – Discussion and Conclusions

This work is somewhat similar to the work of Escalante-García *et al*. [48, 123], who investigated a slag (with somewhat lower Ca than the one used here) containing amorphous, Si-rich waste from a geothermal power station. In the first paper, the slag was activated by a CaO and NaOH solution, along with varying quantities of the waste additive. It was found that, at 5 wt. % waste, the strength increased from ~ 40 MPa at 90 d to ~ 45 d at 90 d. This increase was based on increased Si, and thus the production of more C-S-H, which was confirmed (along with hydrotalcite) by XRD and thermal analysis.

In a second paper, 10 wt.% replacement by the waste increased strength from 30 MPa to 40 MPa at 28 d for a NaOH-activated formula, but decreased strength from 45 MPa to 35 MPa in an NaOH/waterglass activated formula. This was judged to be an effect of the waste material reacting with the activating solution, increasing viscosity, and creating air bubbles. The overall lower strength reported by Escalante-García et al. is likely due to the lower amount of Ca in their slag, and a relatively weaker activating solution, that no new crystalline phases are created, and changing strength by only a few percent. They also report reduced porosity, which was not investigated here, but could be beneficial.

As was seen above, for formulae without DE, the Si/Ca ratios of the Na_2CO_3-activated formulae, as well as those of all Ips, fall roughly within the range described by the literature. The Op of the NaOH/waterglass activated formula shows an even higher Si/Ca ratio than before, due to added Si from DE. FTIR spectra and TGA curves have changed little, only broadening peaks related to Si-O bonds and shifting peak positions

slightly in FTIR while scrambling the order of TGA curves for reasons that are not readily apparent.

4.3 – Addition of Al_2O_3

Al_2O_3 was added to the basic formulae in an attempt to encourage the growth of 'geopolymers,' for which the Si/Al ratio is extremely important. Therefore, Al_2O_3 was added to the powdered reactants to create three new formulae with Si:Al ratios of 1, 2, and 4 for each activator.

4.3.1 – Mechanical Properties (Fine Aggregate Concrete)

The samples were compression tested after grinding both ends to ensure parallelism. For the NaOH/waterglass activated formula, the strength increased depending on the quantity of Al_2O_3 added (Fig. 4.9.)

Formulae with ratios of 1, 2, and 4 reached strengths of 21 ± 3 MPa, 47 ± 5 MPa, and 45 ± 4 MPa, respectively, after 1 day. After 7 d, the strengths had reached a more uniform 61 ± 4 MPa, 64 ± 3 MPa, and 60 ± 5 MPa, with little change afterward, reaching 61 ± 6 MPa, 64 ± 12 MPa, and 67 ± 4 MPa after 28 d. Overall, these numbers represent a 33 %, 39 %, and 46 % increase in strength over the strength of the unadulterated formula.

The Na_2CO_3 activated formulae did not show this large strength gain with the addition of Al_2O_3 (Fig. 4.9.) The formula with an Si:Al ratio of 1 increased from no strength at 1 d, to 29 ± 1 MPa after 7 d and 34 ± 7 MPa after 28 d. The formula with an Si:Al ratio of 2 went from no strength at 1 d, to 28 ± 1 MPa after 7 d and 38 ± 4 MPa after 28 d. Finally, the formula with an Si:Al ratio of 4 went from no strength at 1 day to 29 ± 3 MPa after 7 d and 35 ± 2 MPa after 28 d. The results are, respectively, a 6 %

decrease, 3 % increase, and 4 % decrease in strength when compared to the unadulterated formula.

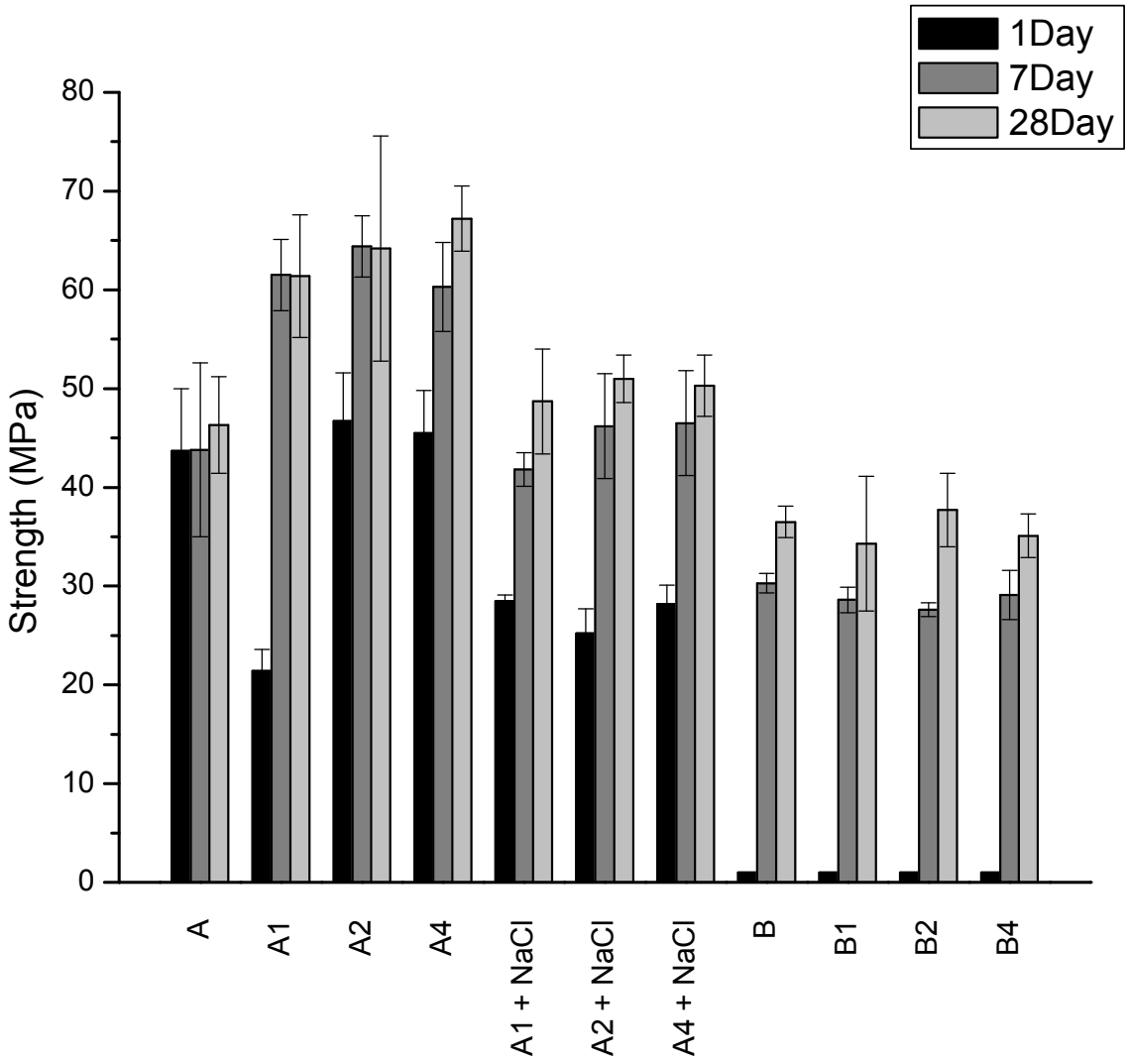

Figure 4.9 – Compressive strength at 1, 7, and 28 days of formulae activated by NaOH/waterglass (formula A) or Na_2CO_3 (formula B) with the addition of Al_2O_3 to reach Si:Al ratios of 1, 2, and 4 (formulae A1, A2, A4, respectively), and NaOH/waterglass activated formulae containing NaCl as a retardant.

A set of samples was made using the NaOH/waterglass activated basic formula, but containing both the three different levels of Al_2O_3 and NaCl as a retardant. The

addition of the Al_2O_3 to this formula led to a shortening of the already short set time, whereas it had little or no effect on the set time of the Na_2CO_3 activated formula. As always with the addition of NaCl, the strength at 1 day was lower (Fig. 4.9.), only 29 ± 1 MPa, 25 ± 3 MPa, and 28 ± 2 MPa for formulae with Si:Al ratios of 1, 2, and 4, respectively. At 7 d these strengths had risen to 42 ± 2 MPa, 46 ± 5 MPa, and 47 ± 5 MPa, and reached 49 ± 5 MPa, 51 ± 2 MPa, and 50 ± 3 MPa after 28 d. These final strengths represent a roughly 10 % increase in strength over the basic formula, but a 25 % decrease when compared to the strength at 28 d of the three formulae that contained Al_2O_3 and no NaCl.

The addition of Al_2O_3, and the gains in compressive strengths that it brought, were reflected in the tensile splitting strengths, although pinning down definite trends is difficult. For the NaOH/waterglass formula (Table 3.1) with Si:Al = 1, strength decreased slightly from 3.4 ± 1.1 MPa after 1 day to 2.7 ± 0.2 MPa after 28 d. The formula with Si:Al = 2 increased from 2.3 ± 0.9 MPa after 1 day to 3.9 ± 0.3 MPa after 28 d. The formula with Si:Al = 4 followed neither trend, increasing from 2.2 ± 0.4 MPa after 1 day to 4.0 ± 1.0 MPa after 7 d and then decreasing to 2.8 ± 0.4 MPa after 28 d. The addition of NaCl as a retardant (Table 3.1) lowered splitting tensile strengths across the board as well as changed the overall trends: from 2.3 ± 1.0 MPa after 1 day falling to 2.2 ± 0.3 MPa after 28 d for the Si:Al = 1 formula; from 1.4 ± 0.5 MPa after 1 day increasing to 3.5 ± 0.8 MPa after 7 d and then falling to 2.3 ± 0.8 MPa after 28 d for the Si:Al = 2 formula; and from 1.2 ± 0.3 MPa after 1 day increasing to 2.6 ± 0.5 MPa after 28 d for the Si:Al = 4 formula.

The Na_2CO_3 activated formulae (Table 3.2) showed a more straightforward trend: at least in terms of strength; all of them slightly increased over time despite still not being strong enough to test at 1 day. From 1.7 ± 0.6 MPa at 7 d to 2.9 ± 0.3 MPa after 28 d for the Si:Al = 1 formula; 2.1 ± 0.8 MPa after 7 d to 2.4 ± 1.3 MPa after 28 d for the Si:Al = 2 formula; and from 2.3 ± 0.6 MPa after 7 d to 2.6 ± 0.1 MPa after 28 d for the Si:Al = 4 formula. In the same manner that the addition of Al_2O_3 had little, if any, effect on compressive strength, so it had little effect of tensile splitting strength.

4.3.2 – XRD (Cement Paste)

Specimens of the basic formulae with three different levels each of Al_2O_3 as an additive were investigated by XRD, however, the highly crystalline Al_2O_3 masked the appearance of most other peaks (Fig. 4.10.) The amorphous hump due to unreacted slag is still in evidence, as well as the peak at 30^o -2θ due to the poorly crystalline C-S-H. This peak again appears somewhat sharper for the formulae activated by Na_2CO_3, perhaps indicating the presence of calcite, though none of the secondary peaks can be observed.

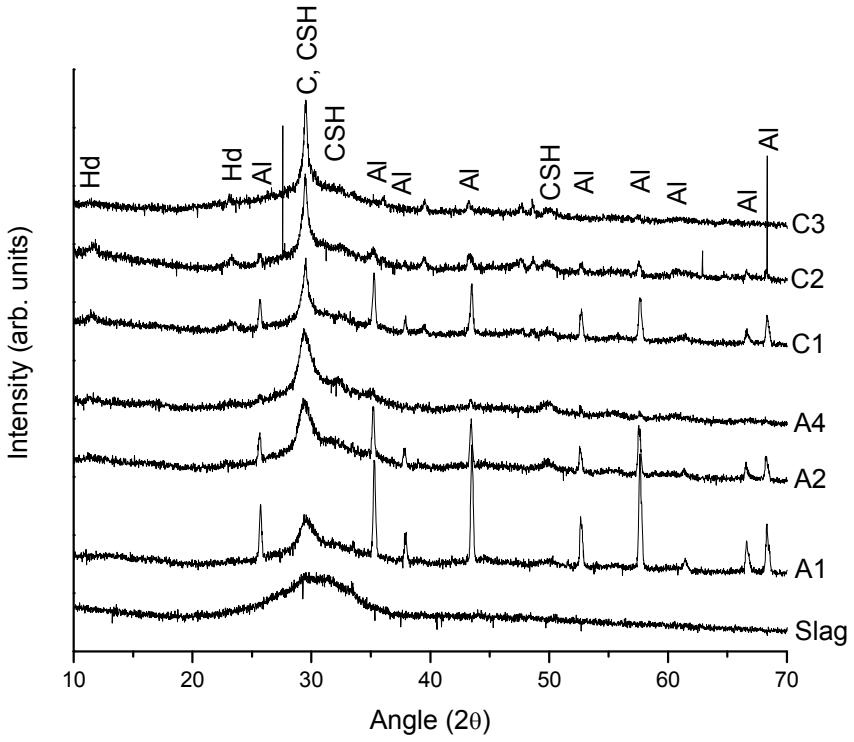

Figure 4.10 – XRD diffractograms of the NaOH/waterglass formula with Al_2O_3 added to bring the Si:Al ratio to 1, 2, or 4 (A1, A2, and A4, respectively) and the Na_2CO_3 formula with Al_2O_3 added to bring the Si:Al ratio to 1, 2, or 4 (A1, A2, and A4, respectively) at 28 d. Diffractogram of raw slag (bottom) provided for comparison. Hd = Hydrotalcite, Al = Al_2O_3, C = Calcite, CSH = Calcium Silicate Hydrate (C-S-H.)

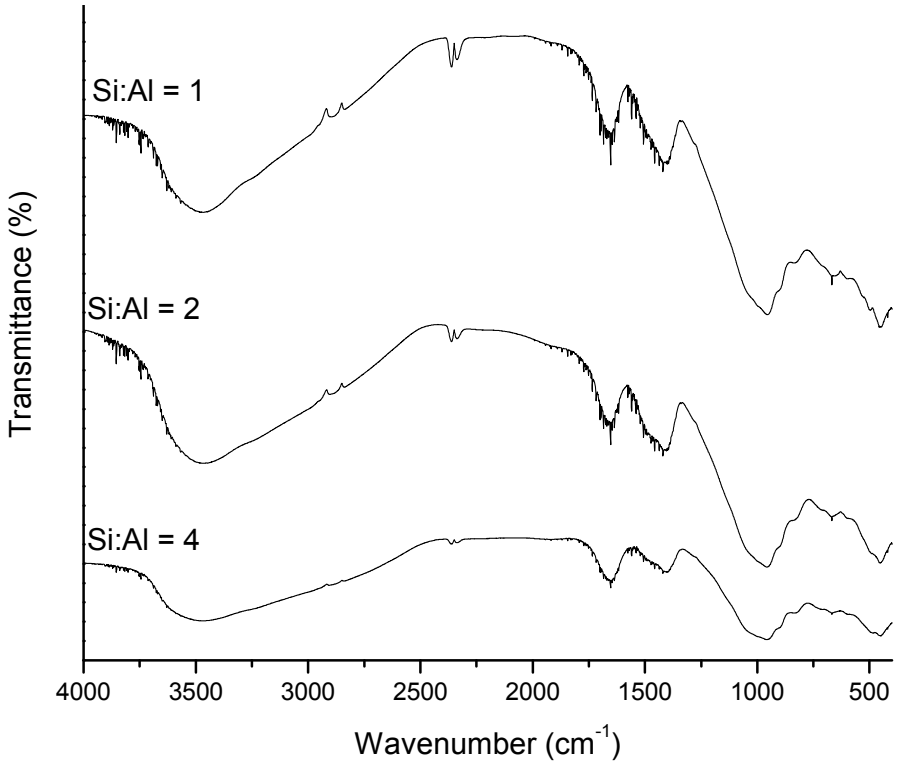

Figure 4.11– FTIR spectra of NaOH/waterglass-activated cements with Al_2O_3 at 28 d.

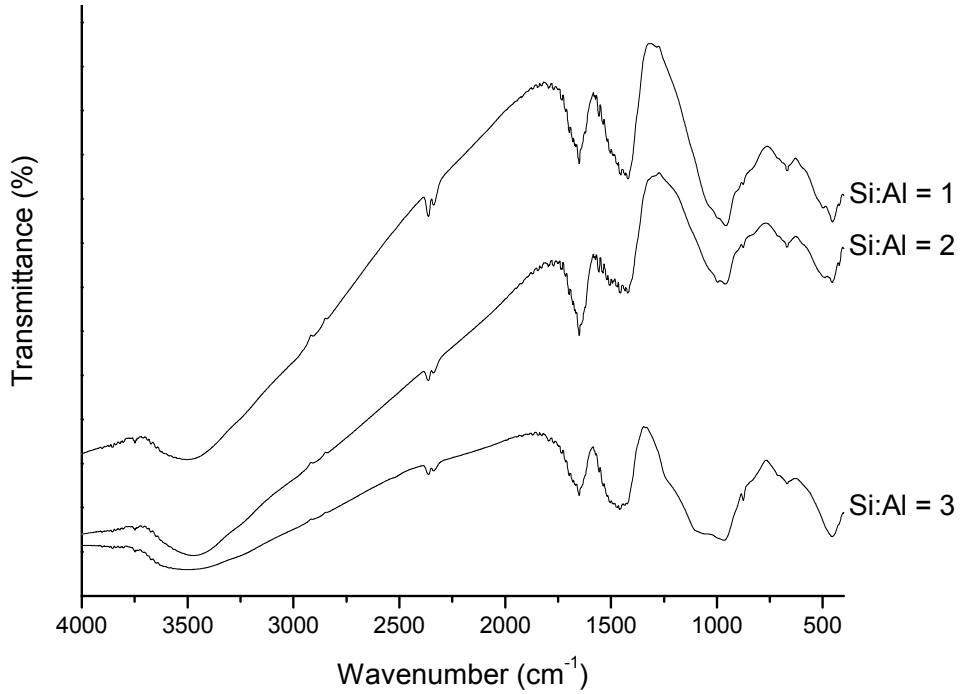

Figure 4.12 – FTIR spectra of Na_2CO_3-activated cements with Al_2O_3 at 28 d.

4.3.3 – FTIR (Cement Paste)

FTIR spectra of cement paste samples from the NaOH/waterglass- and Na_2CO_3-activated formulae (Figs. 4.11 and 4.12, respectively) contain a number of similarities. The NaOH/waterglass activated formulae had nearly identical spectra; each had a peak at 460 cm^{-1} corresponding to O-Si-O and Si-O-Si bending; a peak at 950 cm^{-1} corresponding to the Si-O and Al-O stretching; a peak at 1420 cm^{-1} corresponding to CO_3^{2-} ions, likely formed from atmospheric CO_2 incorporated during the mixing process or residual carbonate from starting materials. Finally, peaks at 1640 cm^{-1} and broad peaks in the 2700-3700 cm^{-1} range, which are due to the OH vibrations of water, which again may hide other hydroxide minerals. [124] These spectra are very similar, but not identical, to the spectra of the formula without Al_2O_3. First, the peak centered 500 cm^{-1} in the as-received slag had previously shifted to 470 cm^{-1}; the addition of Al_2O_3 here shifts it further, to 460 cm^{-1}. The shifting itself is presumably due to the SiO_2 found in the as-received slag moving into more ordered, that is, more crystalline or polymerized conditions as reaction products form. [124] As little crystallinity is seen in the C-S-H by XRD, it is more likely that this increase in order, and thus shift in peak position, occurs due to the increasing polymerization of the Si-rich gel portion of C-S-H.

The spectra of Na_2CO_3 activated formulae (Fig. 4.12) share many similarities. All formulae showed the same peaks at 460 cm^{-1}, 1650 cm^{-1}, and between 2700 and 3500 cm^{-1} due to O-Si-O and Si-O-Si bending, water, and water, respectively. The peak at 1420 cm^{-1} has again shifted slightly higher, to about 1440 cm^{-1} due to carbonate ions from the activator, as has a peak shifting from 950 cm^{-1} to 975 cm^{-1}, again implying a greater

degree of order. Another peak, at 1420 cm^{-1}, appears different in each formula, shifting to 1440 cm^{-1} with an Si:Al ratio of 1 and 1470 $cm^{-1}$with an Si:Al ratio of 4.

All of these spectra are quite similar to both spectra reported by Delgado et al. for pure C-S-H gel [81] and the spectra of formulae without Al_2O_3. Compared to the spectra of sodium polysialate (Na-PSS) geopolymers as reported by Barbosa et al. [75], however, there are some slight differences. The peaks reported here at 1420 cm^{-1} and 960 cm^{-1} have shifted to lower wavenumbers, and the peak centered around 460 cm^{-1} is higher. A greater shift in the location of the peaks in these directions denote that the chemical species are moving into a more ordered system, therefore the C-S-H formed in the slag-based system reported here is possibly less ordered than that formed in a geopolymer/C-S-H system. As above, the overall interpretation here is that the FTIR describes, when combined with other analyses, a C-S-H based system.

4.3.4 – SEM (Cement Paste and Fine Aggregate Concrete)

Particles of unreacted Al_2O_3 were observed in the SEM (Fig. 4.2f-h.) At the lowest magnification (Fig. 4.2f), the particles were difficult to see due to the dominance of microstructural features such as unreacted slag or aggregate particles (in the mortar/concrete specimens.) At higher magnifications (Fig. 4.2g) the unreacted particles became more clearly discernable, as well as particles of unreacted slag, pores, etc. Finally, at the highest magnifications (Fig. 4.2h) the morphology and shape of the individual particles of unreacted Al_2O_3 could be observed. As with the NaCl and DE, no difference was noted in the morphology of the particles in one basic formula compared to another.

BSE image analysis of formulae containing Al_2O_3 was also performed (Table 3.2.) Overall, regardless of activator, or whether NaCl was added as a retardant, the amount of unreacted slag increased only slightly as the amount of added Al_2O_3 decreased. The NaOH/waterglass activated formulae with Si:Al ratios of 1, 2, and 4 contained 16 ± 2 vol.%, 13 ± 1.5 vol.%, and 26 ± 7 vol.% unreacted slag, respectively. The reason for the high error on the last formula is not clear; that the addition of Al_2O_3 is having a pronounced effect, however, is obvious. Furthermore, the size of the unreacted particles was more or less constant: roughly 3 ± 1 μm^2, regardless of formula. That the amount of unreacted slag is less than in the formulae without addition of Al_2O_3 is not surprising, as they were substantially stronger, and less unreacted material means more cementing phase and therefore higher strength. This analysis is complicated, however, in that the unreacted Al_2O_3 appears to the image analysis software to be unreacted slag; therefore, these numbers should be considered primarily as guidelines rather than concrete data points.

For samples activated by NaOH/waterglass, and containing both Al_2O_3 and NaCl as a retardant, the general trend was the same, with all three formulae falling in the range of roughly 20 ± 2 vol.% unreacted slag, each particle of which was 2.5 ± 1 μm^2 in size (Table 3.2.) These numbers are consistent both with each other and in that they are not as high as for the formulae without NaCl; since these formulae had roughly the same strength, but not as high as the previous formula, this is a reasonable result.

Finally, the Na_2CO_3 activated formulae were investigated; as with the NaCl containing formulae, they all contained roughly the same amount of unreacted slag (26 ± 2 vol.%), with similarly sized particles (3.5 ± 1 μm^2) regardless of the quantity of Al_2O_3

added (Table 3.2.) The reason why this number is somewhat lower than that of the formula without additives, despite the fact that the strength did not increase, is not clear at this time.

4.3.5 – EDS (Cement Paste)

The average Ca, Si and Al elements distributions in 9 cement paste formulae including Al_2O_3 were investigated (Fig. 4.13.) The Si:Ca ratio in the all formulae is roughly 1:1 as evidence by the tight grouping of data (Fig. 4.13a.) The Ca:Al (Fig. 4.13b) and Si:Al (Fig. 4.13c) ratios show greater scatter and no clear trends as regards the initial Al_2O_3 concentration. The reason for this is not clear; one possible reason may be the limitation of using EDS in non-homogeneous materials, as the interaction volume of the electron beam can detect phases below the surface. This is unlikely, however, for two reasons: first, a similar scatter was not found for the Si:Ca ratio. Second, these analyses were taken at high magnifications and did not (knowingly) include any un-reacted slag or Al_2O_3 particles. Nevertheless, it is possible that the analysis unwittingly included unobserved and unreacted alumina particles.

The target Si:Al ratios for most samples do fall within the broader range detected by EDS at lower magnification if standard deviations are taken into account. The exceptions are formulae A2 (NaOH/waterglass activated, Si:Al = 2.2 instead of 2), C1 (Na_2CO_3 activated, Si:Al = 2.7 instead of 1) and C4 (Na_2CO_3 activated, Si:Al = 1.7 instead of 4). Reasons for this are unclear and are possibly due to poor mixing.

In contradistinction, within each cementing region of the various formulae, there was little variation concerning the Ca and Na concentrations. No Na-free regions of unaltered C-S-H gel were observed, nor were any Ca-deficient geopolymer regions

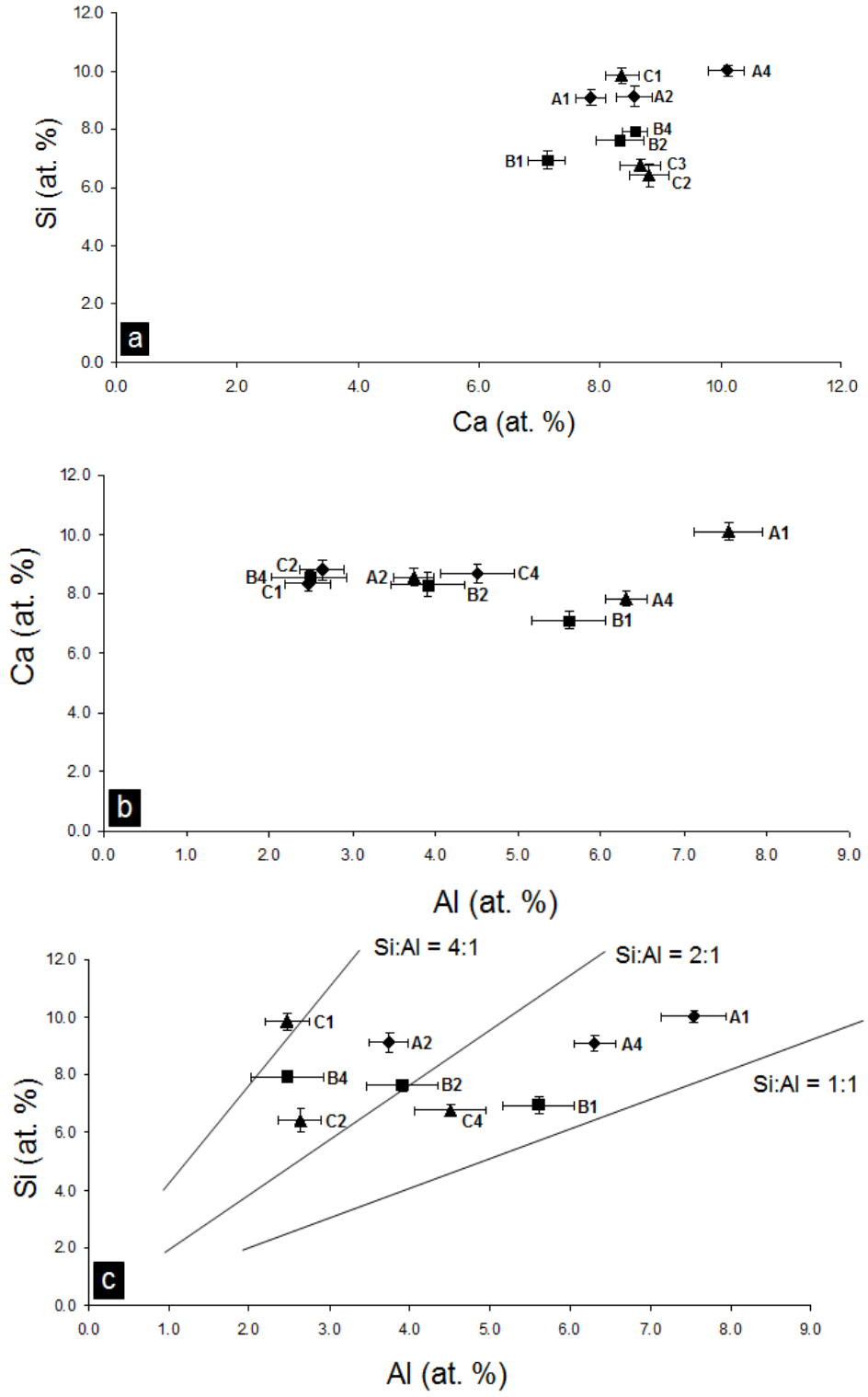

Figure 4.13 – Average elemental ratios as determined by EDS of the nine formulae containing Al_2O_3. a) Si/Ca ratio, b) Ca/Al ratio, and c) Si/Al ratios, with lines indicating target Si:Al ratios. 'A' formulae are NaOH/waterglass activated; 'B' formulae are NaOH/waterglass activated with NaCl as a retardant; and 'C' formulae are Na_2CO_3 activated. All data taken at 28 d.

found. Combined with the XRD results and the fact that the Na level stays more or less constant throughout the binding phase of all formulae, it is likely that the Na is in the form of a Na salt trapped in the spaces between the C-S-H molecules or is playing a charge balancing role by replacing Ca in C-S-H.

4.3.6 – Heat of Reaction (Fine Aggregate Concrete)

It was noted during the production of samples including Al_2O_3 that the heat of the reaction taking place seemed to increase. Therefore a simple experiment was designed to see if there was, in fact, an effect of this nature. A batch of concrete was mixed and poured into a mold which was sitting in a Styrofoam box so as to limit heat conduction away from the sample. A thermocouple was then placed as near to the center of the curing concrete as possible and the temperature at various times recorded (Fig. 4.14.) These experiments showed an increase in reaction temperature (1 or 2 ^oC for the formula with the least added Al_2O_3, up to 4-5 ^oC for the formula with the most) of the material. It could be this increase in temperature (due to the exothermic dissolution of Al_2O_3) that is responsible for the increase in strength, due to the increase production of C-S-H at slightly higher temperatures. It is known that alkali-activated slags respond very well to even modest increases in reaction temperature [23].

4.3.7 – Conclusions

The addition of Al_2O_3 did not, as was hoped, encourage the production of ‘geopolymers.’ It did, however, produce an increase in strength for the NaOH/waterglass activated formulae, the reason for which is unclear. It is possible that increased heat produced during dissolution spurred the reaction, or that a zone too small to be viewed by

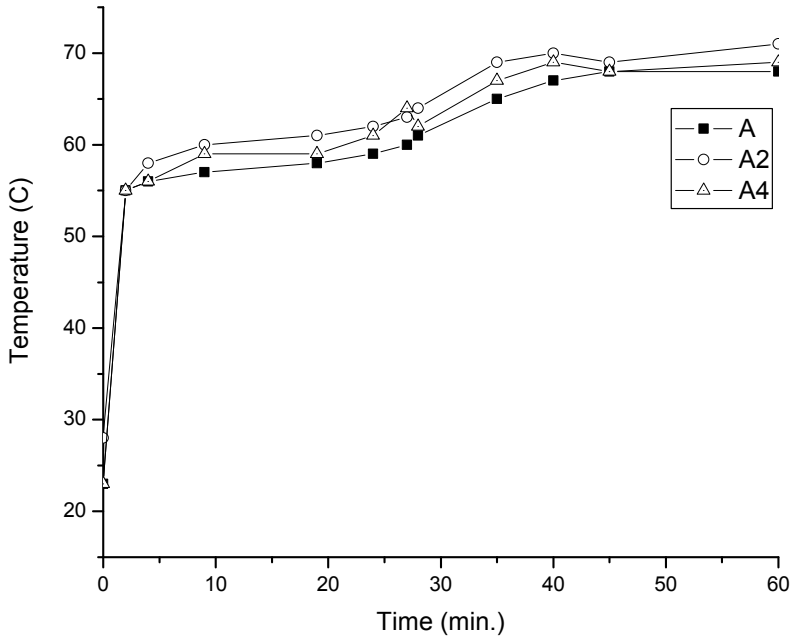

Figure 4.14 Plot of temperature in the center of a fine limestone aggregate concrete sample vs. time, showing increase in reaction temperature with increasing Al_2O_3 content. A = Basic NaOH/waterglass formula with no additional Al_2O_3; A1 = NaOH/waterglass formula with Si/Al = 1, etc.

electron microscopy is being produced that alters the mechanical properties. Na_2CO_3 activated formulae saw no strength gain. NaCl was shown to still be an effective retardant.

4.4 – Addition of Fly Ash

Fly ash, a common aluminosilicate material used as a supplement to OPC [125-127], was added in an attempt to reproduce claims of the superiority of blended slag/fly ash systems over purely slag-based materials. Fly ash replaced 10 wt.% of the slag in the initial reactants. These claims rest mainly on the fact that in a mixed C-S-H/'geopolymer' system, the 'geopolymer' particles act as micro-aggregates, ensuring a more dense final product.

4.4.1 – Mechanical Properties (Fine Aggregate Concrete)

Fly ash was added to the powder reactants after dehydroxylation for 2 hours at 750 ^{o}C. It was added as a powder and was compression tested using the steel cap method. Tensile strength results were not obtained. For the NaOH/waterglass activated formulae, strength increased from a 56 ± 1 MPa after 1 day, to 70 ± 4 MPa after 7 d, to 96 ± 1 MPa after 28 d (Fig. 4.15a.) While the 1- and 28-day strengths are slightly lower than they are in the unadulterated formula, the 7 day strength is somewhat higher. The mechanism for this is unclear, but may be due to the fact that fly ash does not dissolve in very high alkaline solutions [31, 33, 87], and thus waited until the cement had lost some of its alkalinity before it began to react. The 28 d strength is about what it is in the unadulterated formula; however, at an age of 6 months the formula with fly ash performs at about a 20 % loss of strength (112 ± 1 MPa, compared to 139 ± 1 MPa for the basic formula.) That the addition of fly ash definitely changes the strength development profile of the material is clear; however, it does not result in any increase in strength over the long run. That having been said, 112 MPa is a high strength useful for many applications.

The addition of fly ash behaved in a similar manner for the Na_2CO_3 activated formulae (Fig. 4.15b.) From a strength of 10 ± 1 MPa at 1 day, to 24 ± 0.4 MPa at 7 d and 40 ± 2 MPa at 28 d, the addition of fly ash results in a decrease in strength at early ages; however, at 6 months, the strength of the formula with fly ash was within 1 MPa of

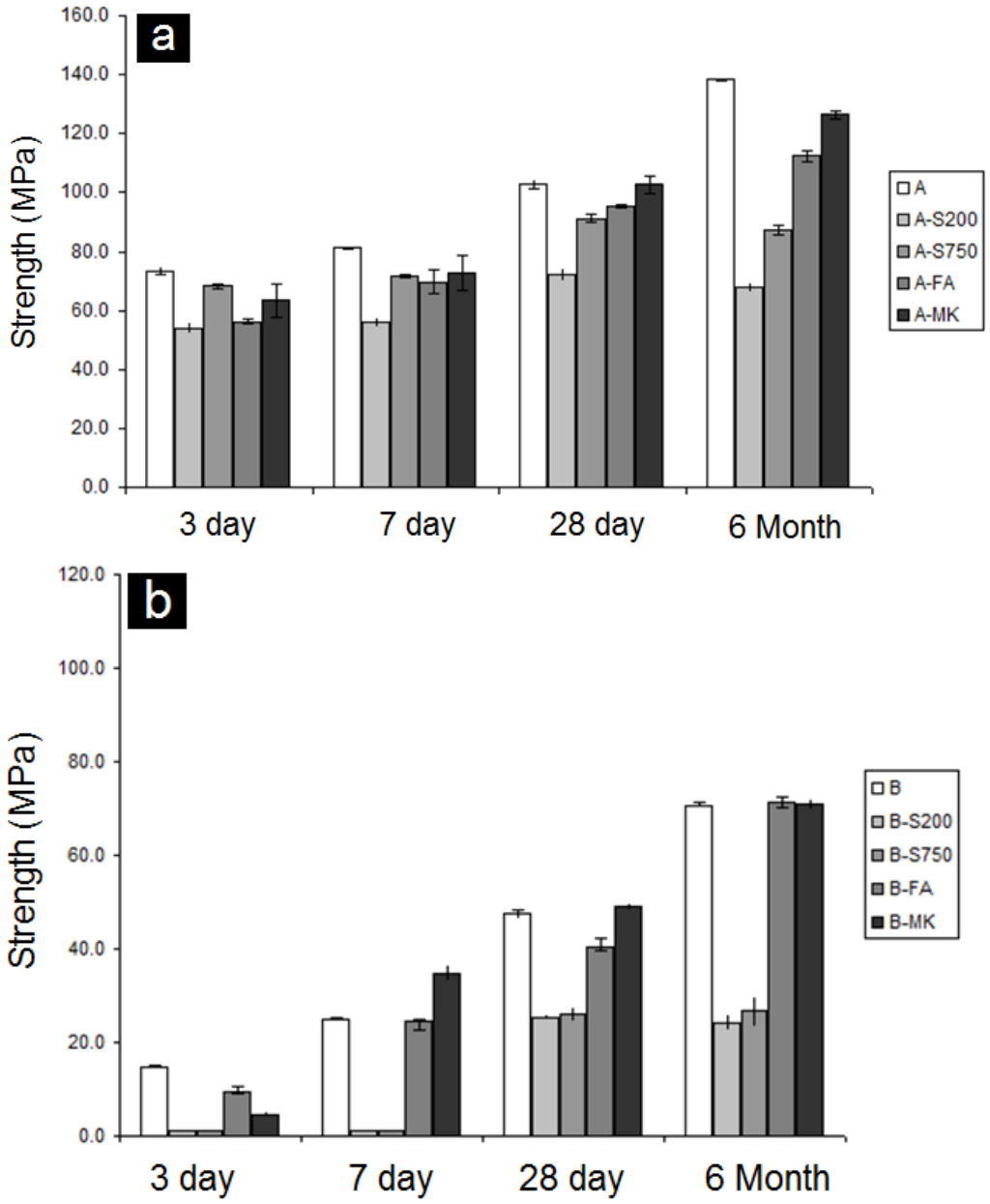

Figure 4.15 – Compressive strength at 1 d, 7 d, 28 d, and 6 months of formulae activated by NaOH/waterglass (formula A) or Na_2CO_3 (formula B) with 10% addition of acid rock treatment sludge dried at 200 ^{o}C (S200) or calcined at 750 ^{o}C (S750), fly ash, and metakaolin.

the strength of the basic formula (71 ± 1 MPa.) Whether the slight decrease in strength at early age is offset by a reduction in the price of the final product due to cutting it with fly

ash is a question whose answer is determined almost entirely be geography, and would have to be investigated on a case-by-case basis.

Zhao *et al.* [128] investigated a 90/10 mix of slag/fly ash, using an activator based on a number of ingredients (65 wt.% gypsum, 25 wt.% lime, and others) and found a maximum strength of about 45 MPa at 28 days, slightly better than the strength of the lower-pH Na_2CO_3-activated formula reported here. Puertas *et al*. [129] performed a similar study, though their minimum fly ash content was 30 wt.%, in which they found that increasing amounts of fly ash lowered strength for a variety of activators and curing regimes. In general, their room temperature strengths varied from 20 – 50 MPa depending on activator.

Substantial work has gone into describing the ternary OPC-slag-fly ash system, in which the OPC could be considered as a somewhat low-pH activator. Xuequan *et al*. [127] reported an optimal strength of 57 MPa in one such system. Li *et al.* [65] report strengths of 30 – 60 MPa (though not exact formulae) at 28 d. In another study, Li *et al*. [126] report strengths of 65 MPa at 28 d for a 60/40 OPC/fly ash blend, 80 MPa at 28d for both an OPC and 60/25/15 OPC/Slag/fly ash blend, and 95 MPa at 365 d for these two formula but 108 MPa for the 60/40 blend. It should be noted that they were testing concrete with a mixture of fine and coarse aggregate, which was not done here. Overall, they conclude that fly ash lowers strength before the first 56 days; after this, they are superior. This is in contradiction to the data reported here, for no readily obvious reason; it may be due to the mix design, use of coarse aggregate, or subtle differences in the slag and fly ash used (which are fairly similar to those used here.)

Fu *et al*. [130] reported a strength of 59 MPa at 28 d for a 65/30 OPC/slag blend. The addition of fly ash to this system only lowered strength: a 55/30/10 blend of OPC/slag/fly ash achieved strengths of 58 MPa, while a 45/30/20 blend achieved strengths of 52 MPa. The addition of only 2 wt.% of a high-pH Na-based activator, however, boosted the compressive strength to 62 MPa at 28 d. Their final conclusions were that, first, fly ash can be added to make OPC more environmentally friendly, but slag should also be added to counteract the negative effects of fly ash and, second, increasing the pH of the system through added activators increases strength. Both of these results concur with those reported here, where in the higher pH activator (i.e. NaOH/waterglass) and higher slag content (i.e. no fly ash) increase strength.

The strengths found in this study are therefore in general comparable to those found in the literature; the wide range of which is due to variation in chemical composition of reactants, composition of blends, curing regimes, reactant fineness, etc. [51, 131-133]. That fly ash lowers the strength of AAS cements, of course, does not mean that it should not be used; in certainly does not lower strength so much as to make it unusable, it may increase the environmental friendliness of the product, and as detailed in a review paper by Bijen [125], it has positive effects on pore structure and thus resistance to hostile environments (which was not studied here.)

4.4.2 – XRD (Cement Paste)

Diffractograms of formulae activated by the NaOH/waterglass mixture are essentially identical to diffractograms of the basic formula, containing only peaks attributable to poorly crystalline C-S-H and (possibly) calcite (Fig. 4.16), similar to the results obtained by other researchers [128, 129], and as described at length above. The

diffractogram of the formula containing fly ash activated by the Na_2CO_3 solution is substantially more complex (Fig. 4.17.) This diffractogram takes the form of a series of peaks, representing a number of minerals, such as gaylussite ($Na_2Ca(CO_3)_2 \cdot 5H_2O$), tetranatrolite ($Na_2Al_2Si_3O_{10} \cdot 2H_2O$), and margarite ($CaAl_2(Si_2Al_2)O_{10}(OH)_2$). Gaylussite is known to form as a natural evaporite in alkali lake waters [134, 135], which the relatively long set time of Na_2CO_3-activated slag cements apparently mimic; the other two are minerals that both occur naturally and are occasionally mentioned in the literature as byproducts of the alkali-activation of slag [49].

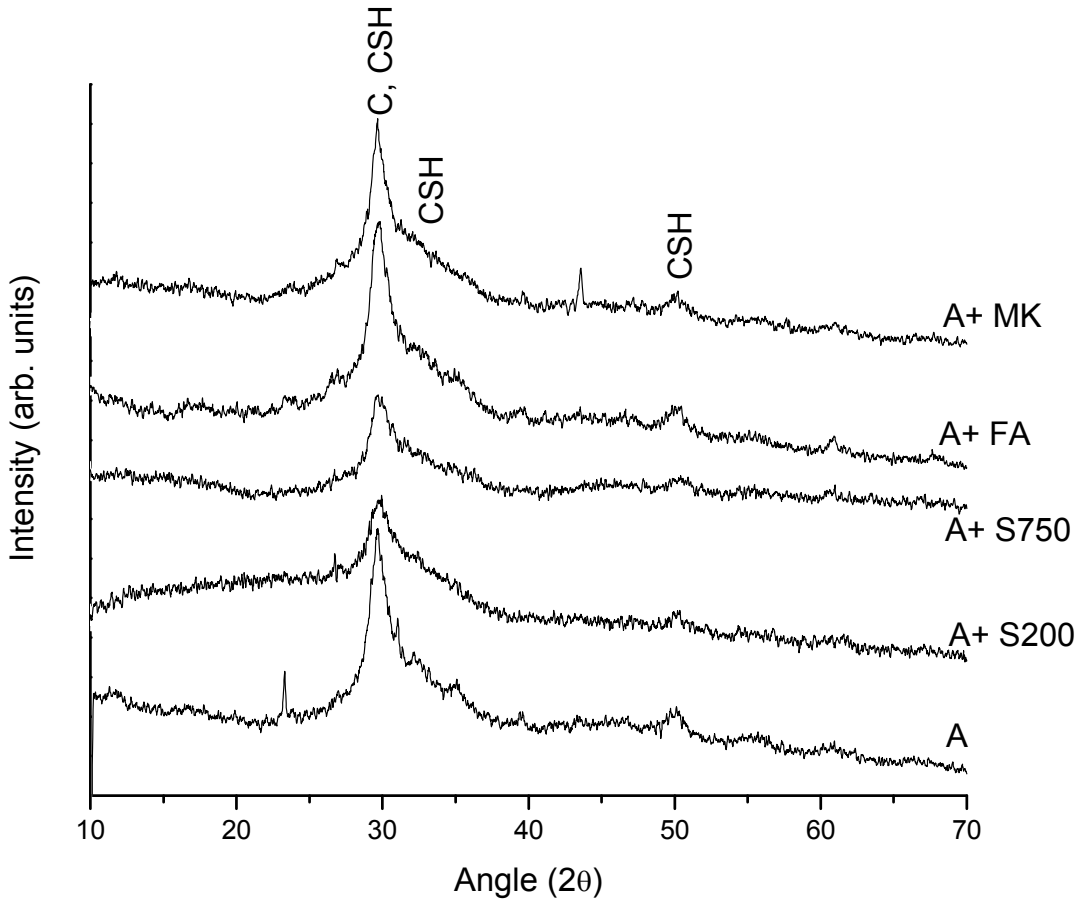

Figure 4.16 – XRD diffractograms of the NaOH/waterglass activated formula with the addition of acid rock treatment sludge dried at 200 ^oC (S200), calcined at 750 ^oC, and with fly ash (FA) and metakaolin (MK) at 7 d. C= Calcite, CSH = Calcium Silicate Hydrate (C-S-H.)

These three minerals, as well as calcite and C-S-H are identified in these three formulae due to the strength of their peaks; a number of smaller and less well defined peaks cannot be identified with absolute certainty, but could be due to the presence of enstatite ($MgSiO_3$), wollastonite ($CaSiO_3$), gehlenite ($Ca_2Al_2SiO_7$), hexahydrate ($MgSO_4$-$6H_2O$), gismondine ($Al_2Si_2O_8$-$4H_2O$), and/or riversideite ($Ca_5Si_6O_{16}(OH)_2$), all of which are naturally occurring minerals.

Overall, the pictured painted here by the XRD diffractograms are essentially identical to the picture painted by the diffractograms for formulae without fly ash: poorly

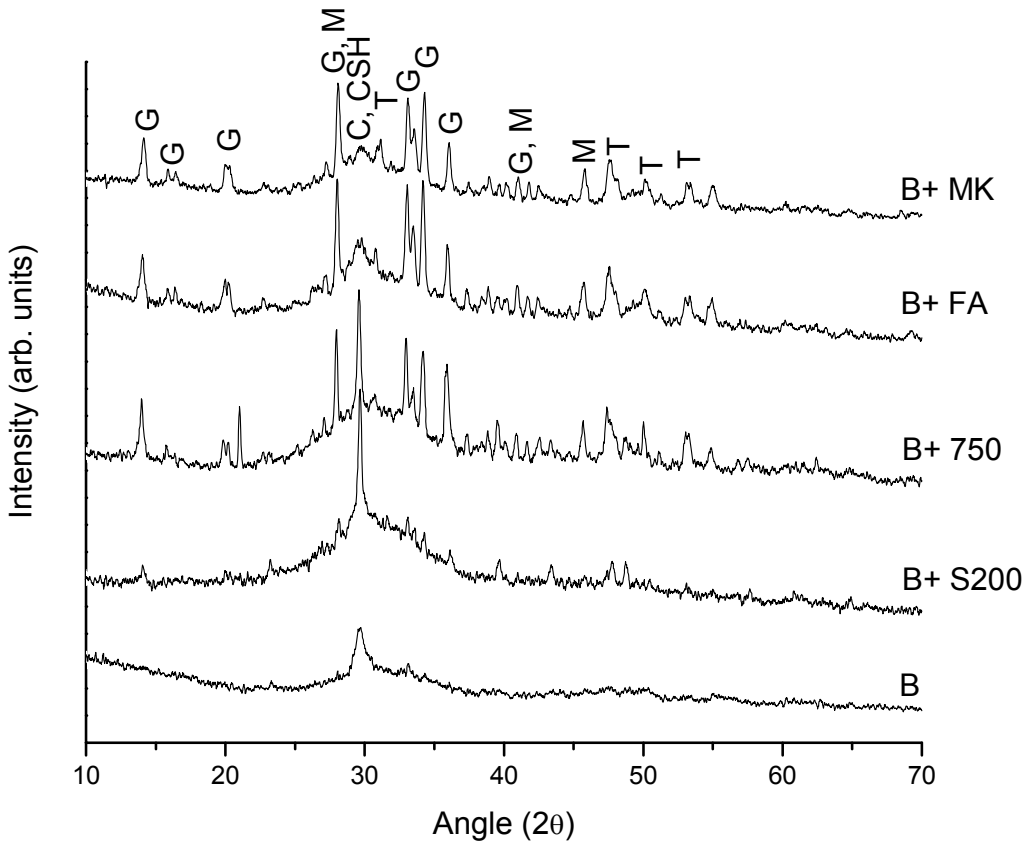

Figure 4.17 – XRD diffractograms of the Na_2CO_3 activated formula with the addition of acid rock treatment sludge dried at 200 ^oC (S200), calcined at 750 ^oC, and with fly ash (FA) and metakaolin (MK) at 7 d. G = Gaylussite, M = Margarite, C = Calcite, CSH = Calcium Silicate Hydrate (C-S-H), T = Tetranatrolite.

crystalline C-S-H, possibly calcite, and some mineral side products (similar to hydrotalcite above) that do not seem to play any major roles.

4.4.3 – FTIR (Cement Paste)

The FTIR spectra of the NaOH/waterglass activated formula (Fig. 4.5) shares many similarities with the basic formula. After 7 d the spectrum contains the same peaks indicative of water, which could possibly hide the presence of –OH bonds associated with hydrated minerals, such as portlandite.

The main peak is again centered around 950 cm^{-1}, representing the Si-O and Al-O stretching. This band is of a slightly different shape and has a pronounced shoulder on the left side; this shoulder (centered at 966 cm^{-1}) is due specifically to stretching of Si-O bonds in C-S-H, confirming the XRD results. In all formulae, at 28 d this peak is both more pronounced and flat-bottomed due to the growth of this shoulder, indicating the increased production of poorly crystalline C-S-H.

The peak at 1420 cm^{-1} again represents stretching in CO_3^{2-} molecules and confirms the presence of minor amounts of calcite, which may have been obscured in the XRD diffractogram. At 28 d, this peak is a little more intense due to increased absorption of atmospheric CO_2. After 28 d, the peak at 450 cm^{-1}, due to Si-O and Al-O bending, has broadened slightly.

FTIR spectra of Na_2CO_3 activated formulae (Fig. 4.5) showed a number of differences when compared to the NaOH/waterglass activated formulae and, as with the XRD diffractograms, were more complicated. At 7 d, the spectrum of the formula containing fly ash also contains a distinct side peak at 3615 cm^{-1}, due to the presence of a crystalline hydroxide [78, 79, 81], possibly margarite, which was detected by XRD. A

pair of very weak double peaks at 2926/2852 cm^{-1} is a harmonic associated with calcite.[79]

Below this, many of the peaks are in the same position but have slightly different shapes. The peak at 1430 cm^{-1}, (due to C-O bond stretching in CO_3^2, indicative of either calcite or the other carbonate materials detected by XRD such as gaylussite) is very pronounced in the formula containing fly ash as well as the basic formula.

A number of minor peaks exist between 815 cm^{-1} and 610 cm^{-1}. They are all sharp, indicating the presence of crystalline species, specifically carbonates (877 cm^{-1} and 700 cm^{-1} due to the bending of –CO groups) and C-S-H (790 cm^{-1} due to Si-O bonds).

Due to the width of the peaks related to Si-O and Al-O bonding, it is difficult to say with confidence that the addition of 10 wt.% of an aluminosilicate material like fly ash has made a difference. The shape of the peaks are slightly different, however, the exact meaning of these slight changes is not readily obvious. As with the basic formulae, these spectra cannot be taken as proof one way or the other of the presence of 'geopolymers'; however, when combined with the XRD data in the manner described above, they most likely indicate C-S-H and an amorphous Si gel, but not 3D, alkali-balanced zeolite-like 'geopolymers.'

4.4.4 – SEM (Fine Aggregate Concrete)

Formulae with fly ash were not investigated with image analysis. As was seen with the addition of DE or Al_2O_3, particles of unreacted additives make image analysis unreliable. In the NaOH/waterglass activated formula containing fly ash, at low magnification (Fig. 4.18a), unreacted particles were difficult to spot due to their small size. At higher magnifications (Fig. 4.18b) they were easier to spot in the form of

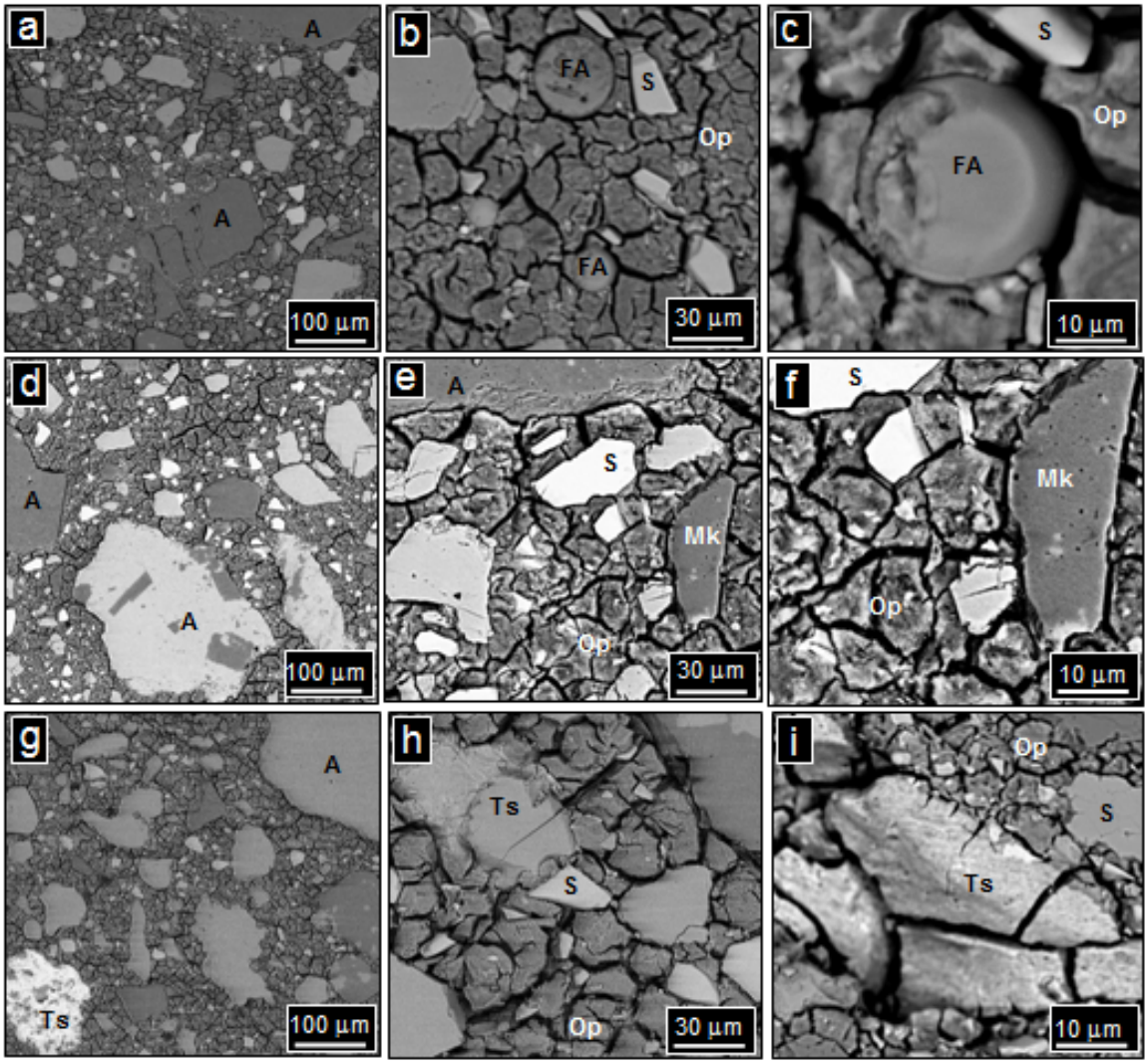

Figure 4.18 – BSE SEM images of NaOH/waterglass activated formulae containing fly ash, metakaolin, and acid rock treatment sludge. a) formula containing fly ash and fine limestone aggregate, in which the aggregate is most easily identified; b) medium magnification image in which particles of unreacted slag and unreacted fly ash become apparent; c) high-magnification image of a particle of unreacted fly ash; d) formula containing metakaolin and fine limestone aggregate, in which the aggregate is most easily identified; e) medium magnification image in which unreacted slag and metakaolin particles become apparent; f) high magnification image of unreacted metakaolin; g) formula containing acid rock treatment sludge and fine limestone aggregate, in which the aggregate is most easily identified; h) medium magnification image showing unreacted particles of slag and sludge; i) a heavily cracked particle of unreacted treatment sludge. A = aggregate, S = unreacted slag, FA = Fly Ash, Mk = metakaolin, Op = outer product, Ts = treatment sludge.

undissolved spheres or parts of spheres. The round shape facilitated identification. At the highest magnification (Fig. 4.18c) the fly ash particles were seen to have, generally speaking, smooth surfaces, and did not seem well bonded to the Op, as evidenced by numerous small cracks (although this is a feature observed in many formulae, and also between the Op and the slag particles themselves in some formulae.)

In Na_2CO_3 activated formulae, fly ash acted in a similar manner; at low magnification (Fig. 4.19a) unreacted particles were difficult to observe, and images were dominated by aggregate; at higher magnification (Fig. 4.19b) other microstructures, such as particles of unreacted slag or fly ash were discernable. At the highest magnifications (Fig. 4.19c) the unreacted fly ash particles took the form of either spheres or parts of spheres. The Op appeared homogenous in BSE mode, suggesting that the fly ash had little, if any, long-range effect on the cementing phase, regardless of activator. That unreacted particles were easily found suggests that fly ash is not, at least at early ages, interacting with the cementing phase on a chemical level.

Even in 'geopolymer' formulae, it is not unusual to see undissolved fly ash particles. Keyte *et al*. [136] observed such particles in a waterglass-activated 'geopolymer'; van Deventer *et al*. [137] and Fernandez-Jimenez *et al*. [138] observed them for NaOH-activated sly ashes; Rattanasak *et al*. [139] reported images showing undissolved fly ash particles over a wide range of concentrations of NaOH solutions; and Andini *et al*. [140] observed them in a KOH-activated formula. It is therefore not unexpected that they are observed here. Whereas Pacheco-Torgal [9] used SEM images of partially-reacted fly ash spheres to back up a theoretical model in his recent review of

the mechanism behind alkali-activation of fly ash, while they were observed here, no such detailed investigation was conducted.

4.4.5 – EDS (Fine Aggregate Concrete)

The Ca/Si ratio of the NaOH/waterglass activated formula (Fig. 4.19a) is generally clustered together, with a handful of outliers. Formulae containing fly ash generally has a higher amount of Si and lower amount of Ca. This ratio is much lower than that expected to be found in the C-S-H of AAS cements; this is likely due to a distinct surplus of Si from both fly ash and waterglass. A similar effect was seen in the formulae with added DE, where the DE was a source of excess Si that pushed the Si/Ca ratio to very high numbers (around 9:1, as opposed to the ≈ 3:1 seen here.) Incorporation of Na and Al into the C-S-H structure, as well as the possible formation of an amorphous Si-rich phase have also been reported [67] and provide plausible explanations.

The Ca/Si ratios of the Na_2CO_3-activated formula with fly ash (Fig. 4.19b) has shifted to lower amounts of Si and slightly higher amounts of Ca when compared to the NaOH/waterglass activated samples; they also show greater scatter due to the presence of a greater number of microconstituents (as observed by XRD.) In general, the data cluster near a Ca/Si ratio of 0.5 – 0.8, which is not unexpected for cements containing C-S-H. When compared to the EDS analyses performed on the OP of the basic formulae in

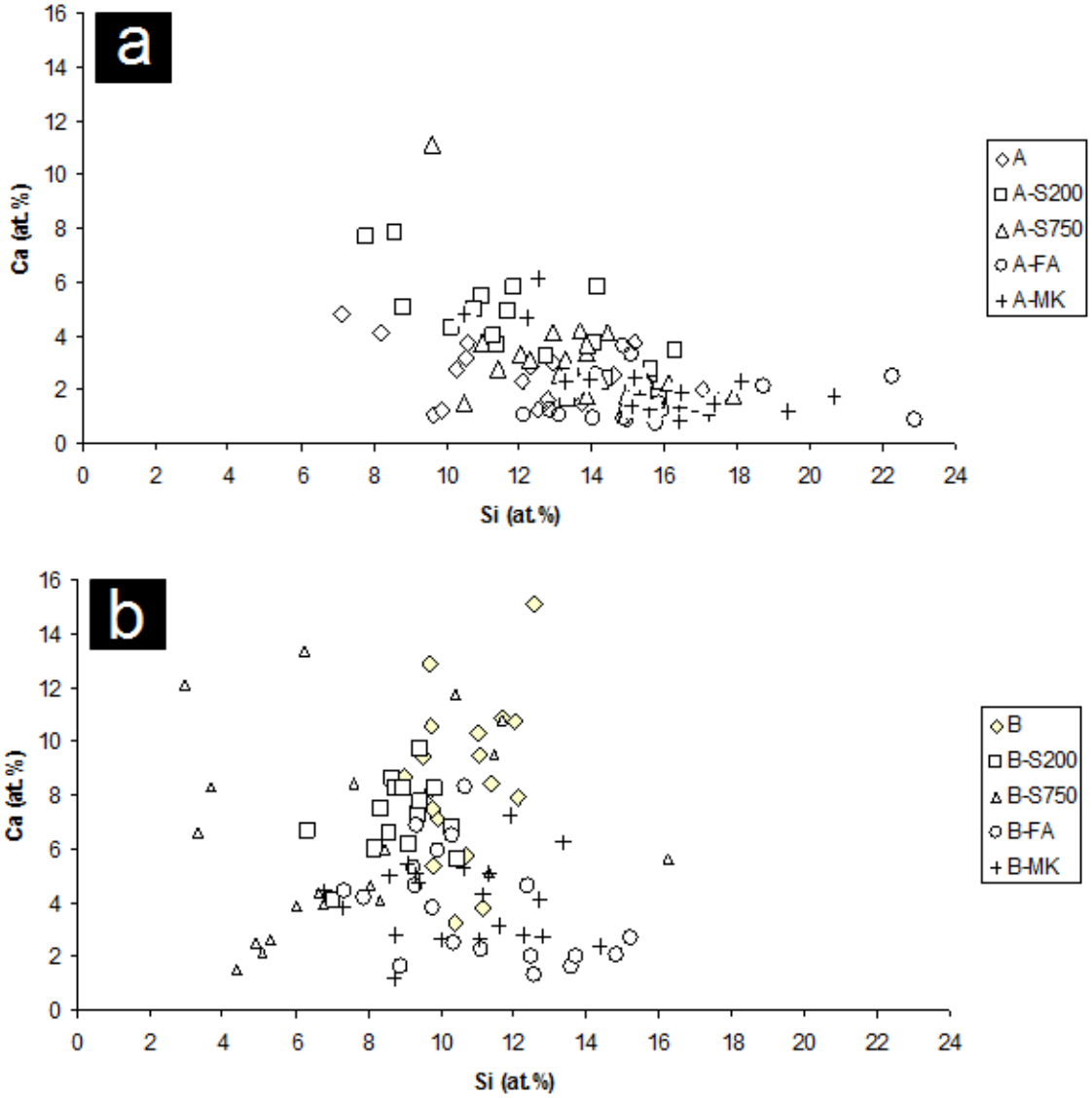

Figure 4.19 – Elemental distribution of Ca and Si in concretes of a) Formulae activated by NaOH/waterglass containing no additives (A), acid rock treatment sludge calcined at 200 and 750 ^{o}C (A-S200 and A-S750, respectively), fly ash (A-FA) and metakaolin (A-MK), and b) Na_2CO_3 activated formulae containing no additives (B), acid rock treatment sludge calcined at 200 and 750 ^{o}C (B-S200 and B-S750, respectively), fly ash (B-FA) and metakaolin (B-MK) as determined through EDS analysis.

chapter 3, these results are fairly similar. Si and Ca concentrations fall in the same general range, though the Si values measured here have a little more scatter; in the Ca values there are occasional outliers with more Ca than was previously seen, but these are too few to draw statistically meaningful conclusions. While care was taken to avoid aggregate particles, it is likely that these points with high Ca are due to the beam impinging on calcite particles.

4.4.6 – Conclusions

The addition of fly ash failed, for the third time in this study, to produce any sort of evidence for the existence of 'geopolymers' in the alkali activated slag cement studied here. Though their existence cannot be ruled out, the overwhelming evidence from the combination of XRD, FTIR, TGA, and EDS suggests that 'geopolymers' are certainly not a major phase, if present at all.

Over 6 months, it produced no increase in strength, though early ages were somewhat lower. Despite this, strengths are still high enough for use in a wide number of applications; whether fly ash is a economically feasible or environmentally preferable additive is a question largely dependant on the geography of cement factories and would have to be settled on a case by case basis. A wide variety of new side products were detected by XRD, though none of them seem to have any great impact on final strength. Finally, undissolved fly ash particles were easily detected by SEM, indicating that it has not reached its full potential as an additive.

4.5 – Addition of Metakaolin

Metakaolin, a naturally occurring material chemically similar to fly ash, was added in hopes of producing 'geopolymers' with reasoning similar to that regarding the use of fly ash. Again, metakaolin was used to replace 10 wt.% of the slag.

4.5.1 – Mechanical Properties (Fine Aggregate Concrete)

Metakaolin was added to the powder reactants after 2 h at 750 ^{o}C; the samples were compression tested using the steel cap method. Tensile strength results were not obtained. Samples containing metakaolin acted in a manner similar to those containing fly ash (Fig. 4.15a), which, as they are both chemically similar aluminosilicates, is not surprising. For the NaOH/waterglass activated formula, strength increased from 63 ± 6 MPa at 1 day, to 73 ± 6 MPa at 7 d, to 103 ± 3 MPa at 28 d and 126 ± 3 MPa at 6 months, for a final loss of 10 % when compared to the basic formula. That is, it began with slightly lower strength but ended at almost exactly the same strength as the basic formula. As before, whether this slight loss in strength would be worth it due to a lowering of cost by cutting the slag with metakaolin would have to be decided on a case by case basis, centered on the geography of the slag production facilities, the metakaolin mines, etc.

When added to the Na_2CO_3-activated formula, metakaolin again behaves in a manner similar to fly ash, but results in stronger material (Fig. 4.15b.) Beginning at 5 ± 1 MPa after 1 day, a significant decrease when compared to the unadulterated formula, strength increased to 35 ± 2 MPa after 7 d, 49 ± 1 MPa after 28 d, and 70 ± 2 MPa after 6 months. As with the Na_2CO_3 activated formula containing fly ash, strength losses during the first month recover after longer curing periods.

The bulk of the work combining slag and metakaolin has been done on adding these materials to OPC [141-145]; Li *et al.* [143] found that incorporating 10 wt.% metakaolin in OPC alone increased compressive strengths from 55 MPa to 65 MPa at 28 d, but reduced fluidity. Adding 20 or 30 wt.% slag in place of OPC increased the strength to 70 MPa and removed the fluidity problem.

Yusheng *et al*. [146] investigated the formation of a 'geopolymer' made from 70/30 slag/metakaolin activated by NaOH/waterglass, cured at elevated temperatures, and with sand aggregate. They found that increasing slag content results in increasing strength, to a maximum of about 75 MPa for a 70/30 formula cured at 80 ^{o}C for 8 h. Hu *et al*. [147] investigated a slag/metakaolin 20/80 blend, much more metakaolin than was used here, activated by NaOH/waterglass. Although the material had roughly the same compressive strength at 28 d than an OPC sample (~ 45 MPa) the slag/metakaolin blend gained strength much more rapidly (22 MPa at 1 d, compared to 8 for the OPC sample.) This is much lower than the strength reported here, most likely due to the substantially higher amount of metakaolin used.

Overall, the trend whereby replacing slag with additives leads to lowered strength (as reported above for fly ash, and here for metakaolin), is confirmed.

4.5.2 – XRD and FTIR (Cement Paste)

The diffractograms (Figs. 4.16 and 4.17) of the formula containing metakaolin are, for all intents and purposes, identical to those of the formula containing fly ash, showing C-S-H, calcite, gaylussite, margarite, and tetranatrolite, with many other possibilities. Similarly, the FTIR spectra (Figs. 4.5 and 4.6) of formulae containing metakaolin have the same peaks, of slightly different shapes, as the spectra of formulae

containing fly ash. The difference in the shape of the peaks, however, is insufficient for the drawing of wider conclusions. The 28 d spectra are essentially identical to the spectra taken after 7 d.

In a study of various cements produced by blending OPC, slag, and metakaolin for purposes of immobilizing radioactive elements (rather than to produce cement with enhanced mechanical properties) Guangren *et al*. [148] obtained very similar FTIR spectra, which they identified as C-S-H; using NMR techniques, they concluded that this C-S-H also contained substitutional Al and Na in the interlayer space, which provides some benefits in immobilizing wastes.

In the work of Yusheng *et al*. [146] the existence of a broad, diffuse hump between 20-40 $^{o}2\theta$ is used to verify the existence of 'geopolymers' made of a slag/metakaolin blend; however, they do not provide a diffractogram of the raw slag, which may contain a hump at similar values. Further, the existence of quartz impurities provide sharp peaks which could be hiding less well defined peaks for products such as C-S-H.

In a study on blending metakaolin with OPC, Love *et al*. [149] reported C-S-H to be one of the main phases (along with other phases common to OPC, such as portlandite) as observed by XRD. Using TEM and NMR, however, they conclude that the use of metakaolin leads to longer chains of C-S-H with a higher degree of Al substitution. While the system reported here likely works differently from the one they report, and such analyses were not here performed, the alteration of the C-S-H is mentioned as a possible interesting area of future inquiry.

4.5.3 – SEM (Fine Aggregate Concrete)

Formulae with metakaolin were not investigated with image analysis. As with fly ash, in the NaOH/waterglass activated formula, individual particles were difficult to observe at low magnification (Fig. 4.18d) due to their small size. At higher magnifications (Fig. 4.18e) particles were still difficult to find, due to its general visual similarity to unreacted slag. EDS, however, positively identified numerous particles as unreacted metakaolin, based on the chemical differences (most notably lack of Ca) between slag and metakaolin. At the highest magnifications (Fig. 4.18f), metakaolin particles appeared as angular, blocky particles, roughly 5 μm wide.

As with the fly ash, metakaolin behaves similarly in both NaOH/waterglass and Na_2CO_3 activated formulae. At low (Fig. 4.18d) or medium (Fig. 4.18e) magnifications, the particles are either difficult to spot due to their small size, or difficult to spot due to their similarity to particles of unreacted slag. At the highest magnifications (Fig. 4.18f) the particles appear slightly rougher than those observed in the NaOH/waterglass based formula. This same phenomenon is observed in particles of unreacted slag, and is therefore more likely due to differences in polishing than any chemical reason.

That unreacted particles of metakaolin are easily found clearly indicates that not all of it is dissolving within the first 28 d, quite similar to the behavior of the formulae containing fly ash.

4.5.4 – EDS (Fine Aggregate Concrete)

The EDS results of both the NaOH/waterglass and Na_2CO_3 activated formulae (Fig. 4.19) containing metakaolin is essentially the same as that of the formulae

containing fly ash. The same general trends (less Si and more scatter in the Na_2CO_3 formula, Ca/Si ratio much lower than what would be expected from C-S-H in materials such as OPC, etc.) are observed.

4.5.5 – Conclusions

Essentially, metakaolin behaves in the same manner was fly ash; it neither produces 'geopolymers' nor negatively effects strength behavior over the first 28 d. A buffet of new mineral side products was produced, none of which seem to have any major effect on properties.

4.6 – Addition of Acid Rock Treatment Sludge

Acid rock treatment sludge from Halifax International Airport was added to alkali cement mostly to find a manner of disposing of acid rock treatment sludge. It was hoped that calcium and silicon in the sludge would make it amenable to incorporation in the cementing phase. As with metakaolin and fly ash, 10 wt.% of the slag was replaced by acid rock treatment sludge.

4.6.1 – Mechanical Properties (Fine Aggregate Concrete)

Acid rock treatment sludge was added to the basic formulae in 2 different ways: after drying at 200 ^oC for 24 hours, and after drying at 200 ^oC for 2 h followed by calcination at 750 ^oC for two h, hereafter referred to S200 and S750, respectively. These formulae were compression tested using steel caps, and thus will be compared to the steel cap data for the basic formulae.

Both of these materials had a deleterious effect on strength (Fig. 4.15a and 4.15b.) In the NaOH/waterglass activated formula, strength for S200 went from 54 ± 2 MPa at 1 d, to 56 ± 2 MPa at 7 d, to 72 ± 2 MPa after 28 d, to 68 ± 2 MPa at 6 months,

representing a total strength loss of almost 30 %. The S750 formulae were stronger, going from 68 ± 1 MPa at 1 d, to 72 ± 1 MPa at 7 d, 91 ± 1 MPa at 28 d, and 87 ± 1 MPa at 6 months. This still represents a roughly 10 % loss in the final strength. Moreover, the loss is consistent at all time stages: samples containing S200 are 30 % less at 1 d than the unadulterated formula at 1 day, 30 % weaker at 7 d, and so on. The reason for this could be due to the large amount of sulfur in the sludge, which is known to have an effect on the setting of portland cement, but this is unclear, as no sulfur compounds were detected by XRD and could not be detected by FTIR (see below.)

The effect of the sludge on Na_2CO_3 activated formulae was more pronounced (Fig. 4.15b.) After 7 d, neither samples containing S200 or S750 had set. It was only after 28 d that the samples were strong enough to test, revealing strengths of 25.3 ± 0.6 MPa and 26 ± 1.5 MPa, respectively, a roughly 50 % loss in strength for each formula. These strengths did not increase after even 6 months of curing; it is therefore clear that even at the longest time periods, the negative effects of adding the acid rock treatment sludge cannot be compensated for. The sludge would make an excellent retardant, except for one thing: this formula's set time is already sufficiently long, and the loss in strength is simply too high.

4.6.2 – XRD (Cement Paste)

The diffractograms of the NaOH/waterglass activated formulae (Fig. 4.16) are essentially the same as those of the formulae without acid rock treatment sludge, except that the peak at 30^o -2θ is sharper, indicative of more calcite than C-S-H. The diffractograms of formulae activated by the Na_2CO_3 solution are substantially more complex (Fig. 4.17.) The formula containing sludge dried at 200 ^oC reveals an extremely

sharp peak at about 30^{o}-2θ as well as a number of minor peaks, all of which correspond to $CaCO_3$ in the form of calcite. This calcite is likely due to the fact that this formula took more than a week to harden; recarbonation of calcium from the CO_3^{2-} ions was made easier due to the higher mobility of species in fluid. The formation of C-S-H may have been retarded by the large amounts of S and Fe in the sludge or, more likely, the C-S-H that was produced was insufficient to account for all the other phases being produced. Gaylussite, margarite, and tetranatrolite are all present; it is difficult to tell due to the size of the peaks, but it is almost certain that riversideite is present.

4.6.3 – FTIR (Cement Paste)

After 28 d of curing, FTIR spectra of the two formula with sludge were obtained (after only 7 d, they had not yet hardened; Figs 4.5 and 4.6.) They contain all of the same peaks as fly ash and metakaolin, but at much lower intensity than the other formulae, likely due to smaller quantities of final reaction products. FTIR is unable to determine if the retardation of setting in these formulae is due to the presence of S-rich compounds such as gypsum, as the peaks for S-O bonds (1650 cm^{-1} and 110 cm^{-1}) overlap with peaks due to water and Si-O bonds, respectively. A pronounced left-side shoulder on these peaks in the 28 d spectra may be indicative of S-O bonds, but is not sufficiently clear.

4.6.4 – SEM (Fine Aggregate Concrete)

Formulae with acid rock treatment sludge were not investigated with image analysis. In the NaOH/waterglass activated formula, particles of the acid rock treatment sludge (Fig. 4.18g) were easily observed due to the relatively large (~ 100 μm) size of some particles and light coloration, possibly due to their high iron content. Many displayed intragranular fractures. At higher magnification (Fig. 4.18h) smaller particles

with the same general characteristics (higher average atomic weight, intergranular cracking) were observed; these characteristics applied to even the smallest particles observed at the highest magnifications (Fig. 4.18i.)

For unclear reasons, the Na_2CO_3 activated formula containing acid rock treatment sludge was the most difficult formula to work with by SEM. Charging due to the electron beam made gathering images difficult; as such, the light coloration of the particles of unreacted acid rock treatment sludge was not seen. This could be due to the fact that the addition of the acid rock treatment sludge retarded the set time of the formula by a large amount, and it likely still contained a substantial amount of unbound water. At low magnification, however, unreacted particles were easily identified (Fig. 4.19g) due to their numerous intergranular fractures; as with the NaOH/waterglass activated formula, this behavior was observed at medium (Fig. 4.19h) and high magnifications (Fig. 4.19i.) It is therefore clear that even the smallest particles of the sludge are not fully dissolving, and are having a detrimental mechanical effect on the material.

4.6.5 – EDS (Fine Aggregate Concrete)

Elemental analyses of the sludge-containing formulae (Fig. 4.19.) are similar to those of formulae containing fly ash or metakaolin. The main difference is that the formulae with sludge, like the basic formulae, contain less Si, as no aluminosilicate materials were added. The Na_2CO_3 activated formulae again show more scatter than the NaOH/waterglass activated formulae, due to a greater number of phases present in the final product.

4.6.6 – Conclusions

It is difficult to imagine a situation in which large quantities of acid rock treatment sludge could be mixed into cement as a method of disposal: the decrease in strength is simply too great. On the other hand, it may be possible to use small quantities as a retardant. This is unlikely to come to fruition, however, because the main goal was to see if large quantities of the material could be disposed of in cement.

CHAPTER 5: CHARACTERIZATION OF ANCIENT BUILDING MATERIALS

5.1 – Bosnian 'Pyramid' Stone

17 samples were received from the site of the Bosnian 'pyramids' (Fig. 5.1.) Their supposed origins can be found in Table 5.1. These samples included:

- 3 samples (samples 2, 4, and 6) which were foul-smelling soils;
- 6 samples (samples 7, 8, 10, 11, 14, and 17) that looked like they could contain aggregate. Of these 6, sample 17 looked different (gray in color with smaller aggregate) and somewhat resembled modern concrete. The other five looked somewhat like concrete, but more like breccia, a naturally occurring mineral (Fig. 5.2.) Sample 10 looked like a hard rock with a layer of "concrete" (possibly breccia) on it;
- 6 samples (samples 1,9,12,13,15, and 16) were more or less normal-looking rocks, with no discernable differences in phases;
- 2 odd samples (samples 3 and 5.) Sample 3 was a solid rock but contained veins of some other mineral. Sample 5 looked like a natural rock containing a layer of some sort of mineral in the form of clear, solid grains. It was referred to as "stalagmite" on the data forms that accompanied the samples.

A number of these samples were investigated using XRD; Table 5.1 lists the phases detected in these experiments. None of the phases detected were particularly exotic and were limited to quartz, calcite, dolomite, and a few unidentified minor peaks.

Sample 17, the one that both contained calcite and visually appeared the most like modern concrete, was investigated in the SEM. The most common phases identified by

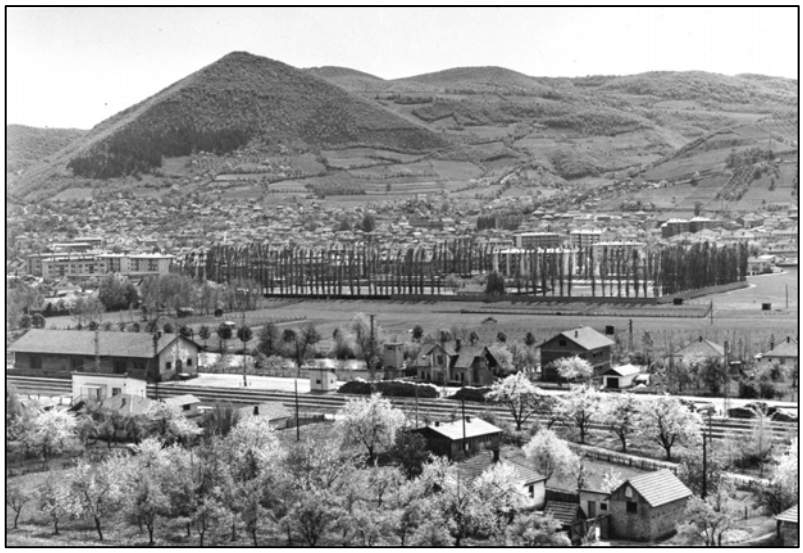

Figure 5.1 – The Bosnian 'Pyramid' (top mid-left) at Visoko in 1973. Photograph courtesy Wikipedia.

Table 5.1 – Descriptions, origins, and summary of XRD analysis of the samples obtained from the Bosnian 'pyramids.' Descriptions are based on visual inspection: SR = 'Solid Rock,' that is, a visually homogenous mineral; S = 'Soil'; Lay = a mineral containing striations of some other mineral; B = most likely Breccia; and Con = a material similar in appearance to modern concrete. Origin is taken verbatim from data sheets that provided by Semir Osmanagić. XRD results are listed in order of highest to lowest peak intensities: Q = Quartz; C = Calcite; D = Dolomite; n/a = XRD not run on this sample; and ? = unknown minor peaks.

Sample #	Description	Origin	XRD Results
1	SR	"Underground Tunnel Complex 'Ravne'"	Q, C
2	S	"Underground Tunnel Complex 'Ravne'"	n/a
3	Lay	"Underground Tunnel Complex 'Ravne'"	n/a
4	S	n/a	n/a
5	Lay	"Underground Tunnel Complex 'Ravne'"	n/a
6	S	"Underground Tunnel Complex 'Ravne'"	n/a
7	B	"Pyramid of the Sun"	n/a
8	B	"Pyramid of the Sun"	n/a
9	SR	"'Tumulus' in Vratnica (Toprakalija)"	D, C, Q
10	B	"'Tumulus' in Vratnica (Toprakalija)"	n/a
11	B	"'Tumulus' in Vratnica (Toprakalija)"	D, C, Q
12	SR	"'Tumulus' in Vratnica (Toprakalija)"	n/a
13	SR	"'Dolovi' hill in Vratnica"	Q, D, C
14	B	"Close vicinity of Temple of the Earth"	D, C, Q, ?
15	SR	"Bosnian Pyramid of the Moon"	Q, C
16	SR	"Bosnian Pyramid of the Moon"	Q, C, D
17	Con	"'Tumulus' in Vratnica (Toprakalija)"	Q, D, C, ?

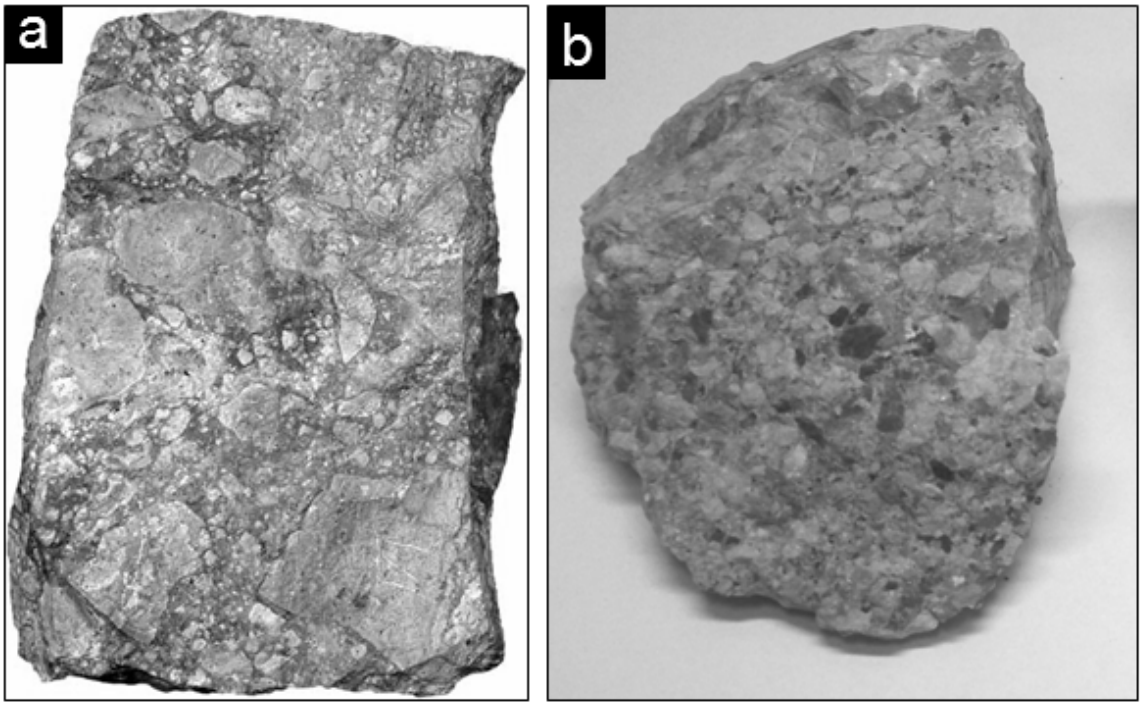

Figure 5.2 – a) Natural breccia, and b) sample #7 from the Bosnian 'pyramid.' Photo of natural breccia courtesy University of Auckland.

EDS (Fig. 5.3) were quartz, calcite, dolomite, small particles of FeS, and small amounts of a phase that is similar to quartz with an additional 7 at.% Al and 7 at.% Na. This is possibly quartz with a small amount of clay as impurities. Though many areas were investigated (not shown), these few phases were the only ones that were identified.

Based on the XRD and EDS results showing that the Bosnian samples contained calcite, two specimens were sent for radiocarbon dating. Sample 17, discussed above, and sample 8, which could be a natural breccia but could also appear to be a concrete, were analyzed; both came back with infinite ages (Table 5.2.) It is therefore likely that at least these two samples are natural; if nothing else, it is definite that they are not made of a recarbonated lime-based material.

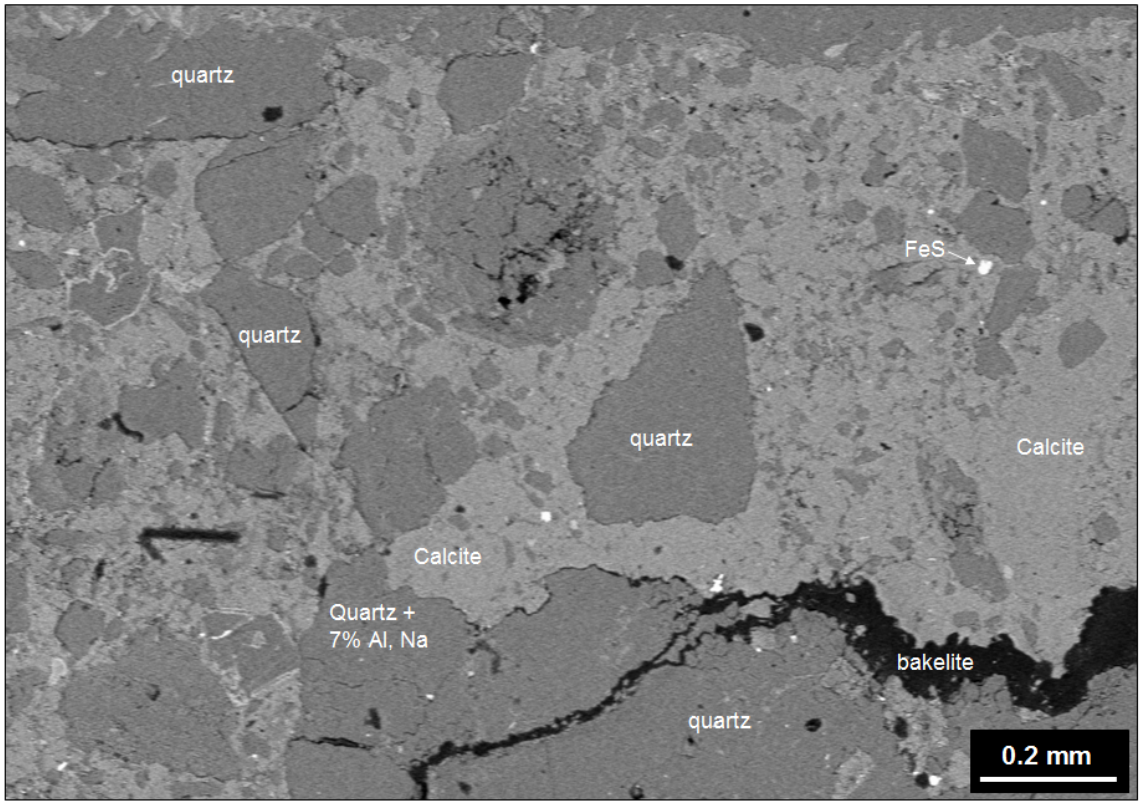

Figure 5.3 – BSE/SEM analysis of Sample #17 from the Bosnian 'Pyramids.' Main phases (quartz, calcite, FeS, bakelite mounting material, and quartz with 7 at.% Na and 7 at.% Al), as determined by EDS, are labeled.

To be totally certain, every sample would have to be radiocarbon dated, at great expense. Bearing in mind that 1) at least one-third of the samples appear to be natural breccia, and one of these samples was shown to be natural; 2) the sample that most resembled modern concrete is, in fact, not concrete; 3) the XRD experiments failed to reveal anything other than naturally occurring minerals; and 4) that 3 of the samples are soils which would be difficult to analyze anyway, it can be more or less safely concluded that the samples are, in fact, not concrete. At least, not concrete as far as the modern conception of the word is concerned.

It is noted here that investigation of the Bosnian 'pyramid' samples provided no evidence supporting the theory that the structures will "break a cloud of negative energy, allowing the Earth to receive cosmic energy from the centre of the galaxy", or that they will "adjust the Earthly frequency and bring it into accordance with the vibrations of our Sun" at the behest of the Maya, the Cosmic Watchmakers. Should either of these events come to pass it will surely be due to reasons other than the geological makeup of the 'pyramids.'

5.2 – Colorado 'Flooring' Stone

Samples from the Colorado 'flooring' stone were obtained from David P. Bailey, curator of history at the Museum of Western Colorado. Two samples were received, each roughly egg-shaped, with a diameter of about 20 mm each. Beige in color, they had a gritty, sandy texture (Fig 5.4a) and were originally obtained from the 'floor', which lay several meters below the surface of the earth (Fig 5.4b.)

Three distinct phases in this material were observed by XRD. The first and strongest was quartz (SiO_2), followed by calcite ($CaCO_3$), and Ca-rich, disordered albite ($(Ca,Na)Al(Si,Al)_3O_8$) which accounts for a number of minor peaks. The origin of a peak at 64^o 2θ is not clear.

At low magnification in the SEM, the Colorado sample looked like what would be expected of a concrete: large grains surrounded by a cementing phase (Fig. 5.5a and 5.5b.) In BSE imaging, the cementing phase was revealed to be itself made of three distinct phases, which appeared as light, medium, and dark gray. The aggregate (phase #1), which was identified by EDS to be SiO_2, appeared as the darkest gray. The lightest colored region (phase #2) appeared to be $CaCO_3$, but with the inclusion of 1 at.% each of

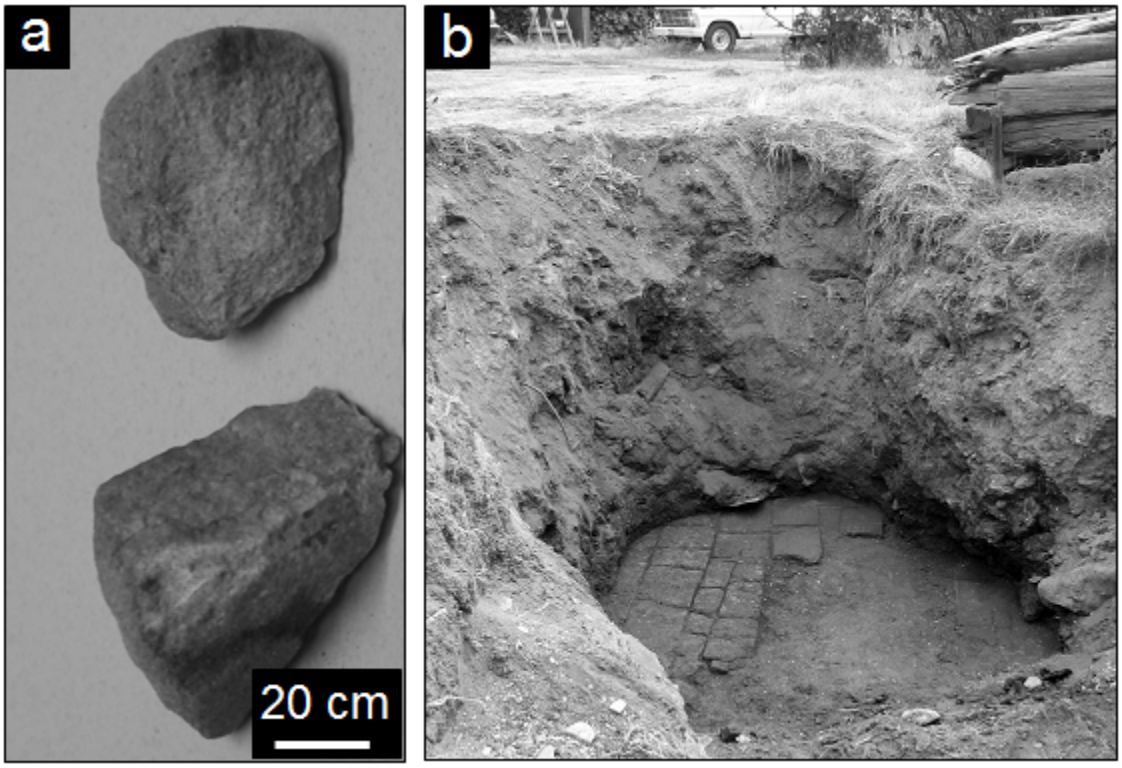

Figure 5.4 – a) Samples from Colorado 'floor' and b) location of the 'floor.' Note truck (top center) for sense of scale.

Na and Al, and 4 at.% Si. It is likely that this was evidence of mild contamination, probably from albite. The medium-gray region (phase #3), which took the form of particles that looked similar to the aggregate particles but went unnoticed in SE2 images, contained 9 at.% C, 57 at.% O, 7 at.% Al, 7 at.% K, 20 at.% Si. The makeup of this region is not clear, but it is possibly a K-aluminosilicate clay. Dark gray regions (phase #4) appear to be $CaCO_3$, but with a Na-aluminate impurity (8 at.% Al, 5 at.% Na.)

EDS mapping of the sample greatly simplified identification of the four phases (Fig. 5.5c-h.) In a map of Si (colored red) and Al (colored green), the aggregate appeared as a bright red, pure-Si phase; phase #2 appeared as an absence of either color, due to the

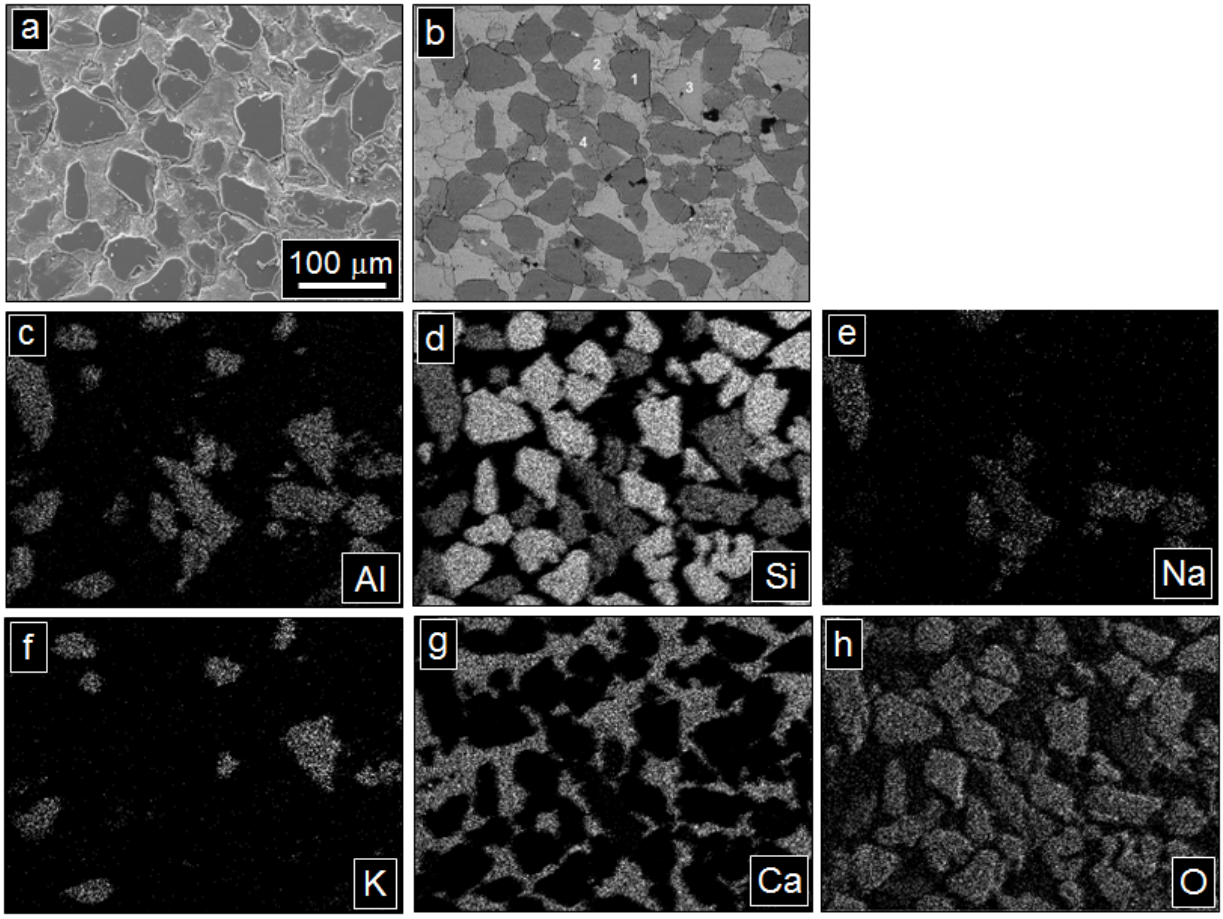

Figure 5.5– SEM images of Colorado sample. a) SE image similar in appearance to a concrete with extremely fine, well-dispersed aggregate; b) BSE image showing four different phases; c) Al EDS map helping to identify phases #3 and #4; d) Si EDS map helping to identify phase #1 (quartz, brighter) and phase #3 (darker gray); e) Na EDS map identifying phase #4; f) K EDS map identifying phase #3; f) Ca EDS map identifying phase #2 ($CaCO_3$); h) O EDS map, showing that all phases are oxides.

Table 5.2– Results of radiocarbon dating 'ancient' samples from the Bosnian 'Pyramids' and Colorado 'Floor'

Description/location	Age (BP)	o/oo	AGG
Colorado Sample	> 45,560	- 4.8	-
Bosnia #17	>44,000	- 0.6	-
Bosnia #8	>44,000	- 1.1	-

low Si and Al levels; phase #3 showed up as yellow (due to the mix of Si and Al); and phase #4 appeared greenish due to the lack of Si.

Based on Fig. 5.5, the only plausible phase that could, based on morphology, act as a binder is calcite (Fig. 5.5g.) The other phases would clearly be considered aggregate. If $CaCO_3$, were the binding phase it would have to have been existed as lime in the relatively near past. As a result a sample was sent for radiocarbon analysis, the result of which was an infinite age (Table 5.2,) indicative of natural $CaCO_3$. It is crucial to note that the same arguments apply to the Bosnian pyramid sample (Fig. 5.3) While a synthetic origin cannot be ruled out, the radiocarbon data effectively shows that, if synthetic, the sample is not made of a recarbonated lime material.

After the analysis, it was learned that the sample which was received was from one of the 'tiles'; analysis on the 'joint' compound (possibly a 'mortar') was not carried out.

5.3 – Pyramid Granite

Investigations of four granites (one natural granite from Aswan, and one each from Menkuare's pyramid, Khafre's pyramid, and the Valley Temple) were carried out by SEM/EDS. According to Davidovits, the granite used in the pyramids must be an alkali-aluminosilicate 'geopoylmer' due to issues pertaining to the quarrying and placement of massive granite blocks. Unfortunately, natural granite is composed of three main ingredients: quartz, alkali feldspar, and plagioclase feldspar. That is to say quartz and alkali (either Ca, Na, or K) aluminosilicates; the presence of these naturally-occurring alkali aluminosilicate minerals thus hampers the search for synthetic alkali aluminosilicate 'geopolymers.'

Table 5.3 – Phases found in granite from four Egyptian sources, as determined by EDS. The bottom four phases are of indeterminate chemistry; thus, they are identified only by their main constituents.

Phase	Valley Temple	Khafre's Pyramid	Menkuare's Pyramid	Aswan (natural)
SiO_2	x	x	x	x
K-Al-Si	x	x		x
K-Al-Si, F-Rich				x
Na-Al-Si	x	x		x
Na/Ca-Al-Si			x	
$CaCO_3$	x			
Fe_2O_3		x	x	x
$BaSO_4$	x	x		
Si, P		x	x	x
Ca, Si, Ti			x	
Ca, P	x		x	x
F-rich phase			x	x

The results of the SEM/EDS investigation (Table 5.3) are indeterminate. In addition to possibly naturally occurring alkali aluminosilicates, a number of minor 'contamination' phases were identified (calcite, barite, ferrite, etc.), as well as several phases with elemental makeups that cannot immediately be identified (F- or P-rich Si or Ca phases, for example.) Due to granite being, for lack of a better term, the 'garbage can of nature,' further analyses were performed instead on limestone, theoretically a more homogeneous system.

5.4 – Pyramid Limestone

Samples of limestone were obtained from a number of pyramids (Table. 5.4.) The provenance of the samples was never in question [150]. The bulk of the samples are from the outer casings, but two are from inner casings (one from the Red Pyramid and the Lauer sample, provided by archaeologist J.P. Lauer, from the Great Pyramid.)

5.4.1 – FTIR

The majority of peaks in FTIR spectra of natural Tura limestone and from 4 other ancient sources (Fig. 5.6) can be attributed to $CaCO_3$. The sharp peaks at 875 cm^{-1} and

Table 5.4 – Names, location, and age of Pyramids whose samples were investigated

Source	Ancient Name	Builder	Location	Completed
Bent Pyramid	Southern Shining Pyramid	Sneferu	Dashur	2596 BC
Red Pyramid	Shining Pyramid	Sneferu	Dashur	2596 BC
Queen's Pyramid	-	Sneferu	Dashur	2560 BC
Collapsed Pyramid	Sneferu Endures	Sneferu	Meidum	2560 BC
Menkaure's Pyramid	Menkaure is Diving	Menkaure	Giza	2504 BC
Great Pyramid	Khufu's Horizon	Khufu	Giza	2560 BC
Valley Temple	-	Khufu	Giza	2560 BC
Khafre's Pyramid	Khafre is Great	Khafre	Giza	2540 BC
Natural Tura Limestone	-	-	Giza	-
Natural Maadi Limestone	-	-	Giza	-
Natural Limestone - Khufu's Quarry	-	-	Giza	-

710 cm^{-1} are indicative specifically of crystalline $CaCO_3$; the broad peak centered around 1470 cm^{-1} indicates the presence of carbonate ions in general. A number of weak minor peaks, at about 2510 cm^{-1} and in the 2900-3000 cm^{-1} range have been attributed to 'harmonics' which occur specifically due to the unique geometry of calcite [79]. Minor peaks in the 1100 cm^{-1} and 510 cm^{-1} neighborhoods may indicate the presence of small amounts of siliceous or aluminosilicate materials, however, they are too small for

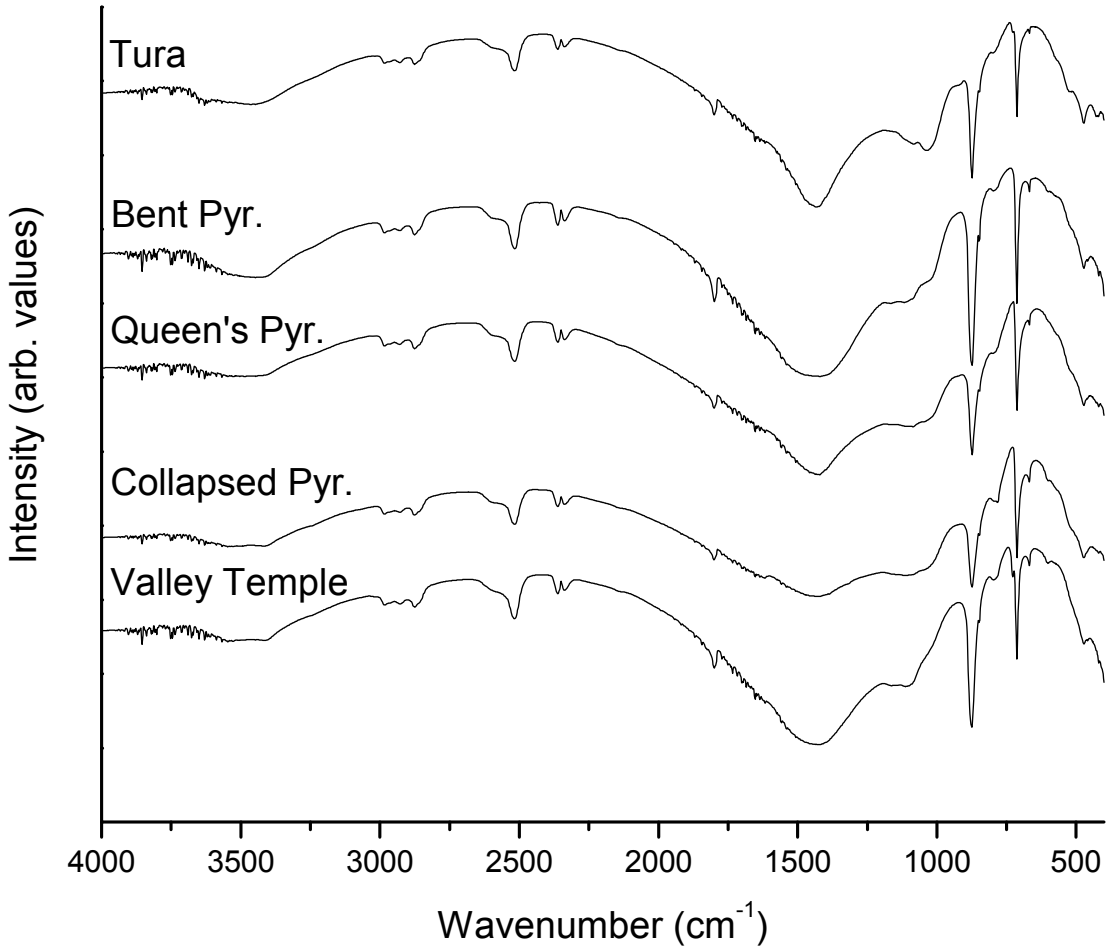

Figure 5.6– FTIR spectra of (from top) natural Tura limestone and limestones from the Bent Pyramid outer casing, Queen's Pyramid in Dahshur, Collapsed Pyramid in Meidum, and the Valley Temple in Giza.

definite conclusions to be reached. The FTIR spectra therefore indicate that $CaCO_3$ is the majority phase in these samples.

The use of FTIR to differentiate between naturally occurring sedimentary limestone and limestone created by the recarbonation of lime has been described [151] in which the ratio of the intensities of the two sharp, crystalline peaks is used. A similar method was attempted here without success: the ratios of the peaks for the spectra collected here are well outside the range detailed by this technique. It is almost certain

that the reason for this is that the technique demands close observation and control of particle size, which was not available at the time this work was carried out.

FTIR analysis therefore confirms that calcite is the main phase in these samples, with some possible silicate or aluminosilicate phases; it was unable to be used, however, to differentiate between natural and recarbonated lime.

5.4.2 – Electron Microscopy

A substantial amount of electron microscopy was performed on a variety of samples; the bulk of these samples came from the outer casing of the Bent Pyramid. Microscopy was performed on polished and/or etched samples, as well as fracture surfaces. In a recent paper, Jana concluded [152] that several pyramid samples including the Lauer sample were natural, based largely on structural evidence (the presence of fossils, etc.) It should be noted that, if lime was in fact used, or limestone used as an aggregate, the presence of fossils would be insufficient to discount the synthetic origin theory.

5.4.2.1 – Fracture Surfaces

Fracture surfaces (Fig. 5.7a-c) contained a number of discernable structures, in addition to calcite and occasional grains of quartz (not shown.) Lepispheres (Fig. 5.7a)

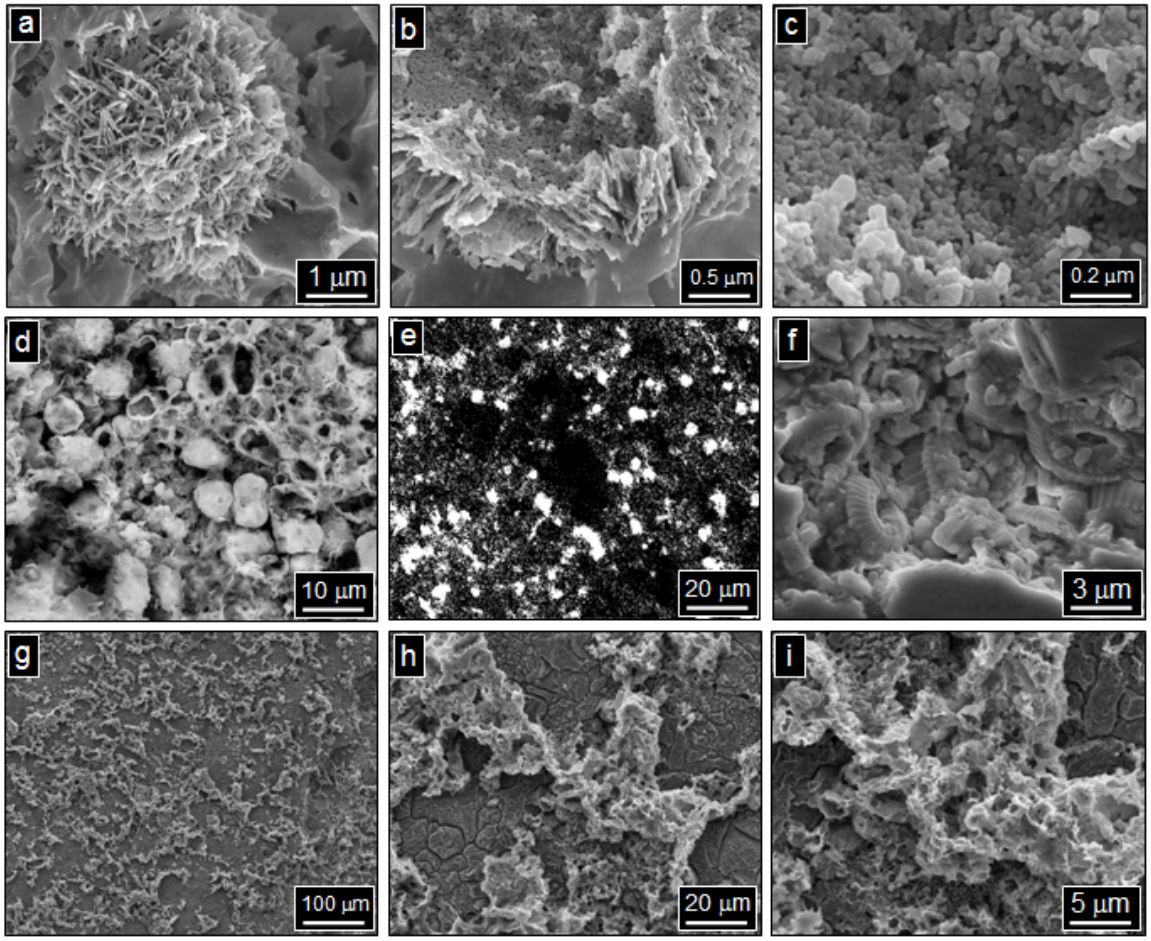

Figure 5.7 – Common structures observed in fracture surfaces of pyramid limestone. a) High-magnification image of a lepisphere, the transition product as amorphous Si becomes quartz; b) outer portion of a fractured lepisphere; c) high magnification image of interior of fractured lepisphere; d) etched sample, showing numerous round structures likely to be lepispheres; e) EDS Si map showing lepispheres as small, bright circles; f) calcareous coccolith skeletons (ridged, donut-shaped objects), of which sedimentary limestone is composed; g) overview of etched sample showing Si-rich residue; h) higher magnification image of Si-rich residue and etched calcite (darker gray); and i) 'flaky' or 'wispy' morphology of Si-rich residue.

were observed fairly frequently; they are small, roughly spherical, agglomerations of opal-CT that are often described as the transition products as amorphous silica turns into quartz. Visually, they look like Christmas tree ornaments made from razor blades. At higher magnifications (Fig 5.7b and 5.7c), the interiors of fractured lepispheres appear to be made of particles with diameters in the 200-300 nm range. They are observed with

increasing regularity in etched samples (Fig 5.7d.) Using EDS Si mapping (Fig 5.7e) it is fairly easy to observe lepispheres – they are shown as circles with a strong Si signal. EDS results show roughly 70% O, 30% Si – deviating from the formula of SiO_2 by only 3%, a reasonable confidence level for using the EDS technique. Finally, coccoliths, the calcite skeletons of microscopic algae of which sedimentary limestone is composed, were frequently observed (Fig 5.7f.)

Judging by the fracture surfaces, there is little evidence that the samples are synthetic – SEM/EDS cannot distinguish between natural limestone and limestone produced through the recarbonation of lime. At no point were Na or Al, the critical hallmarks of 'geopolymers,' found.

5.4.2.2 – Polished Samples

Polished surfaces (Fig. 5.8a) were, as are polished surfaces of any more or less homogenous material, essentially featureless. Occasional impurities (particles containing high amounts of Fe, Zn, Ba, Sr, etc.) were observed, and, due to their much higher average atomic number, could be easily located in BSE mode. Pores were occasionally evident. The vast majority of points investigated were revealed to be calcite; while this was not what was being looked for, at least it provided constant opportunity to check the calibration of EDS. From this, all EDS values are estimated to be accurate to within 3%.

One microstructure that appeared in numerous (though not all) samples were areas that appeared as agglomerations of nanospheres (Fig. 5.8b), approximately 20-50 nm in diameter (Fig. 5.8c.) EDS was inconclusive; while it was clear that the areas are composed mainly of silica, whether Ca is a part of that system, or the signal is bleeding in from outside, is unclear.

These patches of silica, when they were found, were widespread. Elemental mapping (Fig. 5.8d) shows the extent of the phase. That these patches of silica exist could be critical; their microstructure is quite different from that of lepispheres (they are not always round, not the same size, and do not have the bladed structures that make up lepispheres.) Lepispheres are the intermediate step as amorphous silica turns into quartz; there is no readily available explanation for why both lepispheres made of opal-CT and nanospheres of amorphous silica would coexist in the same material. Ingram *et al.* [153] examined samples from a number of pyramids; they found low levels of Si (below 4%) that they dismissed as naturally occurring; however, they also found higher than normal levels of Al, which were not observed here.

5.4.2.3 – Etched Samples

In an attempt to better understand the nature of the silica nanospheres, samples of limestone were etched with HCl. The calcite dissolved away, leaving behind an insoluble residue (Fig 5.7f) which at high magnification appeared to have a lacy, flaky structure (Fig 5.7g and 5.7h.) When the residue itself was investigated, it appeared to be composed entirely of lepispheres and remnants of lepispheres.

Therefore, partially etched samples (Fig. 5.9) were investigated. A typical cross-section of a sample showed a smooth, featureless polished region and an etched region containing two distinct regions: darker, rough regions (Fig. 5.9b) and smoother regions that develop a crack pattern similar to crazed-mud (Fig. 5.9a, inset.) The rough regions were composed of a variety of elements, predominantly Si (Fig 5.9c, with average elemental composition inset.) While structures composed of agglomerations of nanospheres were not observed after etching, plenty of insoluble products remained.

Overall, polished, etched, and fracture surfaces from a number of ancient Egyptian sources have painted a complicated picture. On the one hand, no trace of 'geopolymers' were found; in fact, at no point were amounts of Na or Al greater than 1 at.% ever found, even in impurities. Such structures as lepispheres and coccoliths, which were also found in natural samples, were observed with some regularity.

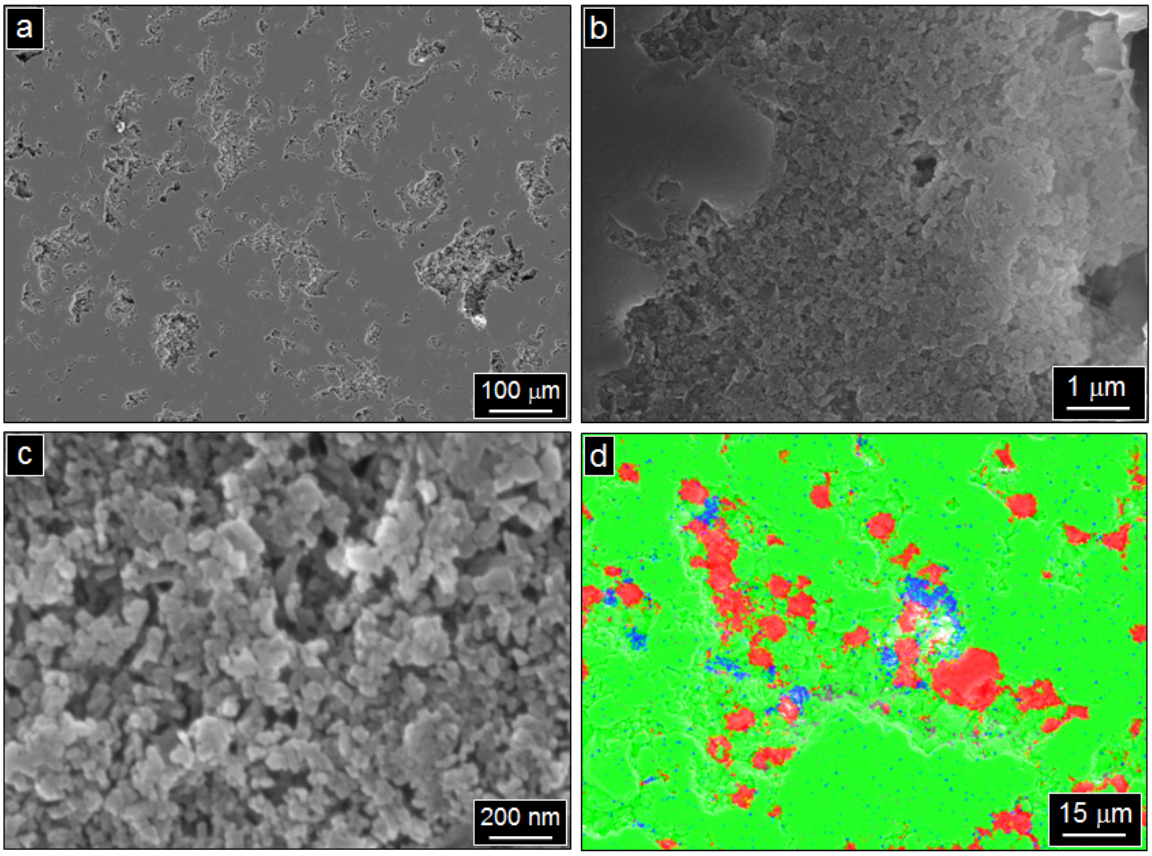

Figure 5.8 – a)Polished surface of limestone from the Bent Pyramid, showing porosity; b) region of Si-rich Nanospheres found in numerous samples; c) high magnification image of Si-rich nanospheres showing average grain size around 20-50 nm; and d) elemental map of Si-rich regions (Si = Red, Ca = Green, S = Blue.)

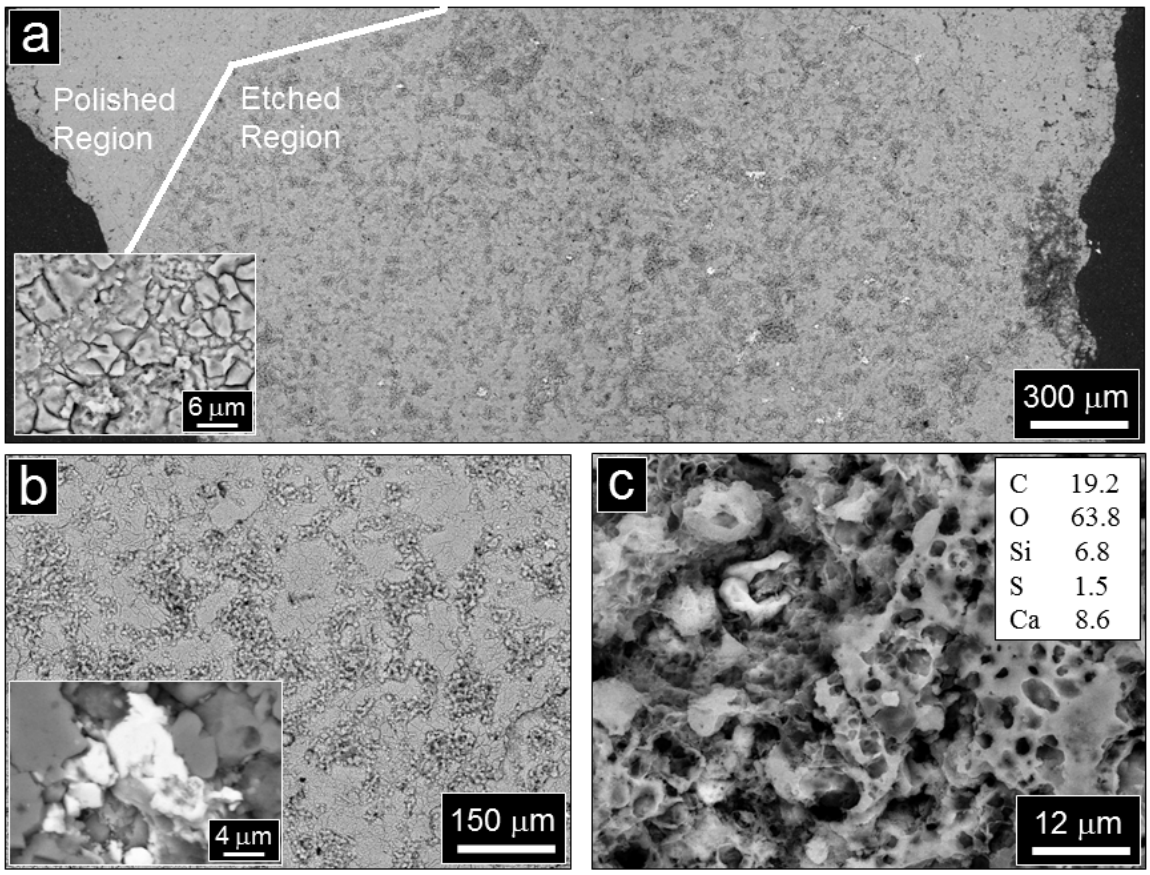

Figure 5.9 – a) Typical BSE-SEM micrograph of a partially etched polished sample. Note lack of contrast in upper top polished corner. Once the limestone is dissolved the extent of the Si-rich phase that is presumably at the "grain boundaries" is revealed. Inset shows a higher magnification of the smoother etched surface. b) Medium magnification of etched area. Inset shows a Ba and S-rich particle. c) High magnification of Si-rich area showing extreme roughness.

On the other hand, nanospheres of amorphous silica were also observed, which were not seen in natural limestone; these may be indicative of a Ca- or Mg-silicate binding phase. Also, EDS is unable to distinguish between natural limestone and calcite produced through the recarbonation of lime.

5.4.3 – TEM

TEM experiments were conducted on samples from the Bent Pyramid in which the presence of SiO_2 nanospheres had been confirmed by SEM. A number of particles

were investigated (Fig. 5.10a) which showed distinct regions of highly crystalline calcite (Fig. 5.10b) and separate regions of amorphous SiO_2 nanospheres (Fig. 5.10c.) These nanospheres were observed to be non-crystalline and roughly 20-40 nm in diameter (Fig. 5.10d-f.) Over time, it is known that C-S-H, such as that produced by mixing amorphous SiO_2 in the form of DE with lime can degrade into two separate regions: calcite and amorphous SiO_2 [154]. As previously observed by SEM, the samples contain semi-crystalline lepispheres; why a mixture of amorphous SiO_2 and semicrystalline SiO_2 would occur in the same sample is not clear; therefore, the possibility of these particles being deterioration products of some sort of calcium silicate binding phase is possible.

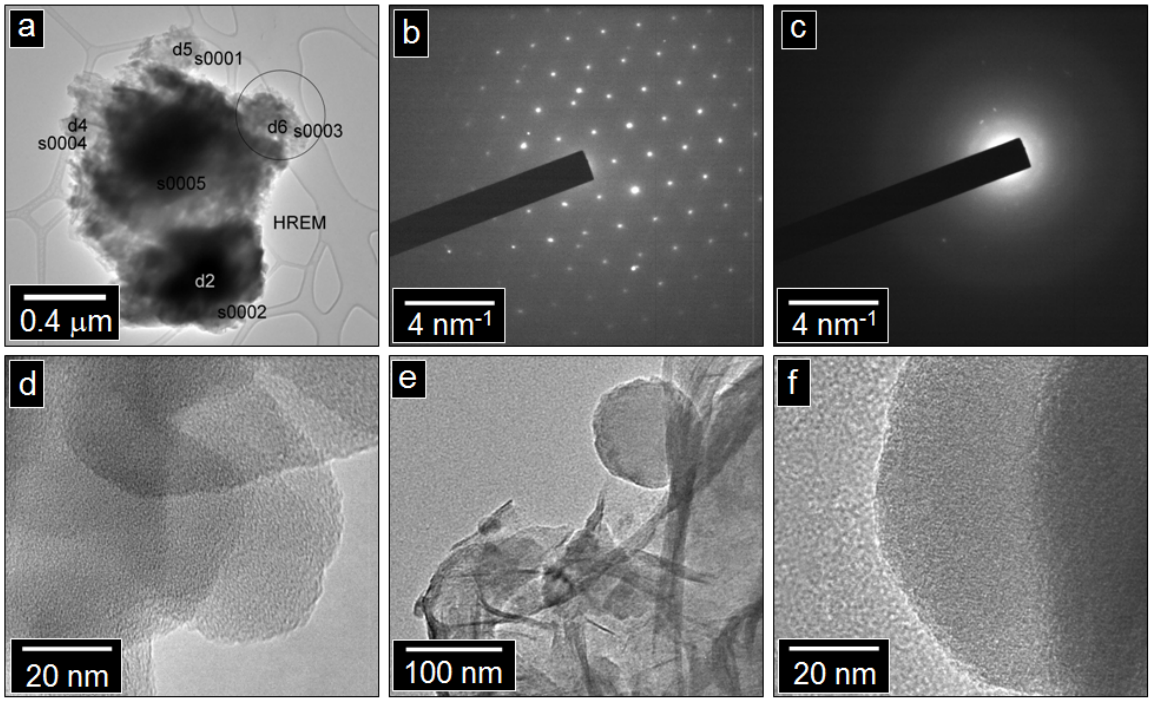

Figure 5.10 – TEM images of limestone from the Bent Pyramid. a) particle of limestone containing regions of pure SiO_2 (D4, D5, D6) and calcite (D2). The circle roughly shows diameter of electron beam; b) diffraction pattern of calcite region; c) diffraction pattern of SiO_2 region, showing no crystal structure; d) close-up image of SiO_2 nanosphere from region marked HREM; e) environment around another nanosphere; f) another SiO_2 nanosphere, showing lack of crystalline content.

5.4.4 – Radiocarbon Dating

Radiocarbon dating can be used to date lime-based mortars due to the chemistry behind their production: first, limestone is burned in a kiln, transforming it into CaO (lime) and releasing CO_2; it is then mixed with water, which hydrates it and forms $Ca(OH)_2$ (portlandite), which, overtime, will absorb CO_2 from the atmosphere and become, once again, $CaCO_3$. (These reactions are shown in Eqs. 1-3, in Ch. 1.) It is the absorption of CO_2 from the atmosphere that enables radiocarbon dating techniques to be applied in the same way that atmospheric carbon from respiration can be used to date plants (or the creatures that eat them.) This technique has been used to successfully date ancient lime materials [155, 156].

Unfortunately, ancient lime was hardly a homogeneous material; the crudes were sufficiently crude that nowhere near all of the limestone was transformed into lime. This is the source of a 'reservoir effect' in which 'dead' carbon (carbon of infinite age) from the unburnt limestone is counted along with the atmospheric carbon fixed by the lime, and the resulting apparent age is much older than the actual age [157]. It is therefore possible to determine the percentage of 'dead' carbon in a sample through well-established means.

If the apparent age (the result of radiocarbon dating), the true age, and the age of any contaminants are known, a straightforward method exists for determining the fraction of the sample that is contamination:

$$\lambda t_a = t - \ln(1-F_c + F_c e^{\lambda(t-tc)}) \qquad \text{(eq. 7)}$$

where t = true age, ta = apparent age, tc = contaminant age, Fc = fraction of contaminant, and λ is the radioactive decay constant (1.24×10^{-4}) [157]. For contamination by infinitely

old material (such as pure cement 'contaminated' by naturally occurring aggregate) the final term drops out:

$$\lambda t_a = t - \ln (1-F_c) \qquad \text{(eq. 8)}$$

This makes the determination of F_c, the amount of contaminant in the sample, relatively easy to determine. It cannot, however, be used in more complex situations; for instance, if contamination is continuously added to a sample, or if there is more than one contaminating event, this equation will provide only a single, average value for any of the values which are to be determined (t, t_a, F_c, etc.) No method capable of describing such complex contamination scenarios exists.

The results of the radiocarbon dating (Table 5.5) are relatively straightforward: some samples are infinitely old (and thus natural) while others have finite, measurable ages. The reason that these ages are older than the ages of the pyramids is due to the previously described 'reservoir effect' in which limestone aggregate with 'dead carbon' has contributes infinitely old carbon to the age.

The percentage of these samples that would have to be infinitely old limestone 'aggregate' were determined through Eq. 5; many samples are calculated to have as much as 4-5% cementing phase. This would indicate only the amount of cementing phase produced through the recarbonation of free lime; if Ca- or Mg-silicates are involved, as the SEM evidence suggests, the quantity of 'cement' could be much higher.

The finding of trends is somewhat difficult; while all of the samples from the Bent Pyramid return finite ages, samples from some pyramids (e.g. Menkaure's Pyramid or the Red Pyramid) return infinite ages, while for samples from Khafre's Pyramid, one sample is datable and another is not. It is possible that the samples returning infinite ages are

Table 5.5 – Results of radiocarbon analyses of ancient samples. 'Crushed' refers to a sample that was coarsely ground and only the fine fraction of powder was tested. The lime/limestone mix was a sample prepared in the lab using commercially available lime. Two natural limestones (bottom) are listed for comparison. 'Organic' refers to the organic residue left over after the sample was dissolved in acid.

Description/location	Age (BP)	o/oo	% Aggregate	Original Code
Lauer Sample	29,010 ± 190	+0.4	95.23	Louis
Collapsed Pyramid	40,980 ± 540	+ 0.6	98.92	Stovetop
"Screwdriver" sample	> 44,000	- 1.0	-	Frank
Menkaure's Pyramid	> 46,000	- 0.1	-	Joseph
Middle kingdom sample	34,800 ± 530	+ 1.8	97.84	Romeo
2 large blocks (pregnant sample)	> 42,000	+ 2.2	-	Lear
Red Pyramid Inner Casing	> 46,000	+ 1.5	-	Onion
Khafre's Pyramid Floor	> 46,000	- 1.2	-	Eggplant
Khafre's Pyramid Floor, SE	33,680 ± 260	+ 0.5	97.34	Cabbage
Khufu's Pyramid, Basement	40,460 ± 550	- 0.3	98.85	Edward
Khufu's Pyramid West Side	40,560 ± 510	0.0	98.87	Beaver
Bent Pyramid cont. nanospheres	38,520 ± 430	+ 1.3	98.53	Aaron
North side, Bent Pyramid	31,180 ± 230	+ 2.1	96.34	Christopher
South side, Bent Pyramid	32,740 ± 270	+ 1.2	96.99	Alex
Bent Pyr East Side	30,000 ± 210	+ 1.1	95.76	Parisbeau
Bent Pyramid - Surface layer	23,620 ± 140	-1.2	90.62	Squid I
Bent Pyramid - Middle layer	21,940 ± 120	1.7	88.44	Squid II
Bent Pyramid - Core layer	21,920 ± 120	2.3	88.41	Squid III
Lime/limestone mix from lab	14,600 ± 140	- 0.7	83.66	Sean
Natural Maadi Limestone	> 45,000	- 1.1	-	Ismail
Natural Tura Limestone	> 43,630	2.2	-	Mike
Tura – Crushed	>44,000	(+ 2.5)	-	Cass
Bent Pyramid (ORGANIC)	4,520 ± 40	-24.1	-	Squid II

simply from pieces of aggregate. As the specimens from which these samples were taken weigh only a few hundred grams, at most, and are smaller than a few cubic centimeters, why a sample would not be evenly contaminated is unclear. It is further unclear why natural samples, which were equally exposed to the elements, would not be similarly contaminated; or why the Lauer sample, which was unexposed until the opening of the pyramid relatively recently, would not show the least contamination. That the modern

sample, prepared in the lab, has 17 % 'contamination' by modern carbon, and not the 20 % expected from the mix proportions, is likely due to incomplete recarbonation.

This is especially shown in a sample from the Bent Pyramid (originally codenamed Squid I, II, and III.) A few cubic centimeters in size, the outer layer was exposed to acid, and the evolved gas measured; then the 'middle layer'; finally, the center of the sample was measured. That the surface of the sample contains less 'cementing phase' (which, it could be argued, is just modern contamination) than the center of the sample is counterintuitive. Why the outside of a sample, which is exposed to the elements, would be less contaminated than the center, is not clear *assuming* contamination from natural sources is the cause of the finite ages. Finally, why the organic residue left over after dissolving the limestone in acid would be so close to the actual age of the Bent Pyramid would have to be addressed if it is contamination; on the other hand, if impure Nile water were used, containing a tiny bit of much older contaminant to skew the age backwards a few years, the result seems quite straightforward.

Numerous researchers, such as Harrell and Penrod [158], Jana [159], and Campbell [160] concluded that samples from the pyramids were natural stone based on detailed petrographic/SEM/XRD. Radiocarbon dating is, however, a much more reliable and *objective* method.

5.4.5 – Conclusions and Discussion

Using FTIR, no evidence for the synthetic nature of the pyramid limestones was found. In the SEM, however, anomalous Si-rich phases in the form of agglomerations of nanospheres 20-50 nm in diameter, and possibly Ca- or Mg-silicates, were observed. Not

even traces of Na or Al were found, discounting the possible use of ‘geopolymers.’ As SEM is unable to differentiate between natural and recarbonated limestones, radiocarbon dating was used. Natural limestones and a minority of pyramid samples had infinite ages; many came back with a measurable age, providing a strong argument for their synthetic nature.

The radiocarbon dating shows that many of the pyramid samples have finite, datable ages. It is not possible to rule out contamination by modern carbon, however, for a number of reasons, this seems unlikely. That the dates are older than expected is likely due to the reservoir effect of limestone aggregate used by the Egyptians, unburnt lime, etc. Though the use of lime as plasters in Egypt and the Levant area in general is well documented, this is the first data that suggest that the Egyptians were able to use lime to form massive blocks, moving the credit for doing so from the Romans back by several thousand years. The conclusions reached herein need to be confirmed by others on more samples, however, before a more definite conclusion, one way or another, is reached.

CHAPTER 6: CONCLUSIONS

6.1 – AAS Cements

A number of conclusions can be drawn from the work here presented:

- C-S-H is definitely present in all of the formulae investigated, confirmed by XRD, FTIR, and possibly TGA. The alkali activation of this slag does not, therefore, lead to wide-scale production of 'geopolymers' (as originally defined by Davidovits) as is sometimes reported in the literature. SEM analysis shows only a single, homogeneous Op.
- The addition of a variety of additives failed to produce 'geopolymer' or mixed 'geopolymer'/C-S-H systems. The addition of Al_2O_3 produced a substantial increase in the strength of the NaOH/waterglass activated formulae, but not through the production of new phases. NaCl was shown to be an effective, if imperfect, retardant, while acid rock treatment sludge has no positive effects at all. Metakaolin, fly ash, and diatomaceous earth show no early positive effects. Neither the additives nor the original slag totally dissolve.
- A number of mineral side products, including margarite, hydrotalcite, gaylussite, and tetranatrolite have been identified. Though not impossible, it is unlikely that any of these phases take an active role in providing strength.
- SEM/EDS analysis has shown that the chemistry of the Op in the cementing phase is slightly different after 20 months of curing, indicating that chemical reactions continue over long periods of time. FTIR evidence confirms this. SEM/EDS analysis also shows little, if any, difference between cement and fine aggregate concretes.

- Substantial recarbonation occurs between 0 and 20 months, though mainly in the Na_2CO_3 activated formulae, implying that the recarbonation is due rather to carbonate ions from the activator, and not absorbed from the atmosphere. This recarbonation forms not just calcite, but also the somewhat more exotic aragonite.
- The AAS cements investigated here have sufficient strength for a wide range of applications (Na_2CO_3 being the weaker, but more practical and environmentally friendly, activator) and deserve further investigation. They could provide a practical, environmentally friendly solution to the quandary of repairing the world's fast-crumbling infrastructure while minimizing greenhouse gas production. Long-term strength could pose a problem, as behavior at long time scales is not yet known; however, recent research on Ukranian slag cements from the 1960s implies that this is a hurdle which can be overcome [21].

6.2 – Ancient Building Materials

- Radiocarbon dating has shown that the calcite content of at least two of the Bosnian 'pyramid' samples are infinitely old and therefore do not contain any recarbonated material. XRD and SEM analyses did not provide any evidence for the synthetic/extraterrestrial/magical nature of the materials.
- Despite the material's appearance in the SEM, radiocarbon dating has shown the calcite content of the sample from the 'ancient floor' in Colorado to be, in fact, infinitely old and therefore of a natural origin. While this does not totally rule out a synthetic origin, it does effectively rule out the presence of recarbonated lime. No data indicative of synthetic phases was found by XRD or SEM.

- That the Egyptian pyramids are made of an amorphous Na-aluminosilicate 'geopolymer' has been effectively disproven, as neither Na nor Al were found in any significant quantities. This does not rule out a synthetic origin; however, no proof at all that the pyramids are composed, or partially composed, of alkali aluminosilicates has been obtained.
- Exhaustive electron microscopy work has failed to provide any macroscale, obvious evidence of a synthetic origin for pyramid stone. On the meso/nanoscale, the presence of Si-rich nanospheres, and possibly Ca- or Mg-silicates, is a potential indicator of the synthetic nature of the materials. Investigation by TEM is far from complete, as sample size is so small, and the pyramids so large, but the presence of amorphous Si could show the existence, at some point, of Ca- or Mg-silicates.
- Radiocarbon dating has been used to obtain definite dates for many pyramids and monuments from Egypt. Through the use of simple mathematical equations, this data has been used to estimate that, in general, the pyramid stones contain up to 5-10 % recarbonated lime. It cannot be ruled out that this material is simply contaminated with modern carbon, however, it is the less likely of the two options.

6.3 – Future Work

This work has provided an excellent foundation for further study of AAS cement systems at Drexel University. An entire laboratory has been built from scratch and equipped with all the necessary chemicals and equipment to work on AAS cements. Naturally, there is no end to the number of additional tests that could be carried out. The

most important of these tests are likely to deal with some of the mechanical, rather than chemical, properties of the cements.

6.3.1 - Shrinkage

One issue that needs to be investigated is shrinkage. It is known from this work that the formulae based on NaOH/waterglass activation show an inordinate amount of shrinkage, enabling them to be removed from their molds simply by taking the lid off and holding them upside down. Quantification of the shrinkage, identification of its origin, and development of a method to combat it is imperative in bringing these AAS cements from the lab to the field. Shrinkage in the Na_2CO_3-based system seems to be less; however, accurate measurement is needed.

6.3.2 – Freeze/thaw Behavior

Another property which deserves investigation is freeze/thaw behavior. During natural weather cycles, concrete and cement can be subjected to freezing temperatures. Any residual water residing in pores will then freeze, which causes an expansion in volume, which puts pressure on the surrounding material and can cause deterioration. Automated machinery which can measure the rate of deterioration of cements due to freeze/thaw (essentially refrigerators with timers on them) exist, and should one be located, the data would provide much needed information on the expected service life and service area of these materials.

6.3.3 – Alternative Materials

The AAS cement system is incredibly robust – any solution containing high-pH water can be used as an activator. In addition to NaOH and Na_2CO_3, which were investigated here, a whole range of alkali solutions exist. Attempts should be made to

determine if any alkali solutions exist which, like slag, are by-products of other industries. Further, unrefined minerals, such as trona, the source from which Na_2CO_3 is produced, should be investigated to determine if they can be used as activators with a minimal amount of processing.

6.3.4 – Advanced Chemical Analyses/Microscopy

Relationships have been established with other universities and other researchers which will enable future students to use more advance chemical analyses than the XRD, FTIR, TGA, and SEM/EDS that make up the bulk of this work. Such techniques include magic angle spinning nuclear magnetic resonance (MAS-NMR), a powerful technique which describes the bond structure of molecules, and Reitveld analysis of XRD diffractograms, a method by which the presence of the various phases can be quantified. An investigation into the microstructure of the cement by TEM or some other high-resolution microscopic method (soft x-ray transmission microscopy, etc.) would elucidate an open question regarding the microstructure of the final products, as well as (if coupled with EDS, diffraction patterns, etc.) provide important chemical information about the C-S-H gel, without (or at least with less) interference from other phases.

6.3.5 – The Bosnian ‘Pyramids’

A number of samples from the Bosnian ‘Pyramids’ were received but not fully investigated beyond XRD experiments. It is possible that continued investigation of these samples would yield enlightening results; in light of the failure of any analysis so far to suggest a synthetic origin of these materials.

6.3.6 – The Pyramid Stones

The samples investigated in this study are by no means exhaustive. Samples from perhaps 5 of the roughly 80 surviving pyramids were investigated, and these samples were certainly of a much smaller scale than the pyramids themselves. Further analysis of more samples may either conclusively prove the tentative conclusions arrived at here or come up with alternative explanations. If the former is the case the implications for, if nothing else, the dating of statuary of uncertain age are enormous; museums all over the world would be urged to perform radiocarbon dating tests on their collections.

LIST OF REFERENCES

[1] Elsen J. Microscopy of historic mortars--a review. Cement and Concrete Research 2006;36:1416.

[2] Gourdin WH, Kingery WD. The Beginnings of Pyrotechnology: Neolithic and Egyptian Lime Plaster. Journal of Field Archaeology 1975;2:133.

[3] Kingery WD, Vandiver PB, Prickett M. The Beginnings of Pyrotechnology, Part II: Production and Use of Lime and Gypsum Plaster in the Pre-Pottery Neolithic Near East. Journal of Field Archaeology 1988;15:219

[4] Regourd M, Kerisel J, Deletie P, Haguenauer B. Microstructure of Mortars from Three Egyptian Pyramids. Cement and Concrete Research 1988;18:81.

[5] Bogue RH. The Chemistry of Portland Cement. New York: Reinhold Publishing Corporation, 1947.

[6] Moropoulou A, Bakolas A, Anagnostopoulou S. Composite materials in ancient structures. Cement and Concrete Composites 2005;27:295.

[7] Moropoulou A, Bakolas A, Moundoulas P, Aggelakopoulou E, Anagnostopoulou S. Strength development and lime reaction in mortars for repairing historic masonries. Cement and Concrete Composites 2005;27:289.

[8] Pollio MV. De Architectura. In: Morgan MH, editor. Boston MA: Plain Label Books, 20 B.C.

[9] Pacheco-Torgal F, Castro-Gomes J, Jalali S. Alkali activated binders: A review. Part I: Historical background, terminology, reaction mechanisms and hydration products. Construction and Building Materials 2008;22:1305.

[10] Association PC. How Portland Cement is Made. vol. 2009. Skokie, Il, 2009.

[11] Scrivener KL, Kirkpatrick RJ. Innovation in use and research on cementitious material. Cement and Concrete Research 2008;38:128.

[12] Gartner E. Industrially interesting approaches to "low-CO_2" cements. Cement and Concrete Research 2004;34:1489

[13] Phair JW. Green chemistry for sustainable cement production and use. Green Chemistry 2006;8:763.

[14] Teoreanu I, Volceanov A, Stoleriu S. Non Portland cements and derived materials. Cement and Concrete Composites 2005;27:650.

[15] Pacheco-Torgal F, Castro-Gomes J, Jalali S. Alkali activated cements: A review. Part 2. About materials and binders manufacture. Construction and Building Materials 2008;22:1315.

[16] Damtoft JS, Lukasik J, Herfort D, Sorrentino D, Gartner EM. Sustainable development and climate change initiatives. Cement and Concrete Research 2008;38:115.

[17] Hendriks CA, Worrell E, Jager Dd, Blok K, Riemer P. Emission reduction of greenhouse gases from the cement industry. Proceedings of the 7th International Conference on Greenhouse Gas Control Technologies. Vancouver, Canada: IEA GHG R&D Programme, 2004.

[18] Worrell E, Price L, Martin N, Hendriks C, Meida LO. Carbon Dioxide Emissions from the Cement Industry. Annual Review of Energy and the Environment 2001;26:303.

[19] Taylor M, Tam C, Gielen D. Energy efficiency and CO_2 emissions from the global cement industry. Energy Efficiency and CO2 Emission Reduction Potentials And Policies in the Cement Industry. Paris: International Energy Agency, 2006.

[20] Roy DM. Alkali activated cements. Opportunities and challenges. Cement and Concrete Research 1999;29:249.

[21] Xu H, Provis JL, Deventer JSJv, Krivenko PV. Characterization of aged slag concretes. ACI Materials Journal 2008;105:131.

[22] Kalyoncu RS. Slag - Iron and steel. USGS Mineral Commodities Summary, 2001.

[23] Bakharev T, Sanjayan JG, Cheng YB. Effect of admixtures on properties of alkali-activated slag concrete. Cement and Concrete Research 2000;30:1367.

[24] Bakharev T, Sanjayan JG, Cheng YB. Resistance of alkali-activated slag concrete to carbonation. Cement and Concrete Research 2001;31:1277.

[25] Bakharev T, Sanjayan JG, Cheng YB. Resistance of alkali-activated slag concrete to alkali-aggregate reaction. Cement and Concrete Research 2001;31:331.

[26] Bakharev T, Sanjayan JG, Cheng YB. Sulfate attack on alkali-activated slag concrete. Cement and Concrete Research 2002;32:211.

[27] Bakharev T, Sanjayan JG, Cheng YB. Resistance of alkali-activated slag concrete to acid attack. Cement and Concrete Research 2003;33:1607.

[28] Duxson P, Fernández-Jiménez A, Provis JL, Lukey GC, Palomo A, Deventer JSJv. Geopolymer technology: The current state of the art. Journal of Materials Sciences 2007;42:2917.

[29] Shi C, Krivenko PV, Roy DM. Alkali-activated cements and concretes. Abingdon, UK: Taylor and Francis, 2006.

[30] Davidovits J. 30 years of successes and failures in Geopolymer applications. Market trends and potential breakthroughs. Geopolymer 2002. Melbourne, Australia, 2002.

[31] Davidovits J. Geopolymers: Inorganic polymeric new materials. Journal of Thermal Analysis 1991;37:1633.

[32] Fernández-Jiménez A, Monzó M, Vicent M, Barba A, Palomo A. Alkaline activation of metakaolin-fly ash mixtures: Obtain of Zeoceramics and Zeocements. Microporous and Mesoporous Materials 2008;108:41.

[33] Davidovits J. Geopolymer chemistry and applications Saint-Quentin: The Geopolymer Institute, 2008.

[34] Komnitsas K, Zaharaki D. Geopolymerisation: A review and prospects for the minerals industry. Minerals Engineering 2007;20:1261.

[35] Davidovits J, Morris M. The pyramids: An enigma solved. New York: Dorset Press, 1988.

[36] Harmon G. Ancient Floor a Work of Nature, Not Nurture. The Daily Sentinel. Grand Junction, CO, 2006. p.1.

[37] Osmanagić S. www.bosnianpyramid.com. 2009.

[38] Bohannon J. Researchers Helpless as Bosnian Pyramid Bandwagon Gathers Pace. Science 2006;314:1862a.

[39] Osmanagić S. The World of the Maya: Gorgias Press, 2005.

[40] Rose M. The Bosnia-Atlantis Connection. Archaeology. Boston, MA: Archaeological Institute of America, 2006.

[41] Rose M. Bosnian "Pyramids" Update. Archaeology: Archaeological Institute of America, 2006.

[42] Rose M. More on Bosnian Pyramids. Archaeology. Boston, MA: Archaeological Institute of America, 2006.

[43] Osmanagić S. Radiocarbon Dating of the Underground Tunnel Complex in the Bosnian Valley of the Pyramids. Sarajevo, Bosnia and Herzegovina: www.piramidasunica.ba, 2009.

[44] Amitava Roy PJS, Harvill C. Eaton, Philip G. Malone, W. Newell Brabston, Lillian D. Wakeley,. Activation of Ground Blast-Furnace Slag by Alkali-Metal and Alkaline-Earth Hydroxides. Journal of the American Ceramic Society 1992;75:3233.

[45] Brough AR, Atkinson A. Sodium silicate-based, alkali-activated slag mortars: Part I. Strength, hydration and microstructure. Cement and Concrete Research 2002;32:865.

[46] Brough AR, Holloway M, Sykes J, Atkinson A. Sodium silicate-based alkali-activated slag mortars: Part II. The retarding effect of additions of sodium chloride or malic acid. Cement and Concrete Research 2000;30:1375.

[47] Escalante-García JI, Gorokhovsky AV, Mendoza G, Fuentes AF. Effect of geothermal waste on strength and microstructure of alkali-activated slag cement mortars. Cement and Concrete Research 2003;33:1567.

[48] Jose I. Escalante-García AFF, Alexander Gorokhovsky, Pedro E. Fraire-Luna, Guillermo Mendoza-Suarez,. Hydration Products and Reactivity of Blast-Furnace Slag Activated by Various Alkalis. Journal of the American Ceramic Society 2003;86:2148.

[49] Komnitsas K, Zaharaki D, Perdikatsis V. Geopolymerisation of low calcium ferronickel slags. Journal of Materials Science 2007;42:3073.

[50] Lecomte I, Henrist C, Liégeois M, Maseri F, Rulmont A, Cloots R. (Micro)-structural comparison between geopolymers, alkali-activated slag cement and Portland cement. Journal of the European Ceramic Society 2006;26:3789.

[51] Puertas F, Fernández-Jiménez A. Mineralogical and microstructural characterisation of alkali-activated fly ash/slag pastes. Cement and Concrete Composites 2003;25:287.

[52] Rajaokarivony-Andriambololona Z, Thomassin JH, Baillif P, Touray JC. Experimental hydration of two synthetic glassy blast furnace slags in water and alkaline solutions (NaOH and KOH 0.1 N) at 40° C: structure, composition and origin of the hydrated layer. Journal of Materials Science 1990;25:2399.

[53] Richardson IG, Brough AR, Groves GW, Dobson CM. The characterization of hardened alkali-activated blast-furnace slag pastes and the nature of the calcium silicate hydrate (C-S-H) phase. Cement and Concrete Research 1994;24:813.

[54] Richardson IG, Groves GW. Microstructure and microanalysis of hardened cement pastes involving ground granulated blast-furnace slag. Journal of Materials Science 1992;27:6204.

[55] Schneider J, Cincotto MA, Panepucci H. 29Si and 27Al high-resolution NMR characterization of calcium silicate hydrate phases in activated blast-furnace slag pastes. Cement and Concrete Research 2001;31:993.

[56] Wang S-D, Scrivener KL. Hydration products of alkali activated slag cement. Cement and Concrete Research 1995;25:561.

[57] Wang S-D, Scrivener KL, Pratt PL. Factors affecting the strength of alkali-activated slag. Cement and Concrete Research 1994;24:1033.

[58] Ana Fernández-Jiménez FP, Isabel Sobrados, Jesús Sanz,. Structure of Calcium Silicate Hydrates Formed in Alkaline-Activated Slag: Influence of the Type of Alkaline Activator. Journal of the American Ceramic Society 2003;86:1389.

[59] Shi C, Wu X, Tang M. Hydration of alkali-slag cements at 150°C. Cement and Concrete Research 1991;21:91.

[60] Alarcon-Ruiz L, Platret G, Massieu E, Ehrlacher A. The use of thermal analysis in assessing the effect of temperature on a cement paste. Cement and Concrete Research 2005;35:609.

[61] Gleize PJP, Motta EV, Silva DA, Roman HR. Characterization of historical mortars from Santa Catarina (Brazil). Cement and Concrete Composites 2009;31:342.

[62] Ingham JP. Application of petrographic examination techniques to the assessment of fire-damaged concrete and masonry structures. Materials Characterization 2009;60:700.

[63] Lawrence RMH, Mays TJ, Walker P, D'Ayala D. Determination of carbonation profiles in non-hydraulic lime mortars using thermogravimetric analysis. Thermochimica Acta 2006;444:179.

[64] Stepkowska ET, Blanes JM, Real C, Perez-Rodriguez JL. Hydration products in two aged cement pastes. Journal of Thermal Analysis and Calorimetry 2005;82:731.

[65] Li D, Shen J, Chen Y, Cheng L, Wu X. Study of properties on fly ash-slag complex cement. Cement and Concrete Research 2000;30:1381.

[66] Kourounis S, Tsivilis S, Tsakiridis PE, Papadimitriou GD, Tsibouki Z. Properties and hydration of blended cements with steelmaking slag. Cement and Concrete Research 2007;37:815.

[67] Puertas F, Martínez-Ramírez S, Alonso S, Vázquez T. Alkali-activated fly ash/slag cement. Strength behaviour and hydration products. Cement and Concrete Research 2000;30:1625.

[68] Palacios M, Puertas F. Effect of shrinkage-reducing admixtures on the properties of alkali-activated slag mortars and pastes. Cement and Concrete Research 2007;37:691.

[69] Cheng TW, Chiu JP. Fire-resistant geopolymer produced by granulated blast furnace slag. Minerals Engineering 2003;16:205.

[70] Mozgawa W, Deja J. Spectroscopic studies of alkaline activated slag geopolymers. Journal of Molecular Structure 2009;924-926:434.

[71] Fernández-Jiménez A, Puertas F, Sobrados I, Sanz J. Structure of Calcium Silicate Hydrates Formed in Alkaline-Activated Slag: Influence of the Type of Alkaline Activator. Journal of the American Ceramic Society 2003;86:1389.

[72] Duda A. Hydraulic reactions of LD steelwork slags. Cement and Concrete Research 1989;19:793.

[73] Pan Z, Cheng L, Lu Y, Yang N. Hydration products of alkali-activated slag-red mud cementitious material. Cement and Concrete Research 2002;32:357.

[74] Yu P, Kirkpatrick RJ, Poe B, McMillan PF, Cong X. Structure of Calcium Silicate Hydrate (C-S-H): Near-, Mid-, and Far-Infrared Spectroscopy. Journal of the American Ceramic Society 1999;82:742.

[75] Barbosa VFF, MacKenzie KJD, Thaumaturgo C. Synthesis and characterisation of materials based on inorganic polymers of alumina and silica: sodium polysialate polymers. International Journal of Inorganic Materials 2000;2:309.

[76] Ichcho S. Materiaux adsorbants a partir des schistes bitumeneux de Timahdit et leurs applications dans l'elimination de metaux lourds et de bacteries. Chemistry, vol. PhD. Casablanca, Morocco: Université Hassan II, 2003. p.162.

[77] Oumam M. Noveaux materiaux adsorbants elabores a partir des schistes bitumineux de Tarfaya. Faculté des Sciences Ben M'Sik, vol. Doctorat. Casablanca, Morocco: Université Hassan II, 2000. p.127.

[78] García Lodeiro I, Macphee DE, Palomo A, Fernández-Jiménez A. Effect of alkalis on fresh C-S-H gels. FTIR analysis. Cement and Concrete Research 2009;39:147.

[79] Farcas F, Touzé P. La spectrométrie infrarouge à transformée de Foruier (IRTF). Une méthode intéressante pour la caractérisation des ciments Bulletin des laboratires des ponts et chaussées 2001:77.

[80] Varas MJ, Buergo MAd, Fort R. Natural cement as the precursor of Portland cement: Methodology for its identification. Cement and Concrete Research 2005;35:2055.

[81] Delgado AH, Paroli RM, Beaudoin JJ. Comparison of IR Techniques for the Characterization of Construction Cement Minerals and Hydrated Products. Appl. Spectrosc. 1996;50:970.

[82] Gao XF, Lo Y, Tam CM, Chung CY. Analysis of the infrared spectrum and microstructure of hardened cement paste. Cement and Concrete Research 1999;29:805.

[83] Lee WKW, van Deventer JSJ. The effects of inorganic salt contamination on the strength and durability of geopolymers. Colloids and Surfaces A: Physicochemical and Engineering Aspects 2002;211:115.

[84] Criado M, Palomo A, Fernández-Jiménez A. Alkali activation of fly ashes. Part 1: Effect of curing conditions on the carbonation of the reaction products. Fuel 2005;84:2048.

[85] Panias D, Giannopoulou IP, Perraki T. Effect of synthesis parameters on the mechanical properties of fly ash-based geopolymers. Colloids and Surfaces A: Physicochemical and Engineering Aspects 2007;301:246.

[86] Bakharev T. Durability of geopolymer materials in sodium and magnesium sulfate solutions. Cement and Concrete Research 2005;35:1233.

[87] Álvarez-Ayuso E, Querol X, Plana F, Alastuey A, Moreno N, Izquierdo M, Font O, Moreno T, Diez S, Vázquez E, Barra M. Environmental, physical, and structural characterisation of geopolymer matrixes synthesized from coal (co-)conbustion fly ashes. Journal of Hazardous Materials 2008;154:175.

[88] Rees CA, Provis JL, Lukey GC, van Deventer JSJ. The mechanism of geopolymer gel formation investigated through seeded nucleation. Colloids and Surfaces A: Physicochemical and Engineering Aspects 2008;318:97.

[89] Ŝkvára F. Alkali activated materials or geopolymers? Ceramics 2007;51:173.

[90] Phair JW, Van Deventer JSJ. Effect of the silicate activator pH on the microstructural characteristics of waste-based geopolymers. International Journal of Mineral Processing 2002;66:121.

[91] Miller S, Jud Sierra E, Sakulich AR, Barsoum MW. The use of Diatomaceous Earth as a Silaceous Material in the Formation of Alkali Activated Fine-Aggregate Limestone Concrete. In Publication 2009.

[92] Richardson IG, Cabrera JG. The nature of C---S---H in model slag-cements. Cement and Concrete Composites 2000;22:259.

[93] Song S, Sohn D, Jennings HM, Mason TO. Hydration of alkali-activated ground granulated blast furnace slag. Journal of Materials Science 2000;35:249.

[94] Juenger M, Monteiro P, Gartner E. In situ imaging of ground granulated blast furnace slag hydration. Journal of Materials Science 2006;41:7074.

[95] Brough AR, Atkinson A. Automated identification of the aggregate-paste interfacial transition zone in mortars of silica sand with Portland or alkali-activated slag cement paste. Cement and Concrete Research 2000;30:849.

[96] Bohác M, Gregerová M. The influence of blast-furnace slag hydration products on microcracking of concrete. Materials Characterization 2009;60:729.

[97] Famy C, Brough AR, Taylor HFW. The C-S-H gel of Portland cement mortars: Part I. The interpretation of energy-dispersive X-ray microanalyses from scanning electron microscopy, with some observations on C-S-H, AFm and AFt phase compositions. Cement and Concrete Research 2003;33:1389.

[98] Escalante-García JI, Fuentes AF, Gorokhovsky A, Fraire-Luna PE, Mendoza-Suarez G. Hydration Products and Reactivity of Blast-Furnace Slag Activated by Various Alkalis. Journal of the American Ceramic Society 2003;86:2148.

[99] Sakulich AR, Anderson E, Schauer C, Barsoum MW. Mechanical and microstructural characterization of an alkali-activated slag/limestone fine aggregate concrete. Construction and Building Materials 2009;23:2951.

[100] Komnitsas K, Zaharaki D, Perdikatsis V. Effect of synthesis parameters on the compressive strength of low-calcium ferronickle slag inorganic polymers. Journal of Hazardous Materials 2009;161:760.

[101] Lawrence R, Mays T, Walker P, D'Ayala D. The use of tg to measure different concentrations of lime in non-hydraulic lime mortars. Journal of Thermal Analysis and Calorimetry 2006;85:377.

[102] Miller S. Use of diatomaceous earth as silaceous material in formation of reconstituted limestone. Materials Science and Engineering, vol. Master's. Philadelphia: Drexel University, 2009.

[103] Lyon RE, Balaguru PN, Foden A, Sorathia U, Davidovits J, Davidovics M. Fire Resistant Aluminosilicate Composites. Fire and Materials 1997;21:67.

[104] Duxson P, Lukey GC, van Deventer JSJ. Thermal evolution of metakaolin geopolymers: Part 1 - Physical evolution. Journal of Non-Crystalline Solids 2006;352:5541.

[105] Barbosa VFF, MacKenzie KJD. Thermal behaviour of inorganic geopolymers and composites derived from sodium polysialate. Materials Research Bulletin 2003;38:319.

[106] Barbosa VFF, MacKenzie KJD. Synthesis and thermal behaviour of potassium sialate geopolymers. Materials Letters 2003;57:1477.

[107] Duxson P, Lukey GC, van Deventer JSJ. The thermal evolution of metakaolin geopolymers: Part 2 - Phase stability and structural development. Journal of Non-Crystalline Solids 2007;353:2186.

[108] Provis JL, Yong CZ, Duxson P, van Deventer JSJ. Correlating mechanical and thermal properties of sodium silicate-fly ash geopolymers. Colloids and Surfaces A: Physicochemical and Engineering Aspects 2009;336:57.

[109] Lin KL, Lin DF. Hydration characteristics of municipal solid waste incinerator bottom ash slag as a pozzolanic material for use in cement. Cement and Concrete Composites 2006;28:817.

[110] Bakharev T, Sanjayan JG, Cheng Y-B. Alkali activation of Australian slag cements. Cement and Concrete Research 1999;29:113.

[111] Li Y, Sun Y. Preliminary study on combined-alkali-slag paste materials. Cement and Concrete Research 2000;30:963.

[112] Fernández-Jiménez A, Palomo JG, Puertas F. Alkali-activated slag mortars: Mechanical strength behaviour. Cement and Concrete Research 1999;29:1313.

[113] Escalante-Garcia JI, Espinoza-Perez LJ, Gorokhovsky A, Gomez-Zamorano LY. Coarse blast furnace slag as a cementitious material, comparative study as a partial replacement of Portland cement and as an alkali activated cement. Construction and Building Materials 2009;23:2511.

[114] Gruskovnjak A, Lothenbach B, Winnefeld F, Figi R, Ko SC, Adler M, Mäder U. Hydration mechanisms of super sulphated slag cement. Cement and Concrete Research 2008;38:983.

[115] Richardson IG. Tobermorite/jennite- and tobermorite/calcium hydroxide-based models for the structure of C-S-H: applicability to hardened pastes of tricalcium silicate, [beta]-dicalcium silicate, Portland cement, and blends of Portland cement with blast-furnace slag, metakaolin, or silica fume. Cement and Concrete Research 2004;34:1733.

[116] Genestar C, Pons C. Ancient covering plaster mortars from several convents and Islamic and Gothic palaces in Palma de Mallorca (Spain). Analytical characterization. Journal of Cultural Heritage 2003;4:291.

[117] Labiadh MR, Ouezdou MB, Hajjem BT, Mensi R. Characterization of waterproof-covering mortars on Ottoman monuments of "Ghar El Melh" (Tunisia). Construction and Building Materials 2009;23:423.

[118] Barsoum MW, Sakulich AR, Miller S, Jud Sierra E, Moseson A. Carbon dating of some re-agglomerated limestones from the pyramids of Egypt. In preparation 2009.

[119] Osborne GJ. Durability of Portland blast-furnace slag cement concrete. Cement and Concrete Composites 1999;21:11.

[120] Chang JJ. A study on the setting characteristics of sodium silicate-activated slag pastes. Cement and Concrete Research 2003;33:1005.

[121] Chang JJ, Yeih W, Hung CC. Effects of gypsum and phosphoric acid on the properties of sodium silicate-based alkali-activated slag pastes. Cement and Concrete Composites 2005;27:85.

[122] Gong C, Yang N. Effect of phosphate on the hydration of alkali-activated red mud-slag cementitious material. Cement and Concrete Research 2000;30:1013.

[123] Escalante-Garcia JI, Palacios-Villanueva VM, Gorokhovsky AV, Mendoza-Suárez G, Fuentes AF. Characteristics of a NaOH-Activated Blast Furnace Slag Blended with a Fine Particle Silica Waste. Journal of the American Ceramic Society 2002;85:1788.

[124] Silverstein RM, Webster FX. Spectromertric Identification of Organic Compounds. New York: John Wiley & Sons, Inc., 1998.

[125] Bijen J. Benefits of slag and fly ash. Construction and Building Materials 1996;10:309.

[126] Li G, Zhao X. Properties of concrete incorporating fly ash and ground granulated blast-furnace slag. Cement and Concrete Composites 2003;25:293.

[127] Xuequan W, Hong Z, Xinkai H, Husen L. Study on steel slag and fly ash composite Portland cement. Cement and Concrete Research 1999;29:1103.

[128] Zhao F-Q, Ni W, Wang H-J, Liu H-J. Activated fly ash/slag blended cement. Resources, Conservation and Recycling 2007;52:303.

[129] Puertas F, Martínez-Ramírez S, Alonso S, Vázquez T. Alkali-activated fly ash/slag cements: Strength behaviour and hydration products. Cement and Concrete Research 2000;30:1625.

[130] Fu X, Hou W, Yang C, Li D, Wu X. Studies on high-strength slag and fly ash compound cement. Cement and Concrete Research 2000;30:1239.

[131] Freidin K, Erell E. Bricks made of coal fly-ash and slag, cured in the open air. Cement and Concrete Composites 1995;17:289.

[132] Goretta KC, Chen N, Gutierrez-Mora F, Routbort JL, Lukey GC, van Deventer JSJ. Solid-particle erosion of a geopolymer containing fly ash and blast-furnace slag. Wear 2004;256:714.

[133] Temuujin J, van Riessen A, Williams R. Influence of calcium compounds on the mechanical properties of fly ash geopolymer pastes. Journal of Hazardous Materials 2009;167:82.

[134] Dheilly R-M, Tudo J. Contribution à létude de la gaylussite: Na2Ca(CO3)2,5H2O. Comptes Rendus de l'Académie des Sciences - Series IIB - Mechanics-Physics-Chemistry-Astronomy 1997;325:407.

[135] Mees F, Reyes E, Keppens E. Stable isotope chemistry of gaylussite and nahcolite from the deposits of the crater lake at Malha, northern Sudan. Chemical Geology 1998;146:87.

[136] Keyte LM, Lukey GC, van Deventer JSJ. The effect of coal ash composition on properties of waste-based geopolymers. International symposium of research students on material science and engineering. Chennai, India, 2004.

[137] van Deventer JSJ, Provis JL, Duxson P, Lukey GC. Reaction mechanisms in the geopolymeric conversion of inorganic waste to useful products. Journal of Hazardous Materials 2007;139:506.

[138] Fernández-Jiménez A, Palomo A, Criado M. Microstructure development of alkali-activated fly ash cement: a descriptive model. Cement and Concrete Research 2005;35:1204.

[139] Rattanasak U, Chindaprasirt P. Influence of NaOH solution on the synthesis of fly ash geopolymer. Minerals Engineering 2009;22:1073.

[140] Andini S, Cioffi R, Colangelo F, Grieco T, Montagnaro F, Santoro L. Coal fly ash as raw material for the manufacture of geopolymer-based products. Waste Management 2008;28:416.

[141] Frías M, Rojas MISd, Rodríguez C. The influence of SiMn slag on chemical resistance of blended cement pastes. Construction and Building Materials 2009;23:1472.

[142] Khatib JM, Hibbert JJ. Selected engineering properties of concrete incorporating slag and metakaolin. Construction and Building Materials 2005;19:460.

[143] Li Z, Ding Z. Property improvement of Portland cement by incorporating with metakaolin and slag. Cement and Concrete Research 2003;33:579.

[144] Ramlochan T, Thomas MDA, Hooton RD. The effect of pozzolans and slag on the expansion of mortars cured at elevated temperature: Part II: Microstructural and microchemical investigations. Cement and Concrete Research 2004;34:1341.

[145] Ramlochan T, Zacarias P, Thomas MDA, Hooton RD. The effect of pozzolans and slag on the expansion of mortars cured at elevated temperature: Part I: Expansive behaviour. Cement and Concrete Research 2003;33:807.

[146] Yunsheng Z, Wei S, Qianli C, Lin C. Synthesis and heavy metal immobilization behaviors of slag based geopolymer. Journal of Hazardous Materials 2007;143:206.

[147] Hu S, Wang H, Zhang G, Ding Q. Bonding and abrasion resistance of geopolymeric repair material made with steel slag. Cement and Concrete Composites 2008;30:239.

[148] Guangren Q, Yuxiang L, Facheng Y, Rongming S. Improvement of metakaolin on radioactive Sr and Cs immobilization of alkali-activated slag matrix. Journal of Hazardous Materials 2002;92:289.

[149] Love CA, Richardson IG, Brough AR. Composition and structure of C-S-H in white Portland cement-20% metakaolin pastes hydrated at 25 °C. Cement and Concrete Research 2007;37:109.

[150] Barsoum MW, Ganguly A, Hug G. Microstructural Evidence of Reconstituted Limestone Blocks in the Great Pyramids of Egypt. Journal of the American Ceramic Society 2006;89:3788.

[151] Chu V, Regev L, Weiner S, Boaretto E. Differentiating between anthropogenic calcite in plaster, ash and natural calcite using infrared spectroscopy: implications in archaeology. Journal of Archaeological Science 2008;35:905.

[152] Jana D. Evidence from detailed petrographic examinations of casing stones from the great pyramid of Khufu, a natural limestone from Tua, and a man-made (Geopolymeric) limestone. 29th Conference on Cement Microscopy. Quebec City, 2003.

[153] Ingram KD, Daugherty KE, Marshall JL. The Pyramids--Cement or Stone? Journal of Archaeological Science 1993;20:681.

[154] Kobayashi K, Suzuki K, Uno Y. Carbonation of concrete structures and decomposition of C---S---H. Cement and Concrete Research 1994;24:55.

[155] Arnold JR, Libby WF. Age Determinations by Radiocarbon Content: Checks with Samples of Known Age. Science 1949;110:678.

[156] Baxter MS, Walton A. Radiocarbon Dating of Mortars. Nature 1970;225:937.

[157] Gupta SK, Polach HA. Radiocarbon dating practices at AnU. Canberra, Australia: Radiocarbon Laboratory, Research School of Pacific Studies, 1985.

[158] Harrell JA, Penrod BE. The Great Pyramid Debate - Evidence from the Lauer Sample. J. Geolog. Ed. 1993;41:358.

[159] Jana D. Evidence from Detailed Petrographic Examinations of Casing Stones from the Great Pyramid of Khufu, a Natural Limestone from Tura, and a Man-made (Geopolymeric) Limestone. Proc. of 29 Conf. Cement Microscopy. Quebe City, Canada, 2007. p.207.

[160] Campbell DH. Geologic Origin of Egyptian Pyramid Blocks and Accocaited Sturctures. Proc. of 29 Conf. Cement Microscopy. Quebe City, Canada, 2007. p.268.

Appendix A: Abbreviations and Symbols

BP	Before Present
C	Celsius
d	Day
DE	Diatomaceous Earth
Ip	Inner Product
ITZ	Interfacial Transition Zone
FA	Fly Ash
FTIR	Fourier Transform Infrared spectroscopy
m	Month
MK	Metakaolin
MPa	Megapascals
NMR	Nuclear Magnetic Resonance
Op	Outer Product
SEM	Scanning Electron Microscopy
TEM	Transmission Electron Microscopy
TGA	Thermogravimetric Analysis
XRD	X-Ray Diffraction
XRD	X-Ray Fluorescence

APPENDIX B: Moroccan Samples

B.1 – Mechanical Properties and General Observations

XRF data collected in Morocco (Table B.1) show that each of the reactants investigated is roughly the same: Some kind of aluminosilicate material, with or without calcium. These chemistries, theoretically, would be sufficient for producing either 'geopolymers' or other alkali-activated cements.

For all the reactants examined in Morocco, four activators were investigated: Solutions of 4M Na_2CO_3, 4M NaOH, 8M NaOH, and waterglass (with 25 wt.% 8M NaOH to improve workability.) These samples were then cured at either 60 ^oC for 24 h followed by 6 d of room temperature curing or at room temperature for an entire week. The strengths of these formulae (Table B.2) were so low as to preclude them from use in all but the lowest-strength of applications. The data is based on 10 mm x 20 mm cylinders produced in Morocco and tested in the United States at ages of 3 months.

Table 6.1– XRF analysis of main reactants used in Morocco. SO = Shale oil

Element	Bizou	Metakaolin	ST Slag	Tata Soil	Tarfaya SO	Temhedit SO
SiO_2	48.01	53.08	4.34	45	16.14	27.19
CaO	22.32	<1	39.48	21.84	52.47	45.21
Al_2O_3	14.43	43.45	1	12.96	5.36	8.95
MgO	5	<1	1.58	11.06	1.23	2.24
Fe_2O_3	4.77	<1	23.76	3.86	<1	5.22
K2O	1.79	1.2	<1	2.04	<1	<1
F	<1	<1	19.07	<1	<1	<1
Fe_2O_3	<1	<1	<1	<1	4.03	<1
Na_2O	<1	<1	1.43	<1	8.17	1.96
P_2O_5	<1	<1	6.1	<1	<1	<1
Cl	<1	<1	1.93	<1	5.03	2.36
S	<1	<1	<1	<1	5.37	3.08

Table B.2 – Compressive strengths (MPa) of various reactants activated by 8M NaOH or 75/25 waterglass/8M NaOH solutions, cured at either ambient temperatures or 60 ^{o}C. SO = Shale Oil. x = no strength

Activator	8M NaOH		Waterglass	
Curing	Ambient	60 ^{o}C	Ambient	60 ^{o}C
Temhedit SO Ashes	x	< 1	x	< 5
Tarfaya SO Ashes	x	x	x	< 5
Marble Dust	x	x	x	< 5
Surface Treatment 'Slag'	x	x	<1	< 1
Tata Soil	x	<1	<1	< 1
Bizou Riverbank Clay	x	x	x	< 5
KT6 Slag	x	<1	x	< 1

Many formulae simply did not react; over the course of the curing regime they either dried out, producing a powder, or they remained moist, without any development of mechanical strength. This is true of nearly all formulae cured at room temperature.

For samples cured at 60 ^{o}C for one day followed by 6 d at room temperature, two general trends were observed. Some samples dried out and began to develop strength; however, these strengths were very low and did not pass 1 MPa. Unlike those samples previously mentioned, these samples could withstand the demolding process and support their own weight. However, under the slightest pressure, they crumbled.

Another group of samples, most notable the two shale oil ashes, marble dust, and riverbank clay materials, when activated by the NaOH/waterglass solution and cured at 60 ^{o}C, began to develop strength. These samples appeared good, however, their strengths did not pass the 5 MPa mark, even after 9 months of curing, when the data was rechecked.

In an attempt to make the formulae more practical for use in developing nations, samples were also made using seawater in the activating solutions. This could be a matter

of critical importance; places such as Temhedit and Tarfaya, the two largest shale oil producers in Morocco, are surrounded by desert. Potable water is a precious commodity; therefore, it would be preferred that the saltwater of the nearby Atlantic Ocean be used in cement production. The use of saltwater did not effect the strengths of the formulae; however, these strengths were so low that such a conclusion is tenuous at best.

B.1.1 - Conclusions

It can therefore be concluded that none of the formulae investigated in Morocco are suitable for any but the very weakest of applications. Possible explanations for this state are discussed in section B.4, however, the claim that 'geopolymer' technology can be rapidly and easily adapted to an area's locally available materials may require some future qualification.

B.2 – X-Ray Diffraction

XRD diffractograms of formulae based on Temhedit and Tarfaya oil shale ashes and the surface treatment slag (Fig. B.1) are generally indistinguishable from each other (differences in peak intensities are likely due to the scans being performed at different times on different machines.

The formulae based on Tarfaya oil shale ash (Fig. B.1a) have many similarities, regardless of activator. The as-received product shows peaks belonging solely to calcite; when burnt, the peaks transform into those of lime (CaO.) After reaction, regardless of activator, only calcite peaks and possibly some minor peaks due to any number of calcium silicates are present. These peaks are, however, so minor as to hinder identification. In samples activated by seawater, halite (NaCl) is also (not surprisingly)

present. This information suggests a number of reasons for the lack of reaction: either the material was not fully burnt before it was reacted (the 'burnt' material was a special batch

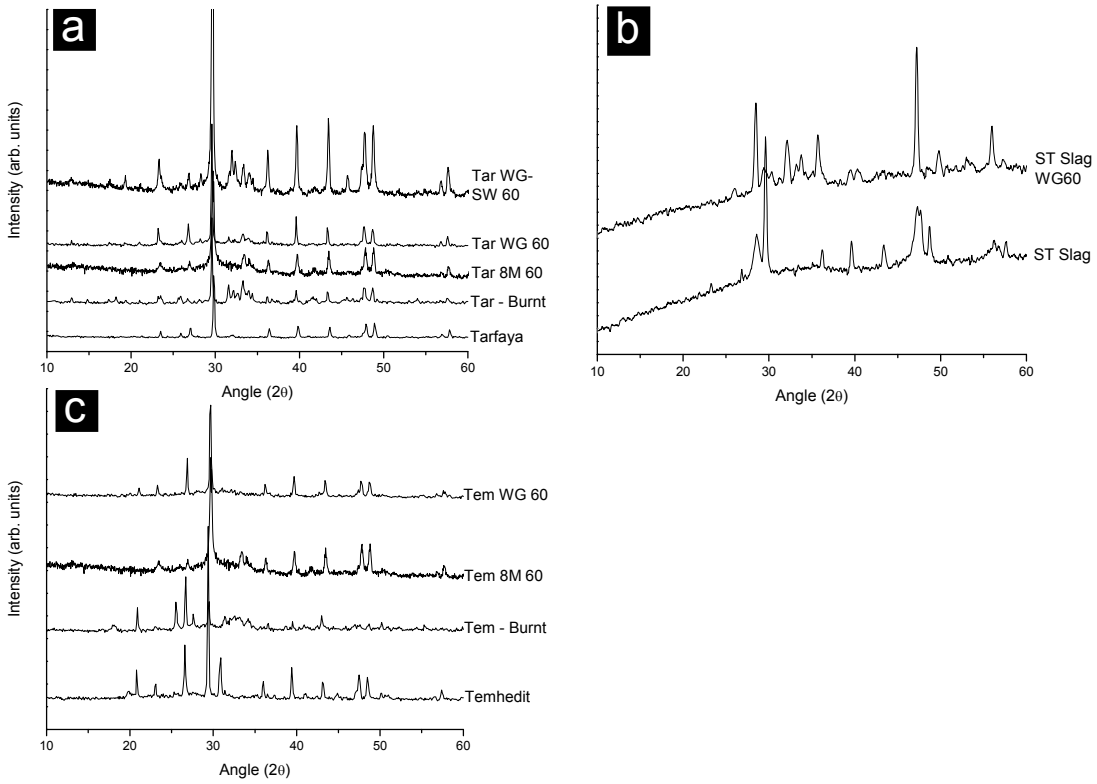

Figure B.1 – XRD diffractograms of (each from bottom) a) Tarfaya oil shale and its ashes, and formulae thereof activated by 8M NaOH, waterglass/NaOH, and waterglass/NaOH with seawater solutions; b) Surface treatment 'slag' and a formula thereof activated by waterglass/NaOH; and c) Temhedit oil shale and its ashes, and formulae thereof activated by 8M NaOH and waterglass/NaOH solutions. All formulae were cured at 60 ^{o}C.

that was finely powdered, then burnt, and immediately scanned), or the recarbonation reaction is occurring so quickly that it prohibits the formation of a cementing phase.

Formulae based on Temhedit oil shale ash (Fig. B.1c) share a number of similarities with the Tarfaya oil shale ash; the main peaks are those of calcite, as well as

those of quartz and anhydrite ($CaSO_4$.) When burnt, the calcite peaks are replaced with those of lime; however, in samples after reaction, the calcite peaks are still present (along with the minor peaks of, possibly, a calcium silicate.) Again, this implies that the burning of the shale oil was insufficient.

Formulae based on surface treatment slag (Fig. B.1b) are complicated; while the untreated material shows peaks belonging to calcite and possibly riversideite ($Ca_5Si_6O_{16}(OH)_2 \cdot 2(H_2O)$), after reaction with waterglass it shows peaks belonging to 'SiO' (PDF #00-030-1127.) How, or why, this is possible is not clear. It should be noted, however, that the result is of little consequence due to the inferior strength performance of the material.

B.2.1 – Conclusions

Overall, the diffractograms of any of the materials failed to show either the presence of C-S-H or the variety of subtle changes that indicate the presence of 'geopolymers.' For the most part, the data seems to indicate that the materials were insufficiently burned before processing.

B.3 – Fourier Transform Infrared Spectroscopy

The FTIR spectra of formulae based on Temhedit oil shale ashes (Fig. B.2a) are all strikingly similar. As with the slag cements, a broad peak centered around 3400 cm^{-1} is due to the presence of water, as is a small peak at 1640 cm^{-1}, almost lost in the noise. Minor peaks at 2920 cm^{-1} and 2860 cm^{-1} are harmonics due to the Ca atom in calcite; a pair of double peaks at 2350 cm^{-1} is an artifact due to differing levels of CO_2 in the chamber when the scan was run compared to when the background was taken. A broad peak centered around 1400 cm^{-1} is due to C-O bond stretching in CO_3^{2-} molecules and

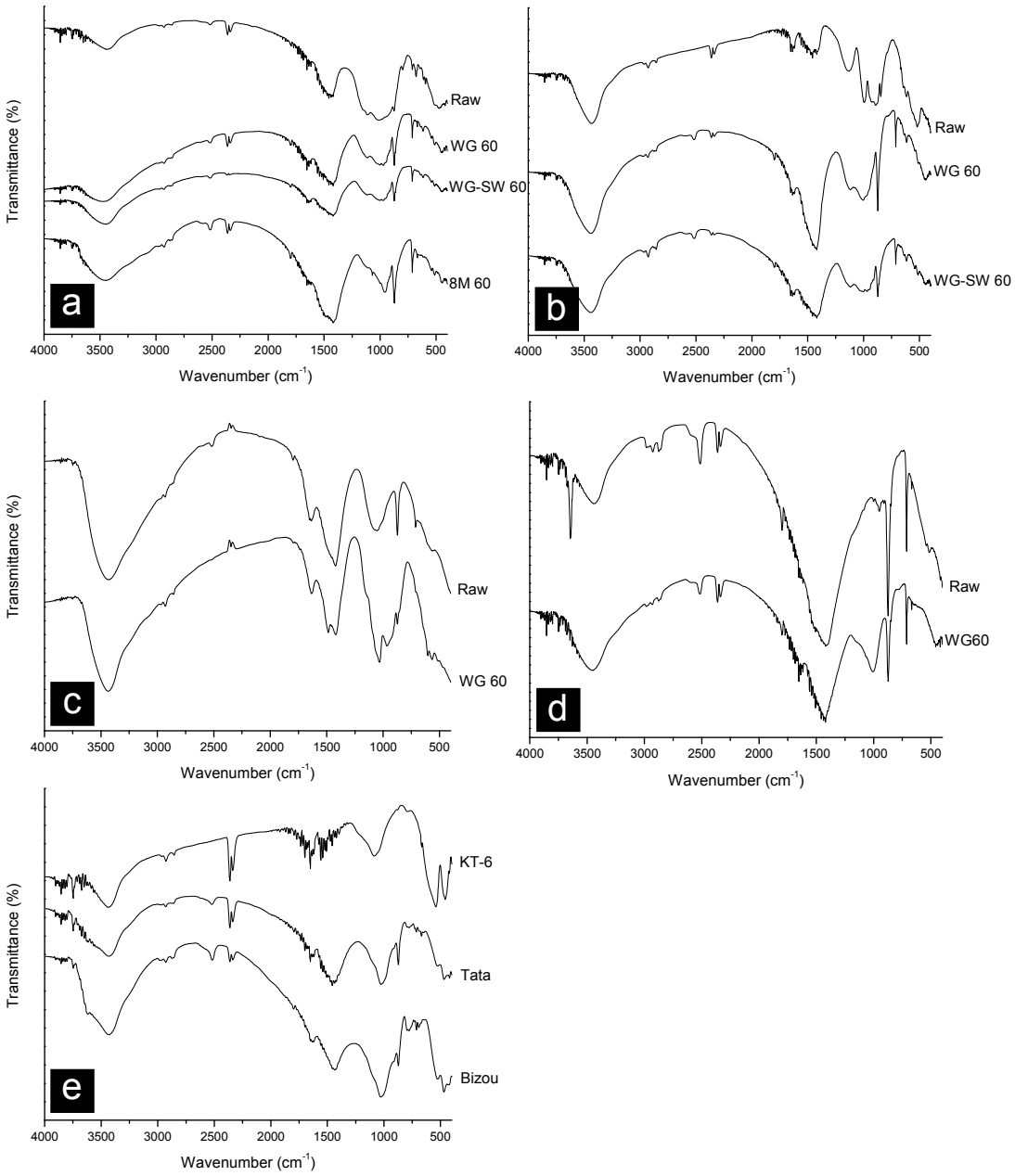

Figure B.2 – FTIR spectra of a) Temhedit oil shale ashes (top spectrum) and formulae thereof activated by waterglass/NaOH, waterglass/NaOH with seawater, and 8M NaOH solution; b) Tarafaya shale oil ashes (top spectrum) and formulae thereof activated by waterglass/NaOH and waterglass/NaOH with seawater; c) Surface treatment plant runoff and a formula thereof activated by waterglass/NaOH; d) Marble dust and a formula activated by waterglass/NaOH; and e) three raw materials from which formulae with strength above 1 MPa were not produced (KT6 'Slag', Tata soil, and Bizou riverbank clay.)

confirms the presence of calcite, further confirmed by the sharp peaks at 870 cm^{-1} and 710 cm^{-1}. The final peaks are those belonging to the various Si-O bond deformations at 960 cm^{-1} and 470 cm^{-1}. Unlike the slag-based formulae, these peaks are relatively weak and shift only slightly between the raw material and the alkali-activated formulae. It is likely that this is due mainly to the presence of the Si in waterglass: the 960 cm^{-1} peak looks different in the formula activated by 8M NaOH. While these results do show some slight reaction, the extent is not as great as that of previously investigated samples, and the presence of calcite is once again a recurring theme.

The FTIR spectra of the formulae based on Tarfaya oil shale ashes (Fig. B.2b) share almost all of the same peaks in the same positions (e.g. the peaks due to water and calcite.) The main difference between the Tarfaya formulae and the Temhedit formulae are the 960 cm^{-1} peak, which becomes more broad and shallow after activation.

In the formulae based on surface treatment slag (Fig. B.2c) the peaks due to water are much stronger and more clearly defined; the peaks of calcite, however, diminish after activation. The reason for this is not clear. Minor peaks appear centered at 1485 cm^{-1} and 970cm^{-1}, most likely due to specific forms of Si deformation. The formulae based on marble dust (Fig. X.Bd) are dominated peaks belonging to calcite and water; finally, the spectra of three materials for which no formulae of measurable strength were developed (Tata soil, Bizou riverbank clay, and 'KT6' slag) show peaks similar to those of the shale oil ashes.

B.3.1 – Conclusions

Overall, the FTIR spectra indicate that a) calcite is present in nearly all formulae, and b)little reaction involving Si is occurring, and what is occurring is likely due to

waterglass. Along with the XRD diffractograms that show no new crystalline products being formed, the FTIR spectra showing no significant change in amorphous products indicates that what little strength was obtained is likely from the drying of waterglass.

B.4 – Analysis

The reason that none of these formulae proved to be a viable construction material is likely to be a combination of factors. Some possibilities include:

- **Water** Although it did not appear to be true based on observation of the mixtures, it is possible that the liquid:solids ratio (0.3) used here included too much water. If this is the case, drying over time would cause micro-cracking and negatively affect final strength.
- **Si Crystallinity** Although it was seen in the XRF results that each material contained a not inconsiderable amount of Si, XRD results indicate that some of this Si was in the form of quartz, and was thus not likely to dissolve in alkali solutions or be available for reaction.
- **Insufficient Burning** To produce the CaO needed to produce C-S-H, the shale oils were burned. In initial trials, much of the material remained black, indicating that the calcite had not been sufficiently burned. Although later runs appeared visually to be much better, XRD and FTIR signatures of calcite can still be seen, implying incomplete burning, and thus a lowered amount of Ca available for reactions. Similarly, the clay materials here investigated as 'geopolymer' precursors needed to be processed at high temperature so as to dehydroxylate the particle surfaces and make them more reactive. If the oil shales were insufficiently burned, so the other materials may have been.

Appendix C: Freeze-Dry Experiments

Several of the formulae previously described were freeze-dried so as to halt the hydration reaction. After being submerged for ~1 h in liquid nitrogen they were stored overnight in a freezer. They were then placed in a lyophilizer for 24 h to sublimate unbound water and thus halt the hydration reactions. XRD and FTIR experiments were then performed so as to provide a 'snapshot' of the chemical reactions occurring in the cement paste at various times (1, 3, 5, 10, 30, and 60 mins.) Unfortunately, not all of the data could be identified, as discussed below.

C.1 – NaOH/Waterglass-activated Formula

Cement pastes of the NaOH/Waterglass-activated formula with and without DE were investigated by both FTIR and XRD.

C.1.1 – XRD

XRD diffractograms for the NaOH/Waterglass-activated formula with and without DE (Figs. C.1 and C.2) show some distinct differences during the first hour despite being almost identical after 7 days. In the basic formula, during the first hour, three minor peaks between 30 and 35 $^{o}2\theta$ are the main features, while a much weaker set of double peaks around 26 $^{o}2\theta$ and another weak set of double peaks around 40 $^{o}2\theta$ seem to be present. Other peaks seem to be present at various curing times, but distinct trends are difficult to observe.

With the addition of DE, however, the three main peaks, and the double peak around 26 $^{o}2\theta$ are more intense; a peak at 39 $^{o}2\theta$ and a peak at 19 $^{o}2\theta$ that were not

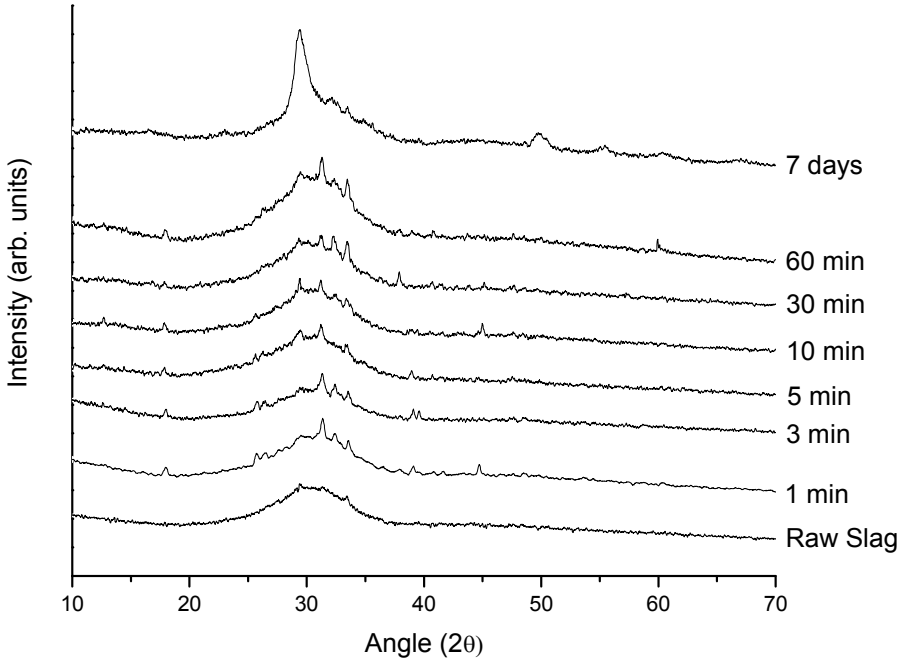

Figure C.1 – XRD diffractograms of basic NaOH/waterglass-activated formula at 1, 3, 5, 10, 30, and 60. Unreacted slag and formula after 7 days of setting shown for reference (bottom and top, respectively.)

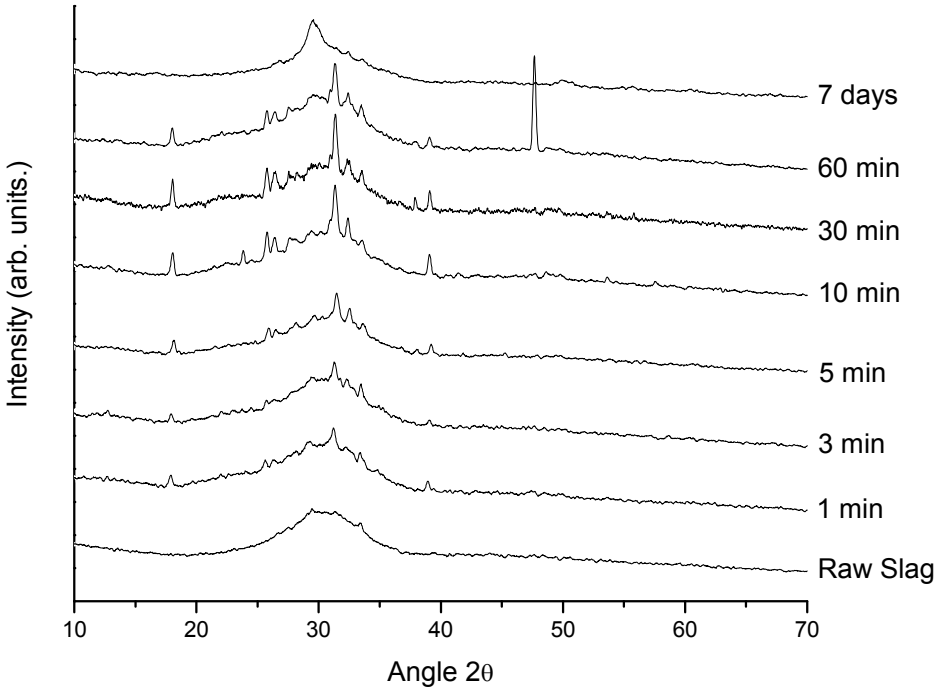

Figure C.2 – XRD diffractograms of NaOH/waterglass-activated formula containing DE at 1, 3, 5, 10, 30, and 60 minutes. Unreacted slag and formula after 7 days of setting shown for reference (bottom and top, respectively.)

present in the basic formula were present. These peaks are sharper and more intense; a very large peak at 47 $^{o}2\theta$ is strange, and possibly erroneous. None of these peaks were identifiable. Because of the large amorphous hump, automatic identification software was unable to spot the peaks; when manual identification was attempted, no matches were found. This is likely due to the weak nature of the peaks: any secondary peaks, which would greatly aid identification, are by far too weak to separate from the background noise.

C.1.2 – FTIR

As always, the FTIR data is more cryptic. Spectra of the basic NaOH/waterglass formula (Fig. C.3) show variations in intensity that complicate analysis. This could be due to errors during the collection of the spectra, inhomogeneity in the cement paste, or a number of other reasons. Overall, the bands are the same as were observed at ages of one week and more: peaks due to the –OH molecules in water in the 3400-3500 cm^{-1} and 1600-1700 cm^{-1} ranges; a peak in the low 1400 cm^{-1} range due to CO_3^{2-} ions that must have been incorporated from the atmosphere; and peaks due to Si-O, Al-O, O-Si-O, etc. bonds around 1000 cm^{-1} and 500 cm^{-1}. The last two peaks are the most important, as the disposition of the Si atoms are what lend the final material strength, whether in 'geopolymers' or C-S-H based materials. The breadth of these peaks, however, makes commentary on trends all but impossible.

The spectra of the formula containing DE (Fig. C.4) show less in the way of variation but are no easier to decipher. The same peaks are present, in the same positions. The two Si-O/Al-O peaks (at 1000 cm^{-1} and below 500 cm^{-1}) seem to be getting much

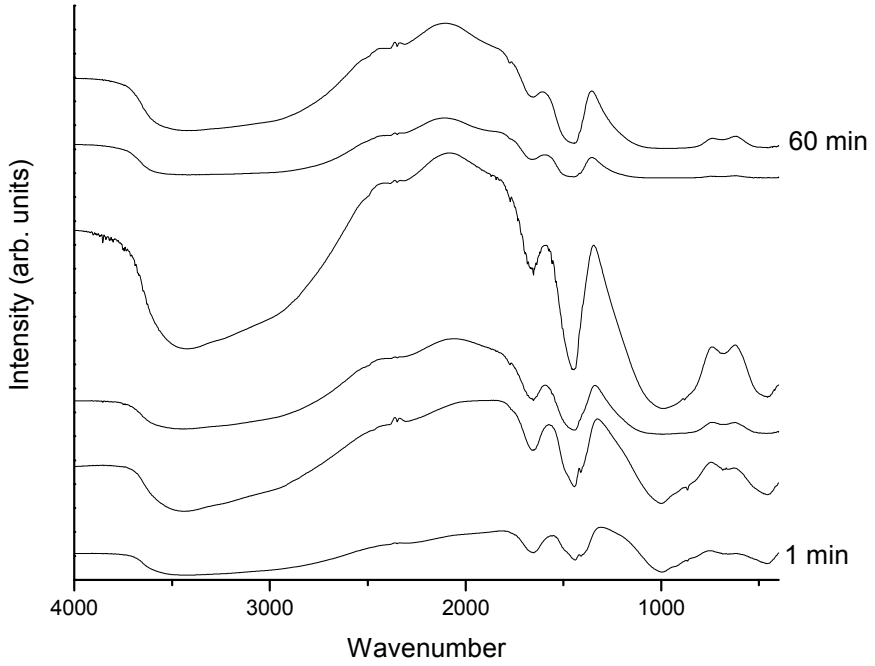

Figure C.3 – FTIR spectra of NaOH/waterglass-activated formula at (from top) 60, 30, 10, 5, 3, and 1 minutes.

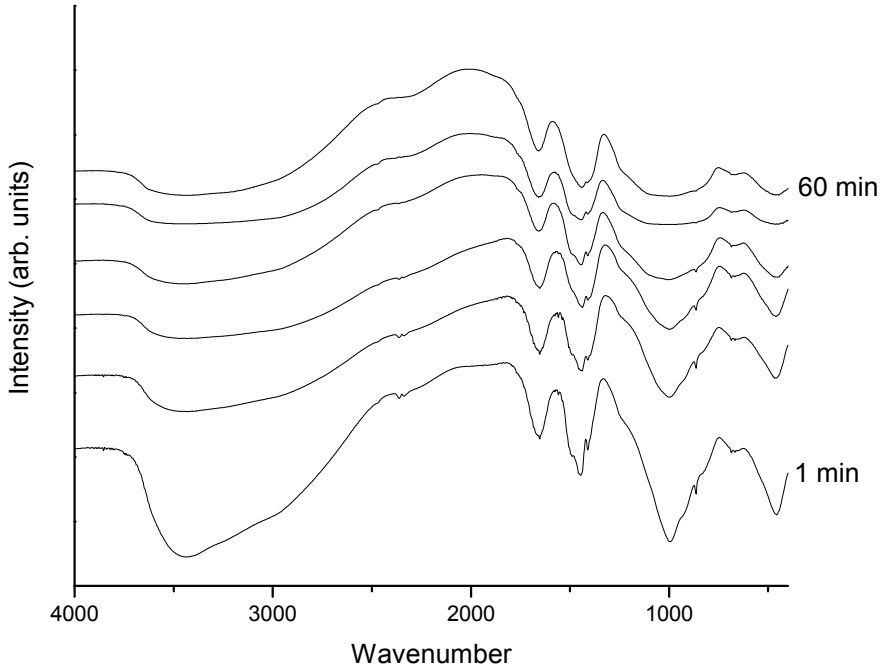

Figure C.4 – FTIR spectra of NaOH/waterglass-activated formula containing DE at (from top) 60, 30, 10, 5, 3, and 1 minutes.

broader, possibly as Si from the DE or the unreacted slag dissolves and forms new types of bonds. Unfortunately, without identification of mineral constituents by other complimentary experimental methods (i.e. XRD) little more than "something is happening to the Si atoms" can be said.

C.1.3 – Conclusions

Despite being unable to identify the peaks in the XRD diffractograms, thus obviating the usefulness of the complimentary technique of FTIR, several important conclusions can be reached. First of all, the reaction products during the first hour are substantially different from those produced after a week of curing time. The addition of DE produces several peaks that do not exist in the diffractogram of the formula without DE; therefore, at least at early ages, the formulae behave differently. It is possible that these new peaks are merely peaks belonging to mineral side-products, the chemical equivalent of a disinterested bystander, however; without identification of the XRD peaks, the importance of these results is unknown.

C.2 – Na_2CO_3-activated Formula

Cement pastes of the Na_2CO_3-activated formula with and without DE were investigated by both FTIR and XRD.

C.2.1 – XRD

In a recurring theme, the XRD diffractograms of the basic Na_2CO_3–activated formula (Fig. C.5) during the first hour have a number of peaks not found in that of the basic NaOH/waterglass formula; these peaks seem somewhat better defined. The addition of DE (Fig. C.6), however, seems to make no difference. In all spectra, the main feature is a set of three well-defined peaks between 30 and 35 $^{o}2\theta$. A peak around 39 $^{o}2\theta$ seems

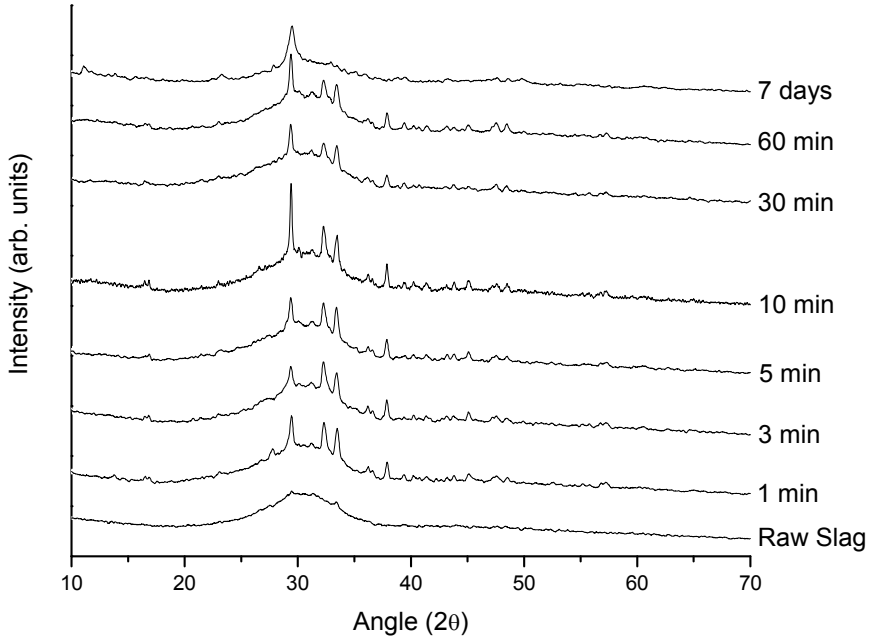

Figure C.5 – XRD diffractograms of basic Na_2CO_3-activated formula at 1, 3, 5, 10, 30, and 60 minutes. Unreacted slag and formula after 7 days of setting shown for reference (bottom and top, respectively.)

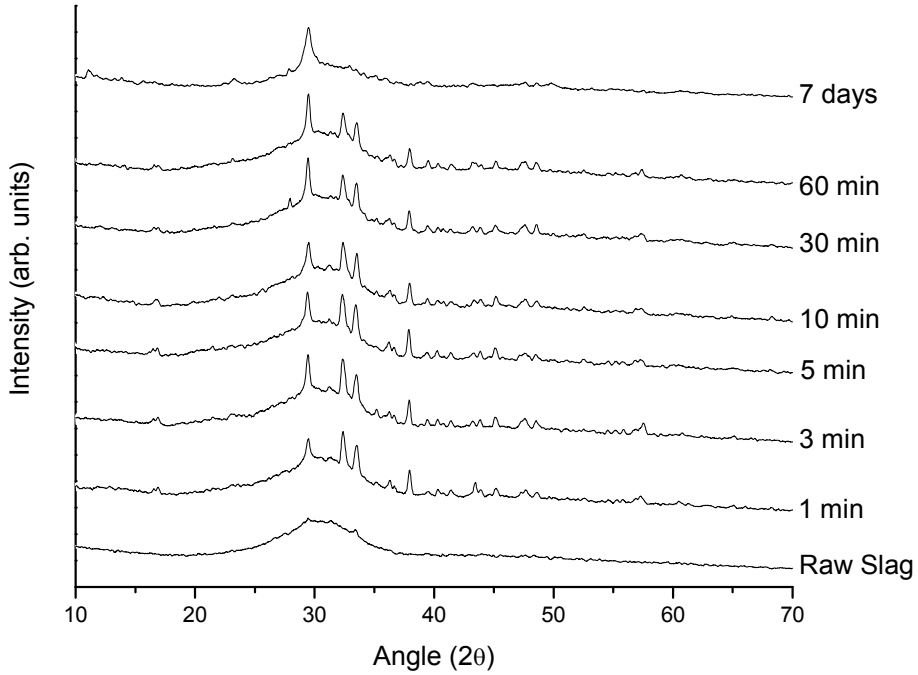

Figure C.6 – XRD diffractograms of basic Na_2CO_3 -activated formula A at 1, 3, 5, 10, 30, and 60 minutes. Unreacted slag and formula after 7 days of setting shown for reference (bottom and top, respectively.)

to diminish slightly over time; a number of other minor peaks can be observed, but are far too weak for identification. That these peaks are so well defined is interesting; it implies that highly crystalline minerals are being produced even after only a minute of curing time. The peak at 30 $^{o}2\theta$ is seen after 7 days; it could be indicative of C-S-H, though the sharpness of the peak argues against that; it could also indicate $CaCO_3$ produced through the absorption of atmospheric CO_2 or CO_3^{2-} ions from the activating solution. Without well-defined secondary peaks, however, this is guesswork at best.

C.2.2 – FTIR

The FTIR spectra of the basic Na_2CO_3–activated formula without DE (Fig. C.7) and with DE (Fig. C.8) are also very similar and contain only the peaks mentioned above for the basic NaOH/waterglass activated formula. The Si-O related peaks (around 1000 cm^{-1} and below 500 cm^{-1}) are substantially broader and flat-bottomed; whether this is due to the wide variety of Si-O bonds in the DE, a special case for the Na_2CO_3 activator, or an artifact of an error in using the equipment is not clear. In the basic Na_2CO_3–activated formula, however, it appears that the peak around 1400 cm^{-1}, due to CO_2 molecules, becomes more broad, possibly due to the production of carbonate minerals (calcite, hydrotalcite, etc.) The sharp peaks due to $CaCO_3$ and the faint resonances that are indicative of calcite are not, however, present in the spectra.

C.2.3 – Conclusions

The XRD diffractograms and the FTIR spectra of the Na_2CO_3–activated formula with or without DE are more or less identical. As before, weak peaks in the diffractograms prohibit definite identification, thus rendering the complimentary FTIR

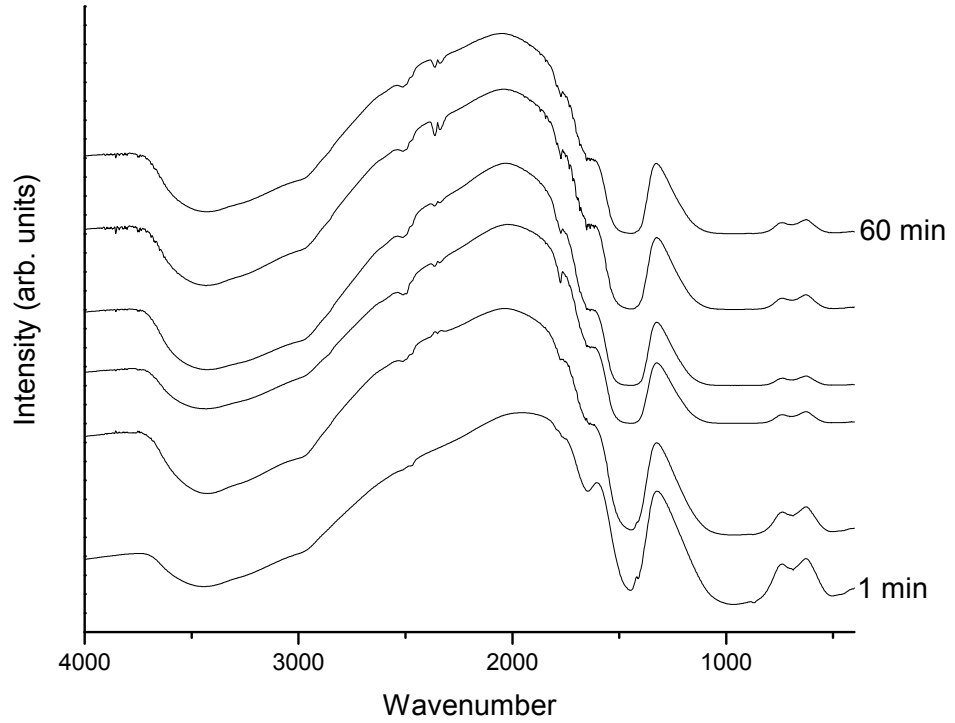

Figure C.7 – FTIR spectra of basic Na_2CO_3 -activated formula at (from top) 60, 30, 10, 5, 3, and 1 minutes.

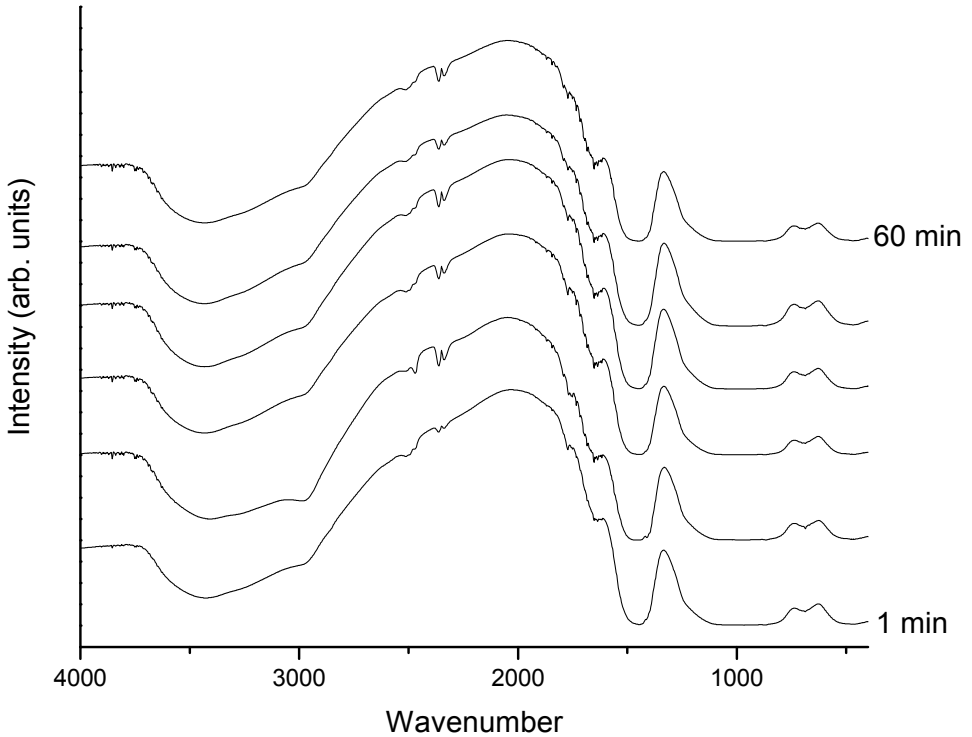

Figure C.8 - FTIR spectra of basic Na_2CO_3-activated formula containing DE at (from top) 60, 30, 10, 5, 3, and 1 minutes.

data difficult to decipher. The broadness of the peaks in the FTIR spectra also makes definite identification of peak location difficult.

C.3 – NaOH/Waterglass-activated Formula with added Al_2O_3

Cement pastes of the NaOH/Waterglass-activated formula with three different levels of Al_2O_3 (bringing the Si:Al ratios to 1, 2, and 4) were investigated.

C.3.1 – XRD

The XRD diffractograms of the NaOH/waterglass-activated formula containing Al_2O_3 are, as was expected, dominated by peaks due to Al_2O_3. These peaks are (naturally) strongest in the formula with the most additional Al_2O_3 (Si:Al ratio of 1; Fig. C.9), less intense in the formula with a medium addition of Al_2O_3 (Si:Al ratio of 2; Fig. C.10) and barely present in the formula with the least s additional Al_2O_3 (Si:Al ratio of 4; Fig. C.11.) The peaks that were previously observed in the basic NaOH/waterglass-activated formula appear to be present; however, they are still impossible to identify, for the same reasons as mentioned above.

C.3.2 – FTIR

The FTIR spectra of the three formulae with added Al_2O_3 (Figs. C.12 – C.14) show only slight differences when compared to the basic NaOH/waterglass based formula. First, the signal was of lower quality, and the curves appear rather a bit more ragged. The peaks due to water are substantially less intense; the peak due to CO_2 appears to shift slightly over time, thought the importance of this is unclear. Again, the SiO-related peaks are so broad as to defy precise analysis.

C.3.3 – Conclusions

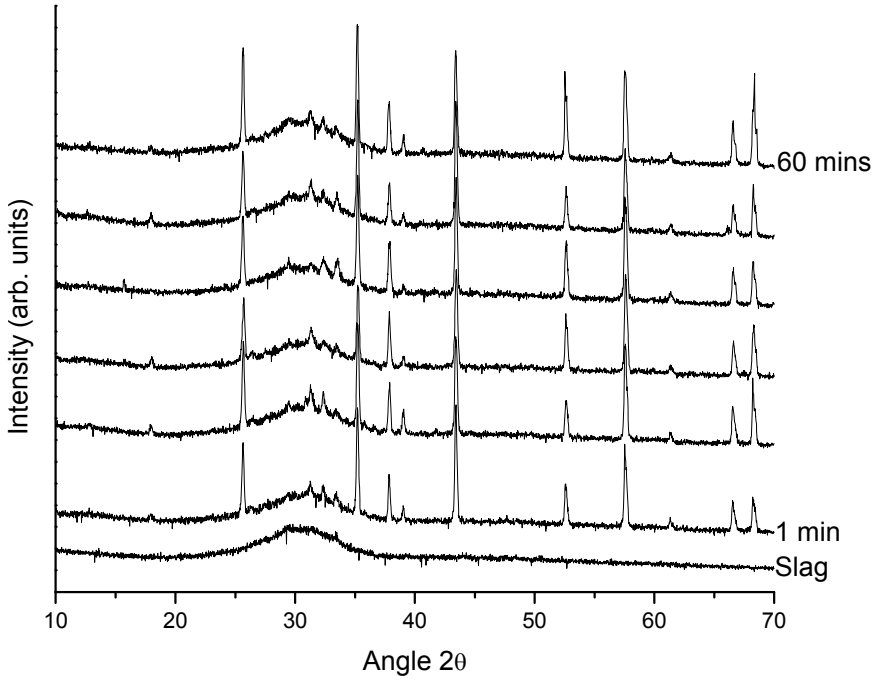

Figure C.9 – XRD diffractograms of NaOH/waterglass-activated formula with Al_2O_3 added to bring the Si:Al ratio to 1 at (from top) 60, 30, 10, 5, 3, and 1 minutes. Unreacted slag shown for reference (bottom.)

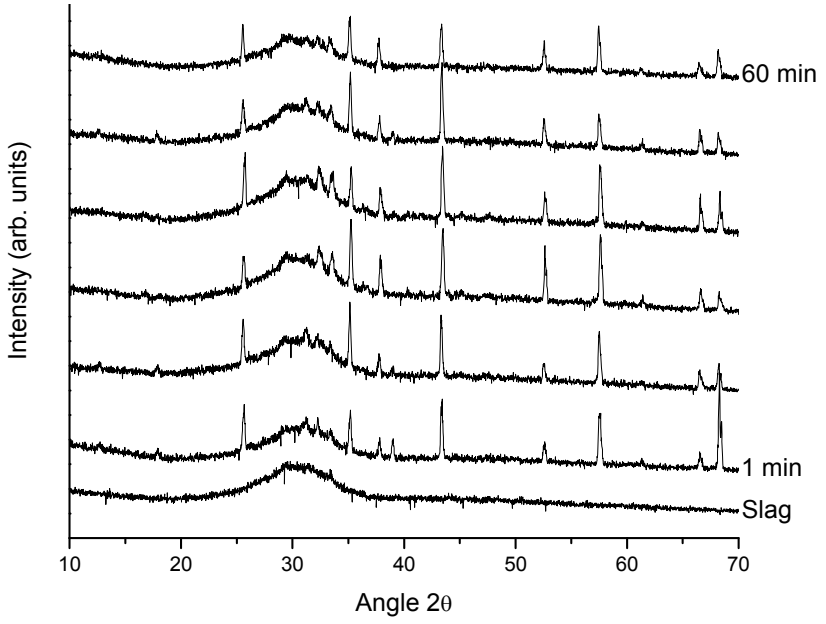

Figure C.10 – XRD diffractograms of NaOH/waterglass-activated formula with Al_2O_3 added to bring the Si:Al ratio to 2 at (from top) 60, 30, 10, 5, 3, and 1 minutes. Unreacted slag shown for reference (bottom.)

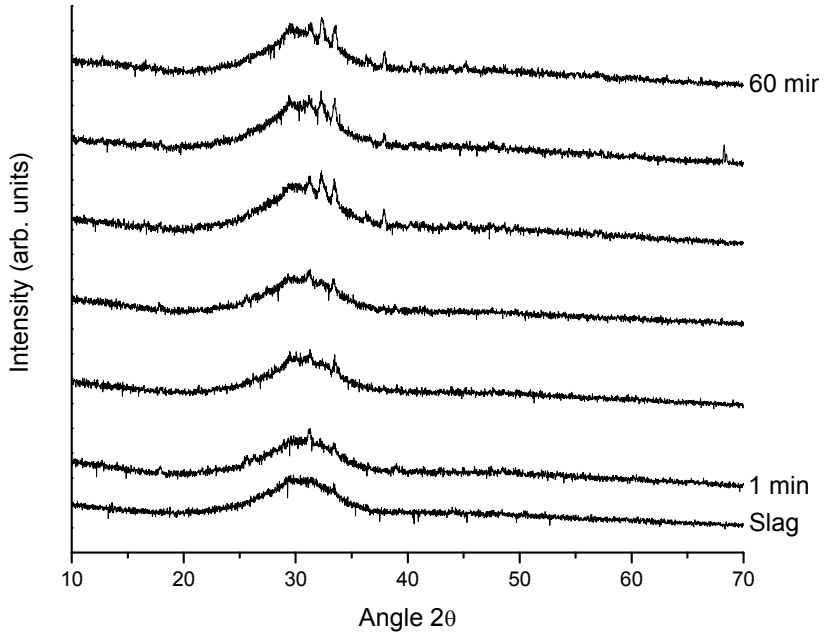

Figure C.11 – XRD diffractograms of NaOH/waterglass-activated formula with Al_2O_3 added to bring the Si:Al ratio to 4 at (from top) 60, 30, 10, 5, 3, and 1 minutes. Unreacted slag shown for reference (bottom.)

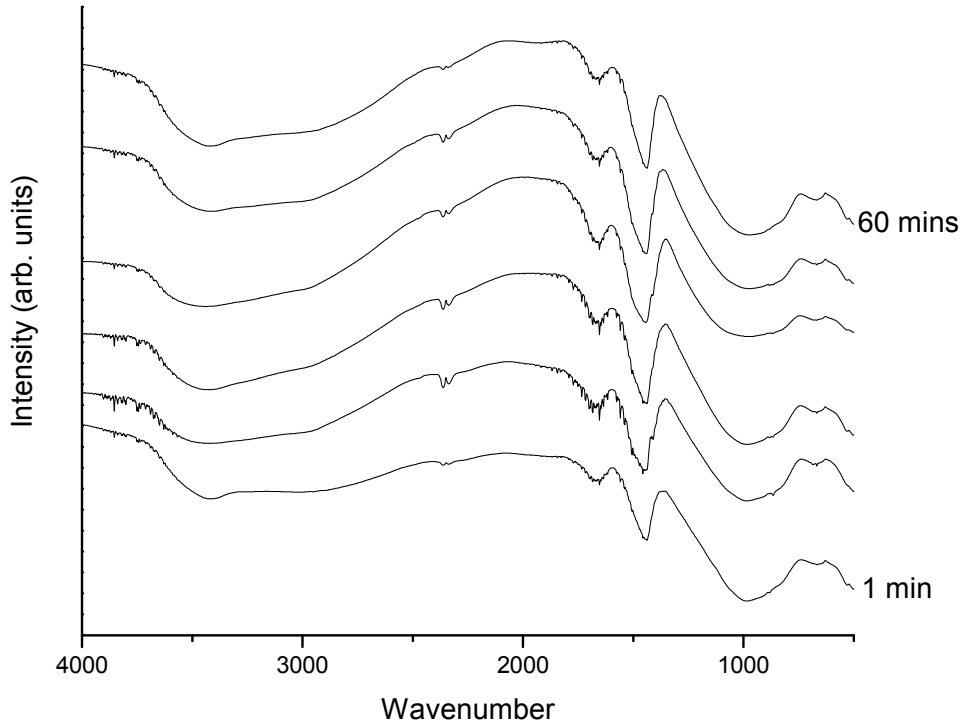

Figure C.12 – FTIR spectra of NaOH/waterglass-activated formula with Al_2O_3 added to bring the Si:Al ratio to 1 at (from top) 60, 30, 10, 5, 3, and 1 minutes.

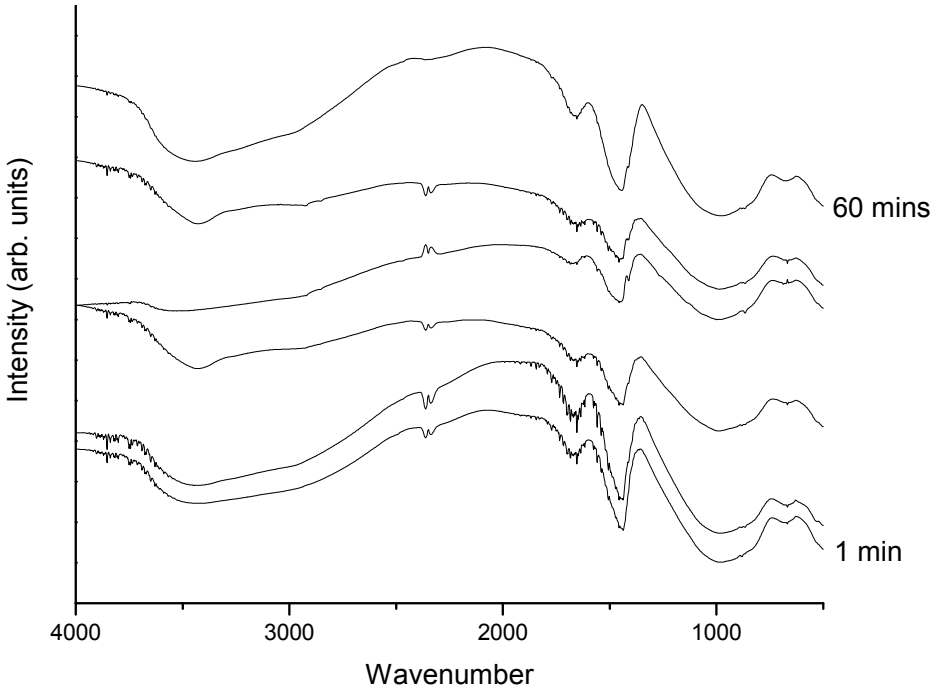

Figure C.13 – FTIR spectra of NaOH/waterglass-activated formula with Al_2O_3 added to bring the Si:Al ratio to 2 at (from top) 60, 30, 10, 5, 3, and 1 minutes.

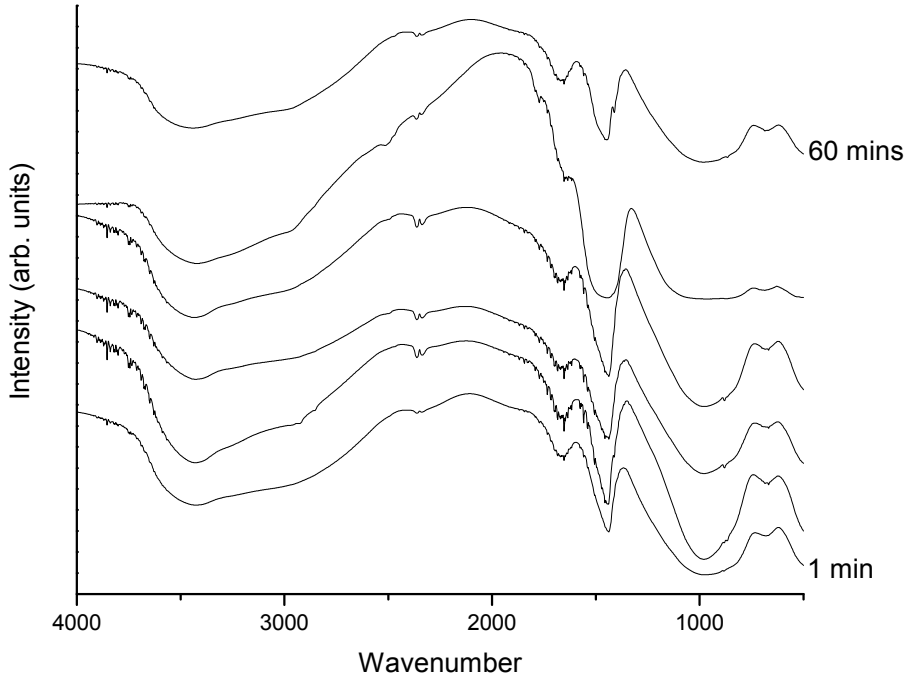

Figure C.14 – FTIR spectra of NaOH/waterglass-activated formula with Al_2O_3 added to bring the Si:Al ratio to 4 at (from top) 60, 30, 10, 5, 3, and 1 minutes.

As above, the main value of the FTIR spectra are as compliments to the XRD diffractograms; without the identification of peaks in by XRD, FTIR does little to describe anything other than the vaguest aspects of the final products.

C.4 – Na_2CO_3-activated Formula with added Al_2O_3

Cement pastes of the Na_2CO_3-activated formula with three different levels of Al_2O_3 (bringing the Si:Al ratios to 1, 2, and 4) were investigated.

C.4.1 – XRD

The XRD diffractograms of the two Na_2CO_3-activated formulae containing added Al_2O_3 (Si:Al ratio of 1 and 2; Figs. C.15 and C.16, respectively) show mostly peaks due to Al_2O_3, however, the new peaks that were previously identified in the basic formula were also observable. In the formula with Si:Al = 4 (Fig C.17), which contained DE rather than Al_2O_3, these new peaks are observable and the diffractograms are no different from those of the basic formula. These peaks were still not identifiable.

C.4.2 – FTIR

The spectra of the three Na_2CO_3-activated formulae described in Section Y.4.1 are, again, quite similar (Figs. C.18 - C.20.) All of the now-familiar peaks are in evidence; strangely, the peak related to water is no less intense than in the formula that does not contain Al_2O_3, as it was in the NaOH/waterglass formulae containing Al_2O_3. On the other hand, as Al_2O_3 has an effect on the strength of the NaOH/waterglass formulae, but not on the strength of the Na_2CO_3-activated formulae, that the spectra are different should not come as a great surprise.

C.4.3 – Conclusions

As the XRD peaks were unable to be identified, the FTIR data was of little use; it does, however, show that the addition of Al_2O_3 does not affect the Na_2CO_3-activated formula as it does the NaOH/waterglass-activated formula.

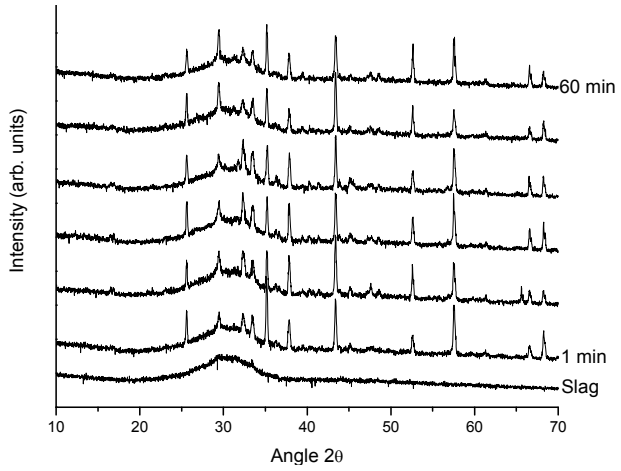

Figure C.15 – XRD diffractograms of Na_2CO_3-activated formula with Al_2O_3 added to bring the Si:Al ratio to 1 at (from top) 60, 30, 10, 5, 3, and 1 minutes. Unreacted slag shown for reference (bottom.)

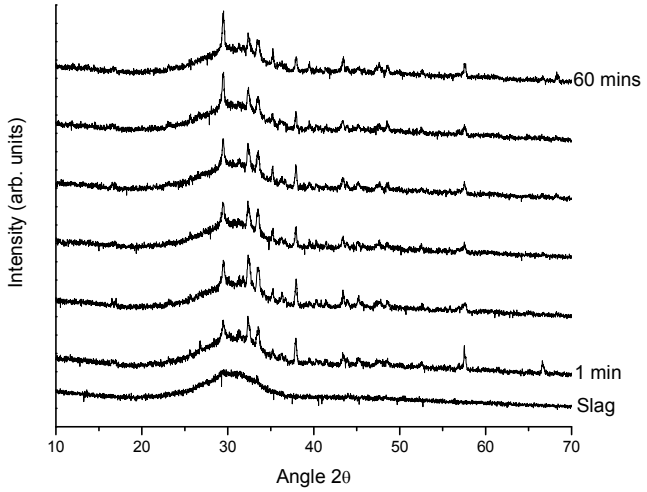

Figure C.16 – XRD diffractograms of Na_2CO_3-activated formula with Al_2O_3 added to bring the Si:Al ratio to 2 at (from top) 60, 30, 10, 5, 3, and 1 minutes. Unreacted slag shown for reference (bottom.)

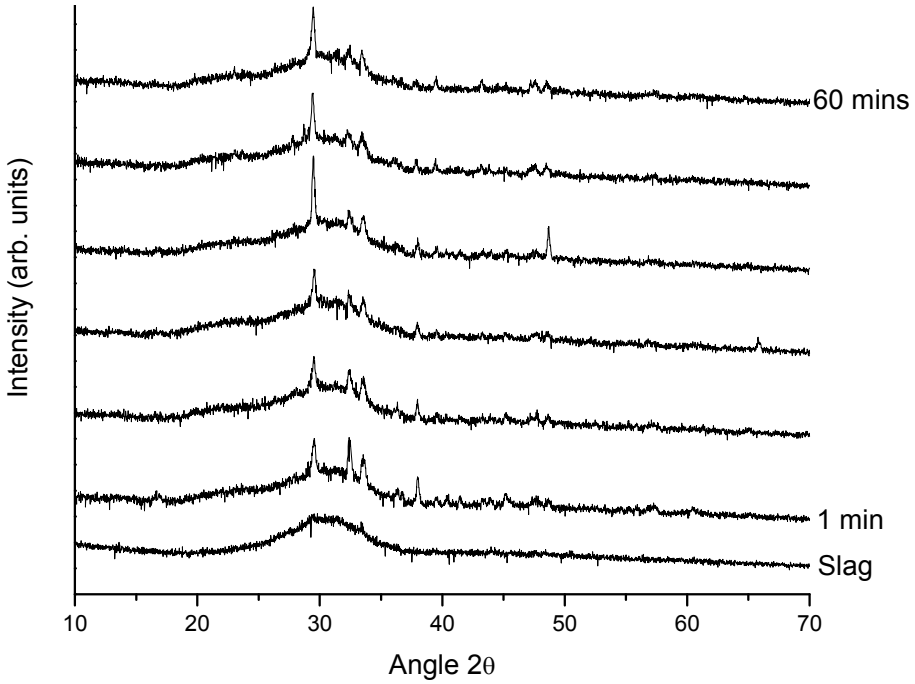

Figure C.17 – XRD diffractograms of Na_2CO_3-activated formula with Al_2O_3 added to bring the Si:Al ratio to 4 at (from top) 60, 30, 10, 5, 3, and 1 minutes. Unreacted slag shown for reference (bottom.)

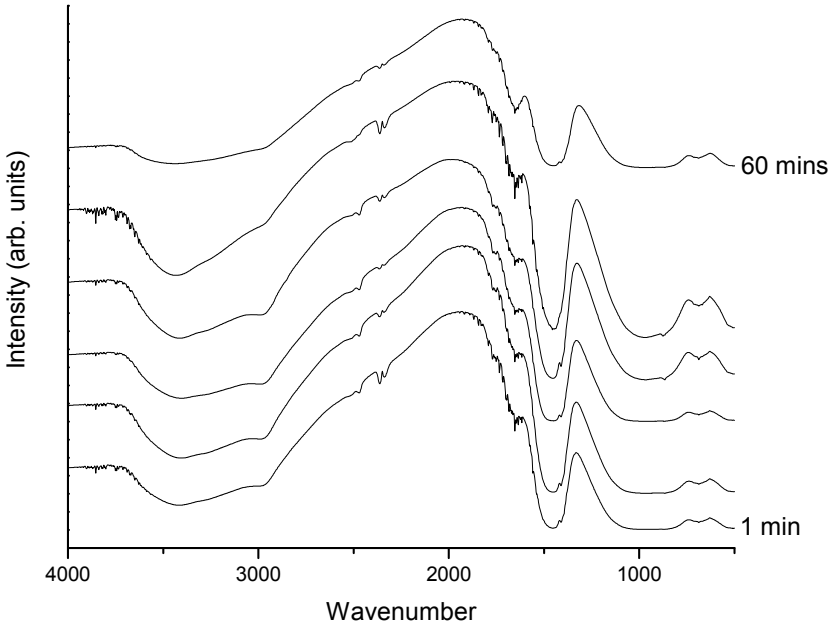

Figure C.18 – FTIR spectra of Na_2CO_3-activated formula with Al_2O_3 added to bring the Si:Al ratio to 1 at (from top) 60, 30, 10, 5, 3, and 1 minutes.

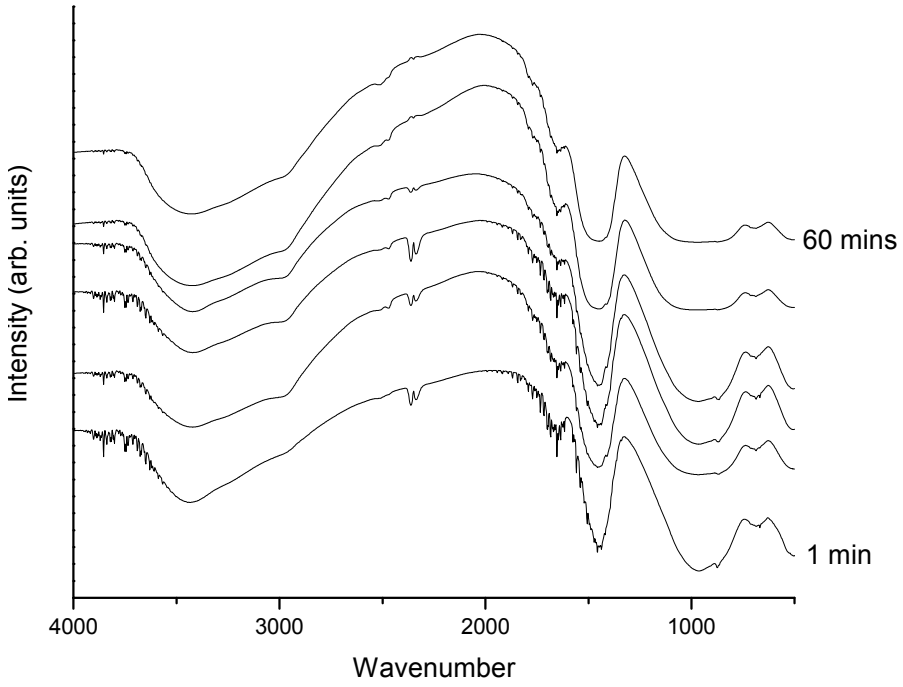

Figure C.19 – FTIR spectra of Na_2CO_3-activated formula with Al_2O_3 added to bring the Si:Al ratio to 2 at (from top) 60, 30, 10, 5, 3, and 1 minutes.

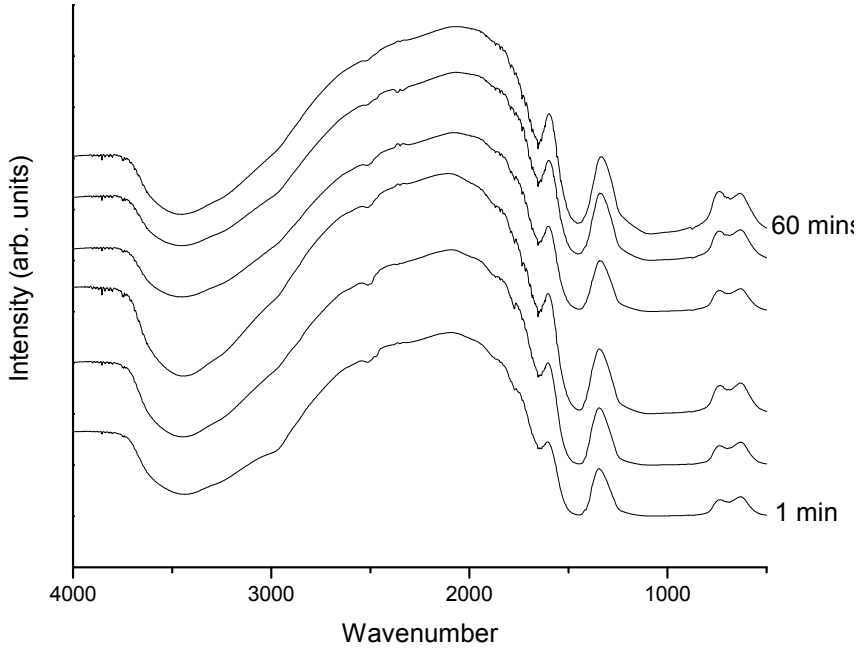

Figure C.20 – FTIR spectra of Na_2CO_3-activated formula with Al_2O_3 added to bring the Si:Al ratio to 4 at (from top) 60, 30, 10, 5, 3, and 1 minutes.

C.5 – Overall Conclusions

That freeze-drying cement paste to gain ‘snapshots’ of the chemical products at various moments in time is a valuable method is clear; however, it is equally clear that there are a number of difficulties involved. First and foremost is that the primary XRD peaks of the various products are so weak that secondary peaks are essentially unobservable; additionally, these weak primary peaks appear on top of a large amorphous hump due to unreacted slag, creating an insurmountable obstacle to the identification of the peaks.

In terms of FTIR, mainly low quality spectra were produced. Peaks related to Si-O bonding were so broad as to defy accurate measurement, and without XRD data to help put the FTIR data in context, only the broadest, most vague statements could be made. It is hoped, though not expected, that at some point in the future, this data will be deciphered and valuable insight into the first hour of reaction will be gained.

Vita – Aaron Richard Sakulich

Education

PhD in Materials Science and Engineering, Drexel University	Oct. 2009
BS in Materials Science and Engineering, Drexel University	June 2005

Professional Experience and Awards

Koerner Family Fellow	Sept. 2008
J. William Fulbright Grantee	Sept. 2007
Critical Language Enhancement Award Recipient	Sept. 2007
College of Engineering Research Excellence Award	April 2007
Materials Science Dept. Outstanding Graduate Student Award	April 2007
Graduate Assistance in Areas of National Need (GAAN) Fellow	2006-2007
Drexel University Outstanding Teaching Assistant Award	Feb. 2007

Publications

A.R. Sakulich, "Shnoo the Hell is Going on Hnaa? A Beginner's Guide to Colloquial Moroccan Arabic Grammar." International Centre for Performance Studies, Tangier, Morocco. Rajae Khaloufi, editor. 2009, 145 Pages. ISBN 978-0-9824409-0-2.

A.R. Sakulich, E. Anderson, and M.W. Barsoum, "Influence of Si:Al Ratio on the Microstructural and Mechanical Properties of Limestone-based Alkali Activated Slag Concrete." *Materials and Structures*. In Press (2009)

A.R. Sakulich, E. Anderson, and M.W. Barsoum, "Mechanical and Microstructural Characterization of an Alkali Activated Limestone/Slag Concrete." *Construction and Building Materials*. **23**(8) p. 2951 (2009)

A.R. Sakulich, Ž. Ivošević, and M.W. Barsoum, "Development of a Diatomaceous Earth, Fine Limestone Aggregate Alkali-Activated Concrete." *Proceedings of the 11th Canadian Masonry Symposium*. pp. 503-513. (2009)

A. Aatiq, R. Bakri, and **A.R. Sakulich**, Preparation and crystal structure of $Sb^{V}_{1.50}In\ (PO_4)_3$ and $(Sb^{V}_{0.50}In)P_2O_7$." *Powder Diffraction* **23**(3) p.195 (2008)

A.R. Sakulich and M.W. Barsoum. "Chemical and Microstructural Characterization of 20-Month Old Alkali Activated Slag Cements." Submitted for publication.

A.R. Sakulich, B. Naylor, and M.W. Barsoum. **"**Effect of Additives on Mechanical and Microstructural Properties of Alkali Activated Slag Cements." In preparation

I.C. Albayrak, S. Basu, **A. Sakulich**, O. Yeheskel, and M.W. Barsoum, "Mechanical Properties of Transparent Yttria: Indentation Techniques." Submitted for Publication

C. Spencer, J. Córdoba, N. Obando, **A.R. Sakulich**, E. Judd-Sierra, M. Radovic, M. Odén, L. Hultman and M.W. Barsoum. "On the Reactivity of Ti_2AlC with SiC Fibers and Powders to 1550°C." In preparation

C. Spencer, J. Córdoba, N. Obando, **A.R. Sakulich**, E. Judd-Sierra, M. Radovic, M. Odén, L. Hultman and M.W. Barsoum. "On the Reactivity of Ti_2AlC with Al_2O_3 Fibers to 1550°C." In preparation

Y. Chung, **A.R. Sakulich**, M.W. Barsoum. "Synthesis of nano-tetragonal $BaTiO_3$ by the Solid State Reaction between TiO_2 and $BaCO_3$" In preparation.

E. Jud Sierra, S. Miller, **A.R. Sakulich**, M.W. Barsoum. "Pozzolanic activity of Diatomaceous Earth for reconstituted limestone." In preparation.

A. Moseson, **A.R. Sakulich**, M.W. Barsoum "Characterization and Optimization of Hydraulic Alkali Activated Fine Aggregate Concrete Using Design of Experiment, Part 2: Chemical Properties" In preparation.